

NORTHWESTERN UNIVERSITY

Cyclic and Post-Cyclic Behavior of Bootlegger Cove Formation Clay

A DISSERTATION

SUBMITTED TO THE GRADUATE SCHOOL

IN PARTIAL FULFILLMENT OF THE REQUIREMENTS

for the degree

DOCTOR OF PHILOSOPHY

Field of Civil Engineering

By

Gabriel J. Colorado Urrea

EVANSTON, ILLINOIS

December 2021

© Copyright by Gabriel J. Colorado Urrea 2021
All Rights Reserved

ABSTRACT

Cyclic, and Post-Cyclic Behavior of Bootlegger Cover Formation Clay

Gabriel J. Colorado Urrea

Cyclic loading, from earthquake, has caused the instability and failure of slopes composed of sensitive clays. During the 1964 9.2 moment magnitude (M) earthquake in Anchorage, Alaska, several slopes comprised of Bootlegger Cove Formation (BCF) clays failed during the strong seismic motion. Some researchers have proposed the use of residual strength to account for strength degradation to overcome the seismic failure of clay slopes. The residual strength is determined in monotonic tests that involves large deformations that may never occur during an earthquake on a clayey slope. This conservative approach fails to provide a comprehensive analysis to consider dynamic parameters (e.g., magnitude and duration) on clay specimens that can control the possible strength degradation during and after a seismic event. The goal of this research is to understand the cyclic behavior and post-cyclic degradation of facies III and IV of Bootlegger Cover Formation (BCF) clay based on laboratory tests to provide key information needed to develop a more comprehensive analysis.

This work evaluates the field and the laboratory investigation performed by Northwestern University and others at Lynn Ary Park adjacent to the Turnagain Heights landslide escarpment in

Anchorage The field exploration consisted of drilling two borings to obtain thin-walled samples for subsequent laboratory testing and one boring to perform field vane and downhole seismic tests. Field data used herein also included the results from CPT, field vane and torvane tests performed by other researchers. These data can provide the necessary elements to establish the soil characterization of the BCF clay at Turnagain Heights.

Laboratory tests were used to establish soil characteristics and in situ conditions of the BCF clay and to evaluate the cyclic and post-cyclic response of BCF clay. For the evaluation of in situ conditions, the laboratory tests include index property, consolidation, monotonic undrained triaxial shearing results. These results complemented the field work and provided a full evaluation of the conditions of the BCF at the site and the possible properties that can impact its cyclic and post-cyclic behavior.

The laboratory testing program also includes cyclic and post-cyclic loading triaxial tests on BCF specimens collected in thin-walled tubes. The analyses focus on the behavior of the BCF clay under equivalent earthquake loadings. Both undrained cyclic and post-cyclic strength are evaluated with respect to stress history and liquidity index. The BCF specimens were tested under stress-controlled cyclic loading with different cyclic stress ratios (CSR). The degradation of undrained shear strength directly is evaluated based on the results of post-cyclic undrained shearing. This degradation is presented as a function of the accumulated strain during the consolidation and cyclic loading or during cyclic loading only. The degradation of post-cyclic strength was also analyzed in terms of effective stresses. The role of sensitivity, quantified by the liquidity index, and conventional axial strain failure criteria are assessed. A limited study of the cyclic loading rate was made to illustrate its effects on the cyclic responses of clay.

Field and laboratory tests were conducted to measure OCR, strength, sensitivity, cyclic and post-cyclic strength. Results from analysis of field and laboratory data showed that the OCR at the BCF at the Lynn Ary Park site decreases with depth, presumably as a result of desiccation. The undrained strengths measured by CPT and field vane were consistent with the OCR and decreased with depth. Material sensitivity measured by field vane varied from 2 to 6 with the highest sensitivity near a sand layer in a predominately clay profile.

The post-cyclic normalized undrained strength of BCF specimens depends on OCR, liquidity index and the total strain prior to the post-cyclic shearing (i.e., axial strain from consolidation and cyclic shearing). Reduction of post-cyclic strength of NC specimens was observed after 15% axial strain accumulated during cyclic loading. There is an influence of the liquidity index in the degradation of the undrained strength when it is higher than 1.0. Based on the current design guidelines, a reduction of 10 to 15% of the undrained strength does not apply to the BCF clays evaluated in this thesis, wherein results indicate more degradation can occur in specimens when accumulating a large amount of axial strain.

The cyclic and post-cyclic strength from specimens prepared by SHANSEP are conservative and may be more representative of the intrinsic behavior of BCF clay.

Acknowledgements

I would like to take advantage of this opportunity to thank many people who joined, helped, and mentored me during my time at Northwestern University. Their support was vital to finish this work.

First, I would like to express my deepest gratitude to my advisor and mentor, Professor Richard J. Finno, for giving me the opportunity to participate in this amazing project, for his extended guidance, support, and patience during the development of the laboratory work and this thesis. I learned so many invaluable lessons not only on the academic setting but also during the professional life as a geotechnical engineer. I would also like to thank the committee members Professor Giuseppe Buscarnera and Professor James Hambleton for their valuable contribution to this thesis.

I want to thank all of my colleagues and friends during my time at Northwestern, Tatiana, Luis, Chang, Molly, Charlotte, Yan, Yida, Zhenhao, Nathan, Sangrae, Jose, Yanni, Zhefei, Thanos, Dillon, Xiang, Nando, and Anastasia. Their friendship and support made this experience a wonderful and unforgettable experience in my life. Very special thanks to Yan Zang and Zhenhao Shi for their incredible help and discussions to carry out the laboratory tests and analysis of results. Their help was crucial for the success of this work. I specially thank Professor Jose Dario Aristizabal-Ochoa, for his guidance and support that paved the future of my academic career in

the US. Very special thanks to Scott Simpson from the Ford workshop for his help during an important part of the laboratory work.

I thank also to all my friends in Evanston, Chicago, and Urbana-Champaign, Jaime, Oliver, Jorge, Daniel, Jessica, Isabel, Filipe, Kevin, Helen, Edwin, Pablo, and Tatiana. Their friendship and innumerable experiences enriched my life during my time in Chicago and Illinois.

I want to thank my family back in Colombia. My mom and my uncle made all of this possible, their sacrifice and guidance under very difficult circumstances made me the person I am today, to Felipe Uribe for his friendship, support and help during all these years.

Lastly, I want to thank my wife, Johanna, for her support during very difficult times without her support and patience this would not be possible. Her company and love during very lonely and frustrating times helped me to keep reaching my dreams. I dedicate this thesis to my beloved Johanna.

Table of Contents

ABSTRACT.....		3
Acknowledgements.....		6
List of Tables		12
List of Figures.....		14
1	INTRODUCTION	21
2	LITERATURE REVIEW	26
2.1	Bootlegger Cove formation.....	27
	2.1.1 Studies Performed on Bootlegger Cove Formation Deposit.....	31
2.2	Cyclic Behavior of Clays	35
	2.2.1 Undrained Cyclic Strength of Clays.....	35
	2.2.2 Sensitive Clay Behavior During Cyclic Loading.....	38
2.3	Post-Cyclic Response of Sensitive Clay	47
	2.3.1 Degradation of Strength as a Function of Accumulated Axial Strain.....	47
	2.3.2 Degradation of Strength as a Function of Accumulated Pore Water Pressure.....	52
2.4	Summary	55

		9
3	EXPERIMENTAL PROGRAM AND PROCEDURES	57
3.1	Introduction	58
3.2	Summary and Experimental Program	58
3.3	Triaxial Device	58
	3.3.1 Bender Elements	63
	3.3.2 Pore Water Pressure Measurements	64
3.4	Testing Protocol	65
	3.4.1 X-Ray Testing	66
	3.4.2 Extraction and Trimming	68
	3.4.3 Specimen Preparation after Trimming	70
	3.4.4 Residual Stress and Saturation	72
	3.4.5 Reconsolidation	74
	3.4.6 Creep or Aging Period	76
	3.4.7 Cyclic Loading	78
	3.4.8 Monotonic and Post-Cyclic Undrained Shearing	82
	3.4.9 Shear Wave Velocity Measurements	84
3.5	Summary	86
4	SITE CHARACTERIZATION AT LYNN ARY PARK	87
4.1	Introduction	88
4.2	Stratigraphy	90

		10
4.3	Northwestern University Exploration	91
	4.3.1 Sampling	91
	4.3.2 Boring Logs.....	92
	4.3.3 Index Properties.....	101
	4.3.4 Field Shear Wave Velocity	105
4.4	Stress History of BCF Clay.....	107
	4.4.1 Results from Reconsolidation in Triaxial.....	108
4.5	Specimen Quality	114
	4.5.1 Shear Wave Velocity.....	114
	4.5.2 Strain During Consolidation.....	118
4.6	Undrained Triaxial (Ck_0U TXC) Results.....	123
4.7	Sensitivity.....	130
	4.7.1 Soil Classification and Sensitivity Based on CPT Normalized Soil Behavior Type (SBTn) Chart.....	130
	4.7.2 Sensitivity Analysis.....	133
4.8	Summary and Conclusions.....	137
5	RESULTS OF CYCLIC LOADING AND POST-CYCLIC UNDRAINED SHEARING OF BCF CLAY	141
5.1	Introduction.....	142
5.2	Results of Cyclic Loading.....	143

	11
5.2.1 Cyclic Responses of Clay Specimens	147
5.2.2 Equalization Period	154
5.2.3 Cyclic Strength.....	156
5.2.4 Effects of Rate of Shearing During Cyclic Loading	160
5.2.5 Analysis of Effective Stresses During Cyclic Loading.....	165
5.2.6 Failure Defined by 5% Axial Strain for Specimens with Equalization Period. .	170
5.3 Post-Cyclic Shearing Results	172
5.3.1 Post-Cyclic Response of BCF Clay	172
5.3.2 Degradation of Undrained Strength of Specimens due Cyclic Loading	179
5.3.3 Effective Stress Parameters Mobilized during Post-Cyclic Shearing	189
5.4 Summary and Conclusions.....	195
6 SUMMARY AND CONCLUSIONS	200
6.1 Summary	201
6.2 Conclusions	203
References.....	209
Apendix A. Boring Logs with Photos.....	217
Apendix B. Triaxial Results of BCF Specimens	231

List of Tables

Table 3.1. Laboratory Experimental Program Borehole NU-1	59
Table 3.2 Laboratory Experimental Program Borehole NU-3.....	60
Table 3.3. Detail Specification of the DYN-TTS (GDS Instruments Ltd, 2013)	63
Table 4.1. Description of Facies proposed by Updike et al. (1988)	90
Table 4.2. Index Properties NU-1	103
Table 4.3. Index Properties NU-3	104
Table 4.4. Parameters of specimens During Consolidation.....	109
Table 4.5. Parameters of specimens During Consolidation.....	112
Table 4.6. Shear Wave Velocity for Specimens Prepared by Recompression Including the Creep Effect.....	115
Table 4.7. Shear Wave Velocity from the Field and Laboratory.....	117
Table 4.8. Shear Modulus from the Field and Laboratory	118
Table 4.9. Ratings of specimen Quality.....	120
Table 4.10. Results of Monotonic Triaxial Compression Tests	123
Table 5.1. Results of Cyclic Loading and Post-Cyclic Shearing (SHANSEP)	145
Table 5.2. Results of Cyclic Loading and Post-Cyclic Shearing (Recompression)	146
Table 5.3. Results of Stiffness Degradation	148

	13
Table 5.4. Excess pore Water Pressure at the End of Equalization.....	155
Table 5.5. Rates of Shearing During Cyclic Loading.....	161
Table 5.6. Results of Effective Strength Parameters for Post-Cyclic Shearing of NC and Slightly Overconsolidated BCF specimens.....	192

List of Figures

Figure 2.1. Turnagain Heights Profile After Failure (Shannon and Wilson Inc., 1964)	28
Figure 2.2. Boring Including Strength and Sensitivity Values (Shannon and Wilson Inc., 1964)	30
Figure 2.3. Plan View of Turnagain Heights Failure (Seed and Wilson, 1967).....	32
Figure 2.4. Liquefaction Potential of Sandy Layer at Fourth Avenue (Stark and Contreras, 1998)	33
Figure 2.5. Undrained and Residual Strength of BCF Clay at Fourth Avenue (Stark and Contreras, 1998).....	35
Figure 2.6. Estimation of Cyclic Shear Strength (Ansal and Erken, 1989).....	36
Figure 2.7. Effect of Soil Stiffness in Cyclic Strength (Lee and Focht Jr, 1976).....	39
Figure 2.8. Typical Specimen after Failure during Cyclic Loading (Lee, 1979)	41
Figure 2.9. Consolidation Response of Drammen Clay (Andersen et al., 1980)	42
Figure 2.10. Cyclic Strength of Drammen Clay (Andersen et al., 1980)	42
Figure 2.11. Stability Threshold Proposed by Lefebvre et al. (1989)	43
Figure 2.12. Cyclic Strength for Specimen with Static Bias (Lefebvre and Pfendler, 1996).....	44
Figure 2.13. Schematic Safe Zones for Foundations on Sensitive Clays (Hanna and Javed, 2008)	45
Figure 2.14. Cyclic Softening for Different Sensitivities (Hanna and Javed, 2014).....	47

	15
Figure 2.15. Post-Cyclic Strength Degradation versus. Normalized Cyclic Strain (Thiers and Seed, 1969).....	48
Figure 2.16. Post-Cyclic Strength Degradation versus Normalized Strain after Cyclic Loading (Koutsoftas, 1978)	49
Figure 2.17. Post-Cyclic Strength vs. Strain Accumulated during Cyclic Loading (Perlea, 2000)	50
Figure 2.18. Degradation of Clay after a Strain Controlled Cyclic Test after Reaching the Failure Strain at Monotonic Loading (Åhnberg et al., 2013).....	51
Figure 2.19. Post-Cyclic Strength Degradation versus Equivalent Over Consolidation Ratio (Matsui et al., 1980).....	52
Figure 2.20. Normalized Post-Cyclic Strength vs Excess Pore Pressure Ratio (Yasuhara, 1994)	54
Figure 3.1. Setup of the DYNTTS at Northwestern University	61
Figure 3.2. Sketch of the DYNTTS Provided by GDS Instruments.....	62
Figure 3.3. Bender Elements at Top-Cap and Pedestal (GDS Instruments Ltd, 2005)	64
Figure 3.4. Cell Base Plan View.....	65
Figure 3.5. X-Ray test on tube NU-1 65-67	67
Figure 3.6. Sample NU-1 65-67(3) (top of the tube).....	68
Figure 3.7. Longitudinal Cutting with Slitting Saw	69
Figure 3.8. Filter Paper Setup in Sample.....	71
Figure 3.9. Sample placed in the Triaxial Pedestal.	72
Figure 3.10. Residual Stress Measurement (NU-1 20-22)	73
Figure 3.11. (a) Pore Water Pressure Ratio and (b) Axial Loading Rate During Reconsolidation with SHANSEP	76

	16
Figure 3.12. (a) Axial Strain Ratio and (b) Pore Water Pressure Ratio During Creep.....	78
Figure 3.13. Stress-Strain-Pore Water Pressure Response During Cyclic Loading (NU-3 60-62)	81
Figure 3.14. Excess pore water pressure Response during Equalization Time (NU-1 22-24(2)) .	82
Figure 3.15. Deviator Stress and Excess Pore Water Pressure versus Axial Strain (NU-1 47-49)	84
Figure 3.16. Change of Shear Modulus with Time (NU-1 27-29 (2)).....	86
Figure 4.1. Plan View of Field Investigation at Lynn Ary Park.....	89
Figure 4.2. Soil Profile Based on Results from Updike et al. (1988).....	91
Figure 4.3. NU-1 Boring Log	96
Figure 4.4. NU-3 Boring Log	100
Figure 4.5. (a) Water Content, PL, and LL (b) Liquidity Index with Elevation.....	102
Figure 4.6. NU-3 50-52 specimen after Cutting.....	105
Figure 4.7. Plasticity Chart with specimens from facies III and facies IV	106
Figure 4.8. Results of in situ Shear Wave Velocity at Lynn Ary Park.....	107
Figure 4.9. (a)Preconsolidation Stress and (b) OCR with Elevation.....	110
Figure 4.10. Coefficient At-Rest Response During Consolidation Stage (a) Loading and (b) Unloading	113
Figure 4.11. Shear Wave Velocity with Elevation	116
Figure 4.12. Reduction of Shear Wave Velocity versus (a) Axial Strain at in situ Stress and (b) Change in Void Ratio	122
Figure 4.13. Stress-Strain Response of Monotonic Undrained Shearing	124
Figure 4.14. Normalized Undrained Shear Strength for Monotonic Compression	126
Figure 4.15. Stress Path of Monotonic Sheared specimens in p' - q Space	127

Figure 4.16. CPT, FV, and TXC Results: (a) Undisturbed Undrained Strength (b) Side Resistance or Remolded Undrained Strength	130
Figure 4.17. Soil Classification Chart for BCF material (Adapted from Robertson (1990))	132
Figure 4.18. Soil Classification Chart for BCF material (Adapted from Robertson (2009))	134
Figure 4.19. Undisturbed Strength after Updike et al. (1988) and in this Research.....	135
Figure 4.20. Sensitivity Distribution of the BCF Clay	137
Figure 5.1. Idealized Stress Path of a specimen Subjected to Cyclic Loading and Post-Cyclic Shearing	144
Figure 5.2. Stress-Strain Response of specimens Subjected to Cyclic Loading	149
Figure 5.3. Pore Water Pressure-Strain Response of specimens Subjected to Cyclic Loading ..	150
Figure 5.4. Axial Strain and Pore Water Pressure Response with the Number of Cycles	153
Figure 5.5. Cyclic Strength of BCF Clay for Different OCR	158
Figure 5.6. Cyclic Strength for NC and Lightly OC BCF specimens	160
Figure 5.7. Time-Axial Strain Response at Cyclic Loading (NU-3 40-42).....	162
Figure 5.8. Axial Strain-Deviator Stress and Pore Water Pressure Responses of Specimens at Different Strain Rates	164
Figure 5.9. Effective Stress Failure Conditions of Specimens that Collapsed During Cyclic Loading.....	167
Figure 5.10. Specimen NU-1 22-24 After Failure during Cyclic Loading.....	168
Figure 5.11. Effective Stress Failure Conditions of Specimens That Did Not Collapsed During Cyclic Loading.....	170
Figure 5.12. Effective Stress Failure Conditions of Specimens with Equalization Period After Cyclic Loading.....	172

	18
Figure 5.13. Axial Strain-Deviator Stress and Pore Water Pressure Post-Cyclic Response	174
Figure 5.14. Normalized Undrained Shear Strength for Post-Cyclic Compression	176
Figure 5.15. Best Fit of Post-Cyclic Sheared specimens in p' - q Space	177
Figure 5.16. Effective Stress Path $OCR = 1.0, 1.05, 2.0$ specimens in p' - q Space	178
Figure 5.17. Post cyclic Undrained Strength Versus the Cyclic Stress Ratio	180
Figure 5.18. Undrained Strength Versus Axial Strain Developed During Cyclic Loading(a) SHANSEP (b) Recompression	182
Figure 5.19. Undrained Strength Versus the Total Axial Strain Prior to Monotonic Shearing...	184
Figure 5.20. Normalized Undrained Strength Related to (a) Cyclic Strain Energy and (b) Total Strain Energy	187
Figure 5.21. Normalized Undrained Strength Related to Pore Water Pressure at the End of Cyclic Loading	189
Figure 5.22. Effective Stress Path of NC and Lightly Overconsolidated Specimens in p' - q Space	191
Figure 5.23. Apparent Cohesion Versus Axial Strain (a) End of Cyclic Loading (b) Total	193
Figure 5.24. Effective Stress Path of NC Specimens Including Boundary Surface	195
Figure A.1. Boring Log NU-1	224
Figure A.2. Boring Log NU-3	230
Figure B.1. Specimen NU-1 17-19	232
Figure B.2. Specimen NU-1 20-22	233
Figure B.3. Specimen NU-1 22-24	234
Figure B.4. Specimen NU-1 22-24(2)	235
Figure B.5. Specimen NU-1 22-24(3)	236

	19
Figure B.6. Specimen NU-1 27-29	237
Figure B.7. Specimen NU-1 27-29(2)	238
Figure B.8. Specimen NU-1 32-34(3)	239
Figure B.9. Specimen NU-1 37-39(2)	240
Figure B.10. Specimen NU-1 40-42	241
Figure B.11. Specimen 40-42(2)	242
Figure B.12. Specimen 42-44(2)	243
Figure B.13. Specimen NU-1 42-44(3)	244
Figure B.14. Specimen NU-1 47-49	245
Figure B.15. Specimen NU-1 47-49(2)	246
Figure B.16. Specimen NU-1 47-49(3)	247
Figure B.17. Specimen NU-1 55-57	248
Figure B.19. Specimen NU-1 60-62	249
Figure B.20. Specimen NU-1 60-62(2)	250
Figure B.21. NU-1 60-62(3)	251
Figure B.22. Specimen NU-1 62-64	252
Figure B.23. NU-1 62-64(2)	253
Figure B.24. Specimen NU-1 62-64(3)	254
Figure B.25. Specimen NU-1 65-67	255
Figure B.26. Specimen NU-1 65-67(2)	256
Figure B.27. Specimen NU-1 65-67(3)	257
Figure B.28. Specimen NU-3 25-27	258
Figure B.29. Specimen NU-3 30-32	259

	20
Figure B.30. Specimen NU-3 40-42	260
Figure B.31. Specimen NU-3 42-44	261
Figure B.32. Specimen NU-3 42-44(2)	262
Figure B.33. Specimen NU-3 47-49	263
Figure B.34. Specimen NU-3 47-49(2)	264
Figure B.35. Specimen NU-3 47-49(3)	265
Figure B.36. Specimen NU-3 55-57	266
Figure B.37. Specimen NU-3 60-62	267

CHAPTER 1

1 INTRODUCTION

Cyclic loadings during major earthquakes have caused the instability and failure of slopes composed of sensitive clayey material. During the 1964 earthquake in Anchorage, Alaska, several slopes comprised of Bootlegger Cove Formation (BCF) clays failed during the dynamic excitation. The failure produced significant economic damages.

The 9.2 moment magnitude (M) earthquake in 1964 triggered several landslides in the city of Anchorage. The largest landslide occurred at the coastline of Turnagain Heights area which was composed of bluffs up to 70 ft high. The slide developed progressively as a sequence of retrogressive rotational slides combined with horizontal sliding. Segments of the slope moved intact as much as 500 ft. Failure first developed in the sensitive clay and was followed by a complete collapse and remolding of similar material (Shannon and Wilson Inc., 1964). Many cracks behind the resulting escarpment developed during the earthquake (Seed and Wilson, 1967).

Considerable research has been conducted to determine the causes of the failures during the 1964 event. Liquefaction in the sand lenses present in the BCF clay was the first mechanism proposed to explain the slide (Shannon and Wilson Inc., 1964; Seed and Wilson, 1967). However, subsequent studies showed that the main cause of the failure was the loss of strength of the sensitive clay, abundant in the Anchorage area (Lade et al., 1988; Updike et al., 1988). Thus, the loss of strength of the BCF clays is one of the major concerns that involve the design of slopes and foundations in the Anchorage area. Sensitivity is a measurement of the loss of strength and can be determined by CPT, vane shear, and fall cone tests. The sensitivity (S_t) of a soil is defined as the ratio of the undisturbed strength (S_u) and the remolded strength or the strength at large strains (S_{ur}), i.e. $S_t = S_u/S_{ur}$. The strength of natural clay materials can be reduced by mechanical factors (e.g. cyclic loading, increment of effective stresses). These factors can reduce or destroy the natural

structure reducing the strength up to its remolded value.

There is considerable variation in design approaches to this issue. An FHWA manual (Kavazanjian et al., 2011), considered the degradation of the undrained strength in the dynamic analysis of slopes composed of fine grain material. The manual notes that clay degrades during cyclic loading when the number of cycles is greater than 10 to 15 and the magnitude of the load is “significant.” The manual suggests that the reduction of strength may be 10-15% of the undisturbed strength for intermediate sensitive soils and recommended that cyclic loading tests must be carried out when the clay is highly sensitive. However, the authors did not define what was “significant” load and a quantified measure of what was “intermediate” sensitivity. In literature, this term is defined different. Skempton and Northey (1952) ($S_t=4-8$), Rosenqvist (1953) ($S_t=2-4$), and Shannon and Wilson Inc. (1964) ($S_t=5-7$) presented different sensitivity intervals for low to medium sensitive material.

Washington Department of Transportation (2015) dictated the use of the residual undrained strength of clay for seismic design of slopes in its geotechnical design manual. This approach is very conservative since many authors have shown that even for highly sensitive clays, the post-cyclic strength is not reduced to the remolded value neither during nor after the cyclic event (e.g. Thiers and Seed, 1969; Koutsoftas, 1978; Andersen et al., 1980; Lefebvre et al., 1989). This range of possibilities in post-cyclic strength suggest a need for a better understanding of the mechanisms that control the loss of undrained strength.

Lynn Ary Park, adjacent to The Turnagain Heights slide, was studied by USGS in the 1980s and is an excellent location to obtain samples of similar to those that failed in the 1964 event. This research quantifies undrained shear strength during and after cyclic loading based on experimental

results of BCF clay obtained at this site. This experimental research is composed of a series of static and stress-controlled cyclic triaxial tests on BCF clays to evaluate the reduction of strength, the accumulation of pore pressure and axial strain during cyclic loading and the soil response during the post-cyclic shearing.

The goal of this research is to establish the parameters that influence the cyclic behavior and post-cyclic degradation of Bootlegger Cover Formation (BCF) clay. The scope of this research is threefold:

1. Evaluate the BCF clay index properties, stress history, strength and sensitivity based on in situ and laboratory tests at Lynn Ary Park.
2. Analyze the cyclic response and strength of the BCF clay samples recovered from Lynn Ary Park.
3. Analyze the post-cyclic undrained shear response of the samples subjected to cyclic loading to evaluate the possible degradation of the undrained strength and clay structure as a result of the cyclic loading.

This thesis presents the results and analyses of this laboratory investigation on the cyclic and post-cyclic response of BCF clay. The laboratory testing program consists of monotonic and cyclic and post-cyclic loading triaxial tests on BCF specimens.

Chapter 2 presents a literature review of the properties of the BCF clay at the Turnagain Heights and Fourth Avenue slides, the cyclic behavior of clays with a focus on sensitive clays, post-cyclic undrained shearing response of sensitive clays and the role of sensitivity in the degradation of the undrained strength.

Chapter 3 summarizes the testing procedures used in this work. It describes the laboratory equipment as well as procedures used to obtain the results presented here in, including sample preparation and details of the triaxial testing under monotonic, cyclic, and post-cyclic conditions.

Chapter 4 presents a geotechnical characterization of the subsurface conditions at Lynn Ary Park with a focus on the BCF clays. The field and laboratory tests presented herein evaluate index properties, stress history, shear wave velocity, undrained strength from monotonic triaxial compression tests and in situ strength and sensitivity from field vane tests. Results obtained by Updike et al. (1988) from the same site are also presented.

Chapter 5 presents the results of cyclic loading and undrained post cyclic shearing of BCF clay. Cyclic response is evaluated in terms of consolidation history and equalization period at the end of cyclic loading. Cyclic strength is evaluated in terms of both total and effective stresses. The undrained post-cyclic shearing response and degradation of strength are discussed in this chapter. The possible degradation of undrained strength is analyzed in terms of the axial strain, pore water pressure, and the energy applied to the specimen before the post-cyclic shearing. Finally, Chapter 5 includes the analysis of effective stress parameters mobilized during the undrained post-cyclic shearing.

Chapter 6 summarizes the thesis and presents the conclusions derived from its results.

CHAPTER 2

2 LITERATURE REVIEW

This chapter presents a review of experimental information regarding fine grained soils under cyclic loading conditions. It includes results developed for BCF soils, as well as results of clays from Canada, Norway, and Sweden. The possible influence of sensitivity on the cyclic behavior is presented. This chapter concludes by reviewing the post-cyclic strength of clays.

2.1 Bootlegger Cove Formation

The BCF is a soil deposit that underlies Anchorage, Alaska. It is composed of silty clays and clayey silts that are interbedded with silt, silty sand, and fine to medium sand. The minimum thickness of the deposit is at least of 30 m (Updike et al., 1988). Figure 2.1 presents the profile section at Turnagain Heights provided by Shannon and Wilson Inc. (1964). Updike et al. (1988) identified seven facies within the deposit in the Anchorage area according to lithological and engineering classification. This research is focused on the facies III (sensitive), and IV, which are composed of fine-grained material. Details of the stratigraphy at the test section at Lynn Ary Park are provided in section 4.2. Studies from the mineralogical composition showed that the clay is composed principally of quartz with some feldspar in a highly weathered form. The BCF clay also included small and variable amounts of kaolinite, illite and chlorite (Shannon and Wilson Inc., 1964).

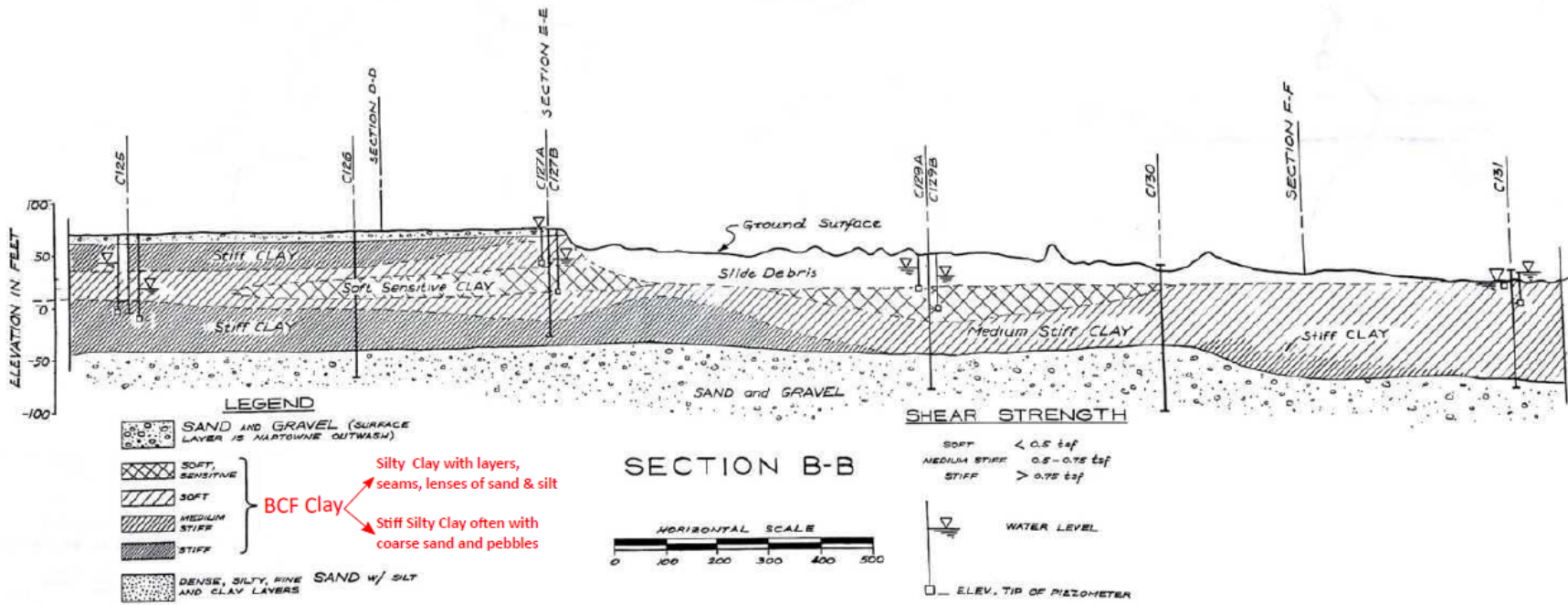


Figure 2.1. Turnagain Heights Profile After Failure (Shannon and Wilson Inc., 1964)

The 1964 earthquake in Anchorage, Alaska triggered several landslides in the area. Shannon and Wilson Inc. (1964) developed a comprehensive geotechnical report discussing the soil characteristics in the Anchorage area. The report focused on understanding the properties of soils in terms of classification, field strength, consolidation, laboratory strength, sensitivity of clay layers, and susceptibility to liquefaction of sand layers. A total of 150 borings were completed in the areas where slides occurred. To obtain undisturbed samples of the sensitive clay, pressure-actuated fixed piston Osterberg and floating piston Lee samplers were used. In stiff non-sensitive clays, undisturbed samples were taken using thin wall steel tubes.

The 1964 field investigations also included field vane tests, installation of piezometers to measure ground water levels, test trenches and bucket-auger borings. Laboratory testing was conducted on specimens from the tubes and consisted of soil classification, laboratory vane, consolidation, triaxial compression, and dynamic triaxial on sand and clay samples. Results from field and laboratory vane showed the presence of sensitive clay in the landslides at Turnagain Heights, Fourth Avenue, and L Street. Laboratory vane results produced higher values of sensitivity than did field vane tests. Figure 2.2 shows boring log C129 and vane results at Turnagain Heights. The undrained strength and sensitivity were obtained by field vane, torvanes and tube vane (performed in every thin walled tube recovered). Results showed significant differences in the sensitivity values based on the type of measurement, with field vane values giving the lowest values of S_t .

Results from triaxial testing on sands showed that the material liquefied when isotropically consolidated and subjected to two directional cyclic loading. Liquefaction occurred after 50 cycles when the cyclic shear stress was 10% of the monotonic strength. For clays, samples were

unconsolidated and cyclic loaded. In these tests, failure occurred after 50 cycles with a cyclic stress of 80 to 100 percent of the static undrained strength obtained from consolidated undrained (CU) and unconsolidated undrained (UU) tests.

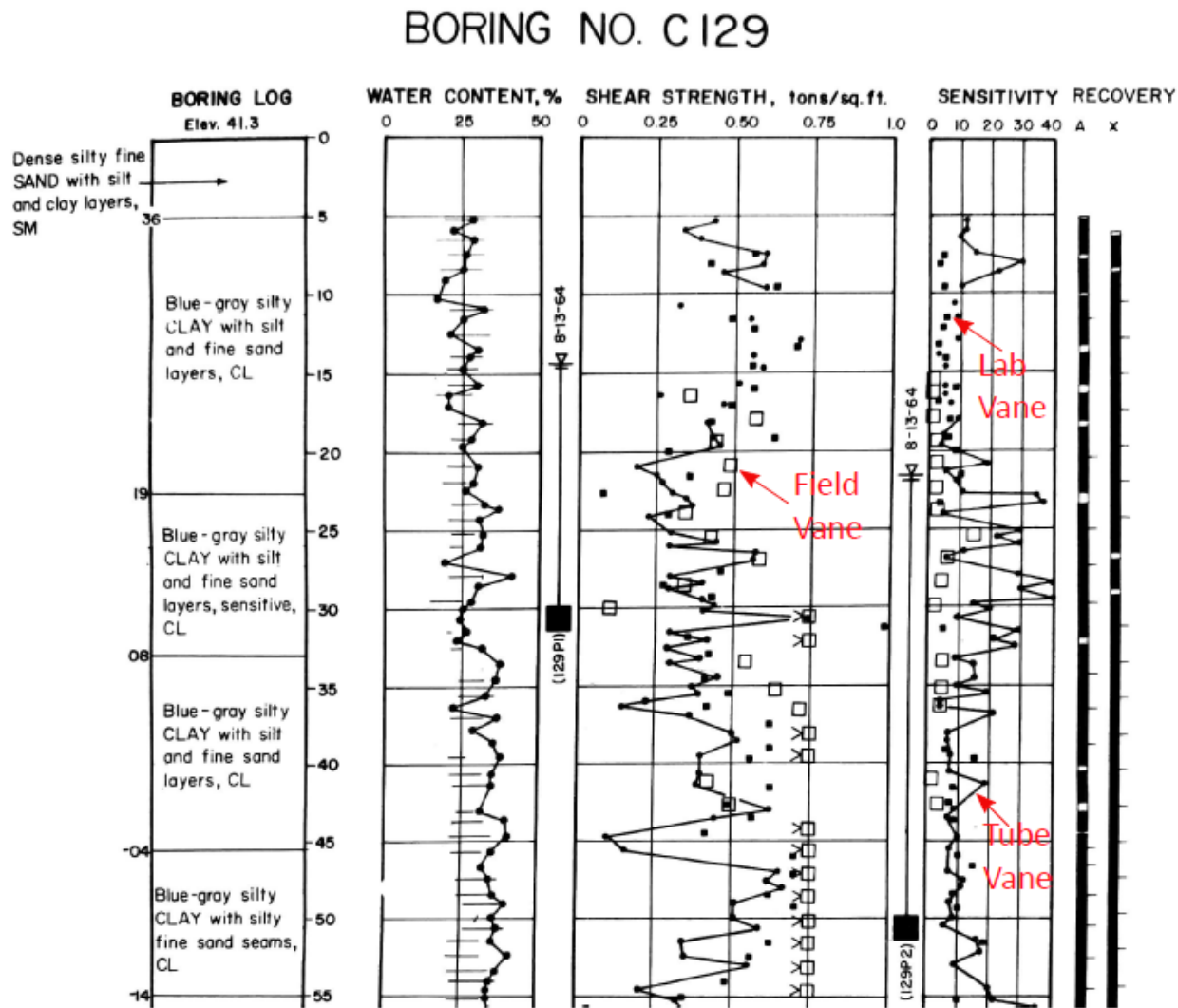


Figure 2.2. Boring Including Strength and Sensitivity Values (Shannon and Wilson Inc., 1964)

The sensitive clay Facies III has been studied since 1964. Mitchell (1973) identified possible sources of sensitivity, including two physical mechanisms, metastable particle arrangement and silt skeleton-bond clay fabric, and six chemical and physicochemical mechanisms, leaching of salt, rupture of cemented bonds, ion exchange, weathering, thixotropic

hardening, and dispersing agents. He concluded that leaching of salt and dispersing agents were the main responsible for the sensitivity values in the BCF clay.

Olsen (1989) carried out a series of chemical tests on the pore fluid of samples obtained at Lynn Ary Park and attempted to establish a correlation between the sensitivity and chemistry of the pore water. In addition, he developed a correlation between sensitivity with the remolded strength. Results showed the lowest remolded strength values, and thus the highest sensitivities occur in the middle of the sensitive layer. These findings were not consistent with the leaching mechanism proposed by Mitchell (1973), because the maximum sensitivities were not found at the interfaces with the sand strata but in the middle of the sensitive clay layer. Dispersing agents were consistent with the low concentration of organic carbon and anions found in the middle of the sensitive layer of the BCF deposit. However both Mitchell (1973) and Olsen (1989) concluded that sensitive clays are present in the Anchorage area. While chemical and environmental analyses are not included herein, determining the sensitivity of the BCF at Lynn Ary Park is an important aspect of the experimental work of this thesis.

2.1.1 Studies Performed on Bootlegger Cove Formation Deposit

The Turnagain Heights area is where the largest landslides occurred in 1964. Figure 2.3 presents the plan view of the failure at Turnagain Heights. The slide impacted an area of about 130 acres. During the initial investigations, Seed and Wilson (1967) conducted a series of monotonic and cyclic triaxial testing on the silt/sand lenses and clay found near the slide. They concluded that the failure initiated with the liquefaction of the sand lenses and was followed by a failure in the sensitive clay. A loss of strength in the clay played a fundamental roll in the development of the slide. Detail results from the triaxial testing are included in Seed and Lee (1966) and Thiers and

Seed (1969). In contrast, Lade et al. (1988) and Updike et al. (1988) concluded that the loss of strength of the clay material during the earthquake was the main mechanism of failure, because the liquefaction and flow of the sand layer was not possible since the sand appeared to be dense enough to preclude liquefaction during the event.

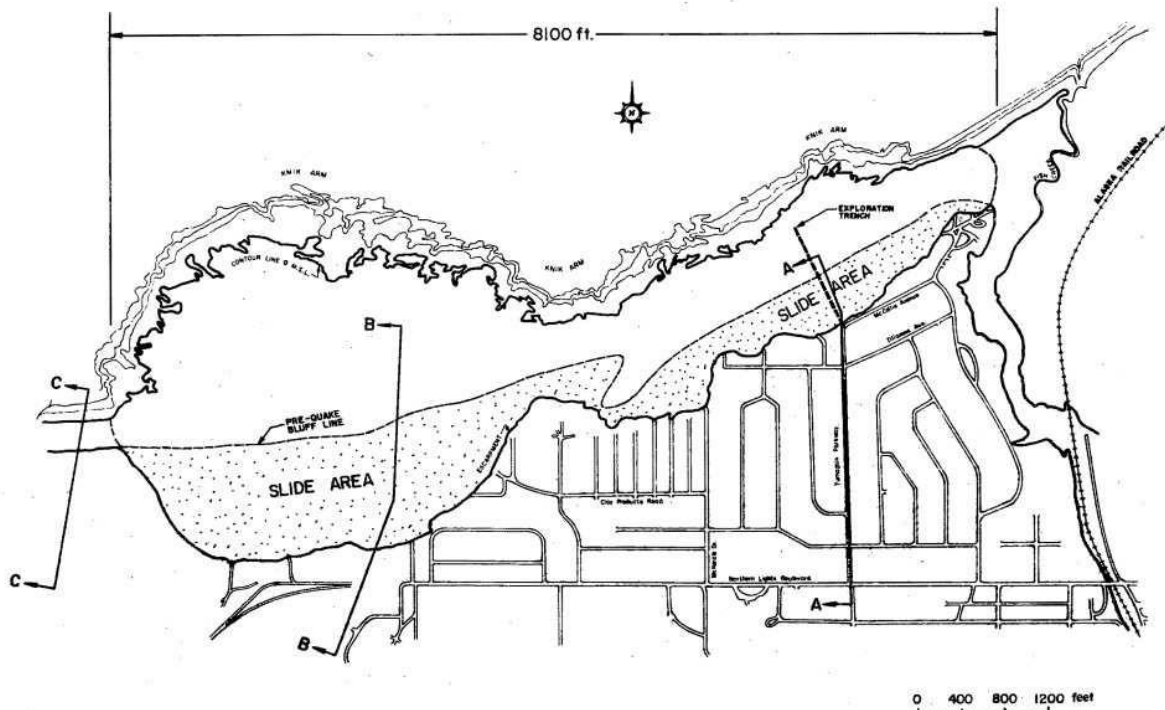


Figure 2.3. Plan View of Turnagain Heights Failure (Seed and Wilson, 1967)

The Fourth Avenue landslide was another major slope failure with a significant presence of sensitive clay. Stark and Contreras (1998) studied the mechanisms of failure of the slope. They first determined the potential for liquefaction of the sand layers. Figure 2.4 shows the results of CPT tests performed on the sandy layer at Fourth Avenue on an empirical chart that relates occurrence of liquefaction to cone tip resistance. Based on the CPT results shown in Figure 2.4, the sand deposits were classified as not liquefiable with a factor of safety of at least 1.5 from the CPT tests.

Stark and Contreras (1998) considered the reduction of undrained strength of the BCF at Fourth Avenue as a function of the significant deformation during the earthquake. After enough lateral movement, the soil could achieve the residual strength after failure was initiated. They used a Newark's sliding block approach to estimate the reduction of undrained strength of the BCF clay.

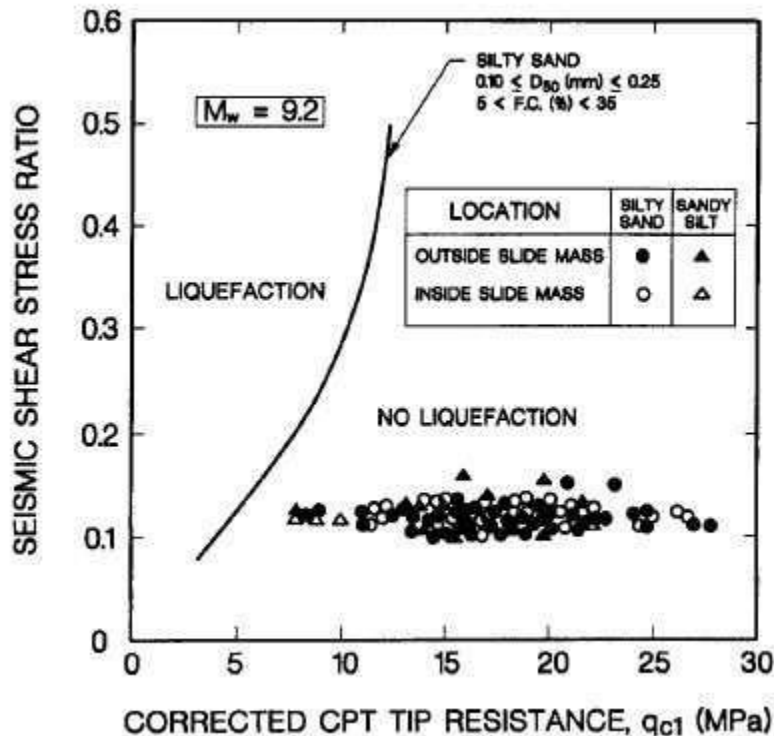


Figure 2.4. Liquefaction Potential of Sandy Layer at Fourth Avenue (Stark and Contreras, 1998)

Figure 2.5 shows the undrained peak and residual strengths of the BCF clay at Fourth Avenue measured by constant volume ring shear tests. Additionally, it includes the mobilized undrained strength for different block permanent displacement. By using Newark's sliding block, the mobilized undrained strength was computed through an iterative process where the input undrained strength was reduced until the sliding block reaches a desired permanent displacement. Results showed a considerable reduction in undrained strength when a sliding block moved between 0.5 m and 2.5 m. The residual strength of the BCF material was achieved after 2.5 m of

displacement; in this same ratio of undisturbed to residual strength was equal to 4, i.e. the sensitivity after the block displacement was equal to 4. The remaining undrained strength was 80% of its initial value after 0.15 m displacement. The authors proposed the reduction of 20% in the undrained strength for the design of new and the evaluation of existing slopes under seismic conditions.

Zapata-Medina (2012) conducted experimental research at Northwestern University for BCF clay. He evaluated the influence of construction-induced stresses in the dynamic properties of BCF material from samples obtained at the Port of Anchorage (POA) project. He carried out a 3D FE simulation to obtain the change of stresses generated by the construction of a new wharf at the port. The laboratory testing aimed to replicate the induced stress path based on the simulation of wharf construction prior to cyclic loading. Specimens tested by Zapata-Medina (2012) belonged to Facies IV. Prior to applying the construction induced stress path, specimens were consolidated by utilizing SHANSEP and recompression techniques. Once the construction stress path was replicated, the samples were subjected to cyclic loading in a triaxial device by applying a loading equivalent to the Contingency Level Earthquake (CLE) for the design, 40 cycles of CSR of 0.2. Post- cyclic shearing was carried out for all cyclically loaded specimens. Results showed no significant degradation of undrained strength occurred as a result of the cyclic loading, based on a comparison of results of undrained monotonic loading conditions. The construction induced-stresses reduced the damping ratio in about 40 to 50% during cyclic loading compared to free-field conditions.

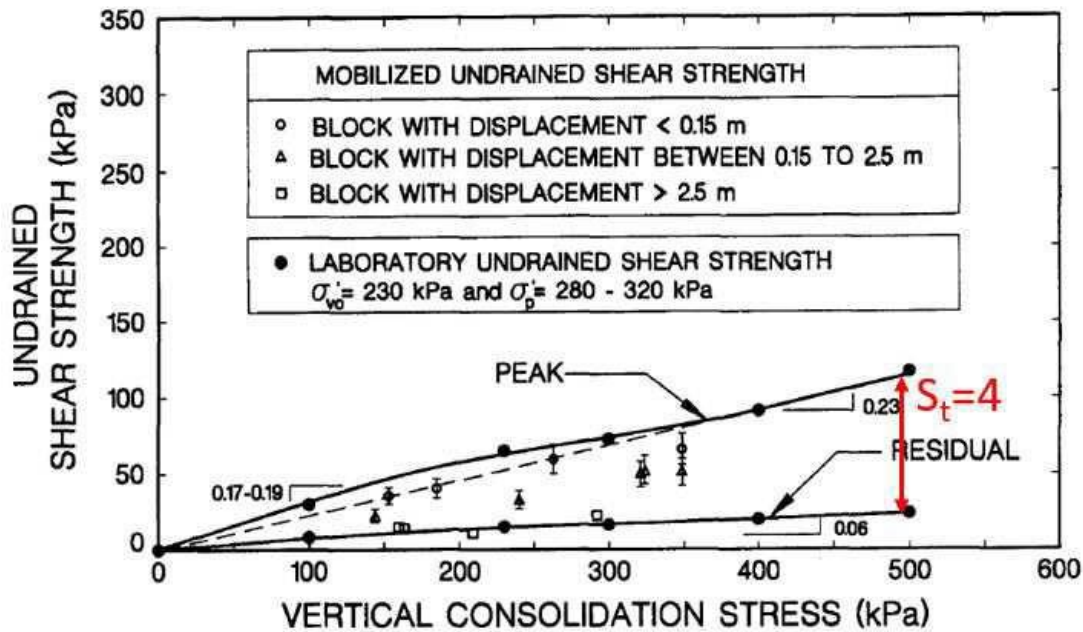


Figure 2.5. Undrained and Residual Strength of BCF Clay at Fourth Avenue (Stark and Contreras, 1998)

2.2 Cyclic Behavior of Clays

Earthquakes and ocean wave loading may have a strong influence in the performance and strength of clayey materials. For these reasons, researchers have studied the influence of cyclic loading on different parameters (e.g. strength, stiffness, pore pressure and strain generation) that might compromise the stability or serviceability of geotechnical structures. Fine grained soils will exhibit clay-like behavior if the plasticity index (PI) is greater than 7 (Boulangier and Idriss, 2006). This means that the material potentially experiences strength and stiffness reduction instead of liquefaction. According to Shannon and Wilson Inc. (1964), the BCF clay has a $PI \geq 7$. This research is focused on BCF clays, a fine-grained material that is expected to exhibit clay-like behavior.

2.2.1 Undrained Cyclic Strength of Clays

Undrained shear strength is a crucial parameter that can be affected by cyclic loading.

Ansal and Erken (1989) conducted cyclic DSS on kaolinite samples to investigate the effects of frequency, degradation of structure, number of cycles, and shear stress amplitude on the undrained cyclic strength of normally consolidated (NC) kaolinite samples. Tests on clay were carried out with frequencies of 0.1, 0.5, and 1.0 Hz. Results showed that cyclic shear stresses up to 65% of the monotonic value can produce excessive shear strains and pore pressures to reach failure depending of the number of cycles. The authors established a yield strength criterion as the intersection of the two tangents for each cycle as shown in Figure 2.6. A criterion for failure was defined based on the yield stress. As noted in the figure, a log-linear relation was established between the yield cyclic stress and the number of cycles.

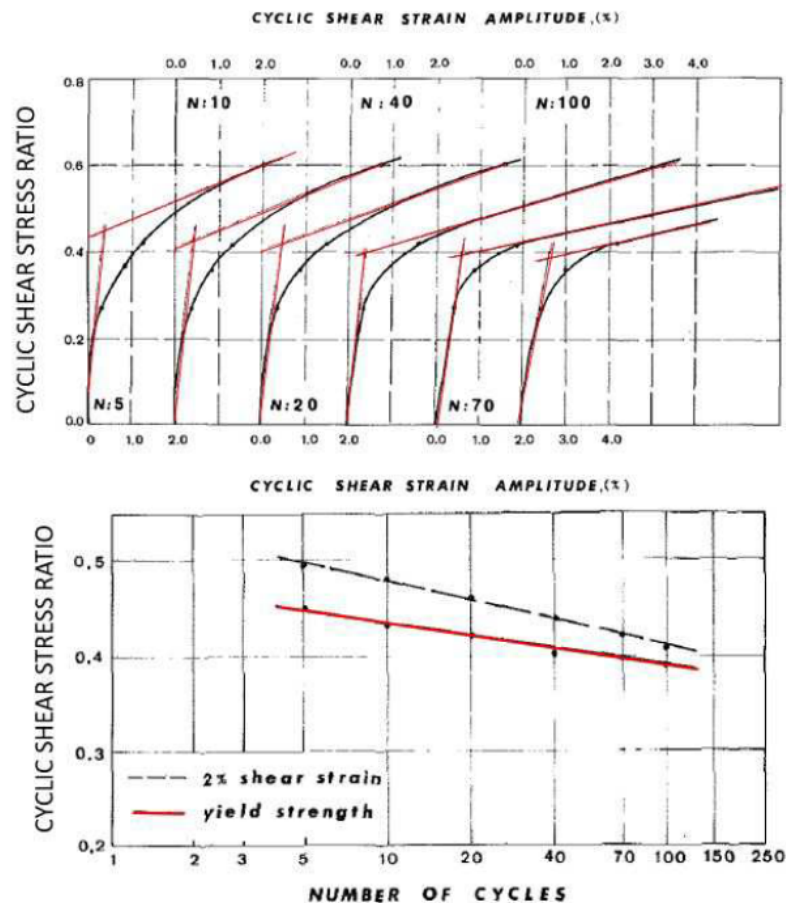


Figure 2.6. Estimation of Cyclic Shear Strength (Ansal and Erken, 1989)

Azzouz et al. (1989) conducted a series of undrained cyclic DSS on reconstituted samples from Boston Blue Clay (BBC). Samples were normally consolidated and lightly overconsolidated before applying the cyclic loading. Cyclic loading tests were conducted under a frequency of 0.1 Hz. Azzouz et al. (1989) introduced the term apparent overconsolidation (AOC). The AOC is different than overconsolidation because in the latter a change in water content is required. The AOC is developed as a reduction of effective stresses due to the increment of pore pressure during cyclic loading. Results showed that the normally consolidated specimens performed as an equivalent overconsolidated material in undrained post-cyclic shearing because of the cyclic loading. Additionally, the authors observed that overconsolidated clay failed at a larger number of cycles compared to the normally consolidated material at the same cyclic stress ratio (CSR).

Yasuhara et al. (1992) studied the effects of cyclic loading on the compressibility and undrained shear strength of reconstituted Ariake clay. Cyclic loading was carried out for one- and two-directional loading using triaxial tests. Samples were isotropically normally consolidated, and then initial shear stresses were applied prior to the one-directional cyclic loading. The failure criterion was assumed as 5% strain accumulated for one-way and 5% strain developed during one cycle for two-way cyclic loading. As found by Lee and Focht Jr (1976) and Perlea (2000), Yasuhara et al. (1992) concluded that the two-directional cyclic loading was more detrimental to the cyclic strength of the material than the one-directional cyclic loading. Studies from Lee and Focht Jr. (1976) and Perlea (2000) will be analyzed in Section 2.2.2.

These works do not present the sensitivity of the clays or were based on reconstituted samples. One of the purposes of this research is to evaluate the influence of sensitivity in the degradation of natural BCF clay. A review of sensitive clay during and after the cyclic loading is

presented in the following sections.

2.2.2 Sensitive Clay Behavior During Cyclic Loading

Several authors have studied the performance of sensitive clays in terms of response during cyclic loading and during post-cyclic undrained shearing for clays that did not fail during the shaking. Lee and Focht Jr (1976) summarized the effects of cyclic loading on the undrained cyclic strength of BCF and San Francisco Bay Mud clays, based on results of triaxial testing found in published and private data. The cyclic strength data of natural specimens was taken from Thiers and Seed (1969) and focused on BCF and San Francisco Bay Mud clays. Two types of BCF specimens were used in this work, natural specimens with sensitivity of 25 and reconstituted specimens with sensitivity of 1.6. San Francisco Bay Mud clay had a sensitivity of 8. Results of their findings showed that reversal of stresses (i.e. two-directional cyclic loading) were more detrimental to strength than one directional cyclic loading. The amount of strength degradation depended on the peak strain and tangent modulus in static loading. Clays with small initial tangent modulus and high peak strain in pre-cyclic loading degraded more during cyclic loading than clays with a high tangent modulus. While not explicitly stated, this finding is consistent with the idea that natural clays with more sample disturbance degrade more than those with less sample disturbance.

Figure 2.7 presented the results obtained by Thiers and Seed (1969) and analyzed in Lee and Focht Jr (1976). During the cyclic loading, San Francisco Bay Mud with a sensitivity of 8 had a higher CSR to reach failure during cyclic loading than the reconstituted BCF clay (sensitivity of 1.6). According to Lee and Focht Jr (1976), the soil stiffness in static loading, and not the sensitivity, controlled the cyclic strength of the clay.

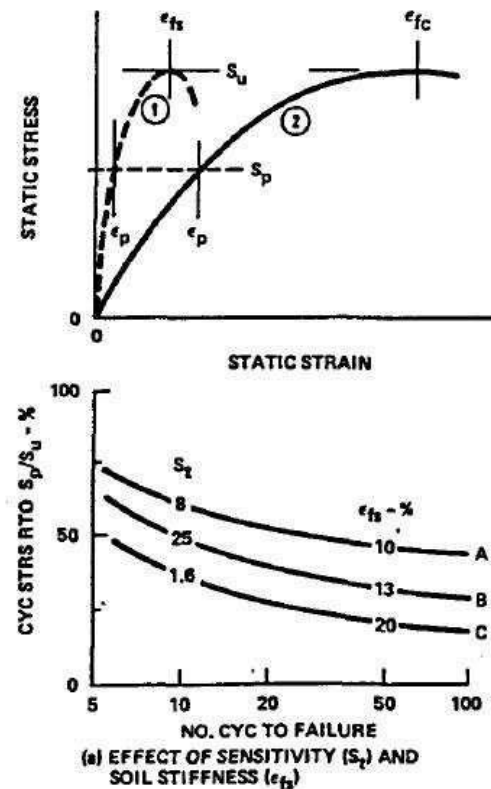


Figure 2.7. Effect of Soil Stiffness in Cyclic Strength (Lee and Focht Jr, 1976)

Lee (1979) tested Champlain marine clay from two different locations from eastern Canada under cyclic triaxial conditions. Samples for each location were named as soil A and B. Soil A exhibited an average of liquidity index of 1.1 and a sensitivity of 350, and soil B exhibited a liquidity index of 1.3 and sensitivity of 35. Sensitivity was obtained from field vane test results. Specimens were consolidated to replicate the *in situ* conditions with an OCR between 2.5 and 5 for both soils. For soil B, some samples were normally consolidated to an effective vertical stress about 2 times the preconsolidation pressure. Specimens were either isotropically or anisotropically consolidated. Undisturbed shear strength was obtained by UU and CU tests. Results of monotonic shearing showed no strain softening after reaching the peak for both soils. For cyclic tests, soils A and B exhibited brittle behavior with the development of one or more shear planes (see Figure 2.8). Once the plane was formed, large deformations were generated leading to collapse of the

sample. At failure, the soil within the shear zones was completely remolded and reduced to liquid, while the material remained essentially intact outside the shear zones. This mechanism of failure was observed in flowslides involving sensitive clay (Lee, 1979). The author presented cyclic strength as a function of the number of cycles. The failure was arbitrarily taken as 3% axial strain accumulated at the end of cyclic loading. For specimens that did not collapse during cyclic loading, the post-cyclic strength reduced to a value 20% lower than the undisturbed strength. Unfortunately, results of post-cyclic strength were not presented and further details were not provided.

Andersen et al. (1980) conducted a total of 129 triaxial and 103 DSS tests on Drammen clay under static and cyclic conditions. While Andersen et al. (1980) did not report the sensitivity of the samples analyzed, Meigh (2013) determined that the sensitivity of Drammen clay varied between 50 and 160 based on results of CPT tests. For both types of tests, undisturbed material was consolidated beyond the *in situ* stress and the unloaded to obtain different OCR. Figure 2.9 presents the material response during the consolidation stage. This procedure altered the original clay structure (Mitchell and Soga, 2005; Vyalov, 2013) and thus presumably the sensitivity of the material.



Figure 2.8. Typical Specimen after Failure during Cyclic Loading (Lee, 1979)

Cyclic loading was performed for one-way and two-way stress conditions. Failure was defined for cyclic triaxial and direct simple shear when samples reached a maximum of 3% shear strain. Figure 2.10 presents the experimental results of cyclic loading on Drammen clay and shows that NC samples failed at higher number of cycles compared to OC at the same cyclic shear stress ratio, defined in their work as the applied shear stress, τ_c , divided by the undrained monotonic strength, S_u . As shown in Figure 2.9, the vertical consolidation effective stress of the NC material was higher than the OC material, and thus the undrained strength is also higher for the NC than OC samples. This difference in monotonic strength can explain the results since the cyclic stresses represented a higher percentage of the undrained strength for the OC samples than the NC ones. Results of post-cyclic response are shown in Section 2.3.1.

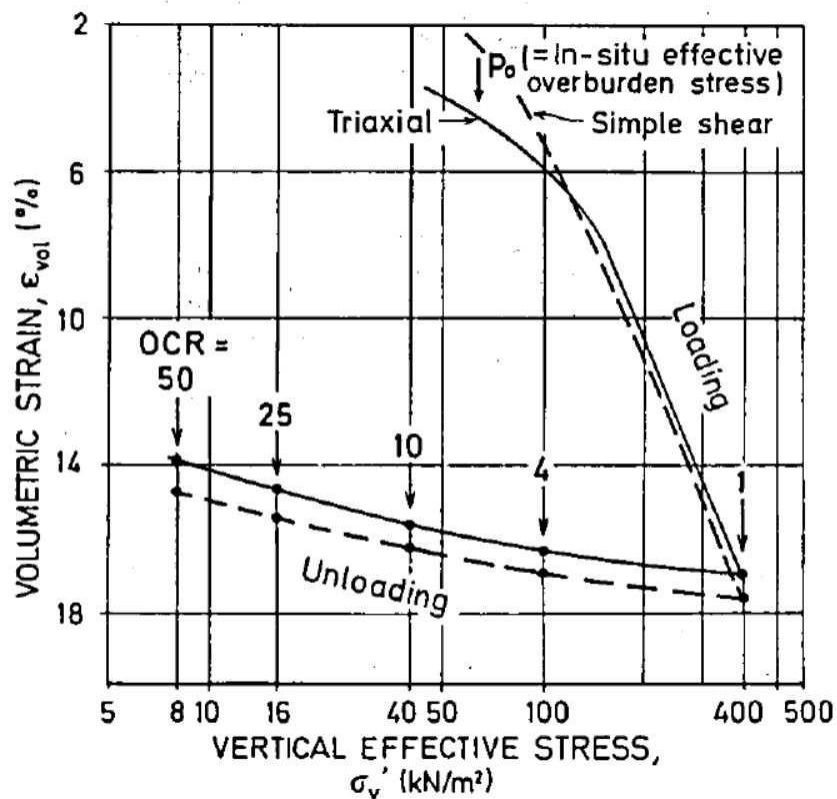


Figure 2.9. Consolidation Response of Drammen Clay (Andersen et al., 1980)

Lefebvre et al. (1989) carried out an experimental investigation to determine the stability threshold of cyclic loading and the post-cyclic strength of Grande Baleine clay. The clay had a sensitivity above 300 measured with the Swedish fall cone test. Figure 2.11 shows the stability threshold for structured and NC Grande Baleine clay. The stability threshold was defined as the maximum cyclic stress that can be applied without producing failure independent of the number of cycles. The authors performed static and cyclic undrained triaxial tests on isotropically consolidated specimens. Consolidation conditions were established above and below of the preconsolidation pressure to evaluate the effect of the material structure. Lefebvre et al. (1989) concluded that the stability threshold was between 60-65% of the static strength. When cyclic stresses were below the stability threshold, no significant reduction in post-cyclic strength was found compared to the monotonic strength. The authors proposed that cyclic loading under the stability threshold causes no significant damage to the clay structure.

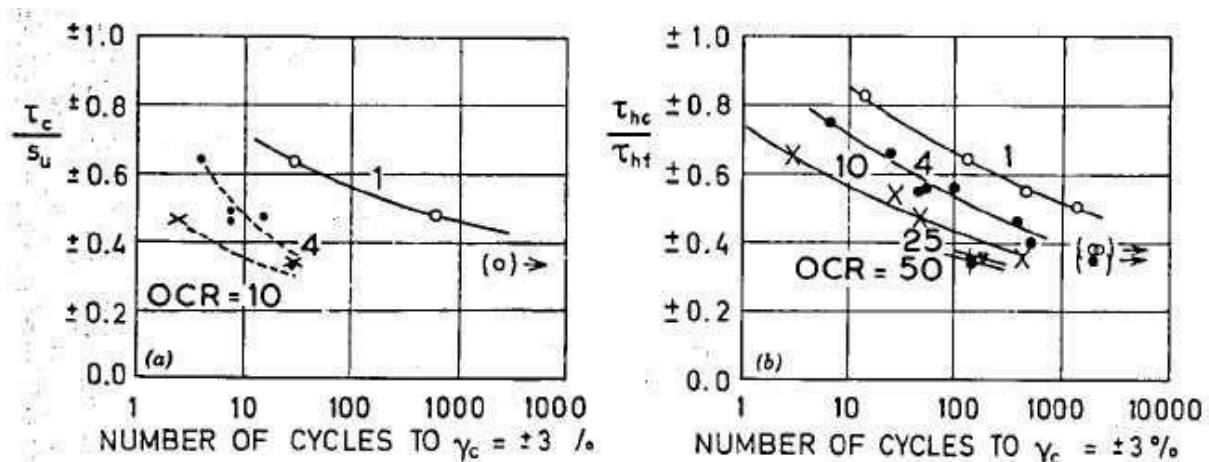


Figure 2.10. Cyclic Strength of Drammen Clay (Andersen et al., 1980)

Lefebvre and Pfendler (1996) conducted a series of cyclic DSS tests on sensitive St. Alban clay consolidated to the *in situ* stress ($OCR=2.2$) to establish the effect of initial shear stresses prior cyclic loading. The failure criterion was established as the number of cycles to reach a rapid increment of shear strain. Lefebvre and Pfendler (1996) defined this failure criteria generally similar to the number of cycles to reach 3 or 5% single amplitude shear strain. Figure 2.12 presents the cyclic strength of St. Alban clay for different initial shear stresses applied after consolidation. Applying an initial shear stress prior to cyclic loading in DSS testing is sometimes called static bias. Results showed that initial shear stresses applied after the end of consolidation reduced the rate of degradation of cyclic strength with the number of cycles compared to specimens with no static bias. However, the cyclic resistance was reduced when the static bias stresses were increased (i.e. lower number of cycles to reach the failure strain).

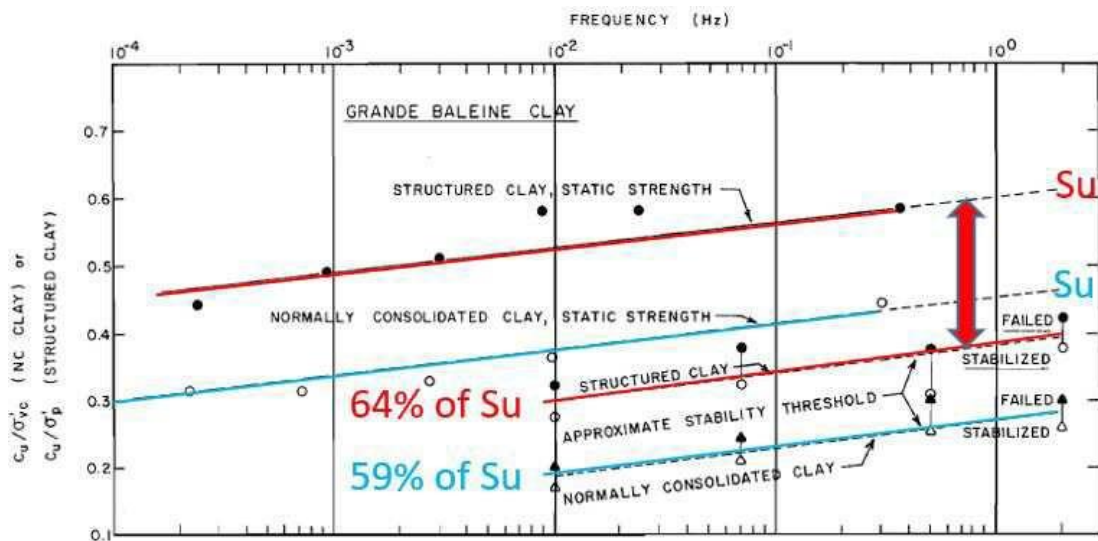


Figure 2.11. Stability Threshold Proposed by Lefebvre et al. (1989)

Wichtmann et al. (2013) tested Norwegian sensitive clay under monotonic and cyclic loading in both triaxial and DSS devices. The authors studied the response of the material under sinusoidal loading at a frequency of 0.1 Hz, 0.01 Hz. Failure was defined when the shear strain

reached 15%. They presented envelopes to quantify the cyclic strength, shear strain accumulation, strain amplitude, and excess pore pressure accumulation as a function of the number of cycles and shear stress amplitude, defined in this work as the applied shear stress, τ_{cy} , divided by the undrained monotonic strength of each device (DSS or triaxial), S_u . These diagrams were proposed for preliminary design of foundation supported on top of clay under cyclic conditions. Wichtmann et al. (2013) also showed the effect of frequency on the cyclic strength. Failure of specimens tested at a frequency of 0.1 Hz required five times more cycles than those tested at 0.01 Hz. When comparing the cyclic strength from both devices, Wichtmann et al. (2013) found that specimens failed at a higher number of cycles in the DSS than the triaxial for the same shear stress amplitude.

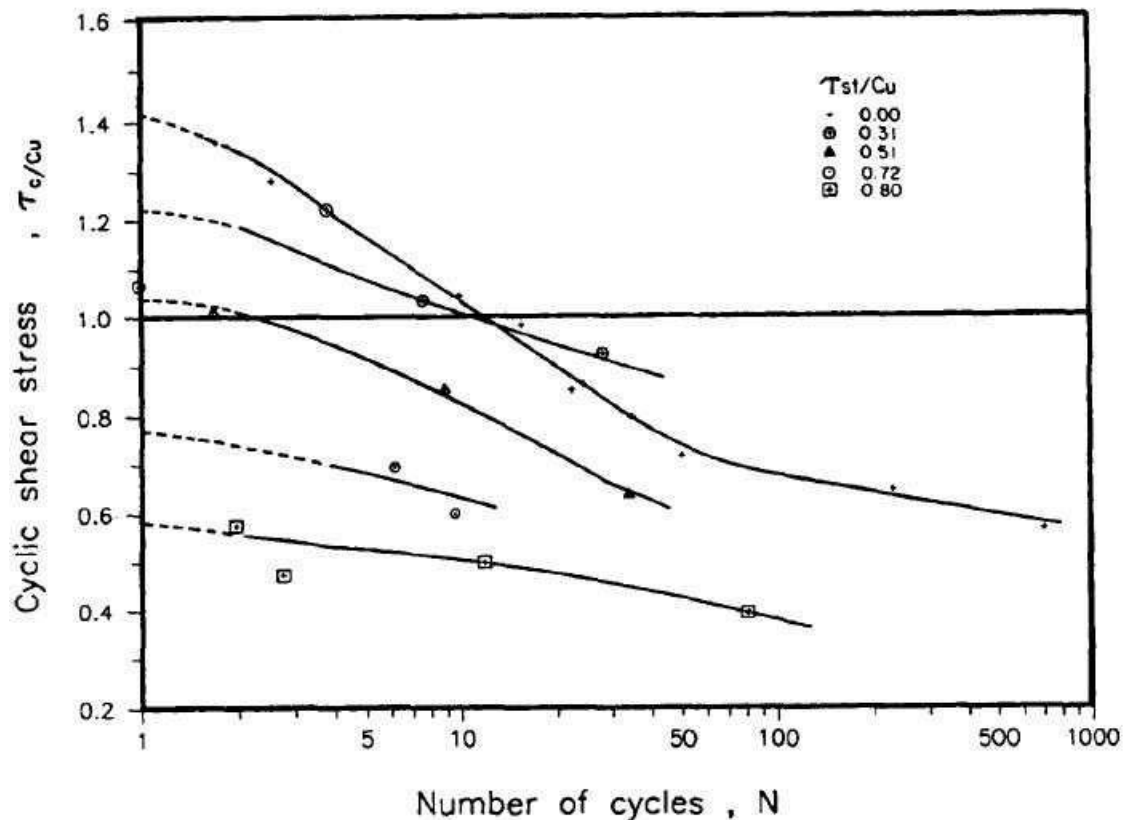


Figure 2.12. Cyclic Strength for Specimen with Static Bias (Lefebvre and Pfendler, 1996)

Hanna and Javed (2008) presented results of an experimental investigation to determine

the cyclic degradation of Champlain clay and its influence on seismic foundation design supported on clays. Samples had sensitivities of 6 to 9 and were tested under stress-controlled cyclic triaxial loading for drained and undrained conditions. Failure criteria were not specified by the authors. From the experimental results, the authors established a safe zone where the sample did not reach the failure in undrained cyclic loading. The zone is larger for drained conditions since more cycles are required to reach failure. Figure 2.13 shows the schematic definition of safe zones proposed for drained and undrained conditions. The authors described a design procedure that included the tests that would be required to design a foundation on top of sensitive clay and subjected to cyclic loading. However, the authors did not clearly define failure, so it is not possible to establish the reduction of strength as a function of the cyclic-induced strain.

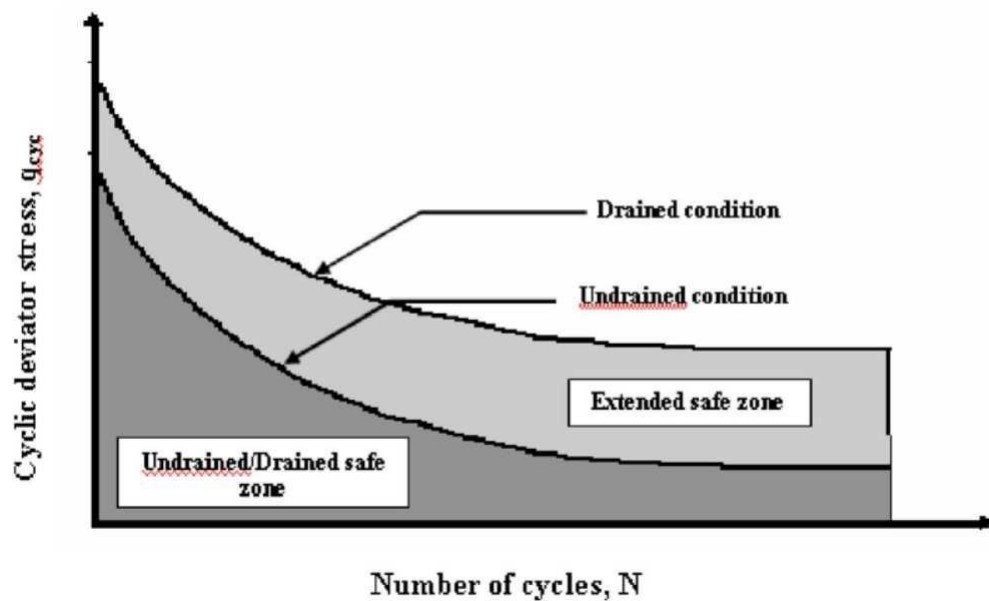


Figure 2.13. Schematic Safe Zones for Foundations on Sensitive Clays (Hanna and Javed, 2008)

A similar study was presented by Hanna and Javed (2014) with clay from Quebec with sensitivities between 5 and 17, higher than their previous work. This time the authors included the cyclic behavior of remolded specimens and the effect of OCR. The OCR for samples tested varied

from 1 to 3. They showed that the cyclic softening of clays was influenced by the frequency of the loading, OCR, confinement pressure, and sensitivity. Figure 2.14 presents the influence of sensitivity on cyclic softening as a function of the number of cycles for failure and includes the failed and the stable soil for a given number of cycles. The cyclic stress applied, q_{cyc} , was normalized with the monotonic strength, q_s . The authors provided different cyclic strength envelopes for 4 ranges of sensitivities. There was not a clear trend of reduction in strength when the sensitivity increased. The cyclic strength for sensitivities between 10 and 16 was higher than cyclic strength for sensitivities higher than 16. As before, they did not define failure, but did provide the final axial strains for the failed samples during cyclic loading. Presumably, the failure occurred when the sample collapsed. As in their previous work, the authors presented a guideline for design of foundations on sensitive clays. The definition of a safe zone was identical to that one presented in Figure 2.13. Although Hanna and Javed (2014) showed that cyclic resistance increased when the OCR increased, the OCR was not included in the definition of the safe zone. The safe zone proposed by the authors may lead one to underestimate the cyclic resistance for clays with OCR greater than one.

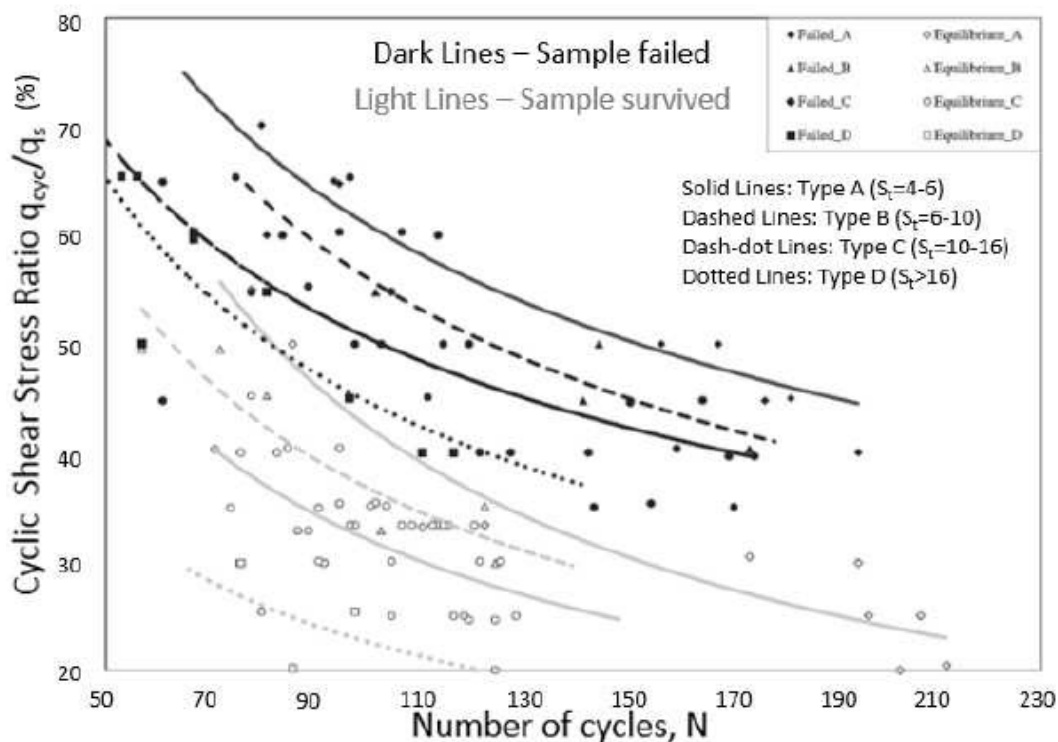


Figure 2.14. Cyclic Softening for Different Sensitivities (Hanna and Javed, 2014)

2.3 Post-Cyclic Response of Sensitive Clay

2.3.1 Degradation of Strength as a Function of Accumulated Axial Strain

Thiers and Seed (1969) conducted one of the first cyclic loading tests on clays. San Francisco Mud and BCF clay were tested under stress-controlled cyclic loading in DSS and triaxial devices. Sensitivities for the samples were 8 and 10 to 20 for San Francisco Mud and BCF clay, respectively. The authors estimated the degradation of both clays during cyclic loading by the reduction of strength and stiffness. Samples were subjected to 200 cycles and post-cyclic undrained shear was carried out for the specimens that did not fail. Figure 2.1.5 presents the results of the post-cyclic strength of the San Francisco Bay Mud and BCF combined. Two aspects to highlight from the Thiers and Seed (1969) results include (1) the static strength is based on unconfined compression tests and (2) they described that the reduction of the strength is related to

the accumulation of strain during cyclic loading normalized by the peaks strain during monotonic tests. Figure 2.15 shows significant reduction in strength when the accumulation of strain during cyclic loading was greater than the 50% of the peak strain for static pre-cyclic shearing.

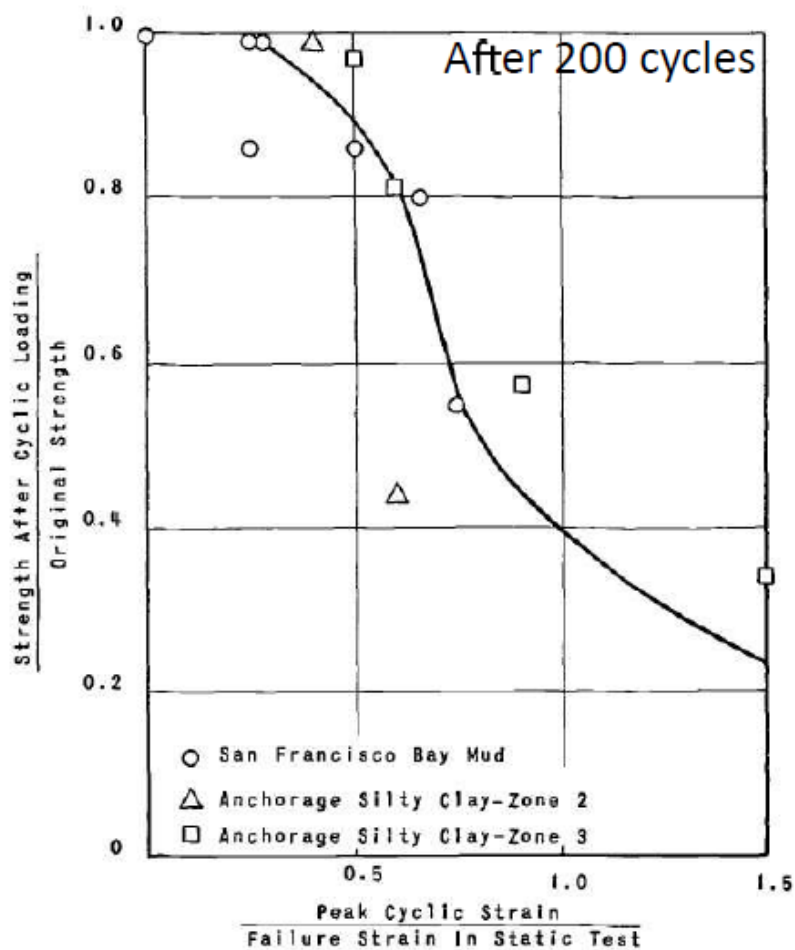


Figure 2.15. Post-Cyclic Strength Degradation versus Normalized Cyclic Strain (Thiers and Seed, 1969)

Koutsoftas (1978) performed a study on cyclic loading and post-cyclic strength on two types of clays. The first was a plastic clay with a sensitivity between 2 and 5, and the second clay, a silty clay, had a sensitivity between 8 and 10. Specimens were tested using a triaxial device with OCRs of one and four. Figure 2.16 shows the degradation of undrained strength for both clays

versus the normalized strain at the end of cyclic loading. Results of post-cyclic shearing for both clays showed a reduction of strength compared to the monotonic strength not greater than 20% even at high strains accumulated during cyclic loading. No difference was observed in post-cyclic strength degradation between both clays. He concluded that the reduction of strength is related to the reduction of the effective stresses as a result of the pore water pressure accumulated during cyclic loading.

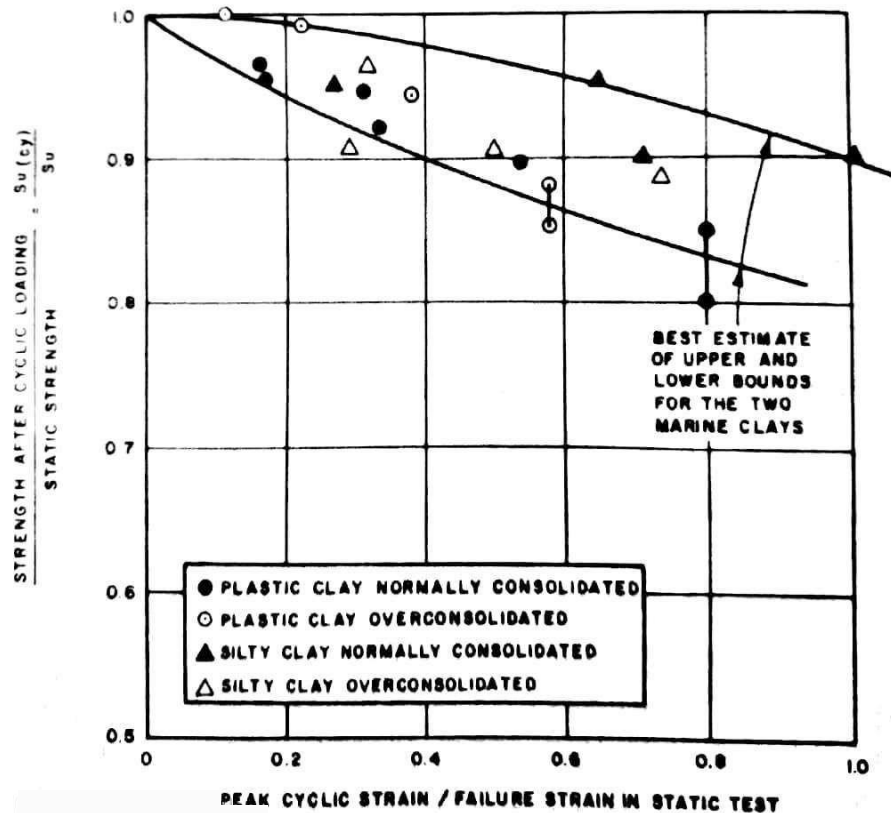


Figure 2.16. Post-Cyclic Strength Degradation versus Normalized Strain after Cyclic Loading

(Koutsoftas, 1978)

Perlea (2000) tested a silty clay in a triaxial device with a sensitivity of 3 measured by the field vane test. Consolidation state and OCR for the test specimens were not presented by the

author. Figure 2.17 presents the reduction of strength as a function of the strain accumulated during cyclic loading. He concluded that when the accumulation of strain during cyclic loading was lower than 10%, a small reduction in strength was observed. On the other hand, higher reductions in strength were observed when the accumulation of strain during cyclic loading was higher than 10%. Additionally, Perlea (2000) showed the importance of two-directional cyclic loading as a main factor in the reduction of strength.

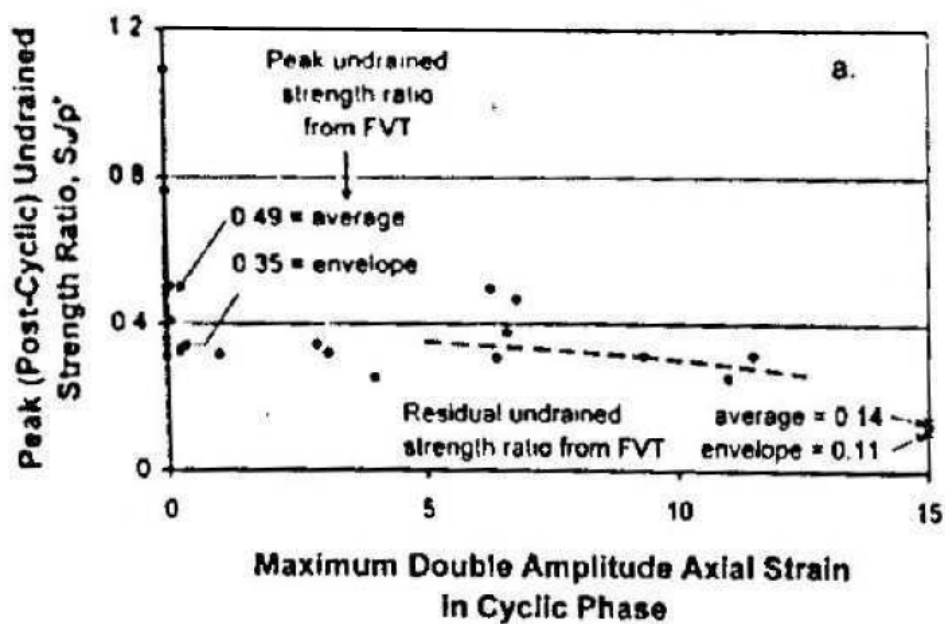


Figure 2.17. Post-Cyclic Strength vs. Strain Accumulated during Cyclic Loading (Perlea, 2000)

Andersen et al. (1980) studied the post-cyclic strength of Drammen clay. The criteria for failure during cyclic loading was established as 3% shear strain. Results from post-cyclic shearing showed greater reductions in undrained strength when the cyclic shear strain and number of cycles increased. The criteria of reduction proposed by the authors established that the post-cyclic undrained strength for NC Drammen clay decreased less than 25% for specimens that developed a shear strain less than 3% when subjected to a maximum of 1,000 cycles. The trend was similar for OCR 4 and 10.

Åhnberg et al. (2013) completed monotonic and strain-controlled cyclic triaxial tests on Swedish clay from different sites. Tests were conducted at different OCR and cyclic stresses. Sensitivity of the clays varied from 10 to 253. Most of the samples were slightly overconsolidated with a typical OCR of 1.3. For cyclic loading, the frequency utilized during the test was primarily 1 Hz; slower rates were applied to evaluate the influence of the frequency. Figure 2.18 presents the stress-strain responses to strain-controlled cyclic loading with cyclic strain larger than the monotonic peak strain. The sample was subjected to a total of 100 cycles and sheared to failure. Results showed a small reduction in strength when the cyclic loading did not impose strains larger than the strain at the peak in monotonic shearing obtained in triaxial compression test. However, when a cyclic strain greater than the pre-cyclic peak strain was imposed during strain controlled cyclic loading, degradation was observed in the material. The undrained strength for this specimen was reduced by 13%.

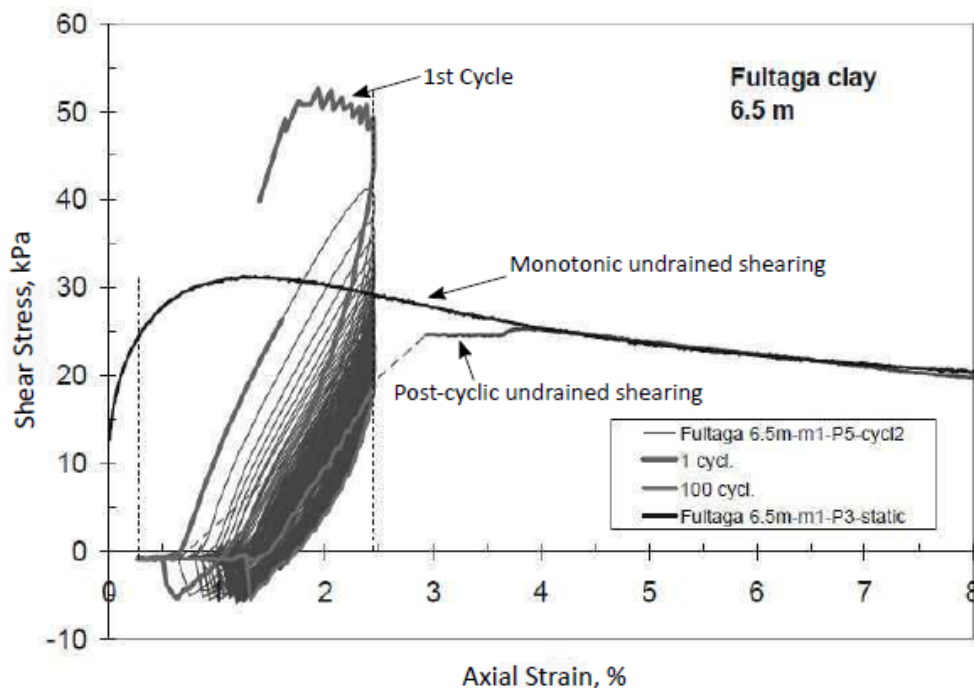


Figure 2.18. Degradation of Clay after a Strain Controlled Cyclic Test after Reaching the

2.3.2 Degradation of Strength as a Function of Accumulated Pore Water Pressure

Matsui et al. (1980) performed a series of cyclic triaxial tests on Senri clay. The authors did not report the sensitivity of the clay. Figure 2.19 presents the degradation of Senri undrained strength versus the equivalent overconsolidation ratio. The overconsolidation ratio was defined as the ratio of the vertical effective stress at the end of cyclic loading to the vertical effective stress at the end of consolidation. The accumulation of axial strain at the end of cyclic loading was less than 10%. Matsui et al. (1980) analyzed the post-cyclic strength with and without dissipation of excess pore water pressure before the post-cyclic shearing. The authors found that when dissipation of excess pore water pressure is allowed the post-cyclic strength increased with respect to the pre-cyclic strength. This is a result of the reduction in void ratio of the specimen. For the case where no dissipation was allowed, the post-cyclic strength decreased up to 45%.

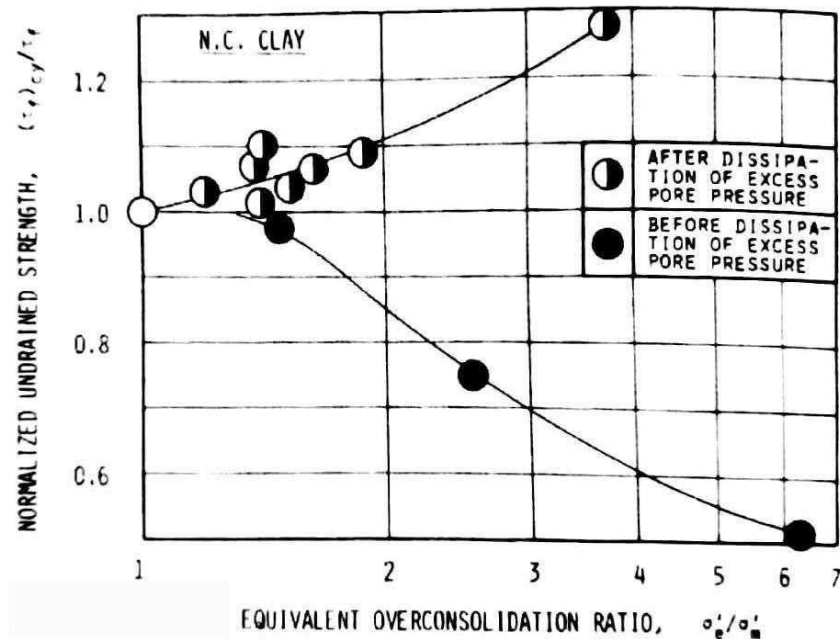


Figure 2.19. Post-Cyclic Strength Degradation versus Equivalent Over Consolidation Ratio

(Matsui et al., 1980)

Yasuhara et al. (1992) and Yasuhara (1994) related the degradation of post-cyclic strength to the accumulation of excess pore pressure at the end of cyclic loading. Yasuhara et al. (1992) performed post-cyclic shearing on samples that did not fail during cyclic loading. Results showed that the two-directional cyclic loading, without drainage after cyclic loading, reduced the undrained strength as a function of the excess pore water pressure during cyclic loading. The author suggested that the reduction of strength without drainage was probably because of the breakdown of the clay structure (Yasuhara et al., 1992). Nonetheless, the reduction of post cyclic strength without drainage after cyclic loading was not greater than 10% of the monotonic strength. On the other hand, the undrained strength increased if drainage was allowed in the sample. The increased post-cyclic shear strength with drainage after cyclic loading was a result of the reduction in void ratio as the cyclically induced pore water pressure dissipated. No significant difference was observed in post-cyclic strength between one-directional and two-directional cyclic loading.

Yasuhara (1994) proposed a closed form solution to quantify the change in post-cyclic strength depending on the OCR, recompression/swelling and compression indexes and the excess pore water pressure accumulated at the end of the cyclic loading as:

$$(2.1) \quad \frac{S_{u,cy}}{S_{u,NC}} = \left(\frac{1}{1 - \Delta u / p'_i} \right) \exp \left(\frac{\Lambda_o}{1 - C_s / C_c} - 1 \right)$$

where $S_{u,cy}$ is the post-cyclic strength, $S_{u,NC}$ is the monotonic undrained strength of normally consolidated specimens, Δu is the accumulated pore water pressure at the end of cyclic loading, p'_i the mean normal effective stress before cyclic loading, Λ_o is a material constant, C_s swelling index, and C_c compression index. No details of pore pressure equalization after cyclic

loading were described by Yasuhara (1994), and presumably none were allowed. The model was applied to clays with different sensitivities. Figure 2.20 shows the results for BCF and Drammen Clay. For BCF clay, the experimental results are based on triaxial tests conducted by Thiers and Seed (1969). The pre-cyclic strength was obtained from unconfined compression tests. Experimental data from Drammen clay was obtained from Andersen et al. (1980). As noted before, Andersen et al. (1980) conducted cyclic triaxial and DSS test with including post-cyclic shearing for specimens that did not collapse. Parameters of the model for Drammen clay were different for the triaxial and DSS tests. The model fit well for the BCF material and triaxial data from Drammen clay but overestimated the reduction in strength of the Drammen clay based on DSS.

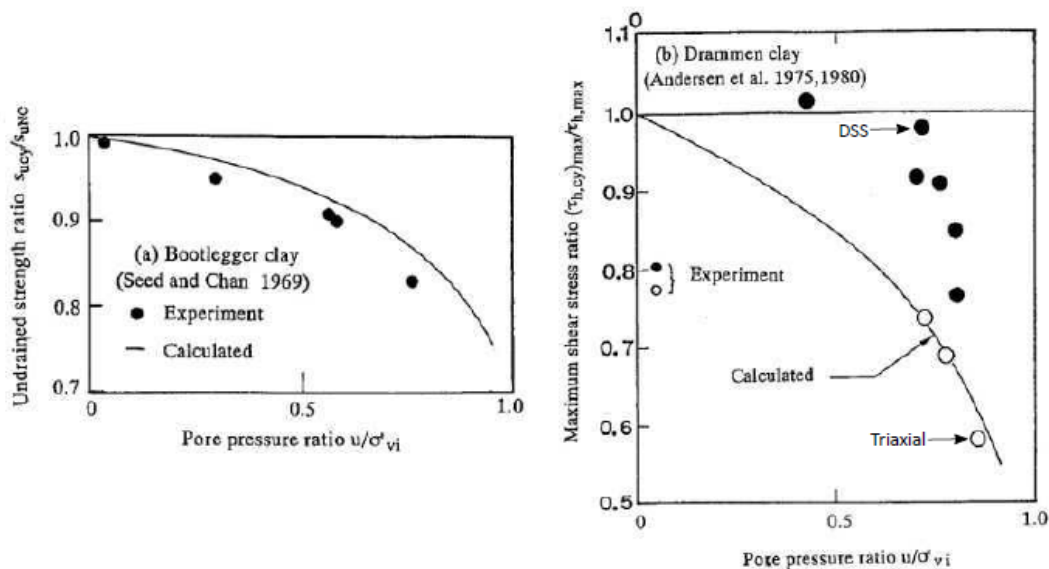


Figure 2.20. Normalized Post-Cyclic Strength vs Excess Pore Pressure Ratio (Yasuhara, 1994)

Based on the literature presented in this work, author showed that the cyclic strength is influence by different factors such as peak strain and OCR. However, there is not a clear roll of sensitivity in the cyclic strength. None of the authors reviewed the effects of preparing the specimens before applying the cyclic loading. There is a need to include the effects of

reconsolidation on the cyclic strength and the effects of the increment of axial strain before cyclic loading on the clay structure.

For post-cyclic shearing two main approaches were described based on axial strain and pore water pressure accumulated during cyclic loading. Both approaches focused on total stress analysis to estimate the reduction of strength by either accumulation of strain or pore water pressure. However, none of the studies presented includes the accumulation of strain during the consolidation of the specimens, an accurate measurement of the pore water pressure at the end of cyclic loading or the effective parameters that control the reduction of strength.

2.4 Summary

The literature review presented herein summarizes the research carried out for clays during and after cyclic loading. During cyclic loading, the literature is consistent in that the degradation of strength and stiffness is a function of the number of cycles and CSR. Some authors found a correlation between the OCR and cyclic resistance (Andersen et al., 1980; Ansal and Erken, 1989; Azzouz et al., 1989; Hanna and Javed, 2014). Stark and Contreras (1998), and Kavazanjian et al. (2011) proposed a reduction of strength between 15 and 20% of the static undrained strength for design, without accounting for number of cycles, CSR, and OCR. For the sensitive clays, Kavazanjian et al. (2011) recognized that sensitive clays might experience significant degradation and recommended cyclic tests be conducted to evaluate this possibility. Hanna and Javed (2014) attempted to correlate the cyclic resistance and number of cycles with sensitivity. Their cyclic results were highly affected by the different OCRs in the specimens and no clear correlation with sensitivity could be established. Results of cyclic loading in triaxial tests show a lack of agreement in the degradation of strength during cyclic loading and its correlation with sensitivity.

For post-cyclic shearing, Lee (1979), Lefebvre et al. (1989), Perlea (2000), and Åhnberg et al. (2013) did not find a significant reduction in undrained strength after cyclic loading. However, Thiers and Seed (1969) and Andersen et al. (1980) found an undrained strength reduction close to 50% compared to pre-cyclic monotonic strength. These differences can be attributed to the amount of strain accumulated during cyclic loading for the different testing programs.

Thiers and Seed (1969) and Yasuhara (1994) proposed two approaches to estimate the post-cyclic strength as a function of the accumulation of strain and pore pressure during cyclic loading, respectively. However, both methods do not consider factors such as OCR or sensitivity that can influence the post-cyclic strength.

Matsui et al. (1980) presented results of post-cyclic shearing including dissipation of pore water pressure between the end of cyclic loading and before post-cyclic shearing. This process allows the material to gain strength after cyclic loading, as results showed. Also Matsui et al. (1980) and Yasuhara (1994) presented results of post-cyclic shearing with no pore water pressure dissipation. However, these authors did not provide details whether pore water pressure equalization was allowed. The pore water pressure equalization period is a different process from dissipation since the equalization required undrained conditions at a constant total vertical and lateral stress so that excess pore pressures could equalize within a specimen. This stage helps to provide more accurate measurements of the accumulation of pore water pressure – typically measured at the end of a specimen - within the clay specimen after cyclic loading.

CHAPTER 3

3 EXPERIMENTAL PROGRAM AND PROCEDURES

3.1 Introduction

This chapter describes the experimental procedures for the cyclic and post-cyclic testing of the Bootlegger Cove Formation (BCF) clay. In particular, it presents descriptions of the monotonic and cyclic tests as a function of the stress history. General features of the triaxial device also are presented in this chapter.

3.2 Summary and Experimental Program

Monotonic triaxial compression and cyclic triaxial compression tests were conducted to characterize the BCF clay strength. Specimens were consolidated by either SHANSEP or recompression techniques. If the specimen did not collapse during cyclic loading, post-cyclic undrained shearing was performed to evaluate the degradation of undrained strength as a result of the imposed cyclic conditions.

Table 3.1 and Table 3.2 summarizes the laboratory tests performed as part of this thesis. Index properties were determined on soil extracted from in all thin-walled tubes collected as part of the field study. Thirty-six triaxial tests were performed, 7 monotonic and 29 cyclic or cyclic/post-cyclic test.

3.3 Triaxial Device

The equipment utilized in Northwestern Geotechnical laboratory is the Advanced Dynamic Triaxial Testing System (DYNTTS) manufactured by GDS Instruments Ltd. The general setup is shown in Figure 3.1. This section describes some pertinent features of the DYNTTS (GDS Instruments Ltd, 2013).

The DYNTTS consists of the following subsystems:

- Actuator Unit, Cell Top and Balance Ram
- Hydraulic Cell and Back Pressure and volume controllers
- GDSDCS-light Control System

Table 3.1. Laboratory Experimental Program Borehole NU-1

Specimen	Facies	Index Properties	Monotonic	Cyclic	Post-Cyclic
NU-1 17-19	IV	X		X	X
NU-1 20-22	IV	X	X		
NU-1 22-24	IV	X		X	
NU-1 22-24 (2)	IV	X		X	X
NU-1 22-24 (3)	IV	X		X	X
NU-1 27-29	IV	X	X		
NU-1 27-29 (2)	IV	X		X	X
NU-1 32-34	IV	X			
NU-1 32-34 (3)	IV	X		X	
NU-1 37-39	IV	X			
NU-1 37-39 (2)	IV	X		X	X
NU-1 37-39 (3)	IV	X			
NU-1 40-42	III	X	X		
NU-1 40-42 (2)	III	X		X	X
NU-1 42-44	III	X			
NU-1 42-44 (2)	III	X			
NU-1 42-44 (3)	III	X	X		
NU-1 45-47	III	X			
NU-1 47-49	III	X		X	X
NU-1 47-49 (2)	III	X		X	X
NU-1 47-49 (3)	III	X		X	
NU-1 50-52	III	X			
NU-1 50-52 (2)	VII				
NU-1 55-57	III	X		X	X
NU-1 60-62	III	X		X	X
NU-1 60-62 (2)	III	X		X	X
NU-1 60-62 (3)	III	X		X	X
NU-1 62-64	III	X		X	
NU-1 62-64 (2)	III	X		X	
NU-1 62-64 (3)	III	X		X	X
NU-1 65-67	III	X		X	X
NU-1 65-67 (2)	III	X		X	X
NU-1 65-67 (3)	III	X		X	

Table 3.2. Laboratory Experimental Program Borehole NU-3

Specimen	Facies	Index Properties	Monotonic	Cyclic	Post-Cyclic
NU-3 25-27	IV	X		X	X
NU-3 25-27 (2)	IV	X			
NU-3 30-32	IV	X	X		
NU-3 30-32 (2)	IV	X			
NU-3 40-42	III	X			
NU-3 42-44	III	X	X		
NU-3 42-44 (2)	III	X	X		
NU-3 47-49	III	X		X	X
NU-3 47-49 (2)	III	X		X	X
NU-3 47-49 (3)	III	X		X	X
NU-3 50-52	III	X			
NU-3 50-52 (2)	VII				
NU-3 55-57	III	X		X	X
NU-3 55-57 (2)	III	X		X	X
NU-3 55-57 (3)	III	X		X	X
NU-3 60-62	III	X		X	X

The actuator unit is the main unit that incorporates the axial actuator with the cell base attached to it. The axial actuator allows the pedestal to move vertically according to the requirements for the type of test that is performed. The cell base includes the hydraulic connections for pore water pressure, back pressure, and cell pressure. Furthermore, the cell base holds the bender element and internal LVDT connections, in case they are required in a test.

Figure 3.2 presents the sketch of the dynamic triaxial testing system (DYNTTS). The DYNTTS is equipped with a balanced ram to maintain a constant cell pressure during fast loading and more importantly for this work, during cyclic loading. When the ram moves up and down in the cell, the change in volume caused by the movement is compensated. This mechanism provides net volume change equal to zero, so that the cell pressure does not need to be adjusted during the test.

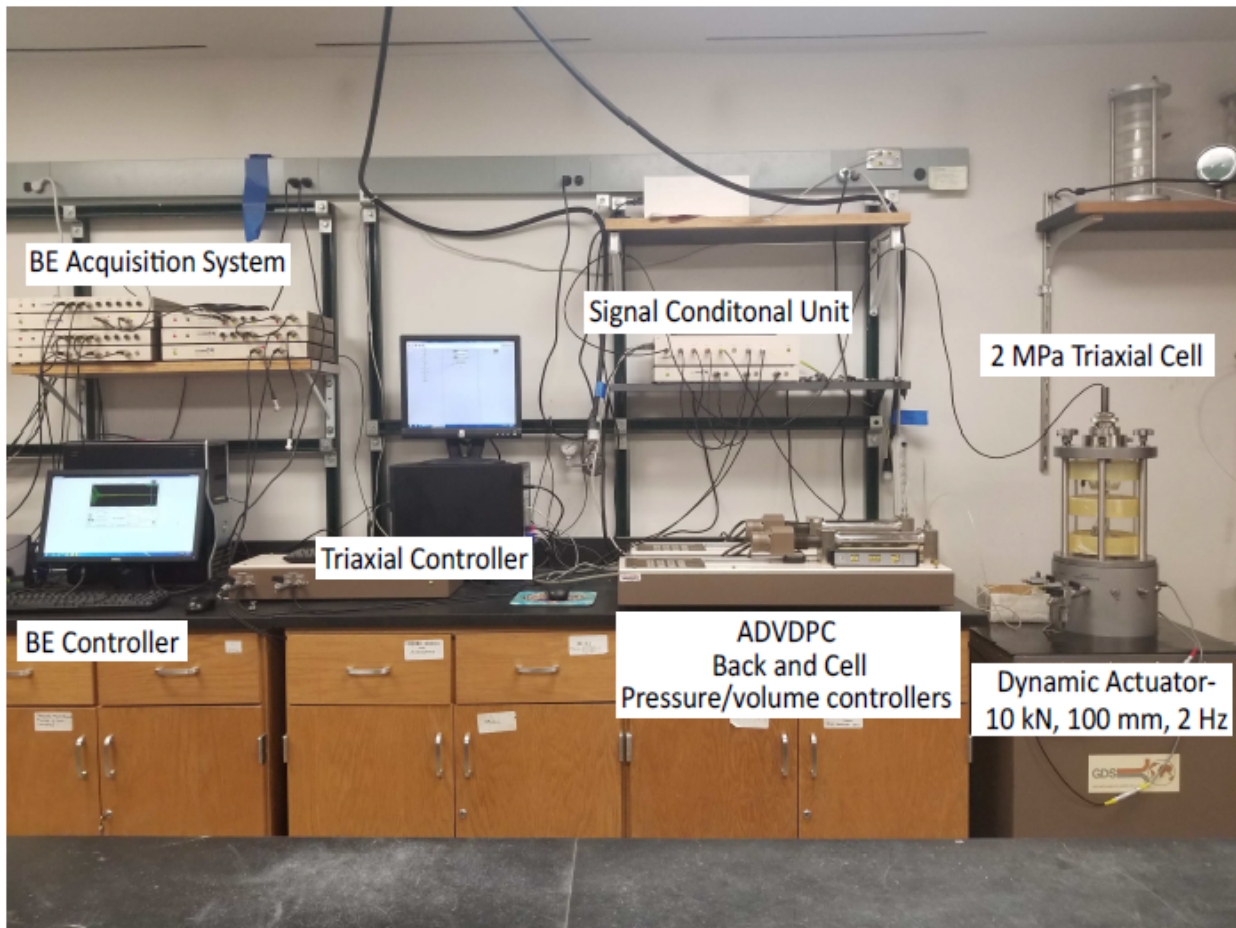


Figure 3.1. Setup of the DYNTTS at Northwestern University

The hydraulic pressure/volume controllers are the advanced 2 MPa/200 cm³ digital controller. De-aired water is pressurized and transported by a piston that moves in the cylinder containing the water. Pressure is measured by a solid state transducer. The controller includes a microprocessor to look for a target pressure or volume. Volume change can be obtained by counting steps of the incremental motor that controls the piston.

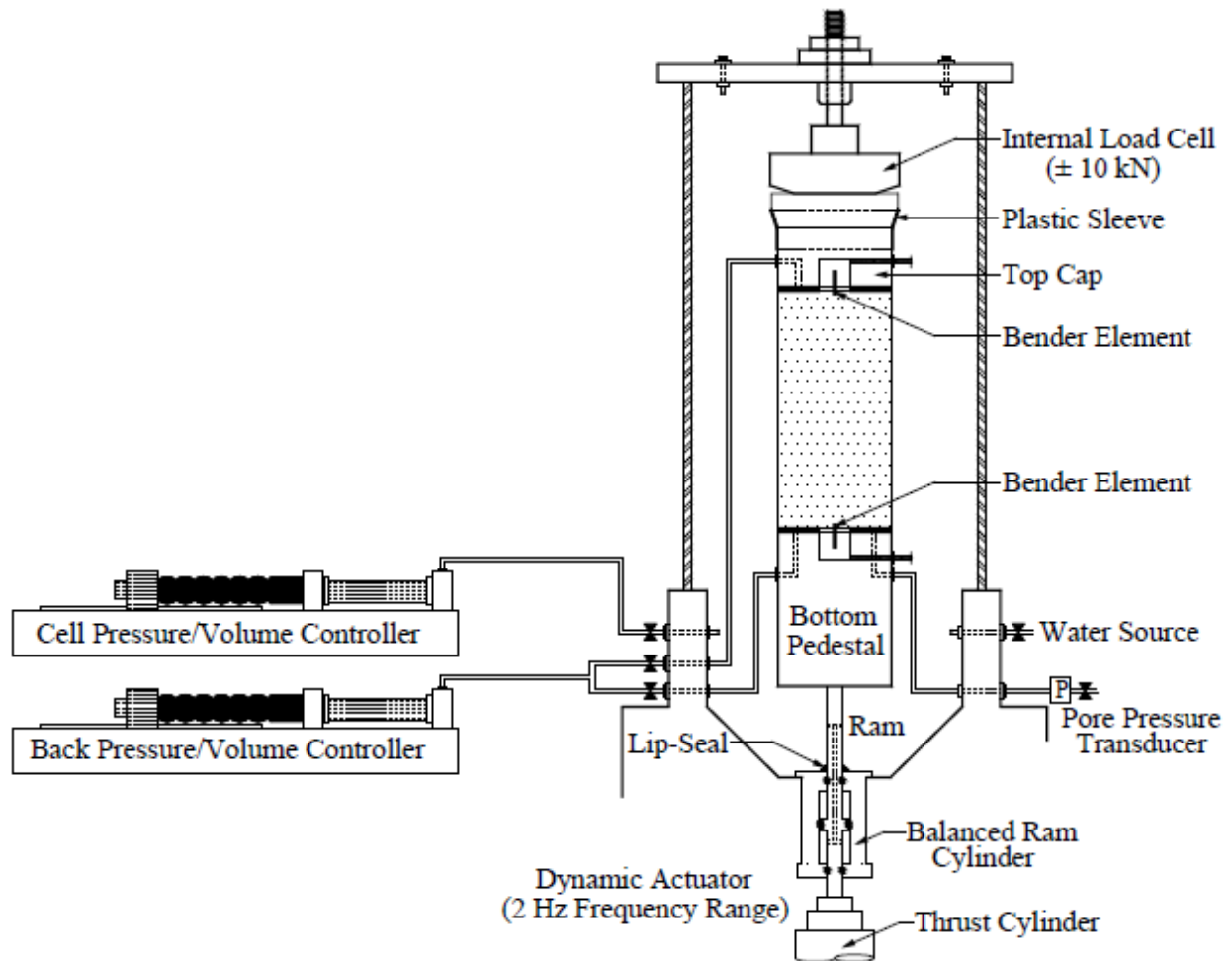


Figure 3.2. Sketch of the DYNTTS Provided by GDS Instruments

The digital control system combines the dynamic control processor and the signal conditioning. The analogue signal conditioning contains an eight channel A/D converter and provides excitation to each transducer. It also provides the correct zero and gain for each transducer input. For this work, the outputs were amplified by ± 10 V. Detail specifications of the DYNTTS are presented in Table 3.3 (GDS Instruments Ltd, 2013):

Table 3.3. Detail Specification of the DYNTTS (GDS Instruments Ltd, 2013)

Actuators	High accuracy electromechanical
Axial force accuracy	<0.1 %
Axial force accuracy	<0.4 <i>N</i> for 10 <i>kN</i> load cell
Axial load	10 <i>kN</i>
Axial displacement range	100 <i>mm</i>
Axial displacement resolution	0.2 μm
Axial displacement accuracy	70 μm in 100 <i>mm</i>
Operating frequency	Up to 2 <i>Hz</i>
Maximum double amplitude when cyclic loading at 1 <i>Hz</i>	14.6 <i>mm</i>
ADVDPCCell/Back pressure range	0 to 2000 <i>kPa</i>
ADVDPCCell/Back pressure resolution	0.2 <i>kPa</i>
ADVDPCCell/Back pressure volumetric capacity	200 cm^3
DVDPC Cell/Back pressure volumetric resolution	1 mm^3
Pore pressure transducer	2 <i>MPa</i> located at the base pedestal
Pore pressure transducer resolution	± 0.2 <i>kPa</i>
Cell-fluid	De-aired water
Sample size used	70 <i>mm</i>

3.3.1 Bender Elements

The bender elements allow the measurement of the shear modulus at small strains by inducing flexural waves into a specimen. The bender elements are made from piezoelectric ceramic bimorphs. Two sheets are confined with a metal shim in between. The insert for the base pedestal is made of stainless steel. The insert for the top cap is made of titanium to reduce its weight by half (GDS Instruments Ltd, 2005).

The vertical bender elements utilized in this research are inserted in the top cap and pedestal of triaxial cell, as shown in Figure 3.3. The flexural-wave is produced by an excitation voltage in the source transducer. The wave travels through the sample and produces a displacement in the receptor transducer. This displacement is transformed into voltage that can be read as an output by

the software Benders provided by GDS Instruments Ltd.

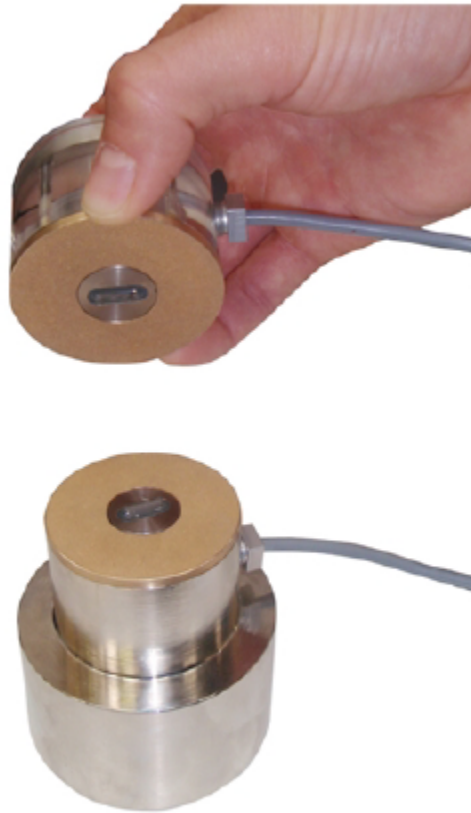


Figure 3.3. Bender Elements at Top-Cap and Pedestal (GDS Instruments Ltd, 2005)

3.3.2 Pore Water Pressure Measurements

The pore pressure can be measured at any time during the test process. The pore pressure transducer is located at the cell base. The capacity of the transducer is 2 MPa with a sensitivity of ± 0.2 kPa.

Figure 3.4 presents the plan view of the cell base. The bottom pedestal provides the connection of the sample with the pore pressure transducer. The tubing from the pore pressure transducer and the bottom pedestal is filled with de-aired water to assure a correct measurement of the pore water pressure of the bottom of the sample.

The pore pressure transducer must have a common zero with the cell and back pressure. One of the limitations of the pore water pressure measurements is the transducer location at the bottom of the sample which may not be representative of the values throughout a specimen during cyclic loading. This condition may occur during fast loading rates such that there is not enough time for the pore pressure to be equalized throughout the sample.

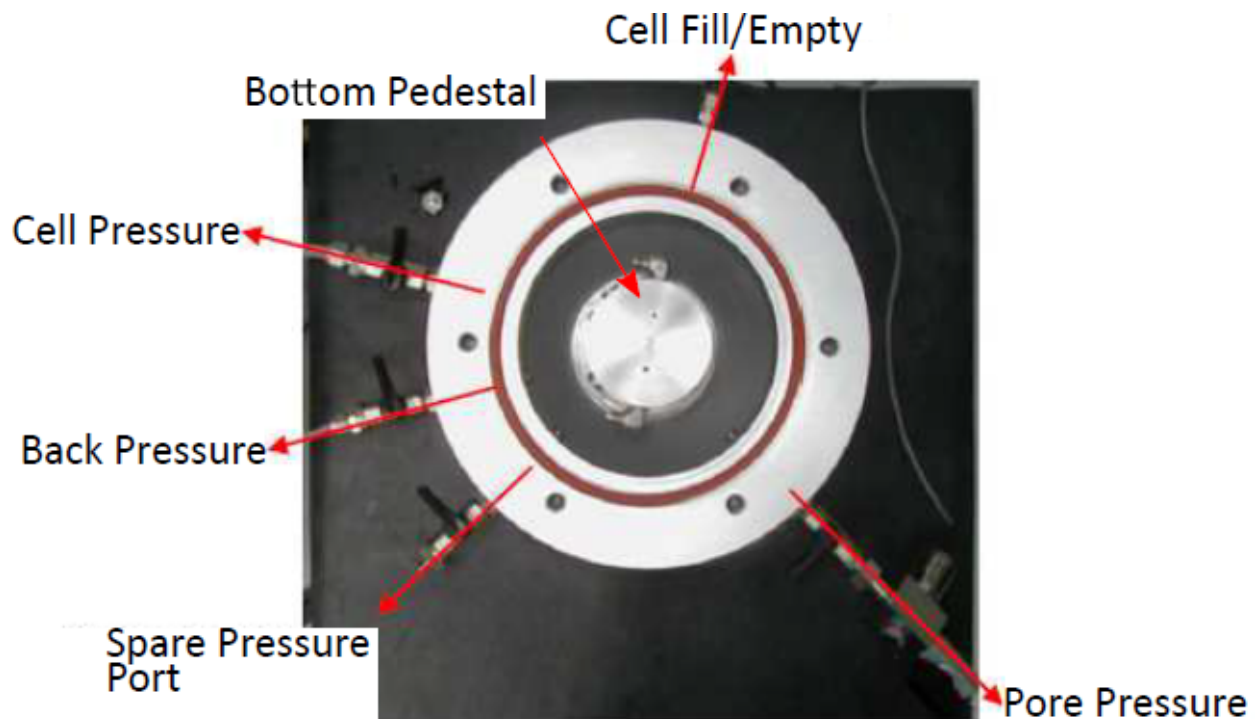


Figure 3.4. Cell Base Plan View

3.4 Testing Protocol

This section describes the procedures utilized to conduct the experimental program including x-ray testing, the extraction of the samples and trimming method, specimen preparation before its placement in the triaxial cell, and the stages followed during each monotonic and cyclic triaxial test.

3.4.1 X-Ray Testing

X-ray testing is a non-destructive testing technique that can help assess the sample quality before extraction. The x-ray testing was not part of the testing protocol for most of this research and only two samples were subjected to x-ray testing to locate potential zones of disturbed material, variability or other type of defects. The x-ray tests were conducted on NU-1 20-22 (from shallow depth) and NU-1 65-67 (from the bottom of Northwestern University exploration). The x-ray tests were performed by using the Nikon XTV 160 high-quality PCB inspection system. The scanner has the capability to identify defects of 500 nm. The test was performed by sections made every 2 inches until the whole length of the Shelby tube was covered. The scans were repeated on the sample rotated 90° about the tube longitudinal axis. The objective was to obtain a better visualization of any defect of disturbance in the material.

Figure 3.5 presents the x-ray test on the sample NU-1 65-67. For reference the bottom of the tube is located on the left of Figure 3.5. Two observations can be taken from the scan: (1) the x-ray showed the wax and possibly discontinuities in the material at the bottom; (2) near the top of the tube, the x-ray image exhibits lighter bands at the edges with a common inclination angle. This might represent disturbance in the sample, as described in ASTM International (2014a).

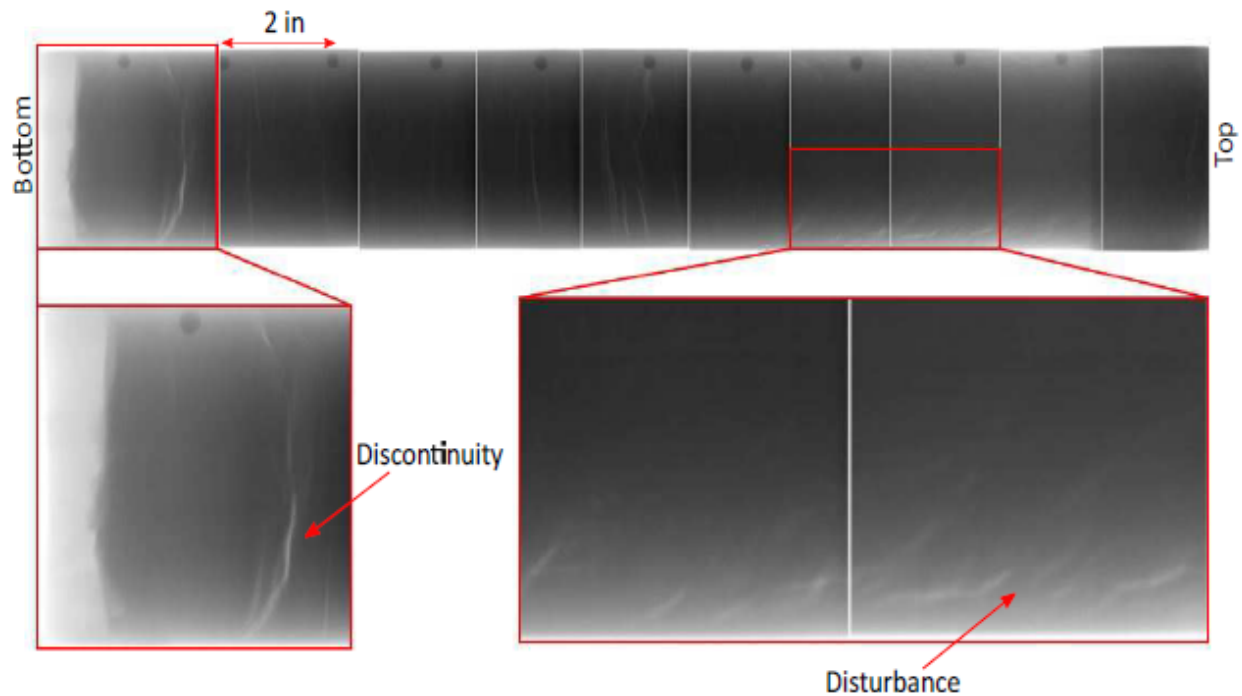


Figure 3.5. X-Ray test on tube NU-1 65-67

Figure 3.6 shows the extracted specimen from NU-1 65-67 that corresponds to the disturbed zone at top of the tube. It can be seen that the sample does not show a noticeable disturbance. Similar results of samples with disturbance are shown in the ASTM 04452-14 (ASTM International, 2014a). However, given that the tubes were all opened by cutting and not extrusion, as subsequently described, the x-ray technique was not needed because all soil collected was observed before selecting the portion to be tested.



Figure 3.6. Sample NU-1 65-67(3) (top of the tube)

3.4.2 Extraction and Trimming

The Shelby tubes containing the BCF samples were shipped from Anchorage, Alaska to Northwestern University. The samples remained vertical during transportation and storage. In the storage, the temperature was maintained at approximately 5°C.

The extraction process consisted of first making 2 longitudinal cuts in a Shelby tube with a slitting saw. Thereafter, the Shelby tube was cut into sections and the sample detached from the Shelby tube with a wire saw. The samples were not extruded. Figure 3.7 shows the sample fixed horizontally in a vertical mill equipped with slitting saw to make the longitudinal cuts. The slitting

saw speed was set at a low speed between 70 to 80 rpm. At the same time, the table was moving horizontally in the longitudinal direction of the tube, at a speed of 1.2 in/min to cover the tube length. The procedure was repeated for the second cut, located 180° from the first cut.



Figure 3.7. Longitudinal Cutting with Slitting Saw

The sample then was set for several transverse cuts to divide the whole tube into smaller sections. Transverse cuts were executed by a chop saw. Each section has a height approximately of 160 to 180 mm. This height was established to meet the required height- diameter ratio between 2.0 and 2.5 for triaxial samples with a diameter of 70 mm. Three to four sections were obtained from each tube, generally resulting in two to three sections suitable for triaxial testing.

Once the cutting was completed, one of the samples was used for testing and the remaining (one or two) were covered with cheesecloth and paraffin wax to be stored for future tests. The samples were extracted from each tube section by using a wire saw to detach the soil from the inner tube wall. A similar procedure was described by Ladd and DeGroot (2003); however, in this case, the tube section had the longitudinal cuts and a fitting tube was not required.

After the extraction, the samples were placed in a rotating pedestal to be radially trimmed

by a wire saw. This procedure was used to eliminate the dry material in contact with the Shelby tube and to obtain samples with a diameter of approximately 70 mm. Then, samples were trimmed transversely to obtain an uniform, horizontal surface, at top and bottom, and additionally to remove the disturbed material after the transverse cutting. The average of diameter and height of the samples used in the triaxial are 70.4 and 147.1 mm, respectively. The height/diameter ratio was intended to be higher than 2.0. For this work, the average height and diameter ratio prior testing was 2.09.

3.4.3 Specimen Preparation after Trimming

The preparation of the samples after trimming consisted of placing filter paper strips, inserting a sample into the latex membrane, and placing it on the triaxial pedestal. First, vertical filter paper strips were installed on the sample surface, see Figure 3.8. The strips have 10 mm thick and cover the entire height. The strips cover about the 50% of the surface area of the sample. The objective of the filter paper is to reduce the time of consolidation by allowing radial drainage and thus shortening the drainage path.

After the installation of the filter paper strips the sample is placed in a non- porous latex membrane. The placement is achieved by using a membrane stretcher and a vacuum pump. The membrane used in this research meets the ASTM D4767-11 standard (ASTM International, 2011) for consolidated triaxial undrained testing on cohesive soils.

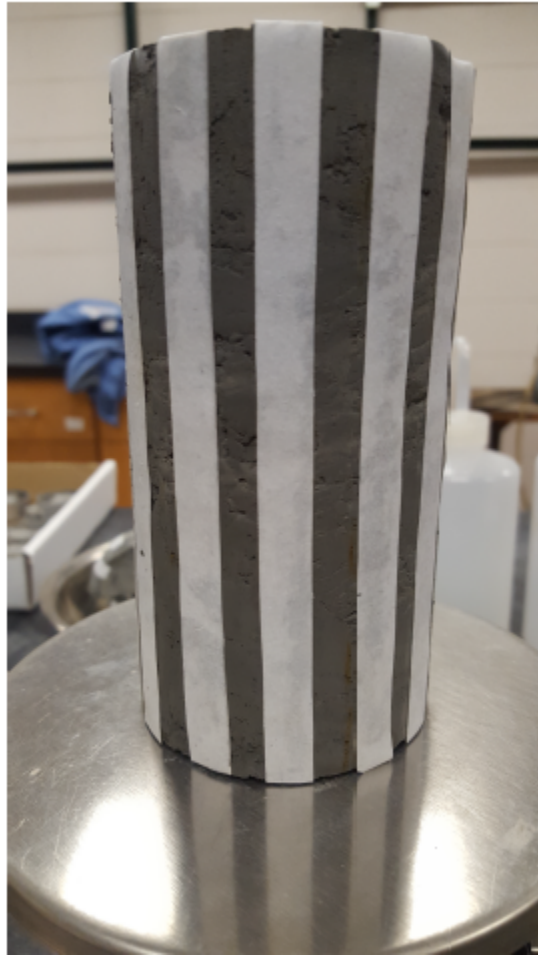


Figure 3.8. Filter Paper Setup in Sample

The sample then is placed on the triaxial pedestal for testing as shown in Figure 3.9. Bronze porous stones with filter paper discs are placed at the top and bottom of the sample. The system cap is sealed by installing o-rings at top and bottom connections between the sample and pedestal and top cap and then applying silicon grease on top of the external o-rings. A vacuum pump is connected to the back pressure lines to eliminate the air trapped between the sample and the membrane. The suction was set at 10 psi and remained on the sample for enough time to let the air flow out of the sample. Then, the valve of the vacuum was closed and suction was measured to verify that there was no leakage in the sample. If the reading of the suction is constant after 30

minutes, it was confirmed that not leakage was present and the test could proceed.

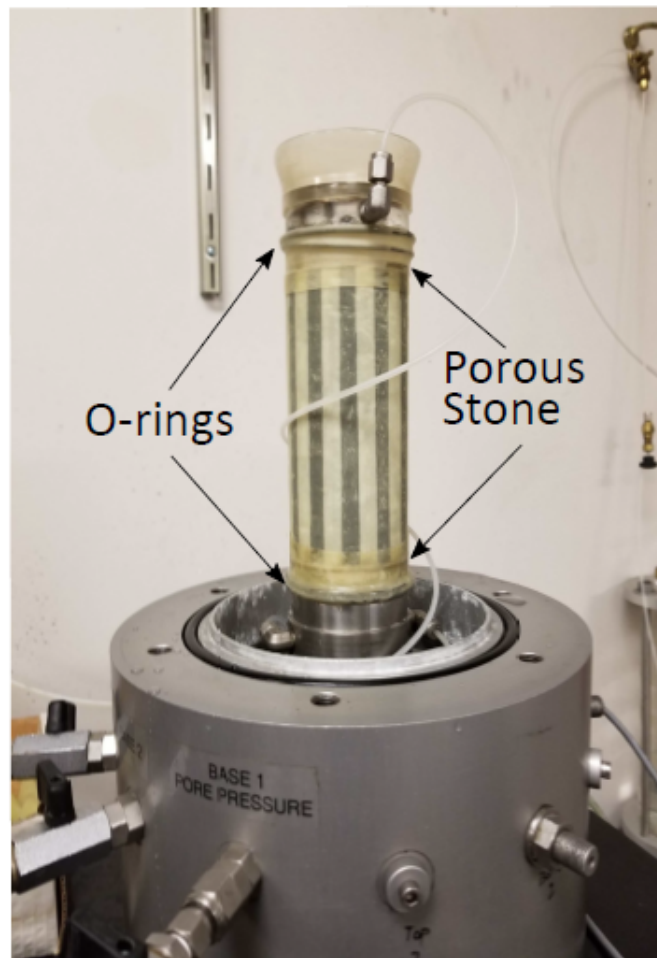


Figure 3.9. Sample placed in the Triaxial Pedestal.

3.4.4 Residual Stress and Saturation

The residual stress measurement is the first stage in each triaxial test described herein. Figure 3.10 presents the measurement and interpretation for determining the residual stress, in this case for specimen NU-1 20-22. The residual stress, p_r , is obtained by increasing the cell pressure, σ_{cell} , and reading the corresponding pore water pressure, u_o , as described by Ladd and Lambe (1964) and Zapata-Medina (2012). For this research, an initial cell pressure of 50 kPa was applied, with subsequent increments of 50 kPa up to 250 kPa. Then, σ_{cell} was decreased from 250 kPa in 100

kPa decrements to return to the initial pressure, 50 kPa. The p_r is extrapolated as the intercept value of the pore pressure when cell pressure equals 0.

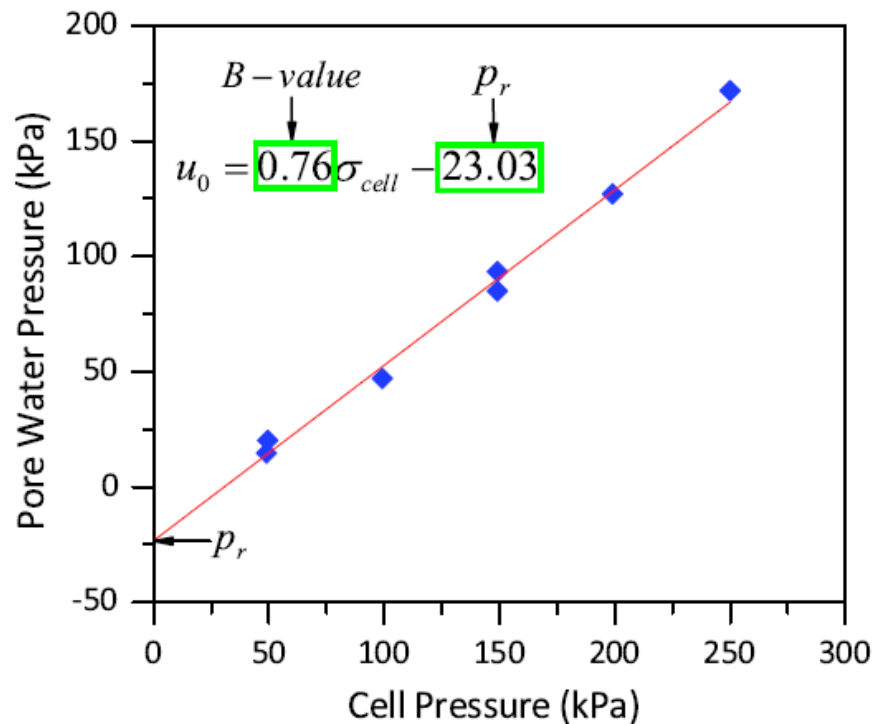


Figure 3.10. Residual Stress Measurement (NU-1 20-22)

After completion of the residual stress stage, saturation begins. The effective stress during saturation was maintained as the measured residual stress. The saturation procedure is described by Cho et al. (2007) and Zapata-Medina (2012). The cell, σ_{cell} , and back pressure, u_{BP} , are increased at a constant rate for 24 hrs. to the target back pressure. The σ_{cell} and u_{BP} difference is kept equal to p_r at all times during saturation. This procedure has shown to produce negligible swelling in both Chicago and BCF clays (Cho et al., 2007; Zapata-Medina, 2012).

The typical back pressure at the end of saturation is 200 kPa. The degree of saturation is checked by increasing the cell pressure by 100 kPa in 1.0 min with the valves closed to record the pore pressure response. Saturation is accepted when the Skempton parameter B was greater than

0.95. If the B-value does not reach the minimum required, the back pressure and cell pressure are increased, repeating the procedure described above, until B is equal or greater than 0.95.

3.4.5 Reconsolidation

The reconsolidation stage was carried out by using either *recompression* or SHANSEP techniques. The *recompression* technique (Bjerrum, 1973; Jamiolkowski, 1985) was adopted to replicate the estimated in situ vertical (σ'_{v0}) and horizontal (σ'_{h0}) effective stresses in the field. This procedure used herein is similar to the one described by Zapata-Medina (2012). Most of the specimens were consolidated anisotropically. The consolidation starts at residual stress and goes directly to the estimated in situ vertical and horizontal stresses. The σ_{h0} and σ_{v0} ratio at the of consolidation are defined as the target for the stage. Five specimens were consolidated under k_0 conditions (i.e. $k_0 = \sigma'_{h0}/\sigma'_{v0}$ changed during this stage to keep the radial strain close to zero, $\epsilon_r \approx 0$); these specimens had an estimated OCR between 1.03 to 1.08. Little difference was noted in the consolidation stresses in the two cases.

The SHANSEP technique (Ladd and Foott, 1974; Ladd, 1991) was utilized to obtain samples with a desired OCR. The samples were loaded at least 1.5 times the maximum preconsolidation stress. Some samples were unloaded to the desired OCR for the test. The consolidation under the SHANSEP technique was always carried out under k_0 conditions. For both techniques, the total radial stress was increased (σ_{hc}) at a rate of 5 kPa/hr for loading and decreased at a rate of 3.5 kPa/hr for unloading. Rates on total vertical stress (σ_{vc}) were higher because k_0 was always lower than one.

The bottom line was closed while the top line remained open during consolidation so that the excess pore water pressure, u_e , was measured at the mid-plane of the specimen. For clays with

low hydraulic conductivity, a non-uniform distribution of pore water pressure arises during load application along the sample's longitudinal axis. However, the mid-plane pore water pressures generated during consolidation were small and the quantity measured at the bottom was assumed to be the average value on the specimen.

The consolidation stage met the ASTM standard D-4186 for consolidation (ASTM International, 2012). Standard D-4186 establishes a control on the pore water pressure ratio (u_e/σ'_{vc}) and axial loading rate (ALR). For the pore water pressure ratio, the ASTM D1486 specifies a maximum ratio of ± 0.15 . Figure 3.11a presents the mid-plane pore water pressure ratio response during consolidation of the specimen NU-1 55-57. The maximum pore water pressure ratio was found at the beginning of the consolidation where σ'_{vc} is close to the p_r , then reduced as consolidation proceeded. The pore water pressure ratio values obtained in this work were always lower than ± 0.15 for all specimens. Typical pore water pressure ratio values were lower than 5% at the maximum value of σ'_{vc} .

Figure 3.11b presents the typical response of ALR at consolidation. For the ALR, the ASTM D-4186 specifies a limit of 1%/hr. As in the case of the pore water pressure ratio, the ALR reached its maximum at small consolidation stresses, then it decreased to approximately 0.05%/hr at maximum σ'_{vc} .

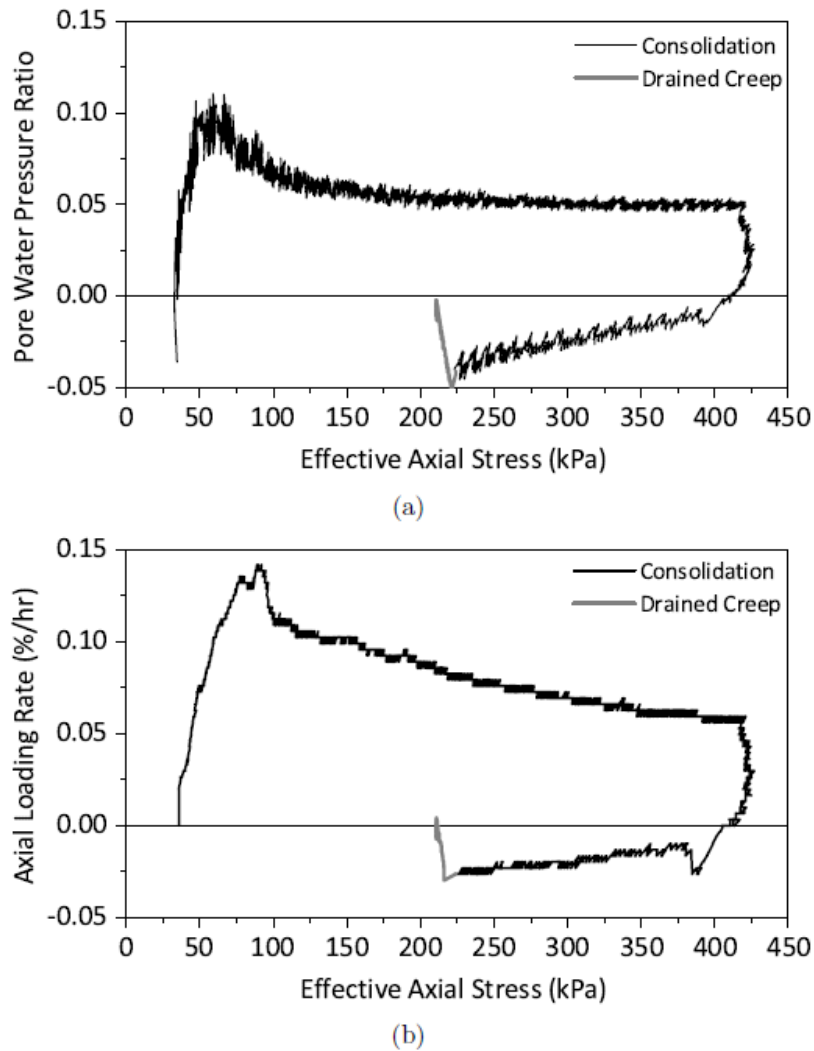


Figure 3.11. (a) Pore Water Pressure Ratio and (b) Axial Loading Rate During Reconsolidation with SHANSEP

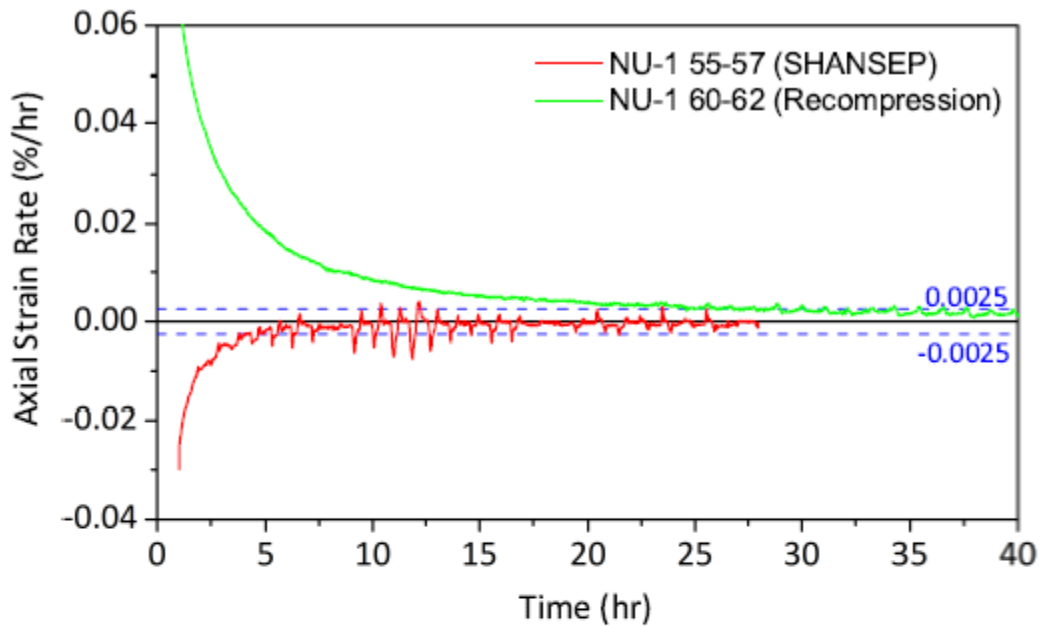
3.4.6 Creep or Aging Period

The specimens were subjected to a drained creep period after the target vertical effective stress was reached. The total stresses were kept constant with the top of the drainage line open during the stage, while tracking both the pore water pressure at the bottom of the specimen and axial strain. A creep stage was terminated once the axial strain rate (ASR) was lower than $\pm 0.0025\%/hr$ and the excess pore water pressure had very low values and about to be constant for

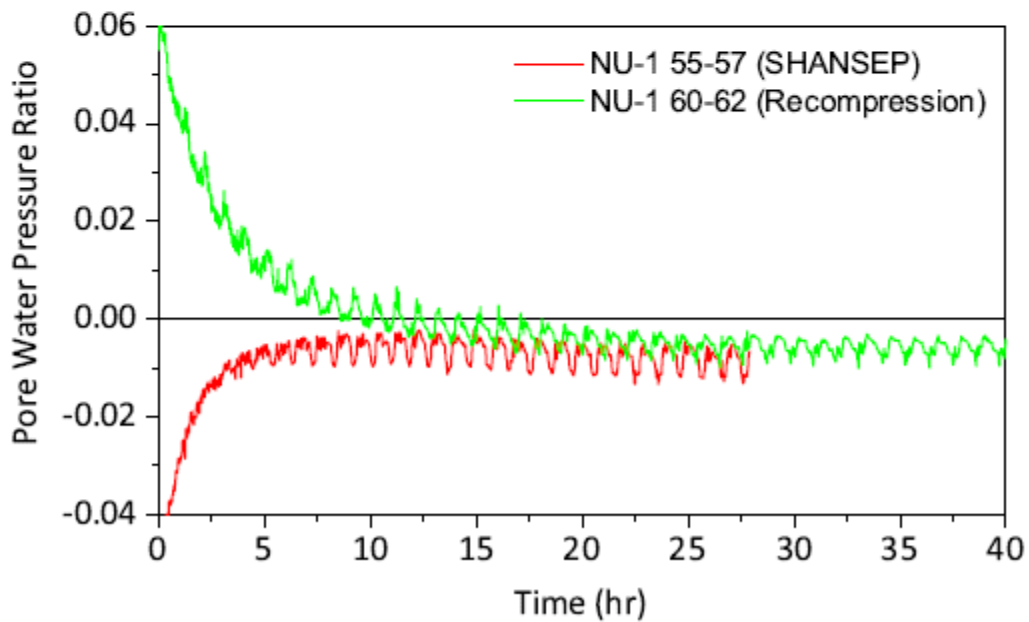
about 4 hrs. For the BCF clay from Port of Anchorage, the minimum ASR and minimum excess pore water pressure was reached after 12 and 24 hours for recompression and SHANSEP reconsolidation techniques, respectively (Zapata-Medina, 2012).

Figure 3.12 presents the ASR and excess pore water pressure response during the drained creep period for specimens NU-1 55-57 (SHANSEP) and NU-1 60-62 (Recompression). The ASR stabilized within the $\pm 0.0025\%/hr$ after 5 hrs for the NU-1 55-57 sample while NU-1 60-62 required about 30 hrs to reach it. Figure 3.11a shows that the creep time varied considerably. The range of creep time was 24 to 48 hrs before continuing with the following stage. The softer and normally consolidated specimens generally had larger periods for reaching stable deformation rates.

Figure 3.12b shows the pore water pressure ratio response of the specimens NU-1 55-57 and NU-1 60-62. The pore pressure decreased rapidly during the first hours corresponding to the reduction in the ASR. The specimens reached the constant pore water pressure ratio of less than 0.01. Similar to the ASR, the specimens consolidated by recompression required more time to reach a constant and low pore water pressure value.



(a)



(b)

Figure 3.12. (a) Axial Strain Ratio and (b) Pore Water Pressure Ratio During Creep

3.4.7 Cyclic Loading

Most of the specimens in this research were subjected to cyclic loading under stress-controlled

conditions. The cyclic stress ratio (CSR) is defined as the ratio between the cyclic shear stress and the effective vertical stress (Kramer, 1996). For triaxial testing, CSR is defined as:

$$(3.1) \quad CSR = q_{cyc} / 2\sigma'_{vc}$$

where q_{cyc} is the cyclic deviator stress and σ'_{vc} is the vertical effective stress at the end-of-consolidation. The CSR varied from 0.15 to 0.35 for this project.

The number of cycles varied for every test. The amount of accumulated axial strain was the failure criteria chosen to stop the cyclic loading. For this work, failure was defined when the axial strain accumulated during cyclic loading was equal to 5%. A maximum number of cycles were applied when this failure criteria was not achieved. The limit was set first as 40 cycles, but then it was increased to 100 cycles. The reason for the increment was that overconsolidated specimens have a high cyclic resistance and more cycles could be applied without reaching failure.

The frequency utilized for most of the cyclically loaded specimens was 1 Hz. Two specimens were tested with a frequency at 0.1, and 0.01 Hz to evaluate the effect of it on the material response. Additionally, two tests were performed under strain-controlled conditions following the cyclic strain path from a stress-controlled test. Although a few tests were subjected to a frequency different than 1 Hz, the study of the material rate effect is not a primary objective of this research.

Figure 3.13 presents the results of the specimen NU-3 60-62 under stress controlled cyclic loading. the specimen was consolidated with SHANSEP technique to a normally consolidated condition. The specimen was subjected to a CSR of 0.175 for 41 cycles. The cyclic loading was terminated once the sample reached failure defined as 5% accumulated axial strain. The deviator

stress range remained relatively constant during the application of the cycles while the axial strain and excess pore water pressure increased gradually. Small reductions of deviator stress are a result of an increment in the lateral strain that the device accounts for to update the cross-section area while maintaining a constant force.

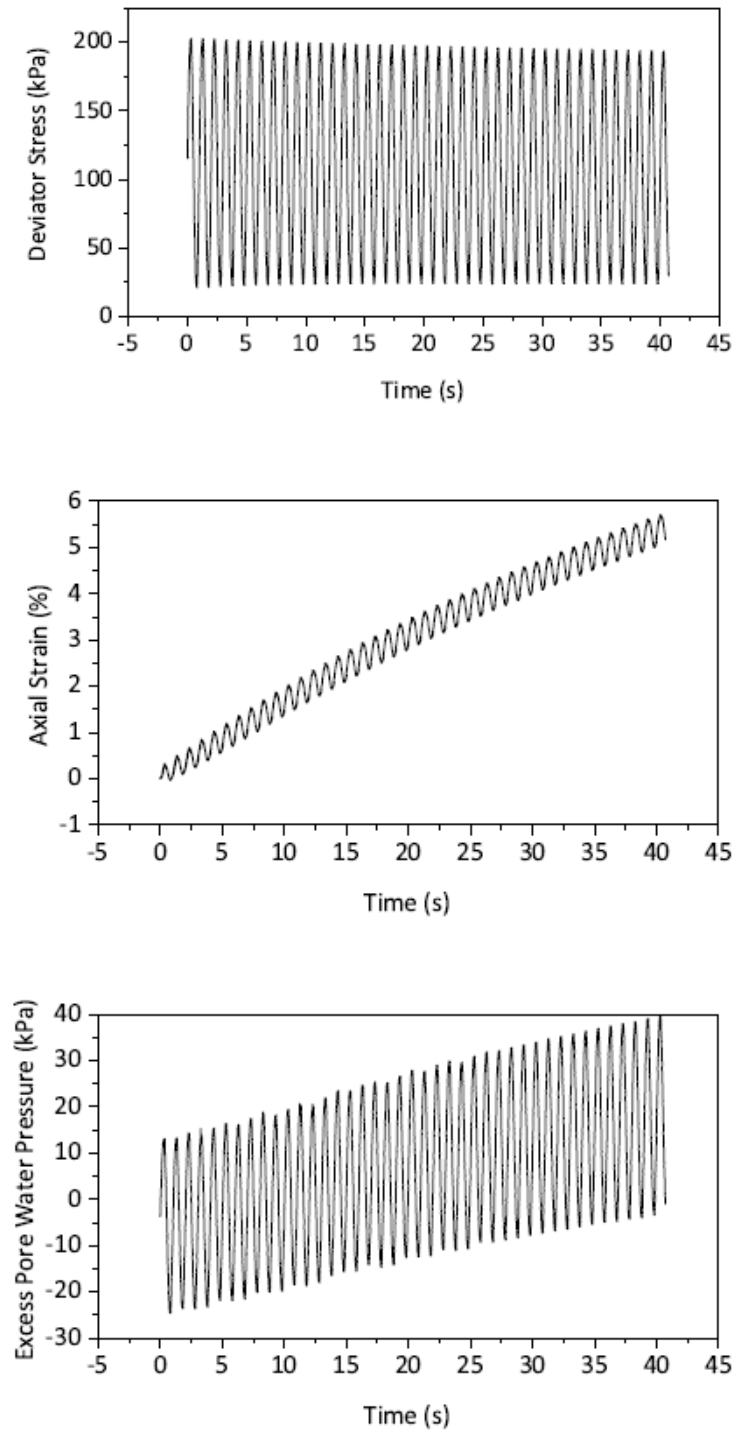


Figure 3.13. Stress-Strain-Pore Water Pressure Response During Cyclic Loading (NU-3 60-62)

For specimens that did not collapse during cyclic loading, either post-cyclic undrained triaxial compression was immediately applied, or an equalization period under undrained

conditions was allowed prior to post-cyclic shearing. The objective of the equalization period was to obtain a uniform distribution of the excess pore water pressure and therefore a more accurate measurement since the pore water pressure was measured at bottom of the specimen. Figure 3.14 shows the excess pore water pressure during the undrained equalization period (i.e. after cyclic loading and before post-cyclic shearing) for the specimen NU-1 22-24(2). The excess pore water pressure typically reached a constant value after 15 min and the excess pore water pressure in this case was almost twice as much as that recorded at the end of the cyclic loading. This response clearly indicates the development of non-uniform pore water pressures during cyclic loading. The type of response is similar in most of the specimens, however the magnitude of the pore water pressure increment was not always as shown in Figure 3.14. The pore water pressure of one of the specimens decreased during the equalization period, further details are provided in Chapter 5.

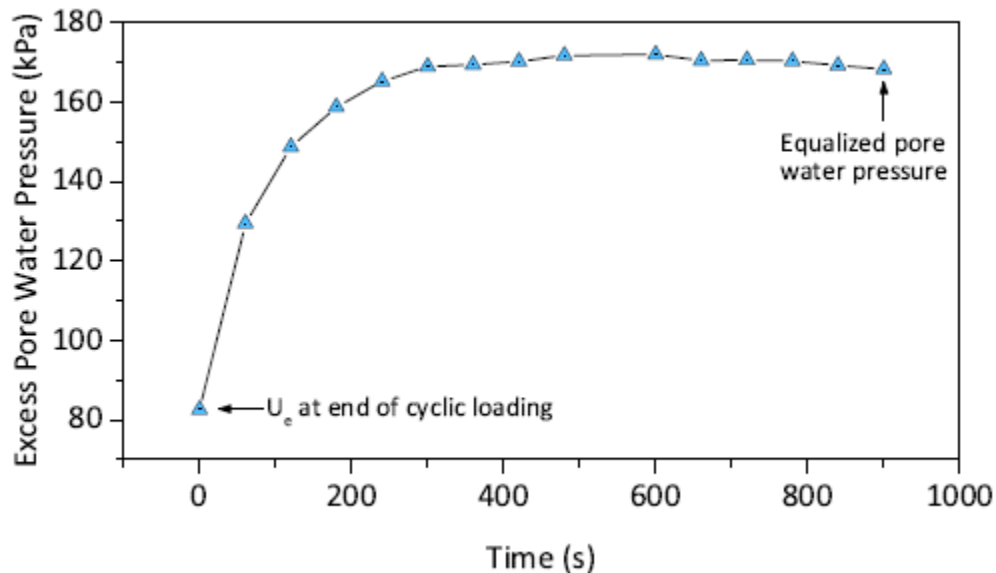


Figure 3.14. Excess pore water pressure Response during Equalization Time (NU-1 22-24(2))

3.4.8 Monotonic and Post-Cyclic Undrained Shearing

Undrained shearing was performed under strain-controlled conditions. For all samples, the shear

rate was kept constant at 0.5%/hr to assure equalized pore water pressure. All samples were sheared to strains between 10% axial strain and 15%.

Both monotonic and post-cyclic shearing was conducted as part of this research. For monotonic tests, samples were sheared after consolidation and a drained creep period. For post-cyclic shearing, two approaches were used. Post-cyclic shearing began either immediately after the cyclic loading or after an undrained equalization period as described in 3.4.7. Most of the samples were subjected to triaxial compression. Two samples were sheared in triaxial extension, one monotonic and one post-cyclic, to establish the material anisotropy.

Figure 3.15 shows a typical post-cyclic stress-excess pore water pressure-strain response for the specimen NU-1 47-49. For this specimen, the equalization period did not take place during the test. It can be seen that the initial excess pore water pressure is not zero and reflects the accumulation during the cyclic loading. After reaching a peak, the specimen experienced a reduction of principal stress difference. The pore water pressure decreased right after passing the peak stress, then increased monotonically until the end of the test.

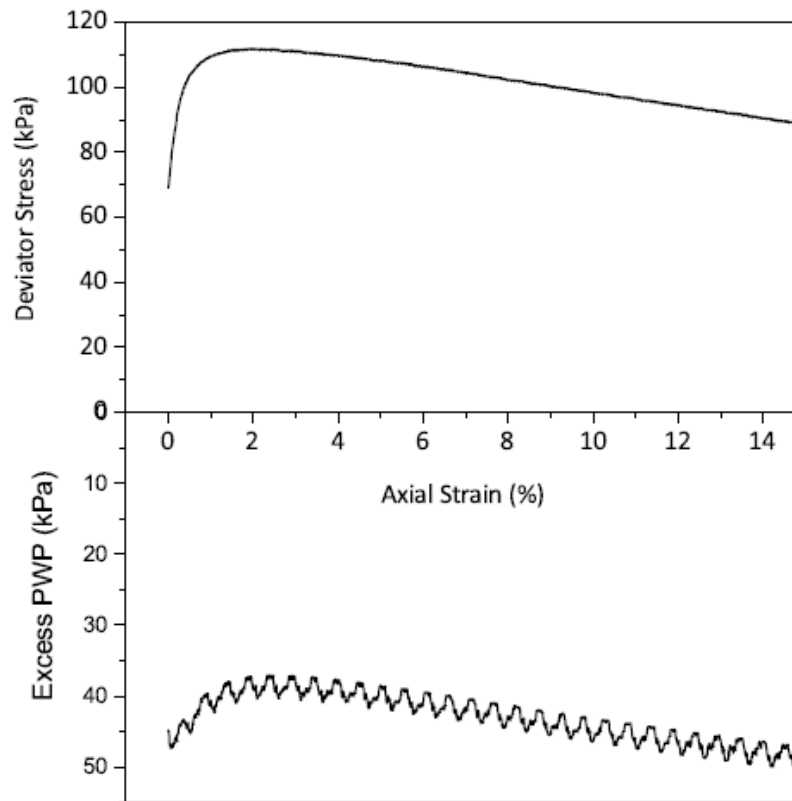


Figure 3.15. Deviator Stress and Excess Pore Water Pressure versus Axial Strain (NU-1 47-49)

3.4.9 Shear Wave Velocity Measurements

The shear wave velocity (V_s) in the laboratory was measured by vertical bender elements installed at the top cap and base pedestal in the triaxial device. From the bender elements, the distance between bender elements and time traveling, t_{BE} , are needed to compute V_{BE} . The t_{BE} is the most problematic parameter to measure.

Zapata-Medina (2012) and Cho et al. (2007) discussed the basic assumptions in bender element tests to obtain a correct measurement of t_{BE} . These assumptions include (1) the induced strains induced are small and the soil behaves linearly elastic; (2) when the flexural-waves generated by the bender elements are generated at a frequency of 5 kHz, guided wave theory indicates that the measured propagation velocity is considered representative of a shear wave

(Holman and Finno, 2005).

The t_{BE} is determined for a flexural-wave generated with a frequency of 5 kHz and an amplitude of 14 Volts. For each evaluation at least 10 received signals were stacked and then analyzed. The three methods used in this work to compute propagation velocity were: (i) frequency domain (Fast Fourier Transformation) analysis; (ii) the measurement of the first significant peak; and (iii) cross-correlation methods. As introduced in Cho et al. (2007), method (ii) can produce up to a 20% error in V_{BE} . For the bender elements measurements performed in this research, the method (i) did not provide a reliable value for all measurements. The values of V_{BE} reported in this research correspond to those obtained by the cross-correlation method (iii).

Figure 3.16 presents the shear modulus, G_{max} for the sample NU-1 27-29 (2) throughout the test. G_{max} is computed as:

$$(3.2) \quad G_{max} = \rho V_{BE}^2$$

where, ρ is the density of the soil. G_{max} increased during the initial loading in consolidation and then is reduced as the specimen was unloaded to the end-of-consolidation vertical effective stress. During creep, G_{max} increased slightly as a result of increment of strain and dissipation of pore water pressure. Measurements of V_{BE} were possible only after cyclic loading. There was a clear reduction of G_{max} at the end of the cyclic loading, in this case after 40 cycles. G_{max} increased during the undrained shearing as a result of negative excess pore water pressure and the corresponding increment in effective stresses.

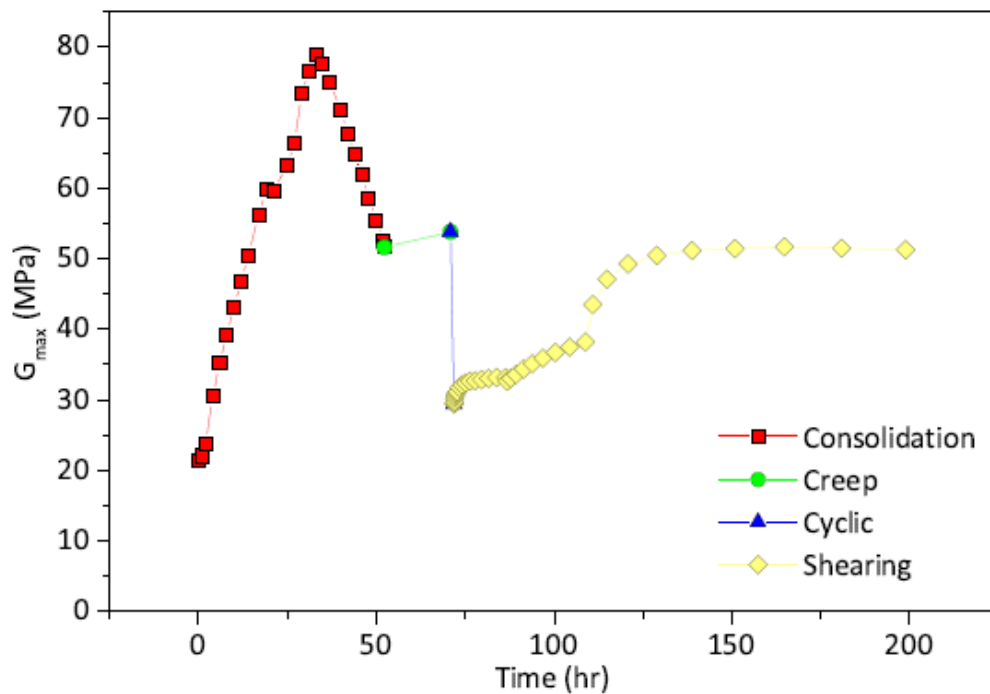


Figure 3.16. Change of Shear Modulus with Time (NU-1 27-29 (2))

3.5 Summary

This chapter describes the procedures used in the experimental program design to evaluate the cyclic and post-cyclic responses of Bootlegger Cove Formation clay. Index properties tests were conducted on specimens from all thin-wall tubes. . Seven specimens were tested under monotonic and 29 under cyclic loading conditions. The main features of the triaxial device used in this research are summarized. This chapter described the procedures used during the specimen preparation, residual stress and saturation, reconsolidation, creep, cyclic loading, and undrained shearing. It also summarized the procedure to measure shear wave velocities during consolidation, creep and undrained shearing.

CHAPTER 4

4 SITE CHARACTERIZATION AT LYNN ARY PARK

4.1 Introduction

As part of the site investigation at Lynn Ary Park, three borings were made and included thin wall sampling of BCF material, downhole seismic testing and field vane tests. The locations of the borings were within the area explored by the USGS (Updike et al., 1988). In this chapter, analyses of the soil conditions at Lynn Ary Park are presented based on the results of the previous investigations and the work performed as part of this research.

Lynn Ary Park is located near the head of the Turnagain Heights landslide scarp that developed during the Great Alaska earthquake of 1964. It is a site previously studied by Shannon and Wilson Inc. (1964) and Updike et al. (1988). Updike et al. (1988) conducted a field investigation to determine the strength and seismic properties of the BCF material. Figure 4.1 presents the location of the borings and CPT tests from all three investigations at Lynn Ary Park. Updike et al. (1988) included in their field investigation inclinometer surveys of the boreholes and downhole and crosshole seismic measurements. For this research, three borings were performed at the same location as Updike et al. (1988) in Lynn Ary Park. Two of the borings (NU-1 and NU-3) were made to obtain undisturbed specimens with thin-walled Shelby tubes. The remaining boring (NU-2) was drilled to perform field vane tests at different depths. Shear wave velocities were measured at the site using downhole seismic tests in one of the borings.

The laboratory tests results presented in this chapter include index property, consolidation and monotonic undrained triaxial shearing results. Index properties include the natural water content, Atterberg limits, and void ratio for each specimen and a number of specific gravity determinations. The initial void ratio was computed based on the initial and dried density taken from each specimen tested.

K_0 -consolidation was performed in the triaxial device. As described in Chapter 3, the device has the capacity to simulate k_0 conditions by keeping the volumetric strain equal to the axial strain. Consolidation was accomplished by using either recompression or SHANSEP approaches to reach the in situ vertical effective stress or overconsolidation ratio, OCR, respectively.

Monotonic undrained triaxial shearing presented in this chapter was performed on specimens that were not subjected to cyclic loading. The undrained shearing was carried out for specimens with a range of OCR values with both SHANSEP and recompression prepared specimens.

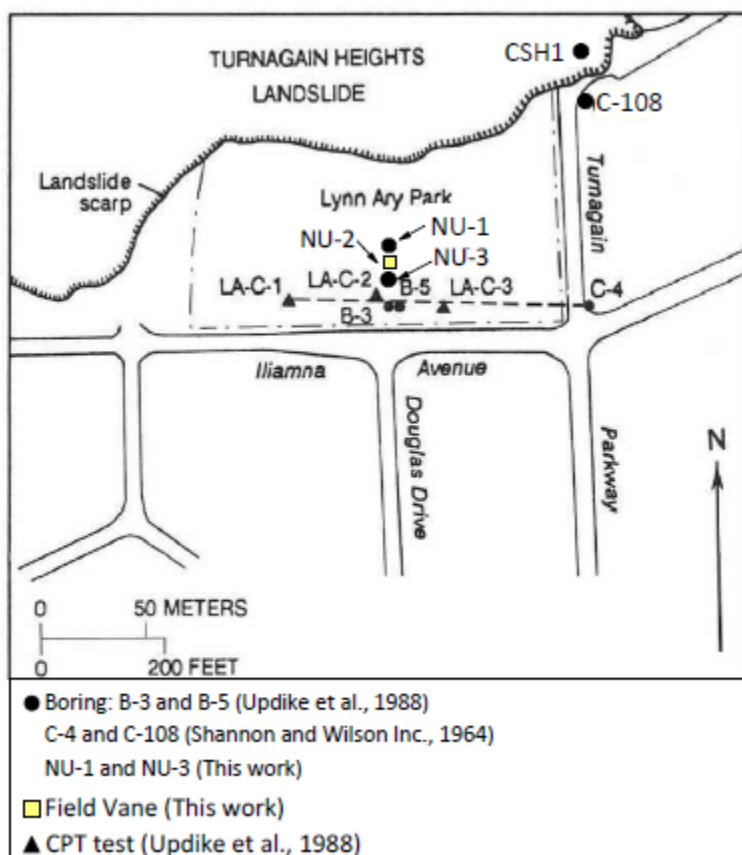


Figure 4.1. Plan View of Field Investigation at Lynn Ary Park

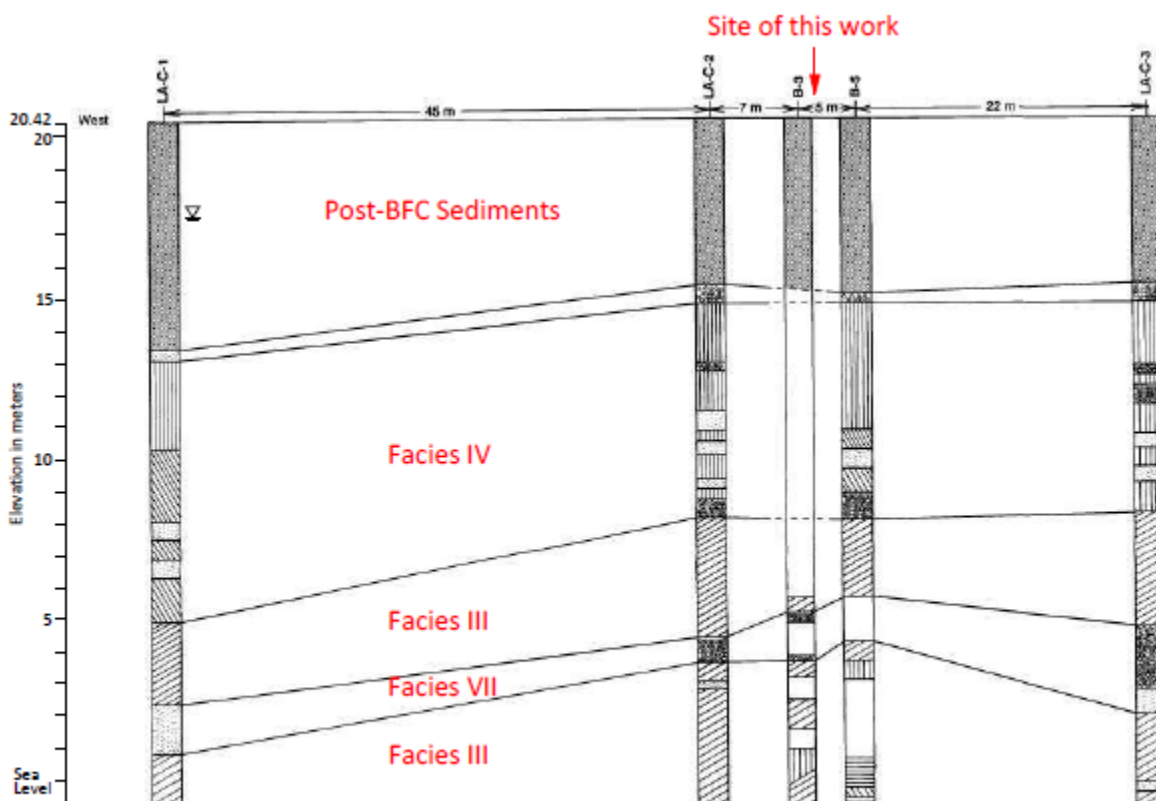
4.2 Stratigraphy

The Bootlegger Cove Formation (BCF) is a marine deposit that lies underneath a granular layer called Naptowne outwash deposited after the retreatment of the last glaciation, called post-BCF sediments in this research. The BCF was deposited mainly in a marine environment, however, it may include some horizons of freshwater origin (Updike et al., 1988). Updike et al. (1988) identified seven facies in the formation as noted in Table 4.1. The classification was based on the lithologic and engineering properties of the materials.

Table 4.1. Description of Facies proposed by Updike et al. (1988)

Facies	Description
FI	Clay, with minor silt and sand
FII	Silty clay (or) clayey silt
FIII	Silty clay (or) clayey silt, sensitive
FIV	Silty clay (or) clayey silt with thin silt and sand lenses
FV	Silty clay (or) clayey silt with random pebbles, cobbles, and boulders
FVI	Silty fine sand with silt and clay lenses
FVII	Fine to medium sand with traces of silt and gravel

Figure 4.2 shows the soil profile from the field investigation at Lynn Ary Park as reported by Updike et al. (1988). They established the soil profile based on the information provided by the two borings and three CPT tests. The dominant facies in the elevations shown are facies III and facies IV. There is a sand layer, facies VII, that divides the facies III deposit. The water table was located at an approximate elevation of 17.5 m mean sea level (MSL) based on data collected from a piezometer installed in the area of exploration (Updike et al. 1988). Water levels in borings made as part of this work showed a similar water table elevation.



F. III: Silty clay and (or) clayey silt, sensitive
 F. IV: Silty clay and (or) clayey silt with thin silt and sand layers
 F. VII: Fine to medium sand with traces of silt and gravel

Figure 4.2. Soil Profile Based on Results from Updike et al. (1988)

4.3 Northwestern University Exploration

4.3.1 Sampling

The soils tested in this research were taken from specimens of the BCF clay obtained from boring NU-1 and NU-3 between elevations 16 and 0 MSL. NU-2 was used to perform field vane shear tests. These soils mostly correspond to facies IV and facies III with a thin layer of facies VII at a few elevations. Undisturbed specimens from both strata were acquired by utilizing three-inch outside diameter thin-walled Shelby tubes. The Shelby tubes had a diameter (B) to thickness (t) ratio of 48. Inevitable disturbance is produced by this type of sampling (Baligh, 1985; Baligh et al., 1987; Santagata and Germaine, 2002). Nonetheless, disturbance can be reduced when the B/t

ratio increases for the tube. Typical B/t values for Shelby tubes are either 20 or 40 (ASTM International, 2015a).

4.3.2 Boring Logs

This section presents the boring logs with the main characteristics found in the specimens recovered from Lynn Ary Park. Blank zones represent elevations where no samples were recovered. Each boring log includes soil descriptions, Atterberg limits, percent recovery in each tube, results of the field vane performed in the boring NU-2 and results of the triaxial tests including OCR and undrained strength. Boring logs including photos of each specimen are shown in Appendix A. The results of boring NU-1 are shown in Figure 4.3. Therein the first samples were located at elevations between 15 to 14 m MSL and composed of the BCF clay and the post-BCF deposits. The BCF at elevations between 15 to 9.5 m MSL, in general, consists of a stiff clay with silty sand lenses of variable thickness within a specimen. This clay coincides with the facies IV material identified by Updike et al. (1988). Results of Atterberg limits showed that the natural water content was always below the liquid limit for all samples of facies IV. A total of 6 thin-walled specimens were recovered identified as facies IV.

For the BCF clay from elevations between 9.5 to 0 m MSL was identified as facies III. The material recovered was, in general, a massive medium to soft gray clay and very wet. Several specimens had natural water content above the liquid limit. The continuity of the facies III layer was interrupted by the presence of two silty sand layers identified as facies VII (Updike et al., 1988). The first layer was found at elevation 5 m MSL with a thickness of approximately 0.40 m in the specimen recovered. At elevation 3.2 m MSL a thin sand layer of 0.08 m thick. A total of 9 thin-walled samples were recovered identified as facies III and some lenses of facies VII.



Depth (m)	Eleva. (m)	Graphic log	Material Description	Water Cont, %		Recov., in		Field Vane S_u (kPa)	Field Vane Sensitivity	OCR _{fast}	σ'_{vc} (kPa)	S_u (kPa)	
				10	20	30	40						50
4	16												
5	15		(SP) Fine sand (post-BCF) from top to 12" with a presence of gravel on top. (CL) Gray, dry, stiff clay with presence of several thin silty sand lenses to the bottom of the tube				22			1	605	215.8	
6	14		(SP) Fine sand (post-BCF) from top to 9" with a presence of gravel on top. (CL) Gray, dry, stiff clay with presence of several thin silty sand lenses to the bottom of the tube. Higher water content at the contact with sand				22			2	800	303.3	
7	13		(CL) Gray, dry, stiff clay with presence of several thin silty sand lenses along the cross section of the samples. 1" thick lense at 7" from the top of the tube				20	247.4	3	2	400	191.2	
8	12		(CL) Material from cutting from top to 6". From 6", stiff clay with presence of some silty sand lenses				18	147.9	3		2.99	114	114
9											3.37	384	105



Depth (m)	Eleva. (m)	Graphic log	Material Description	Water Cont, %		Recov., in	Field Vane S_u (kPa)	Field Vane Sensitivity	OCR_{test}	σ'_{vc} (kPa)	S_u (kPa)
				10	20						
15			From top to 3" material from the cutting. (CL) From 3" to bottom homogeneous, Gray, wet, soft clay. So silty sand lenses observed.			21	57.9	6	1.35	174	-
									1.35	174	70
									1.35	174	56
5			(CL) From top to 6" of homogeneous, Gray, wet, medium stiff clay. Fine sand with 7% of fines from 16" to bottom			22					
16											
17			From top to 13" material from the cutting, probably a mixed of clay and sand. (CL) From 13" to 16" a fine sand layer. From 16" to the bottom Gray, wet, medium stiff clay, no silty sand lenses observed			12					
3							54.9	4	2	213	166
18											
2			From top to 3" material from the cutting. (CL) From 4" to bottom homogeneous, Gray, wet, soft clay. So silty sand lenses observed			24	67.8	2	1	410	126.3
									1	407	78.6
19			From top to 4" material from the cutting. (CL) From 4" to bottom homogeneous, Gray, wet, soft clay. So silty sand lenses observed			20	30.7	2	1.08	221	52.7
									1.05	219	101.7
1									1.05	219	-
									1.05	219	-



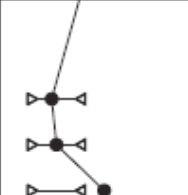

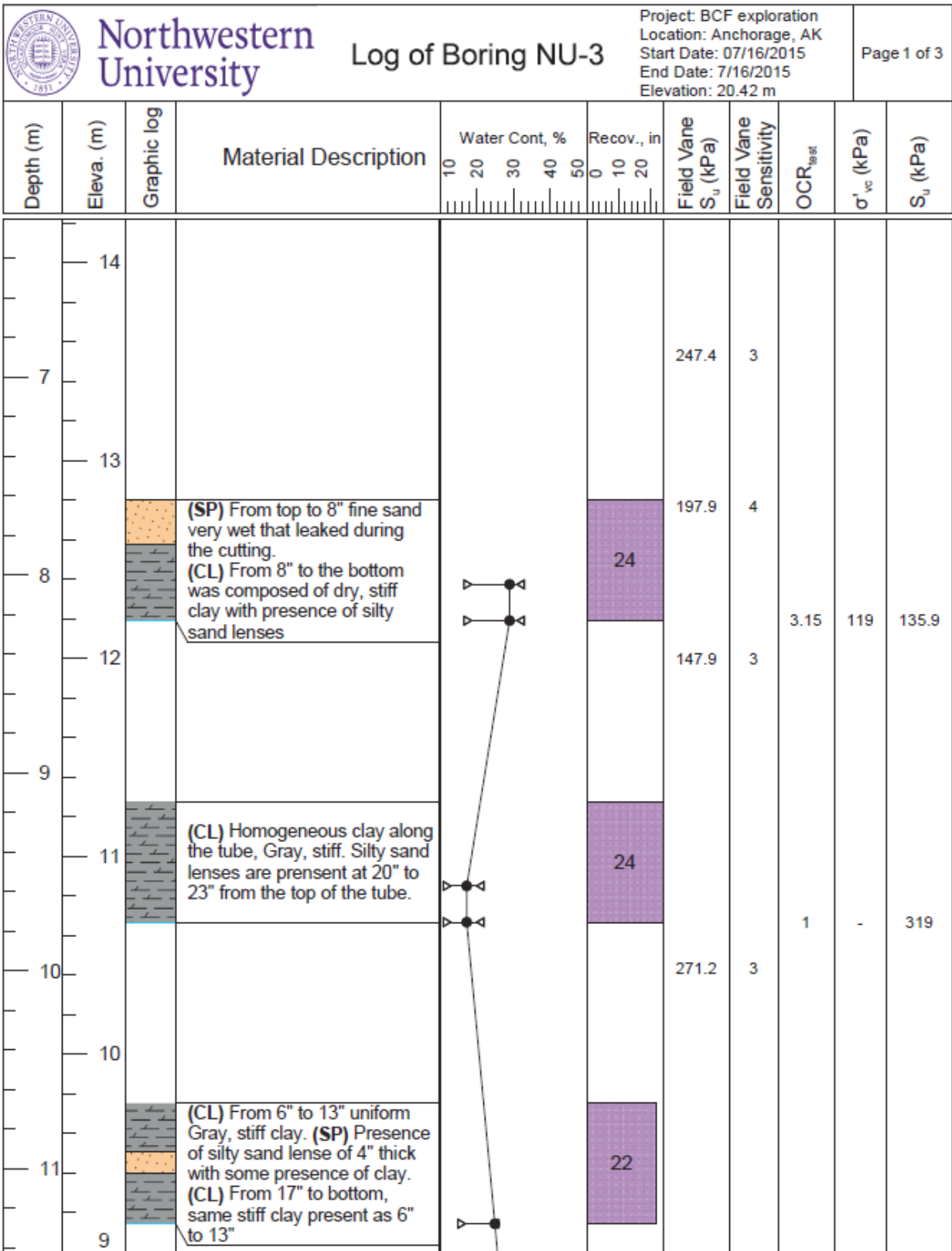
 Northwestern University		Log of Boring NU-1			Project: BCF exploration Location: Anchorage, AK Start Date: 07/13/2015 End Date: 7/14/2015 Elevation: 20.42 m			Page 4 of 4		
Depth (m)	Eleva. (m)	Graphic log	Material Description	Water Cont, % 10 20 30 40 50	Recov., in 0 10 20	Field Vane S_u (kPa)	Field Vane Sensitivity	OCR_{1961}	σ'_{vc} (kPa)	S_u (kPa)
20	0		From top to 4" material from the cutting. (CL) From 3" to bottom homogeneous, Gray, wet, soft clay. Inside the samples, silty sand lenses observed			20.8	2	1	400	-
								1	410	141.6
								1.03	228	98.3
21										

Figure 4.3. NU-1 Boring Log

Similar results were found for the boring NU-3 as shown in Figure 4.4. The clay classified as facies IV was found at between elevations 12.5 to 7.6 m MSL. The facies III layer is interrupted by a silty sand layer of facies VII at elevation 5 m MSL with a thickness of 0.38 m in the specimen recovered. The natural water contents and Atterberg limits of facies IV were similar to those from boring NU-1. For facies III, the natural water content was close to the liquid limit; however, only one specimen showed a value of water content above the liquid limit.

The undrained strength measured with the field vane showed a significant reduction in facies III compared to those measurements obtained from facies IV clay. These results correspond to a reduction in the OCR with depth as a result of desiccation. The sensitivity in the deposit based on field vane results varied between 2 and 6. The maximum sensitivity was measured at an elevation of approximately 5.7 m MSL within the facies III clay.



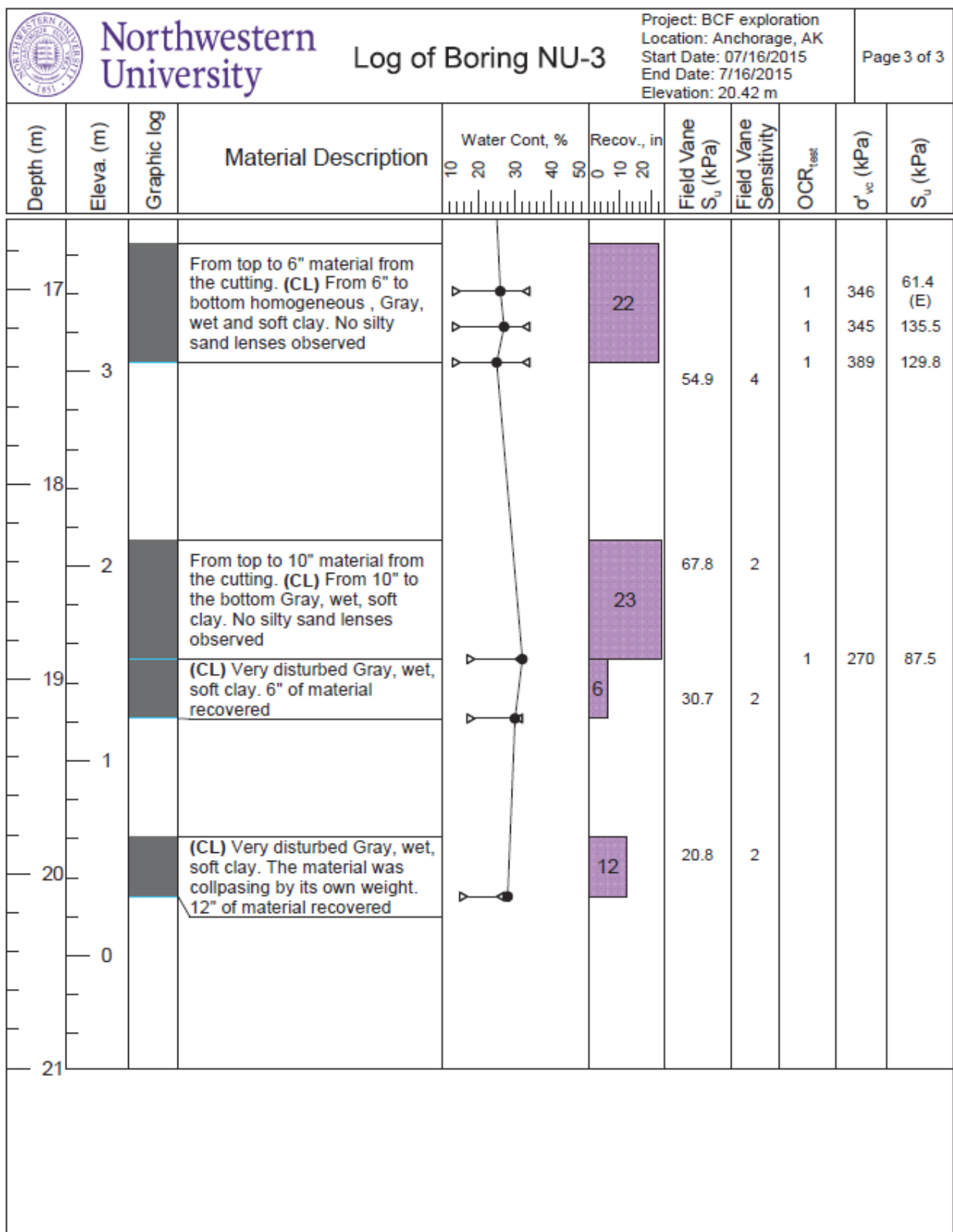


Figure 4.4. NU-3 Boring Log

4.3.3 Index Properties

Index property tests were conducted on the specimens collected from Lynn Ary Park. These tests included water content, ASTM D 2216-10 (ASTM International, 2010), specific gravity, ASTM D 8554-14 (ASTM International, 2014b), and Atterberg limits, ASTM 4318-17 (ASTM International, 2017). Figure 4.5a shows a plot of water content (W_n), plastic limit (PL), liquid limit (LL) versus elevation and Figure 4.5b shows the liquidity index (I_L) versus elevation. Table 4.2 and Table 4.3 present the results of the index properties corresponding to borings NU-1 and NU-3, respectively. For facies IV, the average natural water content was 26%. The average values for the plastic and liquid limits were equal to 16% and 29%, respectively. Clay specimens from facies III had an average natural water content of 29% and PL and LL equal to 18% and 31%, respectively. While the W_n content varied considerably with depth, the W_n are slightly higher within facies III than in facies IV.

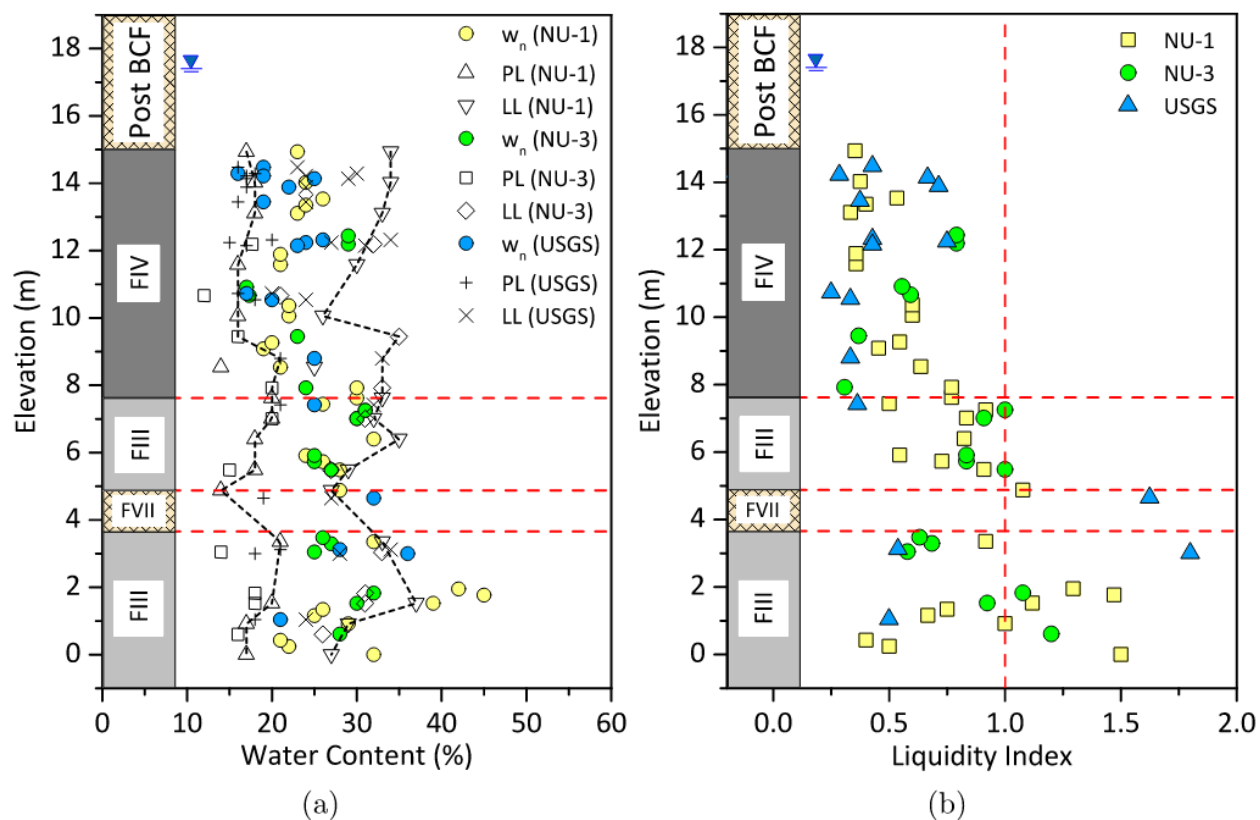


Figure 4.5. (a) Water Content, PL, and LL (b) Liquidity Index with Elevation

As seen Figure 4.5b, the I_L in facies IV was always lower than 1 with an average of 0.5. The average I_L in facies III was 0.8, significantly higher than facies IV. The I_L was higher than one in some specimens, reaching a maximum value of 1.5. Updike et al. (1988) obtained similar values with a maximum I_L of 1.8.

Table 4.2. Index Properties NU-1

Specimen	Elevation (m)	Facies	ω	ω_p	ω_l	I_p	I_L	G_s	e_o
NU-1 17-19	14.93	IV	23	17	34	17	0.4	-	0.65
NU-1 20-22	14.02	IV	24	18	34	16	0.4	-	0.62
NU-1 22-24	13.41	IV	23	18	33	15	0.3	-	0.67
NU-1 22-24 (2)	13.41	IV	24	18	33	15	0.4	-	0.74
NU-1 22-24 (3)	13.41	IV	26	18	33	15	0.5	-	0.82
NU-1 27-29	11.89	IV	21	16	30	14	0.4	-	0.66
NU-1 27-29 (2)	11.89	IV	21	16	30	14	0.4	-	0.68
NU-1 32-34	10.36	IV	22	16	26	10	0.6	-	0.57
NU-1 32-34 (3)	10.36	IV	22	16	26	10	0.6	-	0.65
NU-1 37-39	8.84	IV	21	14	25	11	0.6	-	0.64
NU-1 37-39 (2)	8.84	IV	19	14	25	11	0.5	-	0.55
NU-1 37-39 (3)	8.84	IV	20	14	25	11	0.5	-	0.55
NU-1 40-42	7.92	III	30	20	33	13	0.8	2.7	0.84
NU-1 40-42 (2)	7.92	III	30	20	33	13	0.8	-	0.85
NU-1 42-44	7.31	III	30	20	32	12	0.8	-	0.87
NU-1 42-44 (2)	7.31	III	31	20	32	12	0.9	-	0.83
NU-1 42-44 (3)	7.31	III	26	20	32	12	0.5	-	0.77
NU-1 45-47	6.40	III	32	18	35	17	0.8	2.69	0.86
NU-1 47-49	5.79	III	28	18	29	11	0.9	-	0.74
NU-1 47-49 (2)	5.79	III	25.6	18	29	11	0.7	-	0.68
NU-1 47-49 (3)	5.79	III	24	18	29	11	0.5	-	0.72
NU-1 50-52	4.88	III	28	14	27	13	1.1	-	-
NU-1 55-57	3.35	III	32	21	33	12	0.9	-	0.59
NU-1 60-62	1.83	III	39	20	37	17	1.1	-	1.44
NU-1 60-62 (2)	1.83	III	45	20	37	17	1.5	-	0.87
NU-1 60-62 (3)	1.83	III	42	20	37	17	1.3	-	0.8
NU-1 62-64	1.22	III	29	17	29	12	1	-	0.69
NU-1 62-64 (2)	1.22	III	25	17	29	12	0.7	-	0.68
NU-1 62-64 (3)	1.22	III	26	17	29	12	0.8	-	0.69
NU-1 65-67	0.30	III	32	17	27	10	1.5	-	0.75
NU-1 65-67 (2)	0.30	III	22	17	27	10	0.5	-	0.58
NU-1 65-67 (3)	0.30	III	21	17	27	10	0.4	-	0.57

Because the LL did not vary widely there was a significantly higher I_L in the facies III. Some specimens in facies III had values close or above 1.0. Maximum values of I_L were found close to the sand layer (facies VII) within the facies III soils. Mitchell and Soga (2005) and Holtz et al. (2011) showed that the sensitivity is closely correlated with I_L . Liquidity index values above 1.0 are typical for sensitive clays from Eastern Canada and Scandinavia (Holtz et al., 2011). Based on the results presented in Figure 4.5b, some of the clay close to the sand layer may be sensitive.

Table 4.3. Index Properties NU-3

Specimen	EL. <i>m</i>	F.	ω	ω_p	ω_l	I_p	I_L	G_s	e_o
NU-3 25-27	12.50	IV	29	18	32	14	0.8	-	0.68
NU-3 25-27 (2)	12.50	IV	29	18	32	14	0.8	-	0.68
NU-3 30-32	10.97	IV	17	12	21	9	0.6	2.76	0.55
NU-3 30-32 (2)	10.97	IV	17	12	21	9	0.6	2.73	0.55
NU-3 40-42	7.92	III	24	20	33	13	0.3	-	0.72
NU-3 42-44	7.31	III	30	20	31	11	0.9	-	0.83
NU-3 42-44 (2)	7.31	III	31.3	20	31	11	1	-	0.85
NU-3 47-49	5.79	III	27	15	27	12	1	-	0.73
NU-3 47-49 (2)	5.79	III	25	15	27	12	0.8	-	0.73
NU-3 47-49 (3)	5.79	III	25	15	27	12	0.8	-	0.69
NU-3 50-52	4.88	III	28	15	18	3	4.3	-	-
NU-3 55-57	3.35	III	25	14	33	19	0.6	-	0.68
NU-3 55-57 (2)	3.35	III	27	14	33	19	0.7	-	0.71
NU-3 55-57 (3)	3.35	III	26	14	33	19	0.6	-	0.74
NU-3 60-62	1.83	III	32	18	31	13	1.1	-	0.79
NU-3 62-63	1.37	III	30	18	31	13	0.9	-	-
NU-3 65-66	0.46	III	28	16	26	10	1.2	-	-

Figure 4.6 presents a photograph of a specimen from the NU-3 50-52 tube (Elevation 5 m). This specimen was located at the transition from facies III to the sand lens of facies VII. Figure 4.6 shows the presence of a highly sensitive lens that was apparently disturbed during the sampling and cutting. The lens was in a semi-viscous state and the I_L taken from the very wet zone was 4.3. While no other such wet lenses were noted in any of the tubes, this limited evidence suggests that the BCF deposit at the NU test location contains isolated thin very sensitive lenses that might not be detected with field vane or CPT tests.

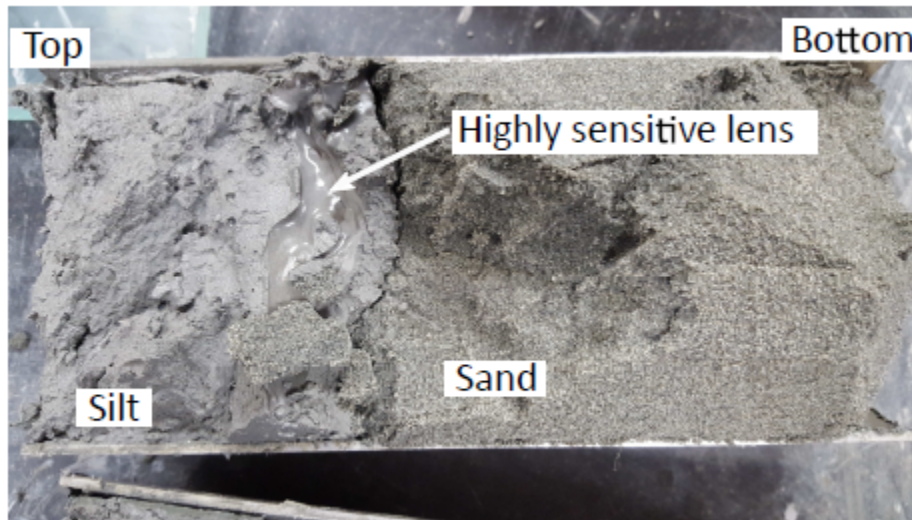


Figure 4.6. NU-3 50-52 specimen after Cutting

Figure 4.7 shows the data from Table 4.2 and Table 4.3 plotted on the plasticity chart. Facies III was divided into the upper and lower layer to identify any possible difference in the material properties above and below the sand seam. All BCF material, except one specimen, was classified as clay of low plasticity or lean clay (CL) according to the Unified Soil Classification (USCS). The specimen from NU-3 50-52 (shown in Figure 4.4) was classified as silt (ML). Clays from facies III and facies IV did not show significant differences in the plasticity chart. Also, no difference was found between the facies III above and below the sand seam.

4.3.4 Field Shear Wave Velocity

Updike et al. (1988) performed downhole and crosshole seismic tests to measure the in-place shear wave velocity. Most of the data were obtained by downhole seismic tests. For the downhole seismic tests, the seismic energy was generated by impacting a sledgehammer against steel anvils supported on concrete blocks. For the crosshole test, the seismic energy was generated by a split-spoon specimen located in the adjacent borehole.

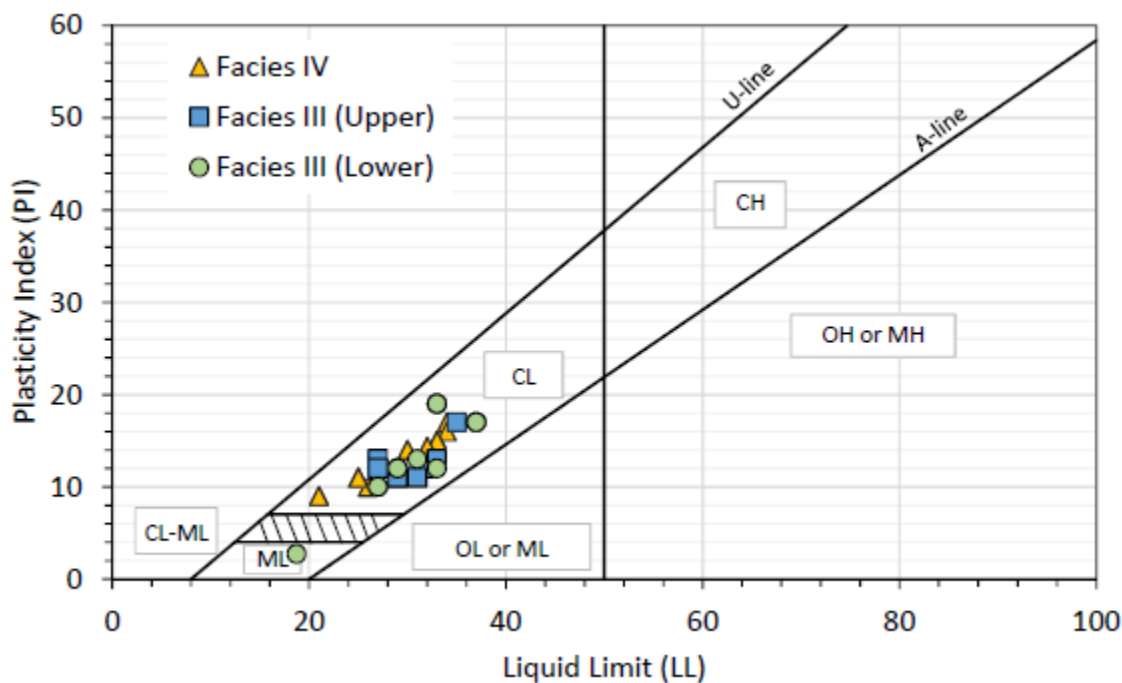


Figure 4.7. Plasticity Chart with specimens from facies III and facies IV

Downhole seismic testing in this project was performed by Global Geophysics. A 24-channel seismograph and 2 horizontal geophones were employed to record the particle velocity at each depth. The testing reached a maximum depth of 18.9 m with particle velocity measurements every 0.9 m. Global Geophysics indicated that the error in the measurements was $\pm 10\%$.

Results of the seismic testing are presented in Figure 4.8. The yellow squares represent the range of V_s values obtained by Updike et al. (1988) by downhole testing. 10% error bars were included for the V_s measured by the downhole seismic test in this research. Results from both downhole tests yielded similar shear wave velocities in facies IV. However, the V_s values differ near the transition to the facies III material and near the facies III and facies VII contact. A possible reason for this difference could be explained as the variation in thickness of the sand layer (facies VII) as shown in Figure 4.2. If so, then the measurements might be made for different materials. The results of V_s in this work did not show any extreme variation for the measurements between

elevation +8 to 0 MSL.

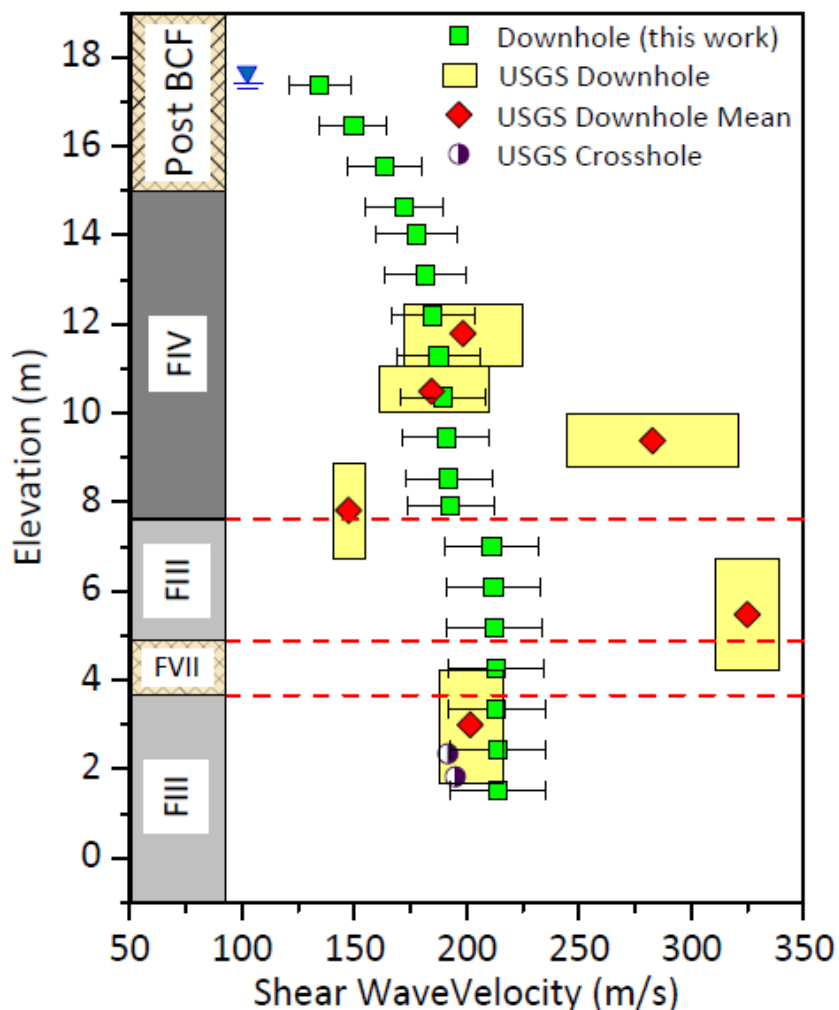


Figure 4.8. Results of in situ Shear Wave Velocity at Lynn Ary Park

4.4 Stress History of BCF Clay

This section presents the results of consolidation tests on specimens of BCF clay. The 1-D consolidation was completed during the triaxial testing by keeping the radial strain close to zero. The consolidation in the triaxial cell allowed the horizontal stresses to be measured to keep the lateral strain close to zero and hence the coefficient of earth pressure at rest, k_0 could be computed throughout the consolidation process.

4.4.1 Results from Reconsolidation in Triaxial

The recompression technique was used to consolidate specimens to the in-situ stress. The SHANSEP technique provides consolidation to a desired vertical stress and OCR (see section subsection 3.4.5). It also alters the original structure of the clay.

Table 4.4 summarizes the consolidation results, including reconsolidation technique, consolidation indexes, effective vertical stresses during consolidation, and OCR. Thirteen specimens were consolidated by the recompression technique as described in section 3.4.5 and were tested at the estimated in situ vertical effective stress. The purpose of this approach was to produce minimal disturbance to the original material structure. Specimens consolidated by recompression belonged to facies III layers, except for one specimen that was part of the facies IV layer. the preconsolidation stress reported for recompression specimens in Table 4.4, was obtained based on the trend presented in Figure 4.9.

Twenty-nine specimens were consolidated by SHANSEP technique. These specimens were tested at an OCR value different from in situ OCR. Most of the SHANSEP specimens were consolidated to a normally consolidated (NC) state. The compression index, C_c , was calculated from response measured near the maximum vertical effective stress and the recompression index, C_r , was calculated from the data collected during unloading. For SHANSEP specimens, the maximum effective vertical stress reached during consolidation was at least 1.5 times the estimated preconsolidation stress.

Table 4.4. Parameters of specimens During Consolidation

Specimen	Elevation (m)	F.	Technique	C_r	C_c	σ'_{vo} (kPa)	σ'_p (kPa)	OCR	ε_{cons} (%)
NU-1 17-19	14.93	IV	SHANSEP	-	0.08	84	350	4.17	0.11
NU-1 20-22	14.02	IV	SHANSEP	0.023	0.097	93	465	5.00	2.97
NU-1 22-24	13.41	IV	SHANSEP	0.018	0.12	99	470	4.75	3.11
NU-1 22-24 (2)	13.41	IV	SHANSEP	0.023	0.111	99	450	4.55	3.02
NU-1 22-24 (3)	13.41	IV	SHANSEP	0.02	0.129	99	420	4.24	3.16
NU-1 27-29	11.89	IV	SHANSEP	0.018	0.120	114	-	3.33	3.15
NU-1 27-29 (2)	11.89	IV	SHANSEP	0.02	0.083	114	-	3.33	1.90
NU-1 32-34	10.36	IV	SHANSEP	-	0.480	129	420	3.26	11.07
NU-1 32-34 (3)	10.36	IV	SHANSEP	-	0.27	129	265	2.05	4.59
NU-1 37-39 (3)	8.84	IV	SHANSEP	-	0.217	144	330	2.29	7.28
NU-1 55-57	3.35	III	SHANSEP	0.021	0.257	198	215	1.09	3.32
NU-1 60-62 (2)	1.83	III	SHANSEP	-	0.206	213	235	1.10	4.63
NU-1 60-62 (3)	1.83	III	SHANSEP	-	0.144	213	230	1.08	4.92
NU-1 65-67 (2)	0.30	III	SHANSEP	-	0.085	228	235	1.03	3.91
NU-1 65-67 (3)	0.30	III	SHANSEP	-	0.088	228	235	1.03	4.11
NU-3 25-27	12.50	IV	SHANSEP	0.02	-	108	340	3.15	2.06
NU-3 25-27 (2)	12.50	IV	SHANSEP	0.02	-	108	340	3.15	2.53
NU-3 30-32	10.97	IV	SHANSEP	-	0.113	123	370	3.01	10.46
NU-3 30-32 (2)	10.97	IV	SHANSEP	0.009	0.085	123	230	1.87	4.35
NU-3 40-42	7.92	III	SHANSEP	-	0.501	153	265	1.73	4.90
NU-3 42-44	7.31	III	SHANSEP	-	0.580	159	225	1.42	9.86
NU-3 42-44 (2)	7.31	III	SHANSEP	-	0.898	159	240	1.51	10.10
NU-3 47-49	5.49	III	SHANSEP	-	-	174	235	1.35	6.82
NU-3 47-49 (2)	5.49	III	SHANSEP	-	-	174	235	1.35	6.74
NU-3 47-49 (3)	5.49	III	SHANSEP	-	-	174	235	1.35	7.18
NU-3 55-57	3.35	III	SHANSEP	-	0.106	198	230	1.16	4.05
NU-3 55-57 (2)	3.35	III	SHANSEP	-	0.126	198	230	1.16	6.55
NU-3 55-57 (3)	3.35	III	SHANSEP	-	0.143	198	230	1.16	7.81
NU-3 60-62	1.83	III	SHANSEP	-	-	213	230	1.08	5.91
NU-1 37-39 (2)	8.84	IV	Recomp	-	-	144	255	1.77	1.06
NU-1 40-42	7.92	III	Recomp	-	-	153	249	1.63	1.26
NU-1 40-42 (2)	7.92	III	Recomp	-	-	153	249	1.63	1.15
NU-1 42-44 (2)	7.31	III	Recomp	-	-	159	240	1.51	2.49
NU-1 42-44 (3)	7.31	III	Recomp	-	-	159	240	1.51	4.22
NU-1 47-49	5.79	III	Recomp	-	-	174	235	1.35	1.84
NU-1 47-49 (2)	5.79	III	Recomp	-	-	174	235	1.35	2.83
NU-1 47-49 (3)	5.79	III	Recomp	-	-	174	235	1.35	1.34
NU-1 60-62	1.83	III	Recomp	-	-	213	230	1.08	2.22
NU-1 62-64	1.22	III	Recomp	-	-	219	230	1.05	0.65
NU-1 62-64 (2)	1.22	III	Recomp	-	-	219	230	1.05	1.19
NU-1 62-64 (3)	1.22	III	Recomp	-	-	219	230	1.05	1.04
NU-1 65-67	0.30	III	Recomp	-	-	228	235	1.03	1.82

σ'_{vo} = *In situ* vertical effective stress, σ'_p = Preconsolidation stress (by strain energy),
 $OCR = \sigma'_p / \sigma'_{vo}$, ε_{cons} = Axial strain at end-of-consolidation

4.4.1.1 Stress History. Figure 4.9a shows the preconsolidation stress, σ'_p , plotted versus elevation and compares these values to the calculated in situ vertical effective stresses, σ'_{vo} . The σ'_p was computed by using the strain energy approach proposed by Becker et al. (1987) and results are shown in Appendix. The values of σ'_p decreased with depth throughout facies IV. Thereafter the σ'_p was approximately constant in facies III. Figure 4.9b shows the corresponding OCR obtained from the consolidation data in Figure 4.9a. Results showed an OCR greater than 4 near the top of the facies IV. Near the transition of between facies III and IV, the BCF clay displayed an OCR close to 1.5. As depth increased below the transition, the OCR decreased with depth until it became approximately normally consolidated near the elevation 0 MSL. It is believed that overconsolidation in facies IV was a result of desiccation (Updike et al., 1988).

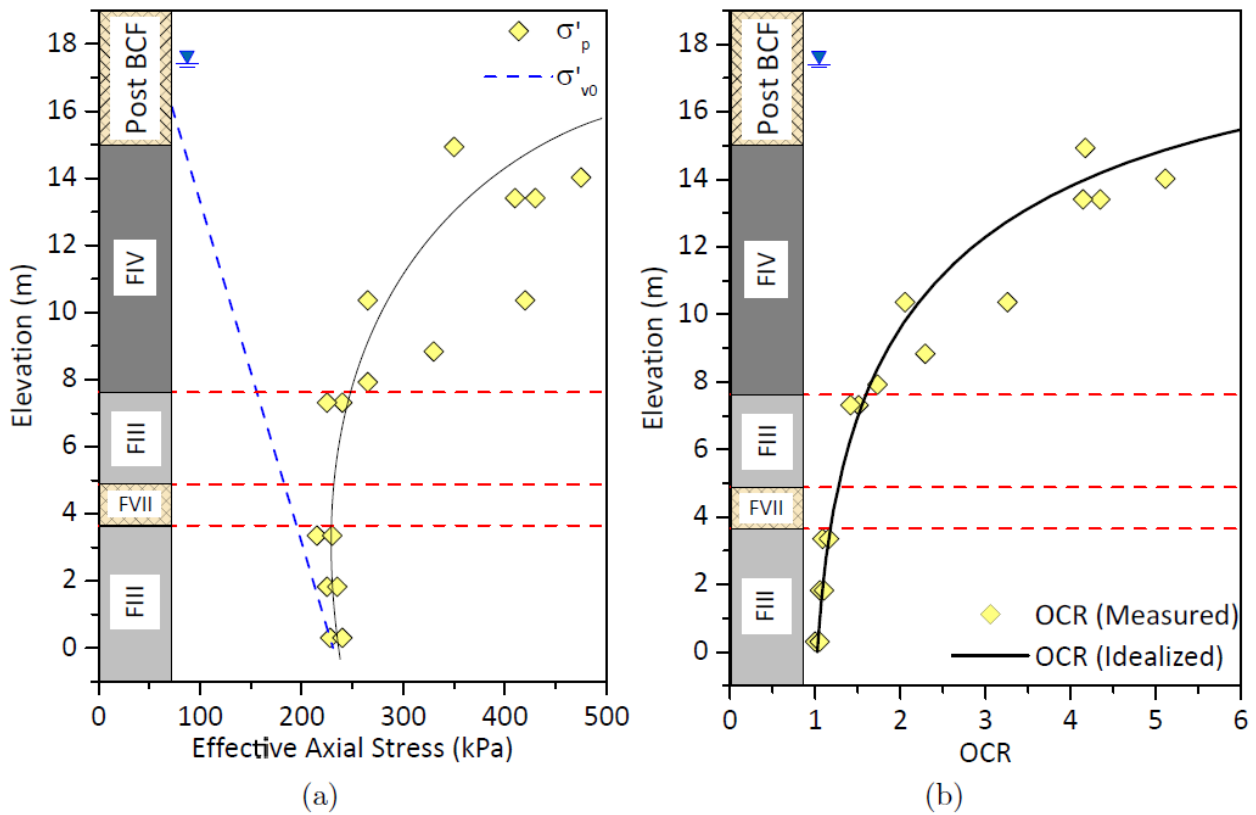


Figure 4.9. (a) Preconsolidation Stress and (b) OCR with Elevation

4.4.1.2 At-Rest Earth Pressure Coefficient. By maintaining zero lateral strain during all portions of consolidation using SHANSEP, the coefficient of earth pressure at rest can be recorded throughout the test. Table 4.5 summarizes the at-rest earth pressure coefficient, k_0 , at a NC state at the end of consolidation. The NC BCF had an average $k_{0(NC)}$ of 0.45 and 0.54 for clay from facies IV and facies III, respectively. Jaky (1944) proposed that k_0 can be calculated as follows:

$$(4.1) \quad k_{0,NC} = 1 - \sin(\phi')$$

where ϕ' is the effective internal friction angle. Using Equation 4.1, ϕ' would be 33° for facies IV and 27° for facies III. Zapata-Medina (2012) presented similar analysis for BCF clay from facies IV at the Port of Anchorage (POA). He reported values of $k_{0(NC)}$ between 0.45 to 0.53. Results from this work agreed with those presented by Zapata-Medina (2012) for facies IV clay, with no significant difference in $k_{0(NC)}$ noted between the two facies. This is consistent with the similarity in LL between the two facies at this site.

Figure 4.10 shows the best fit k_0 values for loading and unloading conditions and the equations presented by Zapata-Medina (2012) and Schmidt (1966). Values of σ'_{vc}/σ'_p greater than one during the loading correspond to stress higher than the estimated preconsolidation stress. During unloading (4.10b), all data started at one since the maximum vertical effective stress during loading is the preconsolidation stress. Results from the best fit during unloading in consolidation presented by Zapata-Medina (2012) are included in Figure 4.10b. The equation proposed by Schmidt (1966) was evaluated at ϕ' values between 27° and 33° . Results showed that the equation proposed by Schmidt (1966) predicts accurately the k_0 during unloading for the BCF at Lynn Ary Park when ϕ' ranges between 27° and 33° . The equation proposed by Zapata-Medina (2012) for BCF from facies IV at POA underpredicts the k_0 value at unloading for the specimens tested in

this work by a maximum of 7%.

Table 4.5. Parameters of specimens During Consolidation

Specimen	Elevation (m)	F.	Technique	$OCR_{specimen}$	OCR_{test}	$k_0(NC)$	k_0 at test cond.
NU-1 17-19	14.93	IV	SHANSEP	4.17	1	0.45	0.45
NU-1 20-22	14.02	IV	SHANSEP	5	2	0.53	0.85
NU-1 22-24	13.41	IV	SHANSEP	4.75	2	0.52	0.7
NU-1 22-24 (2)	13.41	IV	SHANSEP	4.55	2	0.57	0.79
NU-1 22-24 (3)	13.41	IV	SHANSEP	4.24	2	0.52	0.69
NU-1 27-29	11.89	IV	SHANSEP	-	3.37	0.45	0.71
NU-1 27-29 (2)	11.89	IV	SHANSEP	-	2.99	0.5	0.81
NU-1 32-34	10.36	IV	SHANSEP	3.26	1	0.26	0.26
NU-1 32-34 (3)	10.36	IV	SHANSEP	2.05	1	0.36	0.36
NU-1 37-39 (3)	8.84	IV	SHANSEP	2.29	1	-	0.4
NU-1 55-57	3.35	III	SHANSEP	1.09	2	0.54	0.76
NU-1 60-62 (2)	1.83	III	SHANSEP	1.10	1	0.59	0.59
NU-1 60-62 (3)	1.83	III	SHANSEP	1.08	1	0.59	0.59
NU-1 65-67 (2)	0.3	III	SHANSEP	1.03	1	-	0.58
NU-1 65-67 (3)	0.3	III	SHANSEP	1.03	1	-	0.54
NU-3 25-27	12.5	IV	SHANSEP	3.15	4.07	0.49	0.86
NU-3 25-27 (2)	12.5	IV	SHANSEP	3.15	-	0.43	0.63
NU-3 30-32	10.97	IV	SHANSEP	3.01	1	0.49	0.49
NU-3 30-32 (2)	10.97	IV	SHANSEP	1.87	-	0.3	0.32
NU-3 40-42	7.92	III	SHANSEP	1.73	1	0.46	0.46
NU-3 42-44	7.31	III	SHANSEP	1.42	1	0.46	0.46
NU-3 42-44 (2)	7.31	III	SHANSEP	1.51	1	0.46	0.46
NU-3 47-49	5.79	III	SHANSEP	1.35	1	0.47	0.47
NU-3 47-49 (2)	5.79	III	SHANSEP	1.35	1	0.58	0.58
NU-3 47-49 (3)	5.79	III	SHANSEP	1.35	1	0.48	0.48
NU-3 55-57	3.35	III	SHANSEP	1.16	1	0.53	0.53
NU-3 55-57 (2)	3.35	III	SHANSEP	1.16	1	0.55	0.55
NU-3 55-57 (3)	3.35	III	SHANSEP	1.16	1	0.54	0.54
NU-3 60-62	1.83	III	SHANSEP	1.08	1	0.52	0.52
NU-1 37-39 (2)	8.84	IV	Recomp	1.77	1.77	-	0.68
NU-1 40-42	7.92	III	Recomp	1.63	1.63	-	0.68
NU-1 40-42 (2)	7.92	III	Recomp	1.63	1.63	-	0.68
NU-1 42-44 (2)	7.31	III	Recomp	1.51	1.51	-	0.56
NU-1 42-44 (3)	7.31	III	Recomp	1.51	1.51	-	0.56
NU-1 47-49	5.79	III	Recomp	1.35	1.35	-	0.55
NU-1 47-49 (2)	5.79	III	Recomp	1.35	1.35	-	0.55
NU-1 47-49 (3)	5.79	III	Recomp	1.35	1.35	-	0.55
NU-1 60-62	1.83	III	Recomp	1.08	1.08	-	0.67
NU-1 62-64	1.22	III	Recomp	1.05	1.05	-	0.6
NU-1 62-64 (2)	1.22	III	Recomp	1.05	1.05	-	0.54
NU-1 62-64 (3)	1.22	III	Recomp	1.05	1.05	-	0.63
NU-1 65-67	0.3	III	Recomp	1.03	1.03	-	0.57

$$OCR_{specimen} = \text{In situ OCR}, OCR_{test} = \sigma'_{uc(max)}/\sigma'_{uc}$$

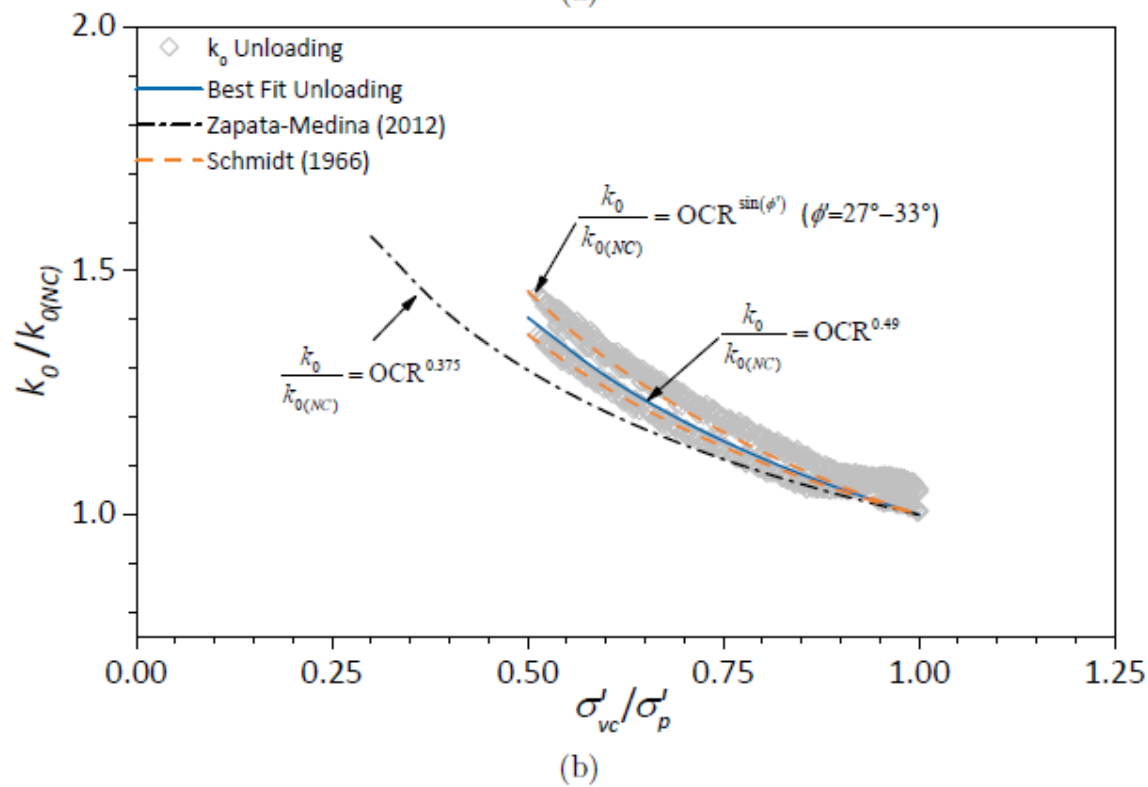
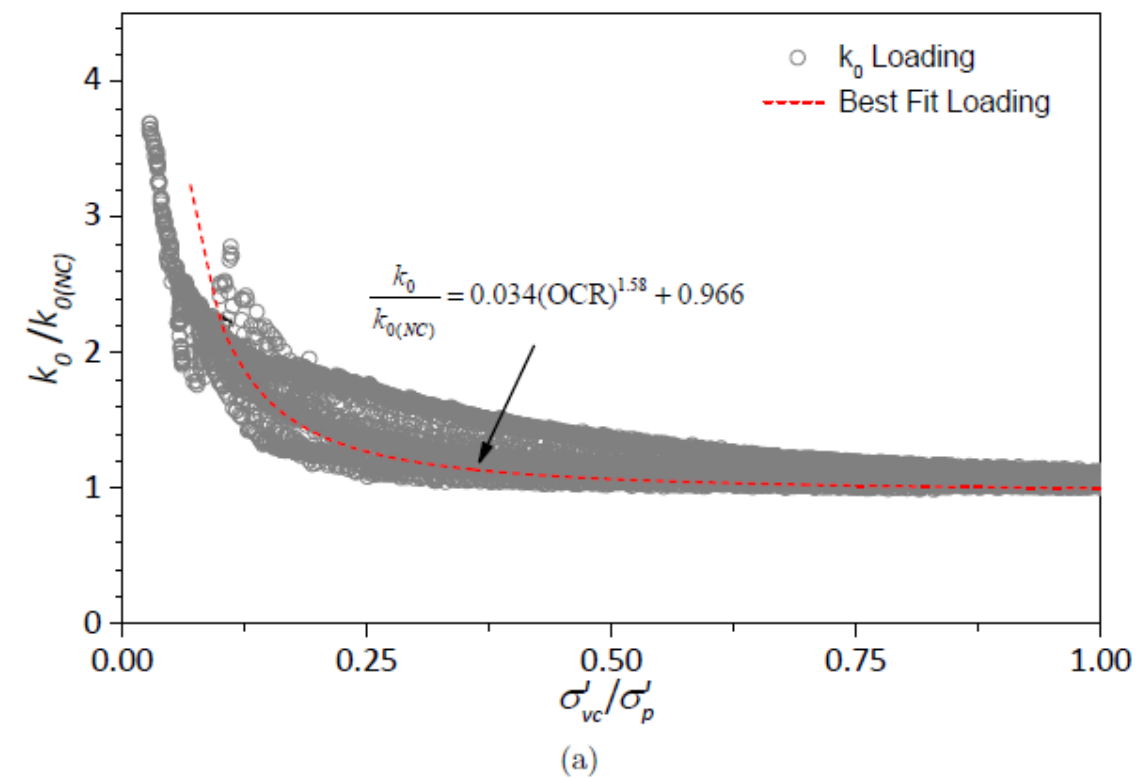


Figure 4.10. Coefficient At-Rest Response During Consolidation Stage (a) Loading and (b) Unloading

4.5 Specimen Quality

4.5.1 Shear Wave Velocity

Downhole seismic testing was performed to obtain the distribution of the shear wave velocities within the BCF deposit. Details of the downhole seismic test are presented in section 4.3.4.

In the laboratory, the shear wave velocity, V_s , of each specimen was measured with bender elements placed at top and bottom of the triaxial specimen, as described in section 3.3.1. The V_s was measured every 2 to 3 hours during the consolidation stages of each test. For specimens consolidated using SHANSEP technique, the V_s measured at the *in situ* vertical effective stress, σ'_{vo} , did not include the effect of creep. When the vertical effective stress at the-end-of-consolidation was higher than *in situ* vertical effective stress, then V_s values at σ'_{vc} are not comparable to the *in situ* measurement. The V_s measured during consolidation by recompression included the effect of creep because σ'_{vc} was the same as σ'_{vo} . Table 4.6 presents the measurements of V_s at the end of consolidation and creep. The V_s increased during creep on average of 6% due to the dissipation of excess pore water pressure and aging effects. As shown in Table 4.6, the increment of V_s after creep accounts for a small amount of the final value. With this trend, the V_s was obtained at the *in situ* vertical effective stress during the SHANSEP tests were increased by 1.06, the average value found from the recompression data in Table 4.6 to compare with the *in situ* values.

Table 4.6. Shear Wave Velocity for Specimens Prepared by Recompression Including the Creep Effect

Specimen	Elevation (m)	End Cons. V_s (m/s)	End Creep V_s (m/s)	Increment (%)
NU-1 37-39 (2)	8.84	173	183	6
NU-1 40-42 (2)	7.92	154	163	6
NU-1 42-44 (2)	7.31	114	120	5
NU-1 47-49	5.79	155	162	5
NU-1 47-49 (2)	5.79	155	164	6
NU-1 47-49 (3)	5.79	159	167	5
NU-1 60-62	1.83	155	167	8
NU-1 62-64	1.22	186	205	10
NU-1 65-67	0.30	178	187	5

Figure 4.11 presents the variation of the V_s with elevation. Figure 4.11 includes the results from downhole seismic and bender element from triaxial tests from this work and downhole and crosshole seismic tests reported by Updike et al. (1988). The V_s of each SHANSEP specimen was increased by 6%. Results of field testing were presented in section 4.3.4. It can be seen that the triaxial specimens from facies IV had V_s values about 12% less than those measured in the field. In contrast, facies III V_s values were 24% less than the field values. The V_s values from boring NU-3 were larger than those at the same elevation in the boring NU-1. Near the boundary between the facies IV and upper facies III, V_s measurements from bender elements were similar to those presented by Updike et al. (1988). For the lower facies III layer, the V_s measured at the laboratory were significantly reduced compared to the values from the field.

Clayton and Heymann (1999) suggested that the seismic measurements in the field might be used as benchmark for measurements in the laboratory. The difference in the measurements of shear modulus at small strain ($G_0 = \rho V_s^2$) can be mainly attributed to sampling disturbance. Table 4.7 presents the results of V_s measured at both locations. Comparisons between field and laboratory measurements were conducted only on the measurements performed in this project. The V_s was

reduced in average by 12.1% in specimens from facies IV. Specimens from facies III experienced a 24.3% reduction. These results showed that the highest disturbance was encountered in the specimens from facies. III where the clay was softer. Specimens from NU-3 had an average 28.3% reduction of V_s including both facies III and facies IV, while those from NU-1 were reduced by 21.4%.

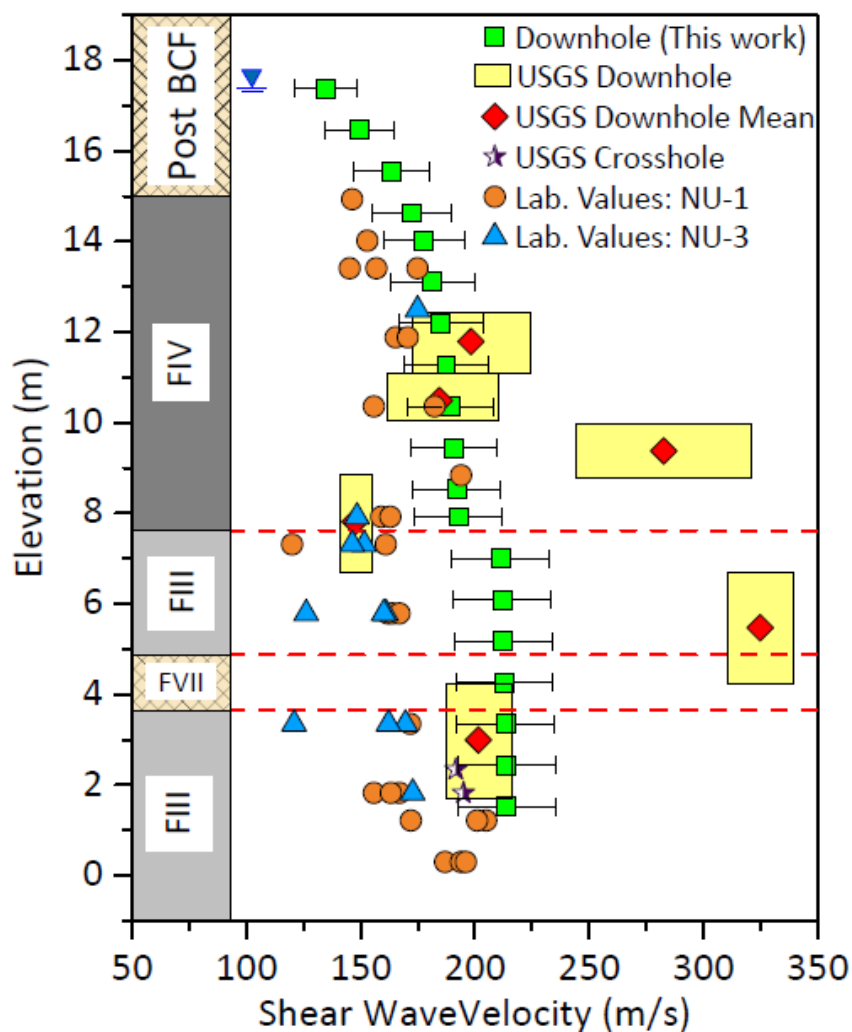


Figure 4.11. Shear Wave Velocity with Elevation

Table 4.8 summarizes the results of the shear modulus based on the laboratory and field V_s measurements. Specimens from facies III had an average 41.8% reduction of G_0 . G_0 was reduced

by 22.3% for specimens from facies IV, this means that the reduction of G_0 was about two times more for facies III than specimens from facies IV.

Table 4.7. Shear Wave Velocity from the Field and Laboratory

Specimen	Elevation (m)	F.	Lab V_s (m/s)	Field V_s (m/s)	Reduction (%)
NU-1 17-19	14.93	IV	146	172	15.0
NU-1 20-22	14.02	IV	153	178	14.1
NU-1 22-24	13.41	IV	175	182	3.9
NU-1 22-24 (2)	13.41	IV	145	182	20.2
NU-1 22-24 (3)	13.41	IV	157	182	13.8
NU-3 25-27	12.5	IV	175	185	5.5
NU-1 27-29	11.89	IV	165	188	12.0
NU-1 27-29 (2)	11.89	IV	171	188	9.2
NU-1 32-34	10.36	IV	182	189	3.5
NU-1 32-34 (3)	10.36	IV	156	189	17.6
NU-1 37-39 (2)	8.84	IV	194	192	-1.0
NU-1 40-42	7.92	IV	159	193	17.6
NU-1 40-42 (2)	7.92	IV	163	193	15.5
NU-3 40-42	7.92	IV	148	193	23.1
NU-1 42-44 (2)	7.31	III	120	211	43.1
NU-1 42-44 (3)	7.31	III	161	211	23.7
NU-3 42-44	7.31	III	152	211	28.2
NU-3 42-44 (2)	7.31	III	146	211	30.7
NU-1 47-49	5.79	III	162	212	23.6
NU-1 47-49 (2)	5.79	III	164	212	22.6
NU-1 47-49 (3)	5.79	III	167	212	21.2
NU-3 47-49	5.79	III	126	212	40.5
NU-3 47-49 (2)	5.79	III	161	212	24.0
NU-3 47-49 (3)	5.79	III	160	212	24.5
NU-1 55-57	3.35	III	172	213	19.4
NU-3 55-57	3.35	III	121	213	43.3
NU-3 55-57 (2)	3.35	III	170	213	20.4
NU-3 55-57 (3)	3.35	III	162	213	23.9
NU-1 60-62	1.83	III	167	214	22.0
NU-1 60-62 (2)	1.83	III	156	214	27.2
NU-1 60-62 (3)	1.83	III	173	214	23.7
NU-3 60-62	1.83	III	163	214	19.3
NU-1 62-64	1.22	III	205	214	4.2
NU-1 62-64 (2)	1.22	III	201	214	6.1
NU-1 62-64 (3)	1.22	III	172	214	19.6

Table 4.8. Shear Modulus from the Field and Laboratory

Specimen	Elevation (m)	F.	$G_{0(lab)}$ (MPa)	$G_{0(field)}$ (MPa)	Reduction (%)
NU-1 17-19	14.93	IV	43.7	60.4	27.6
NU-1 20-22	14.02	IV	48.7	65.9	26.1
NU-1 22-24	13.41	IV	63.6	68.9	7.7
NU-1 22-24 (2)	13.41	IV	48	75.4	36.3
NU-1 22-24 (3)	13.41	IV	56.1	75.6	25.8
NU-3 25-27	12.5	IV	65.8	73.7	10.7
NU-1 27-29	11.89	IV	56.7	73.3	22.6
NU-1 27-29 (2)	11.89	IV	63.5	77	17.5
NU-1 32-34	10.36	IV	71	76.2	6.8
NU-1 32-34 (3)	10.36	IV	50.2	73.8	32
NU-1 37-39 (2)	8.84	IV	80.6	78.9	-2.2
NU-1 40-42	7.92	IV	51.3	75.6	32.1
NU-1 40-42 (2)	7.92	IV	52.2	73.2	28.7
NU-3 40-42	7.92	IV	46.1	77.9	40.8
NU-1 42-44 (2)	7.31	III	27.4	84.7	67.7
NU-1 42-44 (3)	7.31	III	52.4	90	41.8
NU-3 42-44	7.31	III	45.1	87.3	48.3
NU-3 42-44 (2)	7.31	III	39.3	81.8	52
NU-1 47-49	5.79	III	52.5	89.9	41.6
NU-1 47-49 (2)	5.79	III	53.8	89.9	40.2
NU-1 47-49 (3)	5.79	III	44.5	71.7	37.9
NU-3 47-49	5.79	III	33.7	95.2	64.6
NU-3 47-49 (2)	5.79	III	55.4	95.9	42.2
NU-3 47-49 (3)	5.79	III	55.7	97.8	43
NU-1 55-57	3.35	III	62.6	96.3	35
NU-3 55-57	3.35	III	30.9	96	67.8
NU-3 55-57 (2)	3.35	III	61.1	96.4	36.6
NU-3 55-57 (3)	3.35	III	55.6	95.9	42
NU-1 60-62	1.83	III	59	96.8	39
NU-1 60-62 (2)	1.83	III	48.1	90.7	47
NU-1 60-62 (3)	1.83	III	59.2	101.8	41.8
NU-3 60-62	1.83	III	64.6	99.1	34.8
NU-1 62-64	1.22	III	84.9	92.5	8.2
NU-1 62-64 (2)	1.22	III	81.3	92.2	11.8
NU-1 62-64 (3)	1.22	III	59.9	92.7	35.4

4.5.2 Strain During Consolidation

The quality of the specimen can also be measured during the reconsolidation stage. For this, the axial strain, ε_a , measured at the in situ vertical effective stress is used as an assessment of specimen quality. Andersen and Kolstad (1979) and Lunne et al. (2006) proposed two different approaches

to estimate the quality of the specimen. The first approach was developed based on the ϵ_a accumulated during the reconsolidation to reach the in situ vertical effective stress. The approach proposed by Lunne et al. (2006) involved the change of the void ratio to reach the in situ vertical effective stress.

Table 4.9 presents the rating of quality for the specimens from the boring NU-1 and NU-3. From the rating proposed by Andersen and Kolstad (1979), most of the specimens from facies IV were classified as (A):“very good to excellent” or (B):“good”. The specimen from the Shelby tube NU-3 30-32 exhibited large disturbance that was not common in the material from facies IV. The reason of the low rating was that the specimen came from near the top part of the tube that generally contains the most disturbed material. From facies III, only one specimen had an (A) rating and some specimens developed high axial strain during consolidation; therefore, they were classified as (D):“poor”.

General results from the quality rating showed that specimens from facies IV experienced less disturbance than specimens from facies III. Most of the specimens from facies IV reached a “very good to excellent” while specimens from facies III in general varied from “good” to “poor”. Ratings from Table 4.9 demonstrated that the softer clay, from facies III, is more susceptible to disturbance during sampling by thin-walled tube and handling for testing. Table 4.9 also includes the reduction of V_s in percentage. When compared to the rating proposed by Lunne et al. (2006), the specimens rated as (1):“very good to excellent” had a reduction V_s lower than 20%. For ratings (2):“good to fair” and (3):“poor”, the reduction V_s had a range between 20% and 43% and no clear correlation could be established between both approaches. Similar results were obtained for the rating proposed by Andersen and Kolstad (1979).

Table 4.9. Ratings of specimen Quality

Specimen	Facies	ε_a at σ'_{vo} (%)	Quality (Andersen and Kolstad, 1979)	$\Delta e/e_o$	Quality (Lune et al., 2006)	Reduction in V_s (%)
NU-1 17-19	IV	0.39	A	0.01	(1)	15.0
NU-1 20-22	IV	0.39	A	0.01	(1)	14.1
NU-1 22-24	IV	0.34	A	0.01	(1)	3.9
NU-1 22-24 (2)	IV	0.41	A	0.01	(1)	20.2
NU-1 22-24 (3)	IV	0.28	A	0.01	(1)	13.8
NU-3 25-27	IV	0.8	A	0.02	(1)	5.5
NU-3 25-27 (2)	IV	1.4	B	0.04	(1)	.*
NU-1 27-29	IV	1.15	B	0.03	(1)	12.0
NU-1 27-29 (2)	IV	0.65	A	0.02	(1)	9.2
NU-3 30-32	IV	5	D	0.14	(4)	.*
NU-3 30-32 (2)	IV	1.3	B	0.04	(1)	.*
NU-1 32-34	IV	1.2	B	0.03	(1)	.*
NU-1 32-34 (3)	IV	1.02	B	0.03	(1)	17.6
NU-1 37-39	IV	1.2	B	0.03	(1)	.*
NU-1 37-39 (2)	IV	1.06	B	0.03	(1)	-1.0
NU-1 37-39 (3)	IV	2.36	C	0.07	(2)	.*
NU-1 40-42	IV	1.12	B	0.03	(1)	17.6
NU-1 40-42 (2)	IV	1.05	B	0.02	(1)	15.5
NU-3 40-42	IV	1.78	B	0.04	(2)	23.1
NU-1 42-44 (2)	III	2.49	C	0.06	(2)	43.1
NU-1 42-44 (3)	III	3.93	C	0.09	(3)	23.7
NU-3 42-44	III	2.06	C	0.05	(2)	28.2
NU-3 42-44 (2)	III	2.12	C	0.05	(2)	30.7
NU-1 47-49	III	1.7	B	0.04	(2)	23.6
NU-1 47-49 (2)	III	2.67	C	0.07	(2)	22.6
NU-1 47-49 (3)	III	1.34	B	0.03	(1)	21.2
NU-3 47-49	III	5.6	D	0.13	(3)	40.5
NU-3 47-49 (2)	III	4.85	D	0.12	(3)	24.0
NU-3 47-49 (3)	III	5.10	D	0.13	(3)	24.5
NU-1 55-57	III	1.79	B	0.05	(2)	19.4
NU-3 55-57	III	2.49	C	0.06	(2)	43.3
NU-3 55-57 (2)	III	4.89	D	0.12	(3)	20.4
NU-3 55-57 (3)	III	5.9	D	0.14	(3)	23.9
NU-1 60-62	III	2.22	C	0.04	(1)	22.0
NU-1 60-62 (2)	III	2.28	C	0.05	(2)	27.2
NU-1 60-62 (3)	III	2.81	C	0.06	(2)	23.7
NU-3 60-62	III	5.7	D	0.13	(3)	19.3
NU-1 62-64	III	0.65	A	0.02	(1)	4.2
NU-1 62-64 (2)	III	1.19	B	0.03	(1)	6.1
NU-1 62-64 (3)	III	1.03	B	0.03	(1)	19.6
NU-1 65-67	III	1.82	B	0.04	(2)	.**
NU-1 65-67 (2)	III	2.69	C	0.07	(3)	.**
NU-1 65-67 (3)	III	2.87	C	0.08	(3)	.**

Rating Categories Explained: Andersen and Kolstad (1979): (A) Very Good to Excellent, (B) Good, (C) Fair, (D) Poor.

Lune et al. (2006): (1) Very Good to Excellent, (2) Good to Fair, (3) Poor, (4) Very Poor.

Notes: *: No shear wave velocity was measured in the laboratory at the specimen during consolidation.

** : Shear wave velocity was not measured in the field.

Figure 4.12 presents the reduction in V_s versus (a) the axial strain at in situ stress, ε_a at σ'_{vo} , and (b) change in void ratio, $\Delta e/e_o$. The ranges used to evaluate the specimen quality are also included as proposed by Andersen and Kolstad (1979) and Lunne et al. (2006). Figure 4.12 shows as expected that most specimens from facies IV, heavily OC, had the best quality classification: “very good to excellent quality” with the smaller reductions in V_s than facies III specimens. The reduction in V_s was in most of the specimens lower than 20%. Specimens from facies III present the highest reduction in V_s and only two specimens reached “very good to excellent quality”. Reduction in V_s in most of the facies III specimens ranged from 20 to 44%. These specimens were lightly OC and generally very soft making them very susceptible to disturbance during sampling and in preparation for testing. Reduction in V_s lower than 20% essentially corresponded to the highest quality specimens based on both classifications systems (i.e. ε_a at σ'_{vo} lower than 1% or $\Delta e/e_o$ lower than 0.04). When the V_s was reduced more than 20% of the field value, the quality of the sample changes rapidly with small increments of reduction in V_s . Figure 4.12 includes the best fit for both quality classification systems. Although the coefficient of determination is low in both cases, the best fit for the change in void ratio (Lunne et al., 2006) can predict the “very good to excellent quality” when the reduction in V_s is lower than 20% (Figure 4.12b). These results showed that, values of reduction in V_s lower than 20% are a good indicator of a high-quality specimen; however, the V_s did not predict accurately sample quality when reductions in V_s exceeded 20%. Significant degradation of sample quality was apparent in these cases.

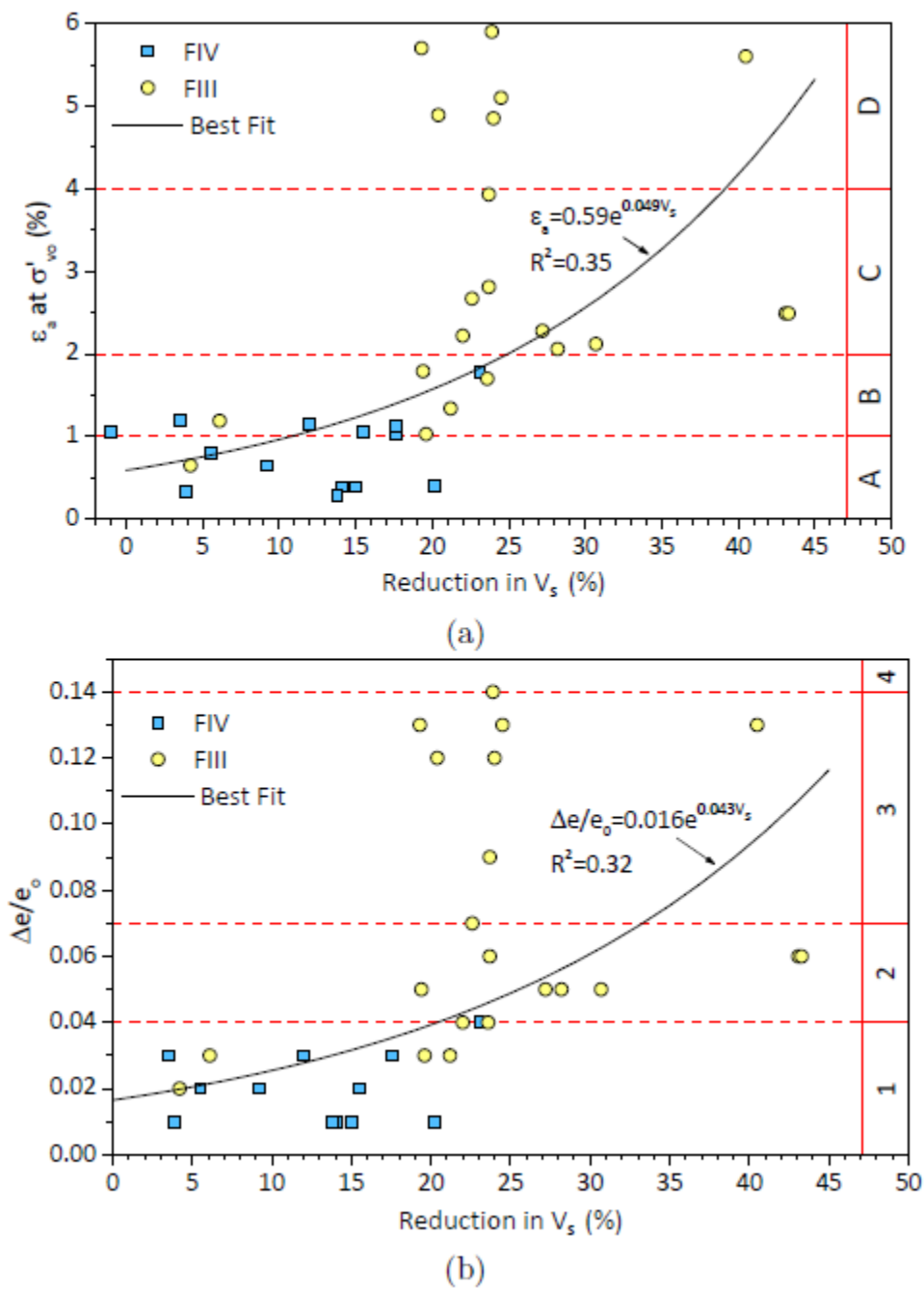


Figure 4.12. Reduction of Shear Wave Velocity versus (a) Axial Strain at in situ Stress and (b) Change in Void Ratio

4.6 Undrained Triaxial (Ck_0U TXC) Results

This section presents the response of the BCF clay to monotonic undrained triaxial compression. The undrained shearing was performed after completion of the consolidation and creep stages. The excess pore water pressure was continuously measured at the bottom of the specimen as explained in section 3.3.2. The undrained shearing was performed under displacement-controlled conditions to capture the post-peak response. Table 4.10 presents a summary of the specimens tested under monotonic conditions. Specimens were sheared at an axial strain rate of 0.5%/hr, unless noted otherwise. Normally consolidated specimens showed good to very poor sample quality by the rating proposed by Lunne et al. (2006). Overconsolidated specimens exhibited a better sample quality rating. Three of them were rated very good to excellent. Only one specimen was rated as poor. Reduction in shear wave velocities is consistent with the quality rating and the lowest reductions were obtained in specimens rated excellent to very good. Shear wave velocity was not obtained in the specimen NU-3 30-32 with the highest disturbance.

Table 4.10. Results of Monotonic Triaxial Compression Tests

Specimen	σ'_{vc} (kPa)	OCR	S_u (kPa)	Quality ⁽¹⁾	Reduction in V_s
NU-3 30-32	912	1.0	319	(4)	-
NU-3 42-44	420	1.0	124*	(2)	28.2
NU-3 42-44(2)	420	1.0	134	(2)	30.7
NU-1 40-42	153	1.63	74	(1)	17.6
NU-1 42-44(3)	159	1.51	73	(3)	23.7
NU-1 20-22	400	2.0	303	(1)	14.1
NU-1 27-29	114	3.4	105	(1)	12.0

Notes:⁽¹⁾: Sample quality by Lunne et al. (2006);

*: Sheared at strain rate of 0.1%/hr

Figure 4.13 presents the normalized stress-strain and pore water pressure-strain response of the specimens subjected to monotonic undrained shearing. Specimens were consolidated under

different vertical effective stresses and OCR. Specimens NU-3 42-44 and NU-3 42-44 (2) with OCRs of 1.0 were sheared up to approximately 2% axial strain. These specimens were part of a slow cyclic loading tests that is presented in more detail section 5.2.4. Specimen NU-3 42-44 (2) was sheared at a rate of 0.1%/hr and that may be the reason why its peak strength is lower than to the peak of NU-3 42-44 that was sheared at 0.5 %/hr. These two specimens were the only one that exhibited post-peak softening. The other four specimens reached peak strength at relatively large axial strains. The OCR for specimens consolidated by recompression were estimated from the preconsolidation stress profile given in section 4.4.1.

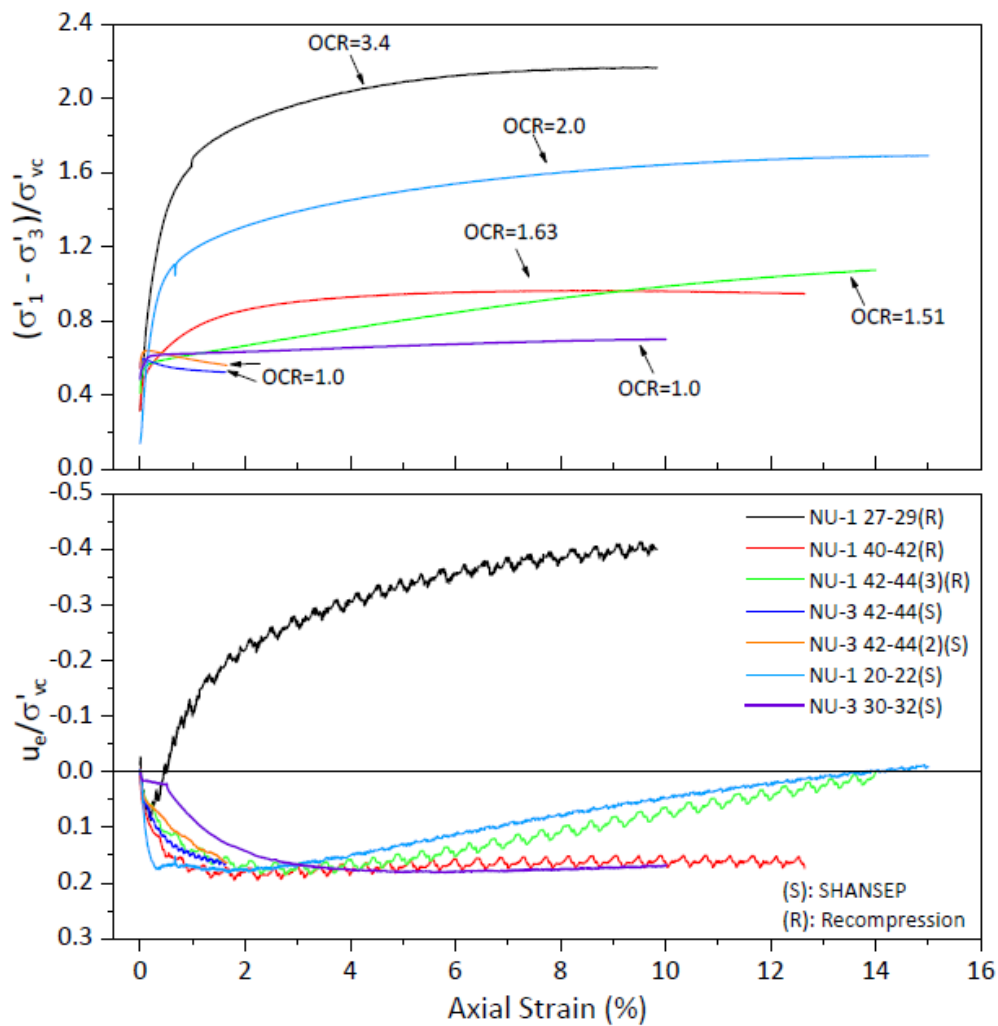


Figure 4.13. Stress-Strain Response of Monotonic Undrained Shearing

Figure 4.14 shows the normalized strength plotted against OCR. The strength was normalized by end-of-consolidation vertical effective stress and plotted versus the OCR of the specimen. The best fit was based on specimens prepared using both SHANSEP and *recompression* techniques. The OCR is estimated for the recompression specimens and thus some uncertainty exists in the reported values. The normalized strength of the BCF clay in triaxial compression can be express as:

$$(4.2) \quad S_u / \sigma'_{vc} = 0.32(OCR)^{1.04}$$

where, S_u is the undrained strength and σ'_{vc} is the vertical effective stress at the end of consolidation. Figure 4.13 also includes the trend line for triaxial compression obtained by Zapata-Medina (2012) for specimens of facies IV from the Port of Anchorage (POA). The results from Zapata-Medina (2012) included the monotonic undrained shear strength of BCF at different OCR. The normalized undrained strength of the BCF from Lynn Ary Park was similar to the BCF from POA, especially at low OCR. No trend was observed between sample quality and results of the normalized undrained strength.

The effective stress paths for representative specimens with different OCR under monotonic undrained shearing conditions are showed in Figure 4.15. For the purpose of this research the deviator, q , and the mean normal effective stress, p' , are defined as:

$$(4.3) \quad q = \sigma'_1 - \sigma'_3$$

and,

$$(4.4) \quad p' = 1/3(\sigma'_1 + \sigma'_3)$$

where, σ'_1 is the vertical effective stress and σ'_3 is the horizontal effective stress.

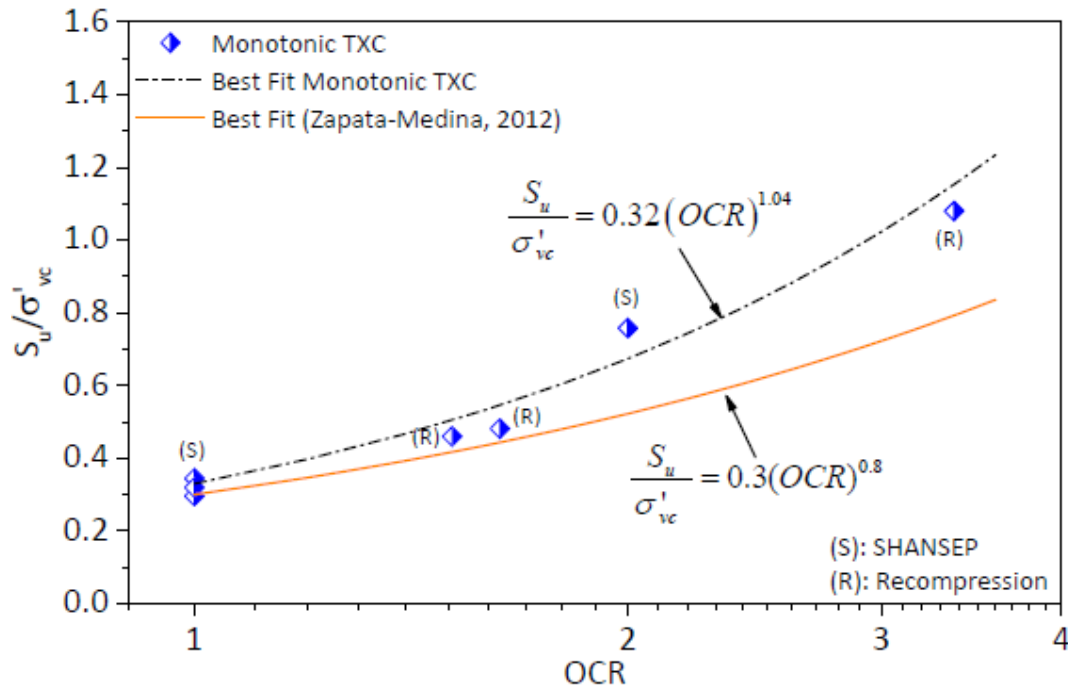


Figure 4.14. Normalized Undrained Shear Strength for Monotonic Compression

The effective stress parameters for a Mohr-coulomb failure, ϕ' and c , can be obtained from the failure line. The failure line was generated as the best fit based on the p' and q coordinates corresponding to the strength value for the NC and slightly OC specimens. The intercept was assumed zero for these specimens, therefore, the equation obtained was $q = 1.17p'$. The value of ϕ' was computed as 29° from:

$$(4.5) \quad \phi' = \sin^{-1} \left(\frac{3\eta}{6 + \eta} \right)$$

where η is the slope of the failure line in p' - q space. The ϕ' obtained in this research was similar to the $\phi' = 28^\circ$ reported by Zapata-Medina (2012) for triaxial compression of BCF material. For specimens with $OCR \geq 2.0$, the failure line was estimated by keeping the same ϕ' and moving the intercept to match the stress path at failure. For reference, Figure 4.15 includes the failure line for

the specimens with OCR of 2.0. In this case, the intercept was computed to be as 22 kPa and the cohesion, c , can be calculated as 18.7 kPa from:

$$(4.6) \quad c = a(3 - \sin \phi') / (6 \sin \phi')$$

where, a is the intercept in p' - q space.

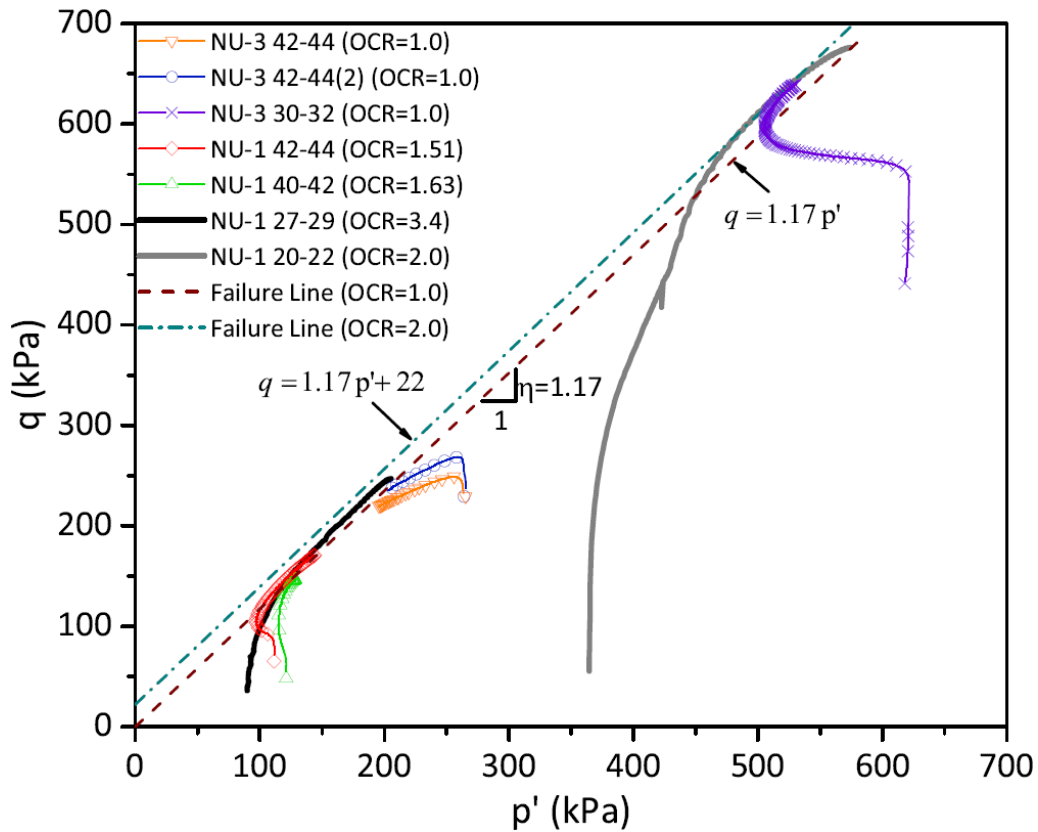


Figure 4.15. Stress Path of Monotonic Sheared specimens in p' - q Space

Three CPT probes were conducted by USGS (Updike et al., 1988) at Lynn Ary Park. From these data, one can obtain the in situ undrained strength, soil classification and sensitivity. The CPT probes reached a total depth of 30 to 45 m and were located as shown in Figure 4.1. The cone penetrometer was composed of a conical tip of 60° apex and a cylindrical sleeve above the tip. The corresponding cross sectional and sleeve area are 15 and 200 cm^2 , respectively. For the CPT test,

the undisturbed strength can be computed as:

$$(4.7) \quad S_u = (q_c - \sigma_{v0}) / N_k$$

where σ_{v0} is the total stress at the elevation of the measurement and N_k is a cone factor that varies between 11 and 19 (Lunne and Kleven, 1981). For this research, it was assumed $N_k=15$ corresponding to a direct simple shear mode of failure (Loehr et al., 2016). Updike et al. (1988) assumed $N_k=16$ in their work.

Additionally, the in situ undrained strength was obtained from the Northwestern University field vane (FV) results completed during the field investigation in this project. The tests were performed every 0.6 to 1.2 m whenever fine grained soil was encountered in the boring. The FV tests were conducted according to the ASTM D2573/D2573M-15 standard requirements (ASTM International, 2015b). The results are summarized in Table 4.11. The FV results provided a range of S_t from 2 to 6. For facies IV, the maximum S_t was 4 and the average was 3. For facies III, the maximum S_t was 6 and the average of 3.

Table 4.11. Results of Field Vane Test

Elevation (m)	S_u (kPa)	S_{ur} (kPa)	S_t
13.53	247	87	2.9
12.77	198	49	4
12	148	44	3.4
10.43	271	13	3
8.94	111	93	1.8
8.14	104	61	3.1
7.26	61	35	4.6
6.61	60	14	5
5.7	58	12	6.4
2.96	55	9	3.6
2.02	68	16	2.5
1.32	31	28	1.7
0.52	21	18	1.8

Figure 4.16a presents the results of the undrained strength, S_u , from the CPT, FV, and monotonic triaxial compression tests (TXC) consolidated by recompression. From the field tests, S_u decreased with depth in the same way OCR decreased with depth in Figure 4.9b. For facies III, the S_u remained approximately constant with depth. CPT and FV results had a similar general trend for the facies III and IV layers.

Laboratory test results followed a similar trend with the field measurements. The specimens from the shallow depth of facies IV were similar to CPT and FV results, only one test result was considerably lower than the FV strength (Figure 4.16a). The normalized triaxial compression strength of the BCF clay in Equation 4.2 was computed by using the trendline of the OCR presented in Figure 4.9b. It predicts a higher undrained strength for the facies III layers, as one would expect for a compression mode of shearing as compared to FV or CPT found using a N_k of 15, representative of direct simple shear mode of shearing. The trend represents a reasonable lower bound for the field tests in the facies IV layer. In the upper portions of facies IV, the relative low values likely reflect the variable OCR representative of a desiccated crust layer.

Figure 4.16b presents the side resistance, f_s , and the remolded undrained strength, S_{ur} , from CPT and FV tests, respectively. As a cone passes a given elevation, large deformations occur and disturbance of the soil results as shown by Baligh (1985). The disturbance should be reflected in the f_s . For the CPT, Lunne and Powell (1997) and Farrar et al. (2008) showed that the values of the side resistance, f_s , were similar to the remolded undrained strength, S_{ur} , for fine-grained soils. The remolded FV data agree reasonably well with the f_s from the CPT results.

Values of f_s were at least 20 kPa in the lower part of the facies III stratum. This is significant because Updike et al. (1988) reported, based on torvane tests on specimens recovered from borings

B-3 and B-5 from the same area (Figure 4.1), the presence of clay with zero-strength at elevations between 2 to 7.5 m. Results presented in Figure 4.16b clearly showed remolded shear strengths between 10 to 30 kPa at these elevations.

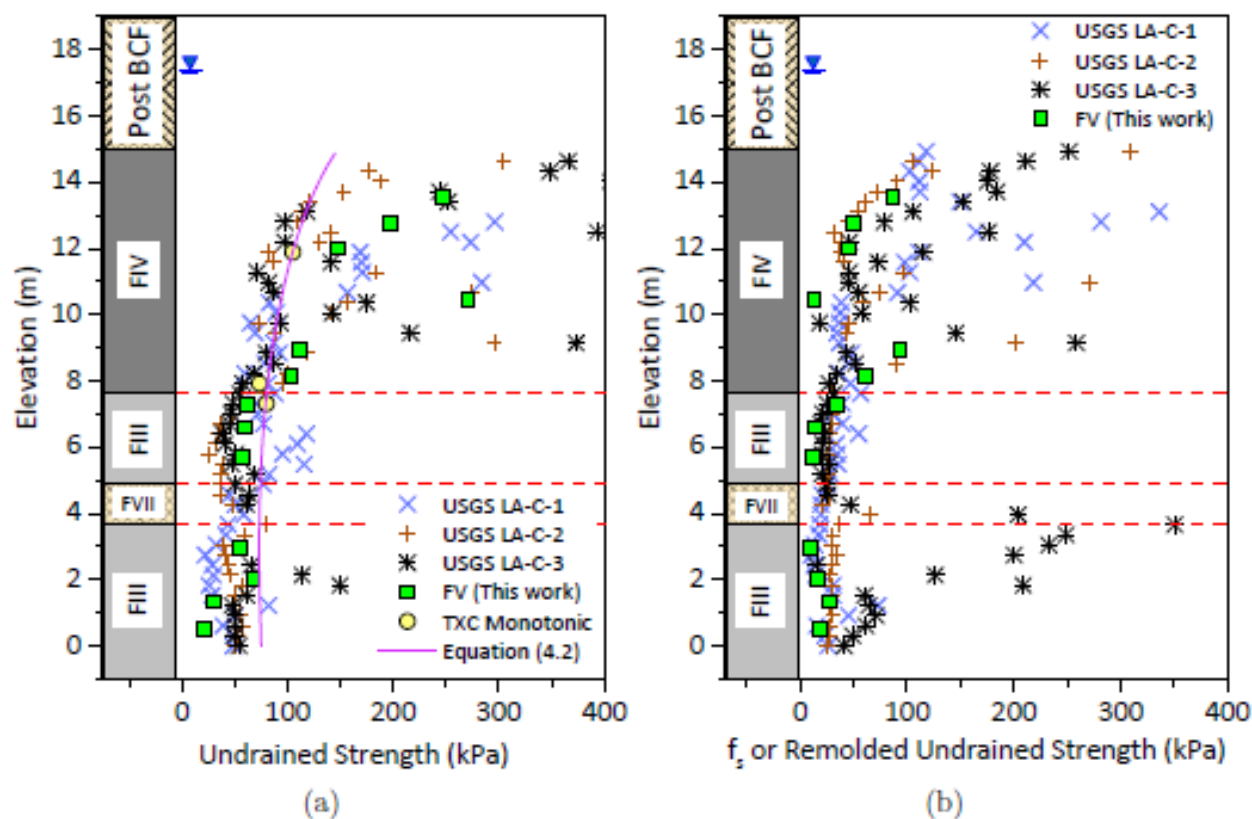


Figure 4.16. CPT, FV, and TXC Results: (a) Undisturbed Undrained Strength (b) Side

Resistance or Remolded Undrained Strength

4.7 Sensitivity

4.7.1 Soil Classification and Sensitivity Based on CPT Normalized Soil Behavior Type (SBTn) Chart

Soil classification based on the CPT data presented by Updike et al. (1988) is shown in Figure 4.17. For this purpose, the normalized soil behavior type (SBTn) chart introduced by Robertson (1990) was utilized to classify the soil and to estimate the sensitivity of the material. The CPT data

shown was taken above the elevation 0 m MSL to be comparable with the maximum depth of the soil exploration performed by Northwestern University. To use the (SBTn) chart (Robertson, 1990), it was assumed that the cone resistance, q_c , was equal to the total cone resistance, q_t , since no pore pressure measurements were obtained by USGS. The total cone resistance is expressed as:

$$(4.8) \quad q_t = q_c + u_2(1 - a)$$

where u_2 is total pressure, $a = d^2/D^2$, d is the diameter of the load cell, and D is the diameter of the cone. According to Robertson (1990), the use of q_c data creates an error in lower part of the SBTn chart where the normalized cone resistance, Q_t , is less than 10. This error affects mainly the estimation of sensitivity and OCR. Results showed that most of the data fell into the soil types 3 and 4. The data from the shallower part of the deposit (facies IV), had higher OCR than the facies III data consistent with the OCR trends shown in Figure 4.9. Some data points from facies IV and upper facies III fell into the soil type 5 (sand mixtures-silty sand to sandy silt), these correspond to the presence of silty sand lenses and thin layer located at elevations about 9 m. A silty sand thin layer was found in the boring NU-3 at the similar elevation (see section 4.3.2). Note that no CPT data falls within Zone 1, the location in the chart for sensitive, fine grained soils; however recall that no pore pressure measurements were made and thus the normalized cone resistance would be lower and normalized friction ratio would be higher if positive pore water pressures were generated, as expect for the normally to lightly overconsolidated facies III soils.

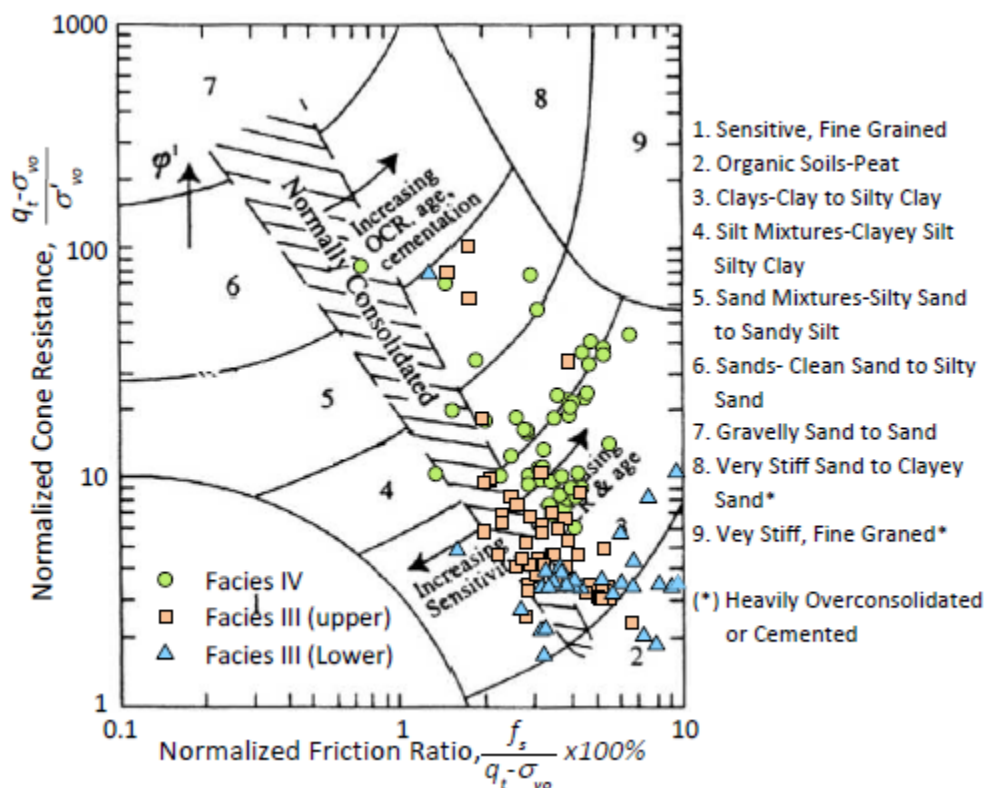


Figure 4.17. Soil Classification Chart for BCF material (Adapted from Robertson (1990))

The sensitivity, S_t , can be computed by using the procedure described by Robertson (2009). The procedure uses the SBTn chart (Robertson, 1990) and is based on a normalized undrained strength of $S_u/\sigma'_{vo} = 0.22$ (average for direct simple shear) and N_k equal to 14. The N_k value is close to the one used by Updike et al. (1988) ($N_k=16$) and in this work ($N_k=15$). Robertson (2009) proposed that the sensitivity can be express as:

$$(4.9) \quad S_t = S_u/S_{ur} = 7.1/F_r$$

where, F_r is the normalized friction ratio. The constant in Equation 4.9 varies between 5 to 10 with an average of 7.1 (Robertson, 2009).

Figure 4.18 shows the SBTn chart including the S_{ur}/σ'_{vo} contours and the sensitivity

associated with them. The sensitivity increases towards region 1, corresponding to “sensitive, fine grained” soil, in Figure 4.17. The data indicated that S_t for the facies III (upper and lower layers) was about 2. Some data points reached a S_t of 5, the maximum sensitivity value obtained based on the CPT data analyzed by the Robertson (2009) procedure. It is recognized that the sensitivity can be different since the pore water pressure was not measured during the CPT testing. The results of the CPT and FV provide a powerful indication that the soil at Lynn Ary Park is not as sensitive as found in other studies (Shannon and Wilson Inc., 1964; Mitchell, 1973).

4.7.2 Sensitivity Analysis

Updike et al. (1988) presented an analysis of the sensitivity based on the “undisturbed” strength, S_u , obtained on tube specimens by pocket penetrometer and torvanes and by results of CPT. Figure 4.19 shows the interpreted S_u from Updike et al. (1988) and that obtained in this research. The S_u from triaxial compression based on the SHANSEP approach (Equation 4.2) is shown for comparison.

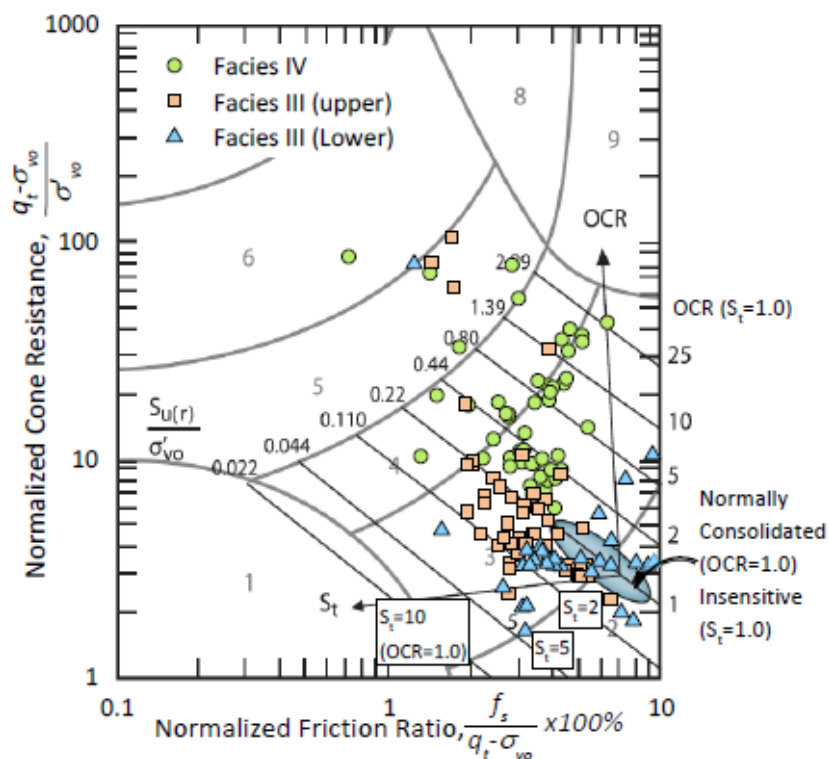


Figure 4.18. Soil Classification Chart for BCF material (Adapted from Robertson (2009))

Updike et al. (1988) recognized that the zones with “zero-strength” (elevation 2.0-7.5 m) were not a result of low in situ strength, but likely reflected the disturbance and high sensitivities of the facies III clay. The CPT results (Updike et al., 1988) and FV performed in this this work did not corroborate the “zero-strength zone”. Updike et al. (1988) used the normalized strength profiles developed for sensitive Norwegian marine clays, presented by Houston and Mitchell (1971), to estimate the S_t of the BCF clay. These relations also are shown on Figure 4.19. The correlation was developed for NC clay, and it is strictly applicable to the soft facies III soils. The S_t estimated by this approach was as high as 1000 for the facies III layers.

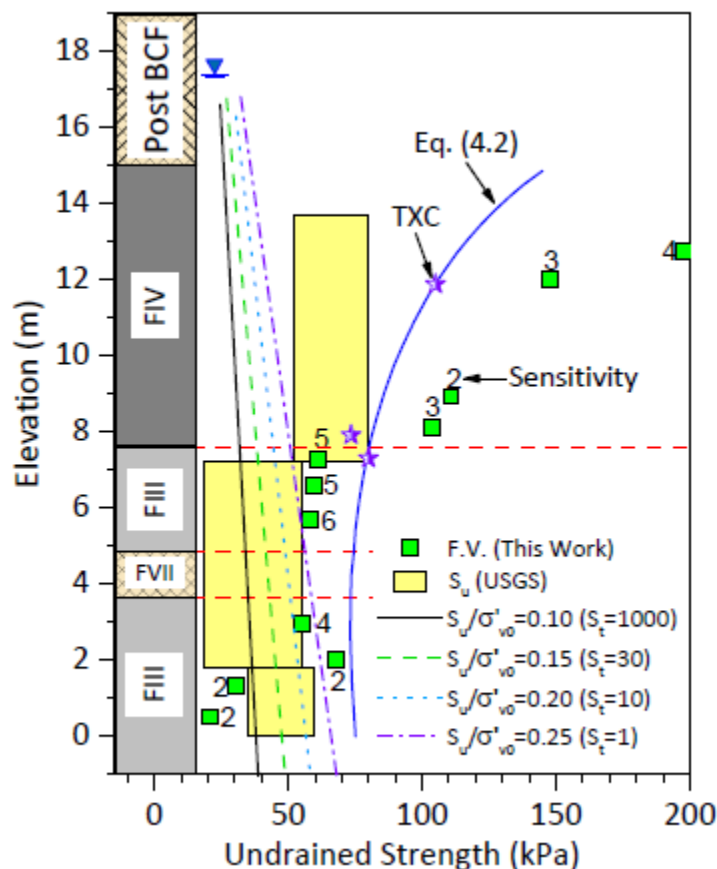


Figure 4.19. Undisturbed Strength after Updike et al. (1988) and in this Research

The two low values of FV near elevation 1 MSL are likely the result of the driller allowing the NX rods to rest on the bottom of the boreholes prior to each test; in these two cases, the rods sank under their own weight, thereby disturbing the soil around the vanes and thus leading to low values of the “undisturbed” strength. Note that the remolded values measured in these two tests were similar to the other values in that zone and thus had very low values of S_t . Therefore the trends of the FV data suggested S_u/σ'_{vc} values were about 0.25. These are lower than the triaxial compression found in the laboratory via SHANSEP procedures and noted by the curved (Equation 4.2) in Figure 4.19. Given that, N_k was taken as 15, representative of DSS strength, these trends are consistent with other lightly OC clays with similar index properties, e.g. Boston Blue Clay

(Ladd and Lambe, 1964) and Chicago clay (Finno and Chung, 1992).

Figure 4.20 presents the results of S_t from CPT, torvane, and FV tests. CPT-based S_t , computed as the ratio between S_u (from q_c , Equation 4.7) and S_{ur} (equal to f_s), exhibited an approximately constant $S_t=2$ for facies III and facies IV. These values differed significantly from the estimation of S_t reported by Updike et al. (1988) since the authors considered f_s as an intermediate strength between the S_u and the S_{ur} and used the correlations proposed for Norwegian marine clays as explained above. Note that S_t from LA-C-3 displayed values lower than 1.0. Based on the approach used in this work, f_s is taken as equal to the S_{ur} and then S_{ur} was higher than the S_u based on q_c data on Equation 4.7. This discrepancy in the measurement can be a result of the assumption made to estimate the S_u (from the q_c) and S_{ur} (equal to f_s) from the CPT test and possibly disturbance in the ground around the cone.

The torvane data reported by Updike et al. (1988) suggested values of S_t that agreed with the approach assumed for CPT data in this work and the results from the FV. At this location, the BCF clay had a S_t as high as 7 for facies III. Results from torvane tests also indicated that the BCF clay at Lynn Ary Park is not quick, according to the classification proposed by Skempton and Northey (1952) and Shannon and Wilson Inc. (1964), respectively.

As can be seen in Figure 4.2, the S_t values from the FV from Northwestern University were lower than those based on FV results presented by Shannon and Wilson (1964) where the maximum S_t was approximately equal to 12. The location of the FV (CSH1) conducted by Shannon and Wilson (1964) is shown in Figure 4.1 and is about 150 m from the Northwestern University test site. It also was below base of the head scarp of the slides. The difference in the results likely reflects natural variability of the material. In general, the S_t values from of Shannon and Wilson

(1964) and Northwestern University, and the approach used herein to interpret the CPT tests performed by (Updike et al., 1988) agreed in the small area tested within Lynn Ary Park. The BCF clay at this location is not as sensitive as indicated by (Updike et al., 1988) with S_t values ranging between 2 and 7 based on CPT, FV, and torvane test results.

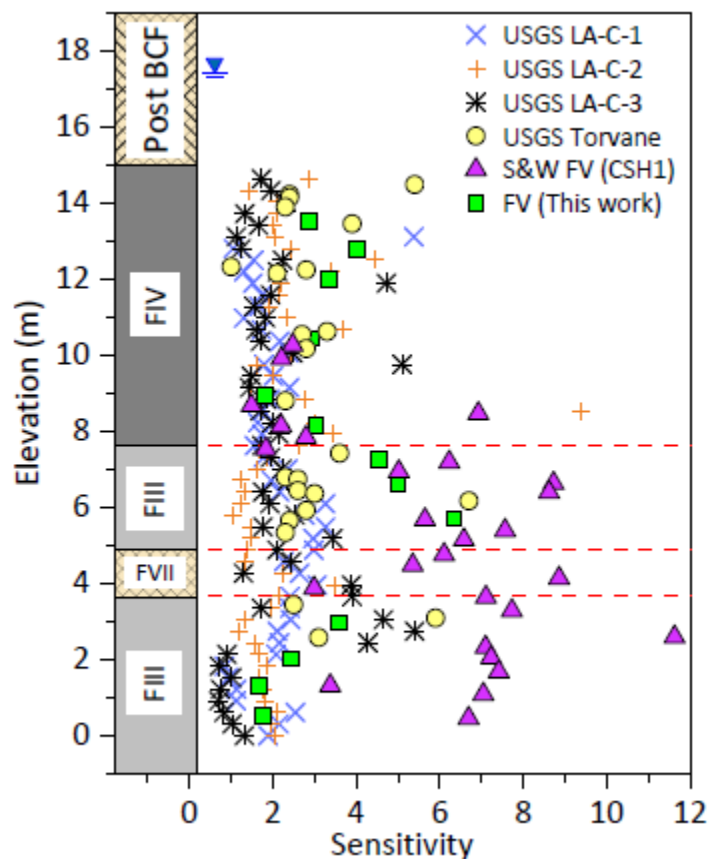


Figure 4.20. Sensitivity Distribution of the BCF Clay

4.8 Summary and Conclusions

This chapter presents the field and portions of the laboratory investigation performed by Northwestern University at Lynn Ary Park adjacent to the Turnagain Heights landslide escarpment. The field exploration consisted of drilling three borings, two of which were used to obtain thin-walled samples for subsequent laboratory testing and one was used to perform field

vane tests. The field vane test results were used to establish the in situ undrained strength and sensitivity of the BCF clay. The field work also included down-hole seismic tests to measure the in-situ shear wave velocity. The information presented by Updike et al. (1988) and (Shannon and Wilson Inc., 1964) was analyzed to help to develop stratigraphy and water table location.

Samples recovered at Lynn Ary Park were used for laboratory testing at Northwestern University. The laboratory data included index properties such as water content, Atterberg limits, specific gravity, and void ratio, consolidation and monotonic undrained triaxial compression tests.

Results obtained in this research were compared to those from the same site presented by Updike et al. (1988) and (Shannon and Wilson Inc., 1964). CPT results presented by (Updike et al., 1988) were analyzed to establish the undrained in situ strength, classification, and sensitivity of the BCF clay by using the SBTn proposed by Robertson (1990). In addition to the undrained strength of the material, in situ and laboratory shear wave velocities were measured to obtain G_o values at the site. The shear wave velocity was also used as an approach to estimate the quality of the specimens taken from Lynn Ary Park. From this chapter the following conclusions can be drawn:

1. The soil profile at Lynn Ary Park consists of an approximately 6 m thick surficial granular soil, geologically called the Naptowne outwash. The BCF is found below the outwash and extended to the bottom of the field investigation conducted as part of this work. A stiff clay (facies IV) lies directly beneath the outwash and is interbedded with silty sand lenses up to depth of 12 m (El. 8.4 m). Underlying the stiff clay, there is a wet medium stiff to soft clay (facies III). The medium to soft clay extends up to the bottom of the boring at 20.4 m (El. 0 m); however, the continuity of this clay layer is interrupted at an approximately 15 m (El.

5.4 m) depth by a 0.6 m thick layer of medium dense fine sand. The water table at the time of the Northwestern field work was located 3.6 m (El. 16.8 m) below the ground surface.

2. Atterberg limits indicated the facies III and IV of BCF clay are a low plasticity clay (CL) with similar liquid and plastic limits. Because of the higher natural water contents found in the facies III clays, the average liquidity index was 0.8 for facies III compared to 0.50 from facies IV. Liquidity indexes as high as 1.5 occasionally were found in facies III.
3. Consolidation test results indicated that OCR decreased with depth, presumably as a result of desiccation. The OCR in facies III decreased from 1.8 at the top of the stratum to 1.03 at elevation 0 m.
4. The SHANSEP parameters α and m in the normalized undrained triaxial compression strength were 0.32 and 1.04, respectively. Specimens used to determine this relation were from both facies III and IV. Zapata-Medina (2012) reported values of 0.3 and 0.8 for the same shearing mode of BCF clay specimens from facies IV at the Port of Anchorage. The drained stress friction angle, ϕ' , based on results on triaxial compression tests on normally consolidated specimens, was 29° .
5. Undrained strength from CPT and field vane tests generally decreased with depth consistent with the observation that OCR decreased with depth.
6. When the CPT results were plotted in the normalized soil behavior type (SBT_n) chart (Robertson, 1990), most of data indicated soil type 3 (clay to silty clay). The facies IV data indicated that the layer was overconsolidated whereas that from facies III was typically normally consolidated. No data from facies III, which was deemed sensitive by USGS, plotted as soil type 1 a sensitive, fine grained soil. CPT results plotted in an updated SBT_n chart that included sensitivity contours (Robertson, 2009) indicated that the sensitivity of

the clays was less than or equal to 5. Note that no pore pressure measurements were made during CPT testing and thus results from use of the SBTn charts are approximate.

7. Results from the field vane conducted by Northwestern University indicated that the sensitivity of the facies III stratum varied between 2 and 6 with the highest sensitivity near the sand layer in facies III. These findings agreed with the results presented by Shannon and Wilson Inc. (1964). However, the maximum sensitivity obtained by Updike et al. (1988) was obtained in the middle of the facies III layer.

CHAPTER 5

**5 RESULTS OF CYCLIC LOADING AND POST-CYCLIC UNDRAINED SHEARING
OF BCF CLAY**

5.1 Introduction

This chapter presents the results and analyses of the cyclic and post-cyclic responses of the Bootlegger Cove Formation (BCF) clay. The analyses focus on the behavior of the BCF clay under equivalent earthquake loadings. Both undrained cyclic and post-cyclic strength are evaluated with respect to stress history and liquidity index. A mechanistic hypothesis regarding the nature of the clay degradation is proposed.

The effects of the type of consolidation prior to cyclic loading, either SHANSEP or *recompression*, are evaluated to determine their influence on cyclic strength, strain accumulation, and stiffness degradation. The BCF specimens were tested under stress-controlled cyclic loading with different cyclic stress ratios (CSR). The cyclic loading consisted of a sinusoidal load applied to the specimen until collapse occurred, axial strain of 5% was reached (i.e. the strain-based failure criterion) or a maximum number of cycles was reached without failure.

The degradation of undrained shear strength directly is evaluated based on the results of post-cyclic undrained shearing. This degradation is presented as a function of the accumulated strain during the consolidation and cyclic loading or during cyclic loading only, accumulated pore water pressure and strain energy. The role of sensitivity, as quantify by the liquidity index, and the axial strain failure criteria are assessed. The hypothesis of this work is that the degradation of clay specimens during post-cyclic shearing is related to the degradation of the structure, represented by the apparent cohesion of the BCF clays. The Appendix B contains plots of all cyclic and post-cyclic tests conducted as part of this thesis and photos of failed specimens.

Figure 5.1 presents an idealized sketch of the effective stress path of a specimen during cyclic and post-cyclic shearing. Each specimen was consolidated to a desired effective stress and

allowed to creep under drained conditions and constant total stress so that excess pore water pressure was equal to zero at the start of cyclic loading. Specimens were subjected to cyclic loading under a certain number of cycles up to failure (i.e. 5% accumulated axial strain, see section 3.4.7) or the maximum number of cycles (i.e. 171 cycles) indicated by (1) in the Figure. After cyclic loading, some specimens were subjected to an equalization period under undrained conditions to allow excess pore water pressure to equalize, (2) in the Figure. This waiting period permits an accurate measurement of the equalized pore water pressure at the end of cyclic loading. If a specimen did not collapse during cyclic loading, an undrained post-cyclic shearing stage was imposed, (3) in the Figure. For some specimens, stage (2) did not occur and the post-cyclic shearing (3) started at the end of stage (1). One could argue that this latter procedure better represents field conditions just after the earthquake shaking has stopped, but the interpretation of the subsequent result is inherently limited by the presence of non-uniform pore water pressure within the specimen.

5.2 Results of Cyclic Loading

This section focuses on the evaluation of the results during cyclic loading for the BCF clay. The stress-strain and pore pressure-strain responses are presented. An evaluation of the cyclic strength and stiffness degradation as a function of OCR is presented. The effect of the rate of shearing is evaluated briefly to illustrate the impact of material rate effects.

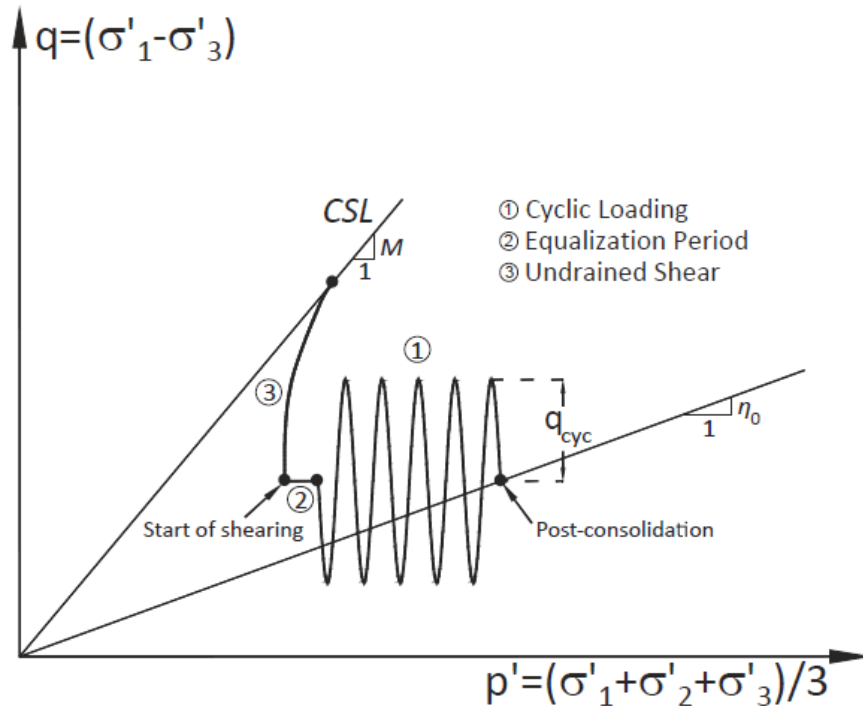


Figure 5.1. Idealized Stress Path of a specimen Subjected to Cyclic Loading and Post-Cyclic Shearing

Table 5.1 and Table 5.2 present summaries of the results of the specimens tested under cyclic loading and post-cyclic shearing for specimens consolidated by the SHANSEP and *recompression* techniques, respectively. Cyclic loading varied with respect to CSR and frequency, although most tests were conducted at a frequency of 1 Hz. Axial strain and pore water pressure accumulated at the end of the cyclic loading are tabulated. The number of cycles to failure are given as both the number of cycles to reach 5% axial strain during cyclic loading and the total number of cycles applied to the specimen (if different). Undrained post-cyclic strength and normalized strength also are given in Table 5.1 and Table 5.2.

Table 5.1. Results of Cyclic Loading and Post-Cyclic Shearing (SHANSEP)

Specimen	El. (<i>m</i>)	Tech.	σ'_{vc} (<i>kPa</i>)	OCR_{test}	f (<i>Hz</i>)	CSR	ε_{acons} (%)	ε_{acyc} (%)	ε_{eq} (%)	$U_{e(cyc)}$ (<i>kPa</i>)	$U_{e(eq)}$ (<i>kPa</i>)	N	σ'_{vcyc} (<i>kPa</i>)	σ'_{hcyt} (<i>kPa</i>)	S_u (<i>kPa</i>)	S_u/σ'_{vc}
NU-1 17-19	14.94	SHANSEP	605	1	1	0.25	3.32	8.55	0.02	120.3	68.2	10	537	207	216	0.36
NU-1 22-24	13.41	SHANSEP	400	2	1	0.30	3.04	7.15	-	54.6	-	41	350	228	-	-
NU-1 22-24 (2)	13.41	SHANSEP	400	2	1	0.25	2.77	0.30	0.05	82.6	168.0	100	228	147	244.3	0.61
NU-1 22-24 (3)	13.41	SHANSEP	400	2	1	0.35	3.16	4.53	0.03	106.3	193.7	23	266	148	191.2	0.48
NU-1 27-29 (2)	11.89	SHANSEP	114	3.3	0.01	0.30	1.79	-0.62	-	42.6	-	40	71	48	114	1.00
NU-1 32-34 (3)	10.36	SHANSEP	394	1	1	0.30	5.23	27.5	-	10.5	-	3(18)	393	138	-	-
NU-1 55-57	3.35	SHANSEP	213	2	1	0.20	3.32	-0.03	-	25.7	-	171	187	137	166	0.78
NU-1 60-62 (2)	1.83	SHANSEP	407	1	1	0.25	5.10	12.82	-	14.5	-	3(4)	379	220	78.6	0.19
NU-1 60-62 (3)	1.83	SHANSEP	410	1	1	0.20	4.92	5.75	0.00	49.1	128.0	12(13)	282	122	126.3	0.31
NU-1 65-67 (2)	0.30	SHANSEP	410	1	1	0.225	4.67	5.54	0.03	131.1	149.4	12(13)	261	88	141.6	0.35
NU-1 65-67 (3)	0.30	SHANSEP	400	1	1	0.225	4.40	18.03	0.005	132.4	139.8	11(100)	280	99	-	-
NU-3 25-27	12.5	SHANSEP	119	3.15	1	0.30	2.06	-0.29	-	2.7	-	40	116.3	98	135.9	1.14
NU-3 40-42	7.92	SHANSEP	420	1	1	0.30	4.90	22.48	-	23.6	-	3(9)	409.38	181.48	-	-
NU-3 47-49	5.79	SHANSEP	342	1	1	0.20	6.82	8.74	-	71.2	-	12(15)	253	100	108.6	0.32
NU-3 47-49 (2)	5.79	SHANSEP	324	1	1	0.15	6.74	3.99	-	77.2	-	40	224	98	112	0.35
NU-3 47-49 (3)	5.79	SHANSEP	367	1	1	0.175	7.18	5.87	-	72.1	-	29	295	114	126.8	0.35
NU-3 55-57	3.35	SHANSEP	389	1	1	0.20	4.05	6.82	-	53.0	-	26(31)	294	117	129.8	0.33
NU-3 55-57 (2)	3.35	SHANSEP	345	1	1	0.25	6.55	11.78	-	105.0	-	4(9)	240	95	135.5	0.39
NU-3 55-57 (3)	3.35	SHANSEP	346	1	1	0.25	8.36	9.81	-	57.0	-	3(4)	222	75	61.4(E)	0.18(E)
NU-3 60-62	1.83	SHANSEP	270	1	1	0.175	5.91	6.91	-	20.0	-	36(40)	226	115	87.5	0.32

El. =Elevation, σ'_{vc} = Vertical effective stress at end of consolidation, σ'_{vcyc} = Vertical effective stress at end of cyclic loading,
 σ'_{hcyt} = Horizontal effective stress at end of cyclic loading, ε_{acons} = Axial strain at end of consolidation,
 ε_{acyc} = Axial strain at end of cyclic loading, ε_{eq} = Axial Strain at end of equalization,
 $U_{e(cyc)}$ = Excess pore water pressure at the end of cyclic loading, $U_{e(eq)}$ = Excess pore water pressure during equalization,
N =Number of cycles to 5% axial strain and total number of cycles, (*E*) = Triaxial Extension

Table 5.2. Results of Cyclic Loading and Post-Cyclic Shearing (Recompression)

Specimen	El. (m)	Tech.	σ'_{vc} (kPa)	OCR_{test}	f (Hz)	CSR	ε_{cons} (%)	ε_{acyc} (%)	ε_{eq} (%)	$U_{e(cyc)}$ (kPa)	$U_{e(eq)}$ (kPa)	N	σ'_{vcyc} (kPa)	σ'_{hcyg} (kPa)	S_u (kPa)	S_u/σ'_{vc}
NU-1 37-39 (2)	8.84	Recomp.	144	1.77	1	0.30	1.07	0.77	-	38.2	-	40	106	60	135.6	0.94
NU-1 40-42 (2)	7.92	Recomp.	153	1.63	1	0.30	1.15	2.47	-	40	-	40	97	46	47.3 (E)	0.31 (E)
NU-1 42-44 (2)	7.31	Recomp.	159	1.51	1	0.30	2.70	30.00	-	30	-	13(40)	122	56	-	-
NU-1 47-49	5.79	Recomp.	174	1.35	1	0.20	1.84	2.91	-	33.8	-	40	129	49	56	0.32
NU-1 47-49 (2)	5.79	Recomp.	174	1.35	0.1	0.25	2.83	4.87	-	17.3	-	12(12)	103	22	70	0.4
NU-1 47-49 (3)	5.79	Recomp.	174	1.35	1	0.20	1.34	4.18	-	46.7	-	82	139	58	-	-
NU-1 60-62	1.83	Recomp.	221	1.08	1	0.20	2.61	9.69	-	42.0	-	49(50)	175	106	52.7	0.24
NU-1 62-64	1.22	Recomp.	219	1.05	1	0.20	0.82	10.00	-	50.0	-	160(170)	161	74	-	-
NU-1 62-64 (2)	1.22	Recomp.	219	1.05	1	0.25	1.40	4.83	0.23	36.8	70.0	18	173	74	-	-
NU-1 62-64 (3)	1.22	Recomp.	219	1.05	1	0.225	1.25	4.31	-0.01	80.4	77.2	48	142	65	101.7	0.46
NU-1 65-67	0.30	Recomp.	228	1.03	1	0.225	2.09	5.49	0.01	83.6	101.6	43(44)	145	48	98.3	0.43

$El.$ =Elevation, σ'_{vc} = Vertical effective stress at end of consolidation, σ'_{vcyc} = Vertical effective stress at end of cyclic loading,
 σ'_{hcyg} = Horizontal effective stress at end of cyclic loading, ε_{acons} = Axial strain at end of consolidation,
 ε_{acyc} = Axial strain at end of cyclic loading, ε_{eq} = Axial Strain at end of equalization,
 $U_{e(cyc)}$ = Excess pore water pressure at the end of cyclic loading, $U_{e(eq)}$ = Excess pore water pressure during equalization,
 N =Number of cycles to 5% axial strain and total number of cycles, (E) = Triaxial Extension

5.2.1 Cyclic Responses of Clay Specimens

Figure 5.2 shows the stress-strain response of three specimens prepared with different OCR and subjected to cyclic loading. The CSR in each test was the same to illustrate the effects of the OCR on the cyclic response. The NC and lightly OC specimens shown in (a) and (b) reached failure at 26 and 49 cycles, respectively. Specimen prepared with $OCR=2.0$, shown in (c), did not fail, and accumulated small axial tensile strain. This outcome was presumably the result of the much larger strength of the OC specimen when subjected to cyclic loading. The results clearly showed that the same CSR created significantly more axial strain in NC specimens. In general, the accumulation of axial strain decreased with OCR.

The degradation of secant stiffness also is illustrated in Figure 5.2 and has been tabulated for each specimen in Table 5.3. The secant stiffness was calculated from the maximum and minimum shear stresses and corresponding strain at every cycle. For the specimens (a) and (b) the initial secant stiffness degraded about 60% and 51%, respectively, at the last cycle with respect to the first cycle. For specimen (c), the degradation of secant stiffness was 60%. Table 5.3 shows degradation of stiffness varied from 0.80 to 0.09. Only Specimen NU-1 47-49(2) showed a qualitatively different response; the specimen exhibited high strain during the first loading followed by stiffer responses in subsequent cycles (see Appendix B). This specimen was cyclically loaded at 0.01Hz and at $CSR=0.25$, the combination of high CSR and a low frequency could explain the weak response at the first loading. From Table 5.3, a relation between the degradation of secant stiffness and OCR could not be established. However, more degradation occurred in specimens subjected to larger CSR values.

Table 5.3. Results of Stiffness Degradation

Specimen	El. (m)	Tech.	σ'_{vc} (kPa)	OCR_{test}	f (Hz)	CSR	N	$G_{sec(i)} / G_{sec(f)}$
NU-1 17-19	14.94	SHANSEP	605	1	1	0.25	10	0.51
NU-1 22-24	13.41	SHANSEP	400	2	1	0.30	41	0.24
NU-1 22-24 (2)	13.41	SHANSEP	400	2	1	0.25	100	0.19
NU-1 22-24 (3)	13.41	SHANSEP	400	2	1	0.35	23	0.15
NU-1 27-29 (2)	11.89	SHANSEP	114	3.3	0.01	0.30	40	0.17
NU-1 32-34 (3)	10.36	SHANSEP	394	1	1	0.30	3(18)	0.13
NU-1 55-57	3.35	SHANSEP	213	2	1	0.20	171	0.40
NU-1 60-62 (2)	1.83	SHANSEP	407	1	1	0.25	3(4)	0.13
NU-1 60-62 (3)	1.83	SHANSEP	410	1	1	0.20	12(13)	0.24
NU-1 65-67 (2)	0.30	SHANSEP	410	1	1	0.225	12(13)	0.31
NU-1 65-67 (3)	0.30	SHANSEP	400	1	1	0.225	11(100)	0.36
NU-3 25-27	12.5	SHANSEP	119	3.15	1	0.30	40	0.28
NU-3 40-42	7.92	SHANSEP	420	1	1	0.30	3(9)	0.09
NU-3 47-49	5.79	SHANSEP	342	1	1	0.20	12(15)	0.23
NU-3 47-49 (2)	5.79	SHANSEP	324	1	1	0.15	40	0.45
NU-3 47-49 (3)	5.79	SHANSEP	367	1	1	0.175	29	0.53
NU-3 55-57	3.35	SHANSEP	389	1	1	0.20	26(31)	0.41
NU-3 55-57 (2)	3.35	SHANSEP	345	1	1	0.25	4(9)	0.28
NU-3 55-57 (3)	3.35	SHANSEP	346	1	1	0.25	3(4)	0.39
NU-3 60-62	1.83	SHANSEP	270	1	1	0.175	36(40)	0.42
NU-1 37-39 (2)	8.84	Recomp.	144	1.77	1	0.30	40	0.63
NU-1 40-42 (2)	7.92	Recomp.	153	1.63	1	0.30	40	0.51
NU-1 42-44 (2)	7.31	Recomp.	159	1.51	1	0.30	13(40)	0.35
NU-1 47-49	5.79	Recomp.	174	1.35	1	0.20	40	0.80
NU-1 47-49 (2)	5.79	Recomp.	174	1.35	0.1	0.25	12(12)	1.25
NU-1 47-49 (3)	5.79	Recomp.	174	1.35	1	0.20	82	0.67
NU-1 60-62	1.83	Recomp.	221	1.08	1	0.20	49(50)	0.48
NU-1 62-64	1.22	Recomp.	219	1.05	1	0.20	160(170)	0.27
NU-1 62-64 (2)	1.22	Recomp.	219	1.05	1	0.25	18	0.56
NU-1 62-64 (3)	1.22	Recomp.	219	1.05	1	0.225	48	0.54
NU-1 65-67	0.30	Recomp.	228	1.03	1	0.225	43(44)	0.76

$G_{sec(i)}$ = Secant shear modulus at N=1, $G_{sec(f)}$ = Secant shear modulus at last cycles

Figure 5.3 shows the pore water pressure versus axial strain during cyclic loading for the specimens presented in Figure 5.2. The excess pore water pressure accumulation decreased with the increasing OCR of the specimen. Specimen (a) with an OCR=1.0 accumulated approximately 60 kPa whereas specimen (c), with OCR=2.0, accumulated only 10 kPa. However, results of the pore water pressure in Figure 5.3 do not include an equalization period at the end of cyclic loading. Pore water pressure values can significantly increase in equalization period is allowed, as subsequently discussed.

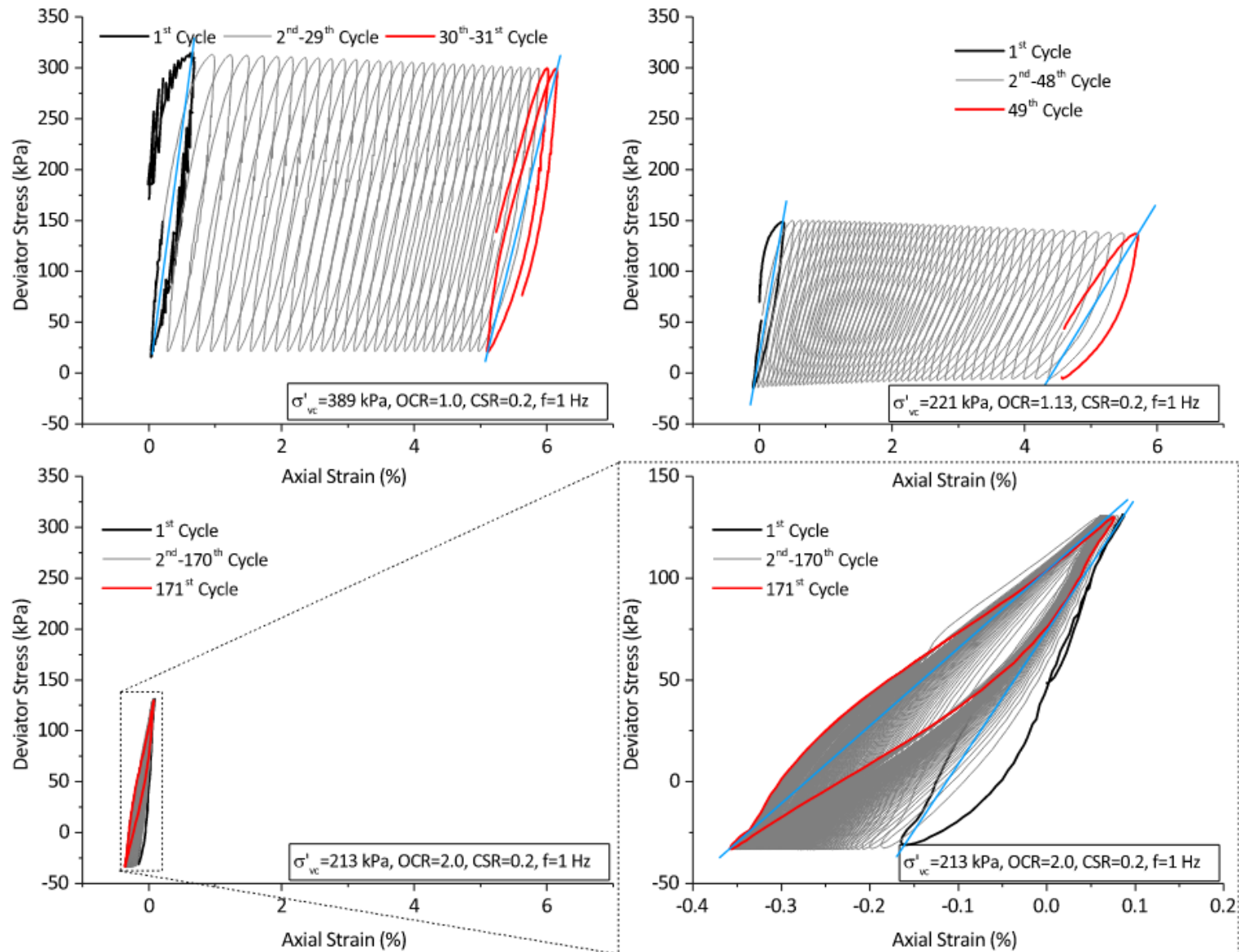


Figure 5.2. Stress-Strain Response of specimens Subjected to Cyclic Loading

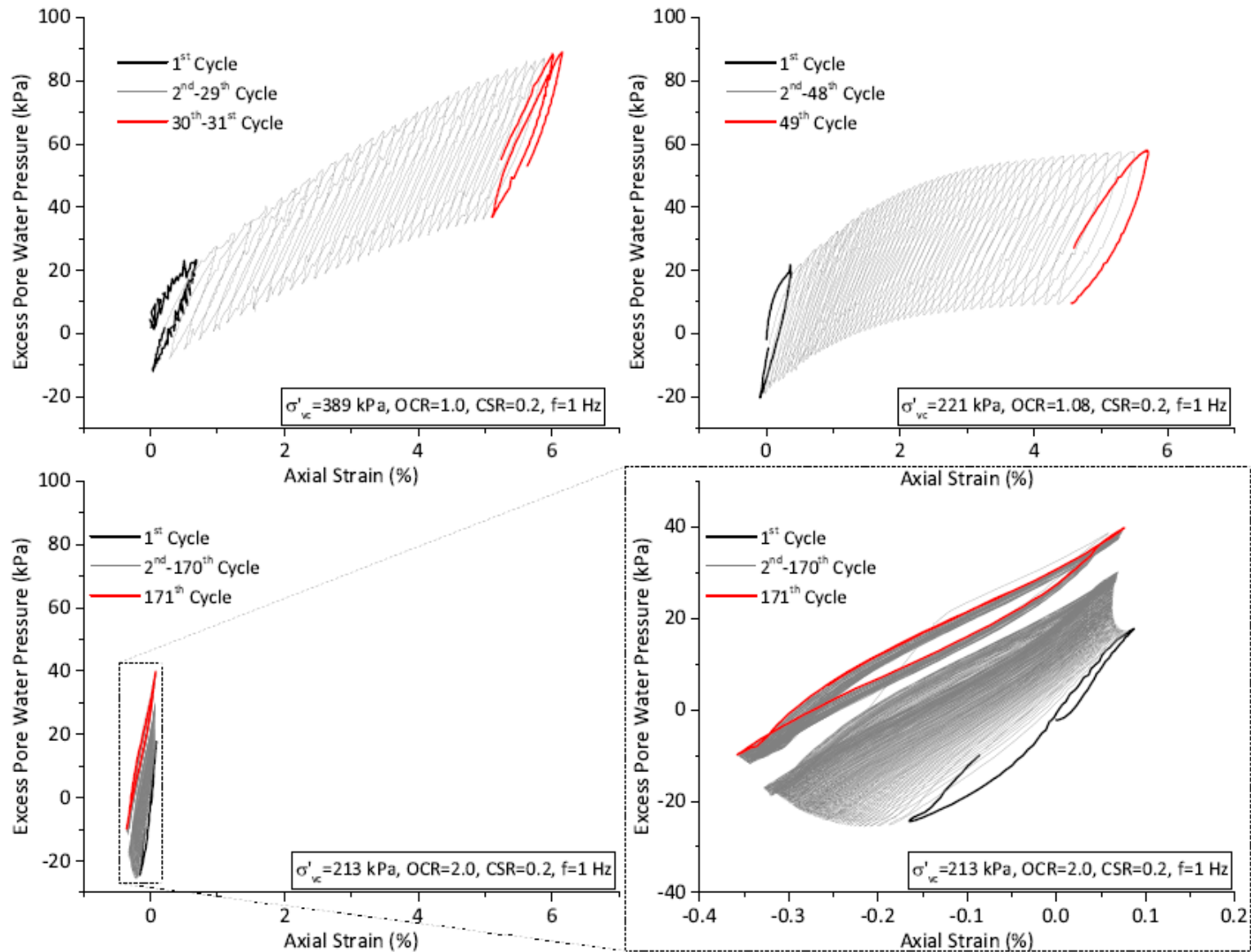


Figure 5.3. Pore Water Pressure-Strain Response of specimens Subjected to Cyclic Loading

Figure 5.4 summarizes the BCF clay axial strain and pore water pressure responses with the number of cycles, as a function of OCR. Figure 5.4 is organized such that pore water pressure responses are shown separately for SHANSEP specimens with $OCR=1$ and 2 and the lightly *OC recompression* specimens. It also shows the effect of the equalization period (undrained creep) after the cyclic loading on the measured pore water pressures. The undrained creep stage is discussed in the next section. Specimens at a constant OCR exhibited a clear trend of axial strains being proportional to CSR. The only exception was for the *recompression* specimens with $OCR=1.05$ which showed very little axial strain until failure occurred at 48 cycles.

The pore water pressure response is normalized to account for the different vertical consolidation stresses applied to the specimen and make a fair comparison for the different OCR. For specimens with $OCR=1.0$, the pore water pressure response is erratic. The specimen with cyclic loaded with $CSR=0.3$ showed minimal increment of pore water pressure for an axial strain increment of 30%. The pore water pressure response during cyclic loading and subjected to high accumulation of axial strain might be a consequence of severe nonuniformities within the sample, including high lateral strain in the middle of the specimen that cannot be accounted by the triaxial device (see specimen photo NU-1 32-34(3) after failure in Appendix B).

For specimens prepared by *recompression*, the pore water pressure response increases with the number of cycles. For specimens with same OCR, the pore water pressure increased when CSR increased. However, specimen cyclically loaded at $CSR=0.2$ and $OCR=1.05$ accumulated more axial strain than the rest of *recompression* specimens; nonetheless the pore water pressure did not follow similar trend and its accumulation was small at the end of the cyclic loading. The reduction of pore water pressure at the end of the cyclic loading, in this specimen, is attributed a non-

uniformity and shear band along specimen due to high axial strain (see photo of failed specimen NU-1 62-64 in Appendix B).

For specimens with $OCR=2.0$, the accumulation of pore water pressure was consistent with the increment of CSR. As noted for specimens with $OCR=1.0$ and *recompression*, the pore water pressure response was not consistent with the increment of axial strain. Specimens with low axial strain accumulated exhibited high pore water pressure accumulation. *Recompression* and $OCR=2.0$ specimens have at the end similar pore water pressure ratios at the end of cyclic loading, but again, the normalized pore water pressure was not proportional to axial strain accumulated. Specimens with low or negligible axial strain accumulated similar normalized pore water pressure as the specimens that failed (reached 5% axial strain) during cyclic loading. Furthermore, allowing an undrained equalization period in some of the specimens showed a significant increment in the pore water pressure accumulated at the end of the cyclic loading, suggesting that the pore water pressures measured during cyclic are not reliable, as one would expect for the 1 Hz rate of loading used for most of the tests.

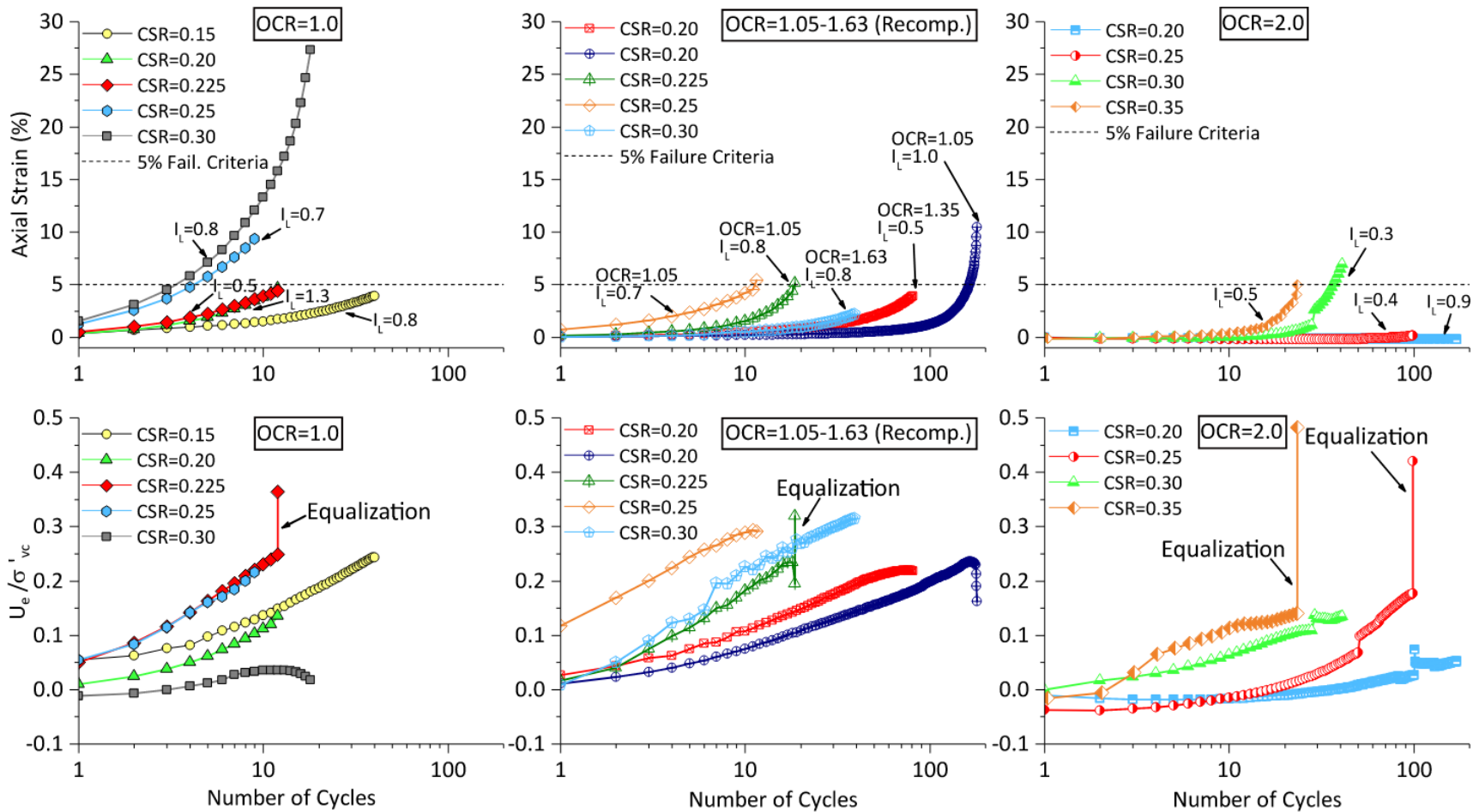


Figure 5.4. Axial Strain and Pore Water Pressure Response with the Number of Cycles

5.2.2 Equalization Period

The equalization period is the stage in which the specimen is subjected to a period of undrained creep after the cyclic loading and before the post-cyclic shearing. This stage lasted until the pore water pressures were essentially constant. The objective of the stage was to obtain a reliable measurement of the U_e accumulated at the end of the cyclic loading. The erratic trend in excess pore water pressure, U_e , response as a function of OCR may be related to the fact that at 1 Hz, pore water pressures are not equalized as noted in four tests with large increment in U_e during the post-cyclic undrained creep. This observation of non-equalized U_e indicates that U_e accumulation is not a reliable way to quantify strength loss during and after cyclic loading. For instance, Yasuhara (1994) proposed an approach to quantify the degradation of post-cyclic undrained strength based on U_e through a closed- form equation. He showed the degradation of the post-cyclic undrained strength increased as $U_{e(cyc)}$ increased. Yasuhara (1994) used tests performed on BCF and Drammen clay to calibrate his model. Presumably, equalization was not allowed in any of those tests. Based on results from Figure 5.4 and Table 5.3, pore water pressure can be significantly higher than the last value reported during cyclic loading leading to erroneous predictions of degradation of undrained strength with Yasuhara's method.

Table 5.4 summarizes the excess pore pressure during the equalization period, $U_{e(eq)}$, for the specimens for which the stage took place. Most of the specimens accumulated positive $U_{e(eq)}$ during the equalization time. The increase in U_e during the equalization period was as much as 161% of that measured at the last cycle during cyclic loading, however some specimens did not show a significant change. These results showed the importance of the undrained creep to obtain an accurate value of the pore water pressure at the end of the cyclic loading.

Some of the variability in the responses was a result of the limitation of the testing system. When the cyclic loading was stopped abruptly after reaching the objective of axial strain of number of cycles, the user does not have control of the state of stresses in the dynamic triaxial testing system (DYNTTS) at the time of the stop. In this case, specimens have to be loaded or unloaded at the end of cyclic loading, so the deviatoric stress can be the same as at the end of consolidation condition. In the case of specimens NU-1 17-19 and NU-1 62-64(3), the deviatoric stress, when the cyclic loading was stopped, was higher than the end of consolidation and then both specimens needed to be unloaded previous equalization affecting the pore water pressure response. The amount of additional deviator stress to reach the end of consolidation value is shown in the table. No clear correlation could be established between the increment of deviator stress and the pore water pressure increment during equalization. Specimen NU-1 60-62(3) had the largest increment of pore water pressure during equalization with a small addition of deviator stress. This change in stress impacted the pore pressure response and likely caused the drop in pore water pressures during equalization.

Table 5.4. Excess pore Water Pressure at the End of Equalization

Specimen	Tech.	OCR_{test}	CSR	$U_{e(cyc)}$ (kPa)	$U_{e(eq)}$ (kPa)	ΔU_e (kPa)	Incr. U_e (%)	Δq (kPa)	$\Delta q/q_{cyc}$ (%)
NU-1 17-19	SHANSEP	1.0	0.25	120.3	68.2	-52.1	-43.3	-115.8	-38.6
NU-1 22-24 (2)	SHANSEP	2.0	0.25	82.6	168.3	85.7	100.4	64.9	32.4
NU-1 22-24 (3)	SHANSEP	2.0	0.35	106.3	193.7	87.4	82.2	119.0	42.5
NU-1 60-62 (3)	SHANSEP	1.0	0.25	49.1	128.0	78.9	160.7	38.1	23.3
NU-1 65-67 (2)	SHANSEP	1.0	0.225	131.1	149.4	76.9	13.9	75.2	40.8
NU-1 65-67 (3)*	SHANSEP	1.0	0.225	132.4	139.8	7.4	5.6	26.4	14.3
NU-1 62-64 (2)*	Recomp.	1.05	0.25	36.8	70.0	33.2	90.2	76.6	68.1
NU-1 62-64 (3)	Recomp.	1.05	0.225	80.4	77.2	-4.0	-1.8	-43.6	-43.6
NU-1 65-67	Recomp.	1.03	0.225	83.6	101.6	18.0	21.5	16.6	16.0

*= No post-cyclic undrained shearing due to collapse,

$U_{e(cyc)}$ = Excess pore water pressure at end of cyclic loading,

$U_{e(eq)}$ = Excess pore water pressure during equalization,

$\Delta U_e = U_{e(eq)} - U_{e(cyc)}$, Incr. = $\Delta U_e / U_{e(cyc)}$

Δq = Change of q during equalization to reach end of consolidation condition,

q_{cyc} = Deviator stress applied during cyclic loading, see Figure 5.1

The equalization time after cyclic loading has the following advantages: (1) it can provide a more accurate measurement of $U_{e(cyc)}$; (2) it can provide the actual effective stress state after cyclic loading; and (3) it can provide uniformity of the pore water pressure within a specimen, so effective stress conditions can be determined accurately in the post-cyclic shearing stage of the test. The disadvantages of allowing U_e to equilibrate after cyclic loading are: (1) the clay can gain some stiffness as a result of the accumulation of axial strain, even if those are small, during the equalization time since it is assumed that the increment in pore pressure is only a result of redistribution at the bottom of the specimen where is measured; (2) the limitation of the DYNTTS when cyclic loading is stopped can create an additional level of uncertainty of the pore water pressure accumulation at the end of cyclic loading; and (3) the non-uniformity of the pore water pressure within the specimen may more accurately represent the conditions in the field. Pore water pressure measurements during cyclic loading without equalization contain potential uncertainties that can lead any possible analysis to inaccurate results. Based on the results from the equalization period, allowing pore pressure to equalize at the end of cyclic loading results is more representative value of the pore water pressure within the specimen recognizing that limitations on the DYNTTS can alter the equalized value.

5.2.3 Cyclic Strength

The failure during cyclic loading of fine grained has been defined a number of ways in the literature. For triaxial testing, the most common failure criterion is the single amplitude axial strain (i.e. strain accumulated at the end of the cyclic loading). Several authors have proposed the axial strain accumulation at different levels (e.g. 3% or 5%) as a failure criterion for cyclic triaxial and direct simple shear (DSS) testing (Lee, 1979; Andersen et al., 1980; Lefebvre and Pfendler, 1996; Wichtmann et al., 2013). As noted in section 3.4.7, the failure is defined herein as when 5% axial

strain has accumulated. Hence, the cyclic strength, in this thesis, is defined as the CSR and number of cycles (N) required to reach 5% axial strain for the specimen at the end of the cyclic loading. Note that these values are for k_0 consolidated specimens.

Figure 5.5 presents the CSR to cause failure of the BCF clay based on the results presented in this thesis. The arrows on specimens that did not reach failure indicate that a higher CSR is required to produce failure at the same number of cycles. Specimens with OCR equal to 1.0 and 2.0 were consolidated by using SHANSEP technique. The slightly overconsolidated (OC) specimens were obtained by *recompression* to the in situ vertical effective stress. Figure 5.5 includes the estimated OCR values for the slightly OC specimens. The OCR values were estimated based on the profile showed in Figure 4.9, so some uncertainty exists in the reported OCR values as a consequence of natural variability. The CSR at failure showed a strong correlation with the OCR of the specimen. Specimens with higher OCR were more resistant to cyclic loading than the lower OCRs. Results also showed a significant influence of the specimen structure on the cyclic resistance. For a given CSR, specimens with OCR values slightly above 1.0 required more cycles to reach failure compared to the NC specimens. The CSR at for 5% axial strain for the NC specimens varied linearly with the log of the number of cycles. The best fit included the specimens from facies III and facies IV without noticing a significant difference in the cyclic response at NC state. The CSR for 5% axial strain for NC specimens can be express as follows:

$$(5.1) \quad CSR = 0.321 - 0.097 \log(N)$$

where CSR is the cyclic stress ratio to produce 5% axial strain and N is the number of cycles. The coefficient of determination, R^2 , for the regression was $R^2=0.83$. The Washington DOT and FHWA design manuals do not recognize the effect of OCR in the cyclic strength. Results of this work

show that specimens with OCR greater than 2.0 can sustained without failure significant amounts of cycles and high CSR.

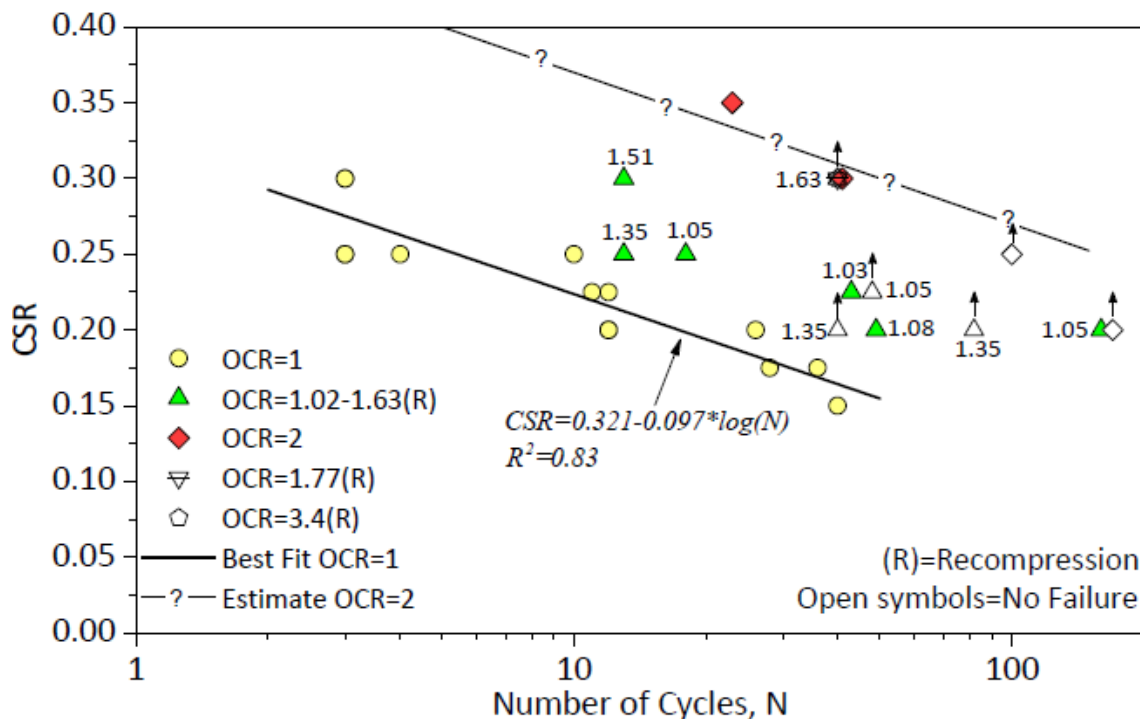


Figure 5.5. Cyclic Strength of BCF Clay for Different OCR

For OCR=2.0, only 2 specimens failed during cyclic loading and the failure line is an estimate. The specimens that did not fail were placed below the failure line to help evaluate the failure line. The one specimen with an OCR=3.4 was subjected to 40 cycles and a CSR of 0.3 with no failure occurring. Clearly heavily OC specimens are very resistant to cyclic loading compared to NC specimens. Zapata-Medina (2012) noted that for the contingency level earthquake (CLE) magnitude, M , of 9 for the Port of Anchorage (POA) wharf construction project the number of cycles and the CSR were established as 40 and 0.2, respectively. None of the specimens with OCR greater than or equal to 2 would have reached 5% axial strain for the POA loading.

Lightly OC specimens were located between the failure lines proposed for the NC and

OCR=2.0 specimens. The *recompression* specimens should preserve the original structure better than the SHANSEP prepared specimens because of the small strains that develop prior to application of the cyclic loading. Figure 5.6 provides an expanded view of Figure 5.5 for the NC and lightly OC BCF clay and includes the LI and the axial strain accumulated during consolidation. For normally consolidated specimens, the axial strain accumulated during consolidation has a strong influence in the cyclic strength. In general, specimens with higher axial strain during consolidation exhibited fewer cycles to reach 5% strain at the same CSR. The liquidity index also has a detrimental effect on the cyclic strength. Some specimens with similar or lower axial strain accumulated during consolidation showed smaller cyclic strength when liquidity index was higher than 1.0 than those with liquidity index lower than 1.0.

For slightly OC specimens, the cyclic strength was significantly stronger compared to normally consolidated specimen when the OCR was marginally higher than 1.0. The preparation for slightly OC specimen was through *recompression* approach where the axial strain at the end of consolidation is generally small compared to SHANSEP specimens. This result demonstrates the influence of the strain accumulated during consolidation in the cyclic strength. A BCF specimen will degrade its structure throughout the whole test process affecting the cyclic response. This means that specimens consolidated using the SHANSEP approach that tend to accumulate more strain than those consolidated using *recompression* are closer to the intrinsic response and can be conservative and used as a lower bound to determine the cyclic strength of clay.

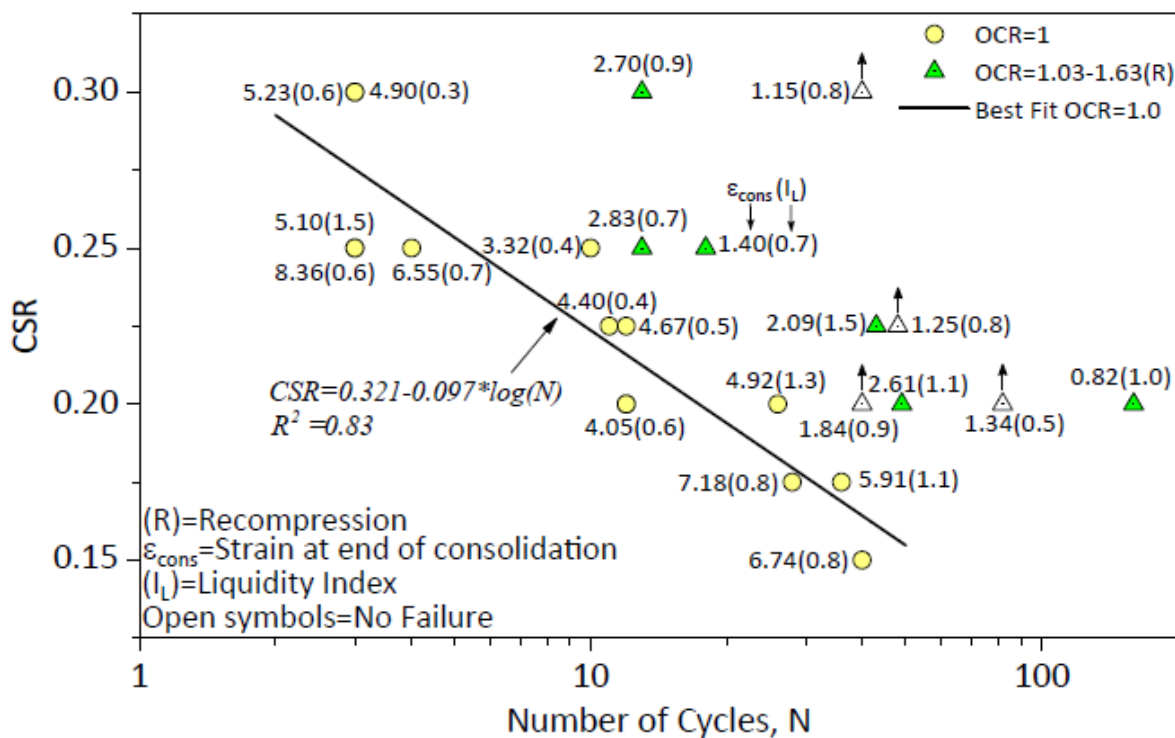


Figure 5.6. Cyclic Strength for NC and Lightly OC BCF specimens

The effect of sensitivity on the cyclic strength was analyzed using *recompression* specimens. These specimens are more likely to maintain the original structure and hence its original sensitivity. The sensitivity for these specimens varied in a relatively small range from 2 to 6, as shown in Figure 5.6. When compared at CSR equal to 0.25, specimen with an OCR of 1.05 and sensitivity of 2 showed a stronger cyclic strength than the specimen with an OCR of 1.35 and sensitivity of 6. However, the small range of sensitivity and the variability of OCR does not allow one to establish a clear trend concerning the role of sensitivity in the cyclic strength.

5.2.4 Effects of Rate of Shearing During Cyclic Loading

The rate of loading is recognized as an important parameter affecting the results of cyclic loading of clays. Lefebvre and Pfendler (1996) carried out an analysis of the rate effect on St. Alban clay. During cyclic loading, some specimens failed during the first cycle. The undrained strength reached at the first cycle was up to 40% higher than the strength determined by the monotonic test

at a slower rate.

Table 5.5 shows the specimens that were tested at rates different than 1 Hz frequency. Two specimens were tested under stress-control at frequencies of 0.1 and 0.01 Hz. Specimens NU-1 27-29 (2) and NU-1 47-49(2) had OCRs of 3.0 and 1.35 and CSRs of 0.3 and 0.25, respectively. Specimen NU-1 47-49(2) reached failure after 12 cycles, while NU-1 27-29 (2) did not reach failure after applying 40 cycles. Both specimens were stable after failure and post-cyclic shearing was performed at the end of cyclic loading.

Also, two specimens were tested under strain-controlled conditions. Specimens NU-3 42-44 and NU-42-44(2) were subjected to strain-controlled following the axial strain path that developed while cyclically testing specimen NU-3 40-42 under stress-controlled with a frequency of 1 Hz and a CSR equal to 0.3. This specimen was normally consolidated to an effective vertical consolidation stress, σ'_{vc} , of 400 kPa.

Table 5.5. Rates of Shearing During Cyclic Loading

Specimen	OCR	Rate	N
NU-3 40-42	1.0	1 Hz	9(4)
NU-3 42-44	1.0	0.1%/hr*	-
NU3 42-44(2)	1.0	0.5%/hr*	-
NU-1 27-29(2)	3.4	0.01 Hz	40
NU-1 47-49(2)	1.35	0.1 Hz	12(12)

*Strain-controlled test

The axial strain response during cyclic loading at 1 Hz of specimen NU-3 40-42 is shown in Figure 5.7. The total number of cycles was 9 and the accumulated axial strain reached 23%. If one computes the equivalent axial strain rate for the first cycle of loading, the specimen reached an axial strain rate of 16,560%/hr. This rate was more than three orders of magnitude higher than

that utilized for undrained shearing (i.e. 0.5%/hr) and should represent a substantial difference in the material response. The NC specimens, given in Table 5.4, were tested under strain-controlled conditions at different slow rates following the strain path showed in Figure 5.7 to directly evaluate the material net effect of the BCF clay.

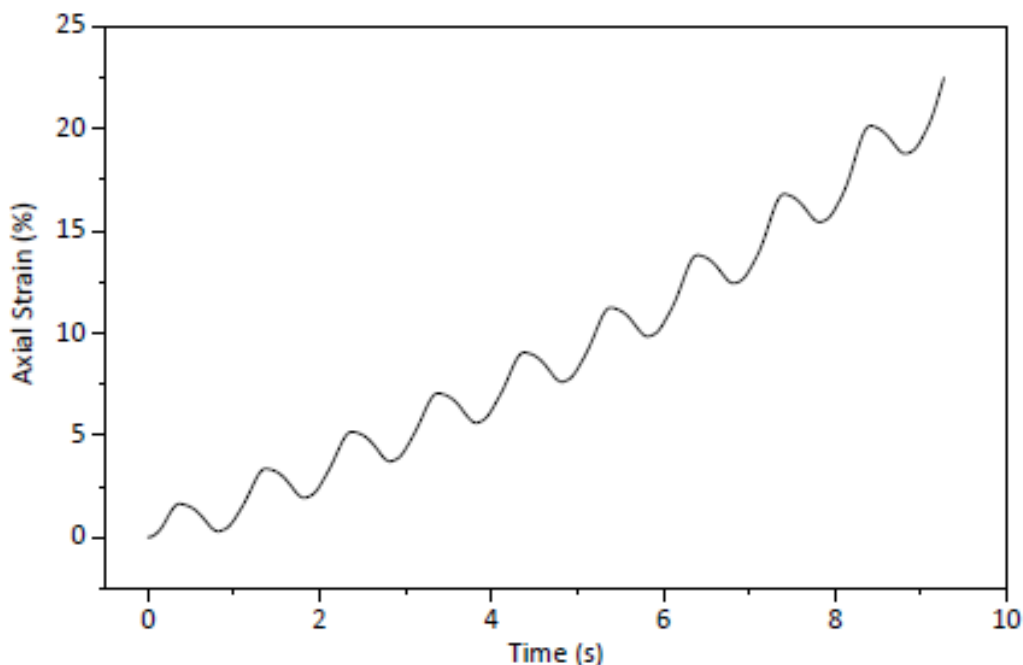


Figure 5.7. Time-Axial Strain Response at Cyclic Loading (NU-3 40-42)

Figure 5.8 summarizes the responses of the BCF specimens subjected to cyclic loading at different rates. Significant differences were observed as a function of strain rate. Figure 5.8(a) was the baseline test that created the strain path showed in Figure 5.7. Values of deviator stress decreased gradually until the specimen collapsed. As in the case of the baseline test, the specimens with strain rates of 0.1%/hr and 0.5%/hr reached the peak deviator stress during the first loading, after which the peak deviator stress decreased with subsequent cycle of loading. The magnitude of the first peak deviator was similar for both specimens but approximately 1.6 to 1.7 times lower than that of the baseline test.

The axial strain and pore water pressure responses during consolidation of both strain-controlled showed very similar responses. It may be assumed then that the difference at the maximum peak deviatoric stress during the first loading is a result of the strain rate. Results from Figure 5.8b and 5.8c seem to indicate that the slower rates of shearing cause more degradation since the deviatoric stresses were smaller and pore water pressures were higher than that for the baseline specimen at comparable strain levels. Lefebvre et al. (1989) recognized the effect of rate of shearing on the cyclic response. The Grande Baleine clay test by Lefebvre et al. (1989) showed required higher number of cycles or higher CSR to reach failure when the rate of shearing was increased. It is clear from the results in Figure 5.8 that the rates of loading significantly less than the typical 1 Hz cyclic loading rate result in more degradation and higher excess pore pressures than the typical cyclic test. More data are required to draw quantitative conclusions of the rate of shearing.

At rates of 0.1 and 0.5 %/hr the excess pore water pressure has time enough to equalize within the specimen. The high loading rate of the baseline tests does not allow one to measure a representative pore water pressure. Thus, a cyclic triaxial test conducted at 1 Hz specimen must be considered as a boundary value problem in terms of effective stresses. In this case, the undrained strength can be evaluated reliably if acknowledging that the rate effect may affect the S_u value. . When interpreting results in terms of effective stresses, one must recognize the limitation of the pore water pressure measurements.

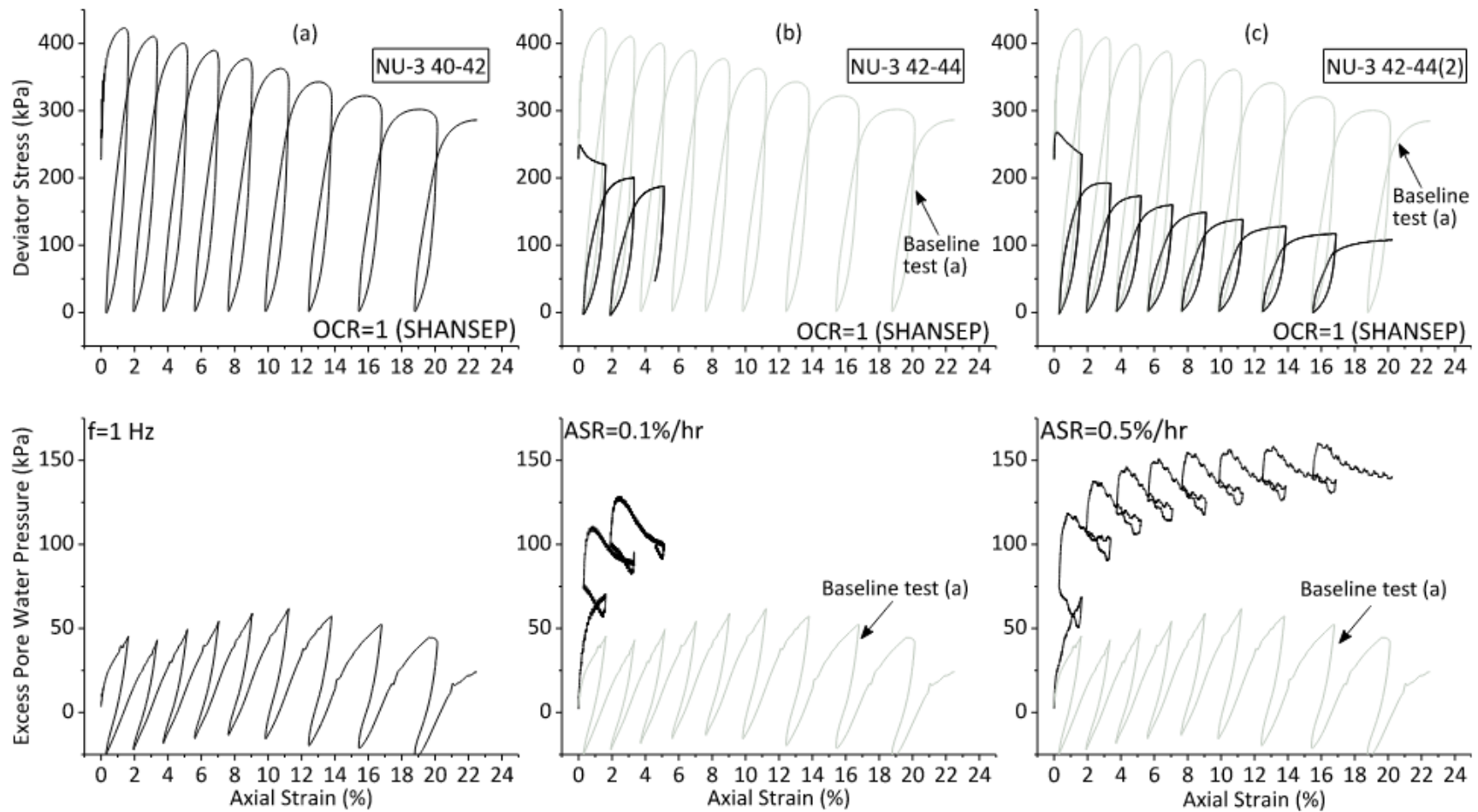


Figure 5.8. Axial Strain-Deviator Stress and Pore Water Pressure Responses of Specimens at Different Strain Rates

5.2.5 Analysis of Effective Stresses During Cyclic Loading

This section shows an analysis of the cyclic loading failure criterion in terms of effective stresses. The analyses presented herein assumes that the excess pore water pressures at the end of cyclic loading are sufficiently accurate. The failure criterion during cyclic loading used in this work was 5% axial strain at the end of cyclic loading. The failure line of BCF clay in p' - q space based on monotonic undrained shearing of NC and slightly OC specimens was defined in section 4.6. It is necessary to recognize that OC specimens of clay typically display some apparent cohesion and thus the intercept in a p' - q diagram is not zero for all specimens.

5.2.5.1 Collapsed Specimens. Figure 5.9 shows the effective stresses at failure in the p' - q space for specimens that collapsed during cyclic loading (i.e., “failure” not defined in terms of 5% axial strain) assuming that the pore water pressures measured at the end of cyclic loading were representative of the values throughout the specimen. Note that these specimens were not suitable for post-cyclic shearing.

A total of 8 specimens collapsed during cyclic loading. It also shows the end-of-consolidation effective stresses in open symbols and the failure line defined for NC specimens under monotonic conditions. The shift of the points to the left on the effective stress space is a result of the excess pore water pressure developed during cyclic loading. Some of the specimens developed small excess pore water pressures at the end of the cyclic loading even when the axial strain was large enough to produce collapse. The limitation in the measurement of the pore water pressure during cyclic loading at 1 Hz, as discussed section 3.3.2, likely is why the obviously failed specimen did not reach the effective stress failure line. The pore water pressures measured at the bottom do not reflect the likely variation of pore water pressures throughout the specimen at the end of cyclic loading at 1 Hz. Specimens had different values of sensitivity and yet no clear effect

of sensitivity was observed in the specimens consolidated by recompression. Effective stress analysis of specimens subjected to equalization period is shown in section 5.2.1.3.

Two normally consolidated specimens reached the failure line and the slightly consolidated specimens were close to it. One of the specimens even at failure accumulated low pore water pressure at an axial strain higher than 20%. This might be an indication that the pore pressure is not representative of the specimen possibly due to unequalized pore water pressure, strain localization or significant horizontal strain at failure. As mentioned above, the measured pore water pressure for a cyclic loading of 1 Hz frequency are usually not reliable, and values of pore water pressure in general tend to increase after sufficient time for equalization is allowed. Results shown in Figure 5.9 can suggest that, even if one considers the limitation of the pore water pressure, the failure line defined by specimens under monotonic conditions may be a reasonable approximation of the failure criteria in terms of effective stresses for normally consolidated to slightly overconsolidated specimens.

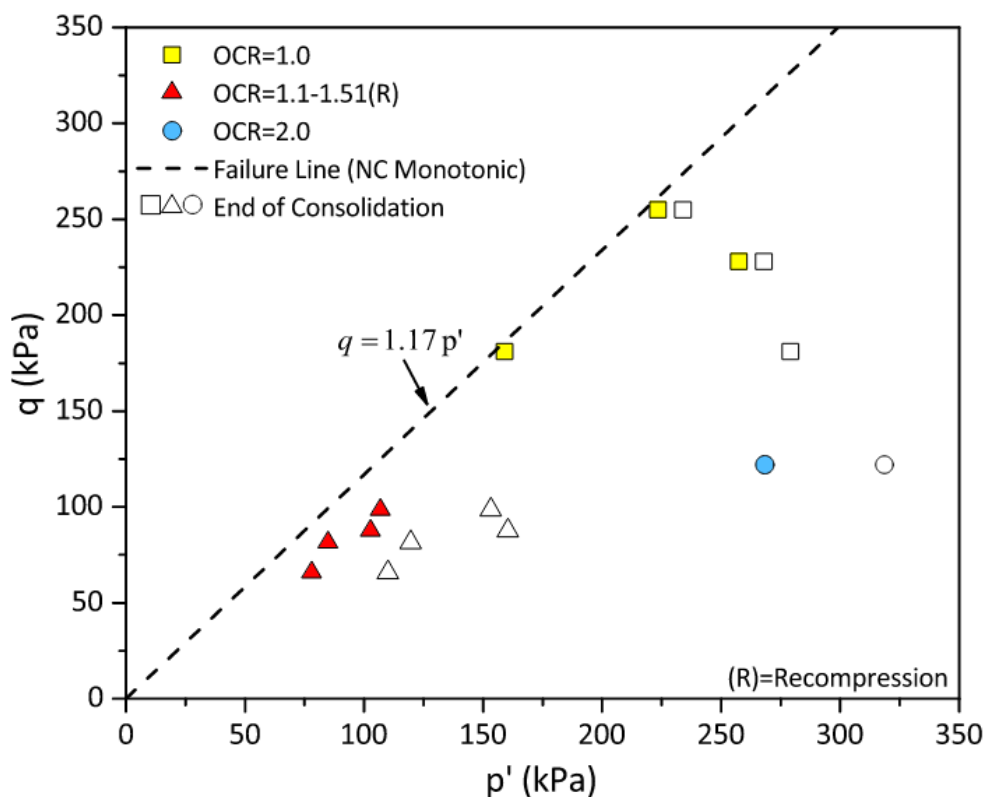


Figure 5.9. Effective Stress Failure Conditions of Specimens that Collapsed During Cyclic Loading

For the specimen with $OCR=2.0$, the increment of pore water pressure during cyclic loading was small when compared to the axial strain strain developed. The failure of the specimen cannot be explained in terms of effective stresses. Figure 5.10 shows a photo of specimen NU-1 20-22 with an $OCR=2.0$ after reaching failure during cyclic loading. The failure occurred in a near horizontal plane with partial collapse of a 3 cm layer (see Figure 5.10a). Figure 5.10b shows the presence of a sand seam at the failure plane that might affect the homogeneity of the cyclic response of the specimen and finally failing without following any trend observed in this study.

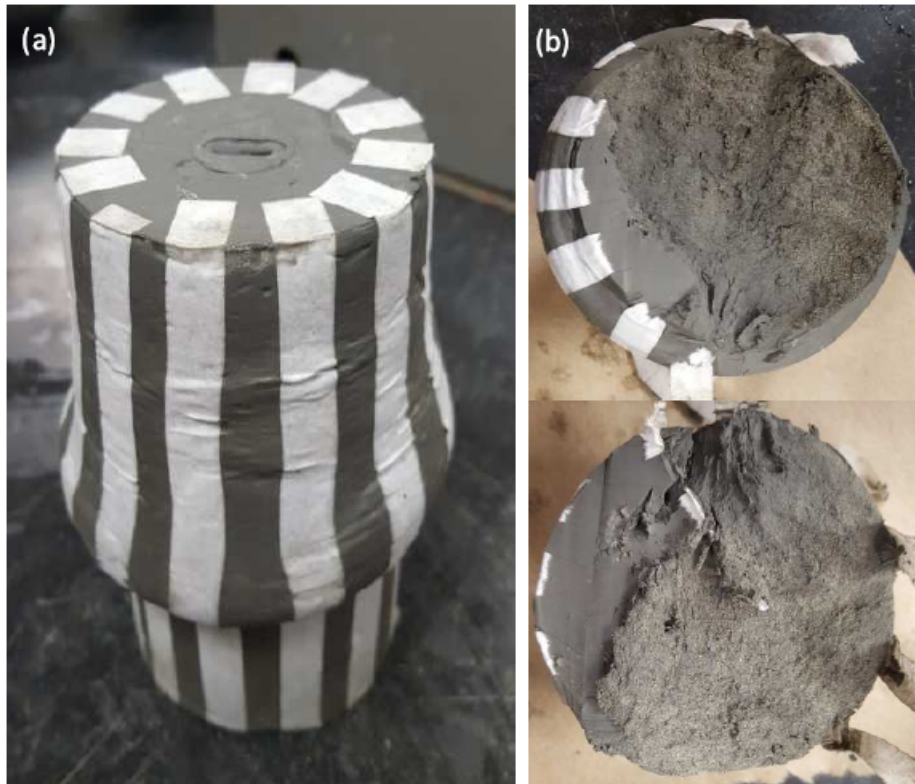


Figure 5.10. Specimen NU-1 22-24 After Failure during Cyclic Loading

Note that the failure line in Figure 5.9 was defined based on the results of undrained shearing at a strain rate of 0.5%/hr. The cyclic loading resulted in strain rates as high as about 250%/min. Lefebvre et al. (1989) and Lefebvre and Pfendler (1996) studied the influence of the rate during cyclic loading and concluded that the rate of shearing must be included in the definition of failure. They showed that faster rates produced higher clay strengths. Conversely, the pore water pressures may have been higher than recorded at the bottom of the specimen. Given these compensating errors, the failure line in terms of effective stresses in Figure 5.9 is an approximation.

5.2.5.2 Failure Defined by 5% Axial Strain for Specimens with No Equalization Period.

Figure 5.10 presents effective stresses at end of consolidation and cyclic loading for specimens that did not collapse during cyclic loading; only specimens with no equalization period are shown. The axial strain was limited to a maximum value close to 5% accumulated during cyclic loading. Some of the specimens did not reach the 5% failure criterion for cyclic loading and the accumulation of axial strain was generally small.

Figure 5.10 shows two NC specimens reached the NC failure line, yet each did not collapse and were suitable for performing post-cyclic shearing. The fact that two specimens reached the NC failure line but remained in a stable condition may be due to the higher available undrained strength for the fast loading rates in cyclic tests. Also note that the excess pore water pressures may not be representative of the actual value in the specimens. Based on the results shown in Figures 5.9 and 5.10 the effective stresses after cyclic loading in specimens that collapsed were closer to the effective stress failure line than those that did not when normally consolidated.

Slightly overconsolidated specimens were closer than the NC specimens to the failure line at the end of cyclic loading. At 5% axial strain, specimens approached the failure line without collapsing. This outcome can be either a result of the significant difference between the rate of shearing that define the failure line and the cyclic loading frequency or the structure that was not completely destroyed during the loading process.

For overconsolidated specimens, the accumulation of axial strain was generally small and only one specimen was close to 5% axial strain. As expected, these specimens are not close to failure line and higher cyclic stress ratios are required to reach failure in terms of effective stresses at 5% axial strain.

Two specimens were cyclically loaded at a frequency of 0.1 and 0.01 Hz with an OCR of 1.35 and 3.3, respectively, and the consolidation and failure stresses are shown with shading in Figure 5.11. These two specimens exhibited a higher excess pore water pressure at the end of the cyclic loading. Only the specimen sheared at frequency of 0.1 Hz reached the failure line, likely a result of a higher accumulation of axial strain during cyclic loading since its OCR is close to 1.0. The values of pore water pressure measured in these two specimens are likely to be closer to a representative value in the specimen.

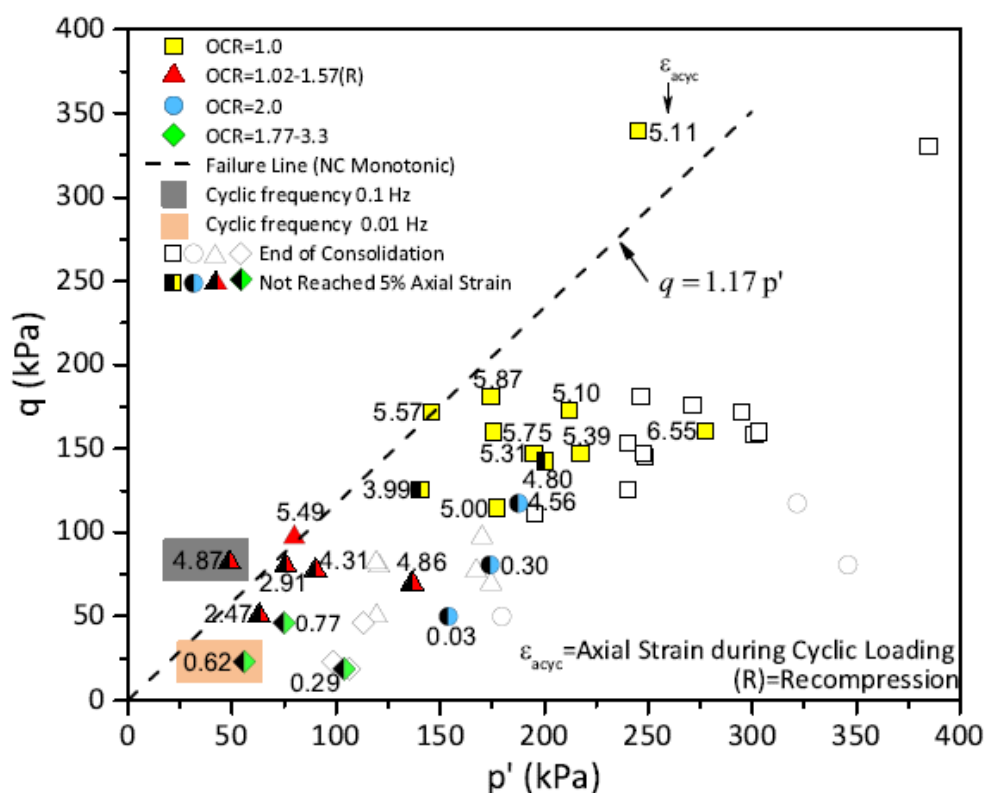


Figure 5.11. Effective Stress Failure Conditions of Specimens That Did Not Collapse During Cyclic Loading

5.2.6 Failure Defined by 5% Axial Strain for Specimens with Equalization Period.

Figure 5.12 presents the consolidation and end of cyclic loading effective stresses of specimens that included an equalization period after cyclic loading. One NC specimen (orange shaded in

Figure 5.12) collapsed during cyclic loading exhibiting a shear band and bulging at the middle of the specimen (see photo of NU-1 65-67(3) in Appendix B). Pore water pressure recorded at the end of equalization might be affected by the non-uniformity of the specimen. This condition may result in unrepresentative values of pore water pressure. Higher pore water pressure values are expected within the shear band than in the rest of the specimen. One slightly overconsolidated specimen (gray shaded in Figure 5.12) collapsed during the equalization period and exhibited shear bands and bulging at the top half of the specimen. This non-uniform condition presumably generates a lower pore water pressure reading at the bottom of the specimen and consequently higher effective stresses recorded moving the specimens far from the failure envelope.

NC and slightly overconsolidated specimens were in general close to failure line after cyclic loading and equalization period. One NC specimen (axial strain 5.57%) that did not collapse and reached the NC failure line stayed stable. As stated before, this may be a result of the fast loading rates during cyclic loading and the fact that the NC failure line may not represent failure for the horizontal effective stress path that the specimens were subjected to during cyclic loading.

It is clear that the 5% strain criterion is not supported by the effective stress responses from the cyclic tests presented herein. However, the actual pore water pressures within a specimen at the end of the cyclic loading are uncertain and is a main reason by a total stress approach is used to define cyclic strength. The 5% strain criteria can be considered conservative and likely does not represent actual failure conditions within the clay specimens, especially when specimens are overconsolidated. This work suggests failure defined by 5% axial strain for OCR greater than 2.0 would be overly conservative.

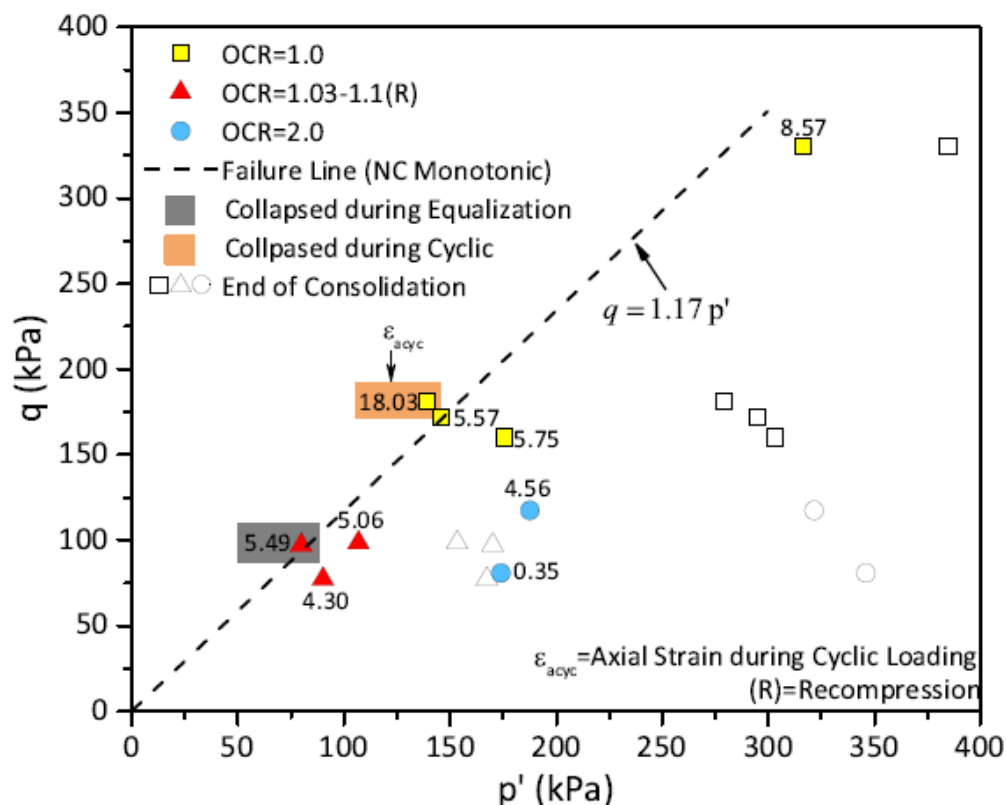


Figure 5.12. Effective Stress Failure Conditions of Specimens with Equalization Period After Cyclic Loading

5.3 Post-Cyclic Shearing Results

This section presents the results of the undrained shearing of specimens after being subjected to cyclic loading. The evaluation of the post-cyclic strength is made to estimate the strength degradation of the BCF clay. After cyclic loading, the axial strains experienced by a specimen may have destroyed some of its structure.

5.3.1 Post-Cyclic Response of BCF Clay

Figure 5.13 shows the deviator stress and pore water pressure response of three specimens subjected to post-cyclic undrained shearing. These specimens were selected to show the post-cyclic response of BCF with different OCR values. As noted on the figure, the liquidity index of

the three specimens is 1.3, 0.8, and 0.9, these values are close or above 1.0 and one can expect that these specimens are sensitive, especially specimen (a). The stress-strain response in case (a) and (b) reached a peak at axial strain about 4 to 5%, while specimen (c) never reached the peak and the estimated undrained strength was obtained based on the maximum effective stress ratio. These 3 specimens did not exhibit degradation of strength when compared to the normalized strength values (Figure 4.14) established for monotonic specimens.

Figure 5.13 also shows the pore water pressure response of the three specimens during post-cyclic shearing. None of the specimens presented in Figure 5.13 was subjected to equalization period. Initially, the specimens developed positive excess pore water pressure during post-cyclic shearing. Specimens developed high excess pore water pressure at small strains during post-cyclic shearing. This response probably included equalization of excess pore water pressure (since the shearing rate was 0.5%/hr) generated during cyclic loading. All specimens showed a tendency to dilate during undrained shearing after the first positive increment of excess pore water pressure. This type of response, typical of OC specimens, shows that NC specimens subjected to cyclic loading become “overconsolidated” as a result of the accumulation of pore pressure.

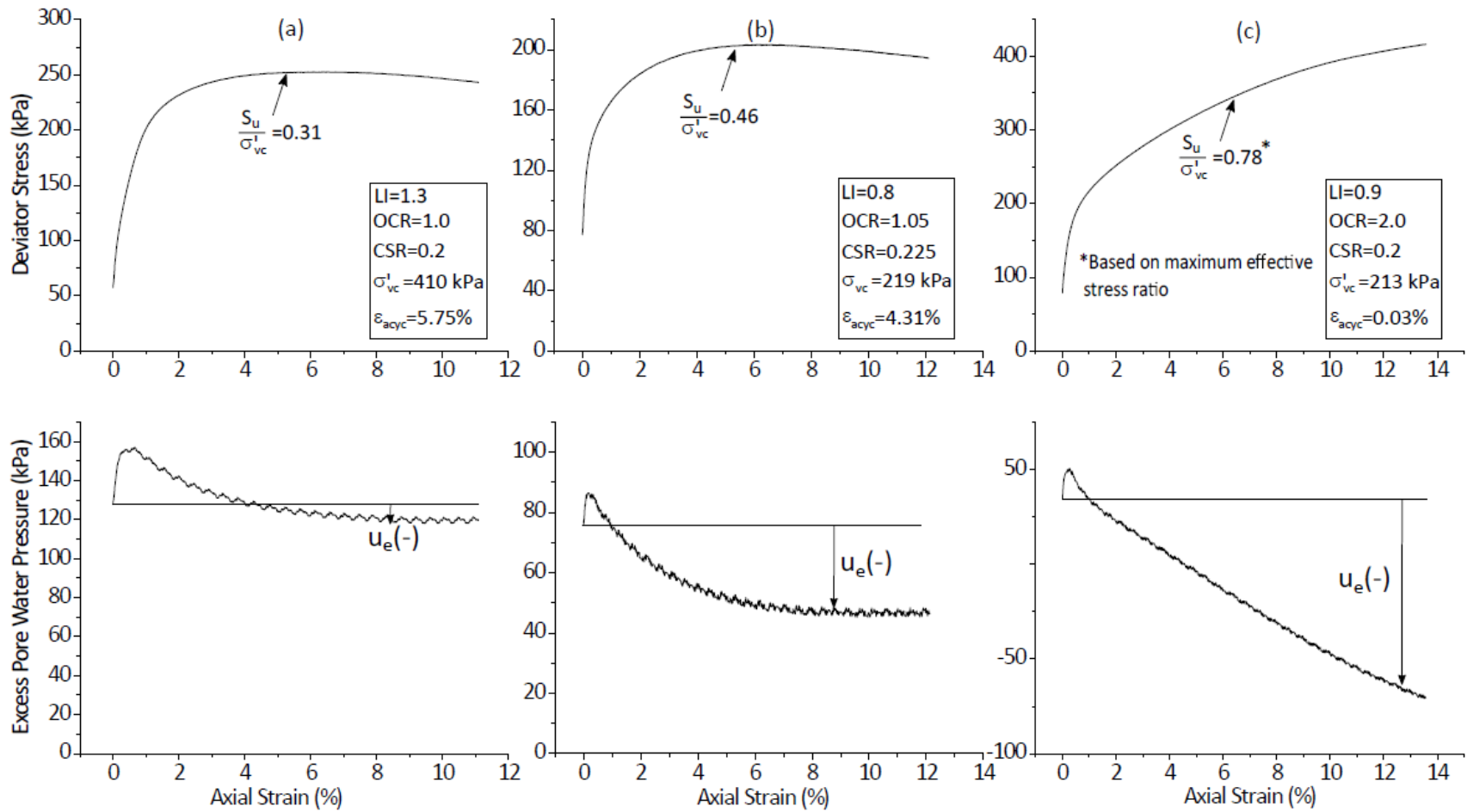


Figure 5.13. Axial Strain-Deviator Stress and Pore Water Pressure Post-Cyclic Response

The results of normalized strength as a function of the OCR prior to cyclic loading are presented in Figure 5.14. The actual OCR of the *recompression* specimens is estimated because the preconsolidation stress is not reached during the consolidation phases of the tests. The preconsolidation pressures were selected based on Figure 4.9, and thus there is uncertainty in the stated OCR for the *recompression* data. Figure 5.14 presents normalized undrained strength versus OCR for monotonic triaxial compression and post-cyclic shearing. The best fit for the post-cyclic strength exhibited some scatter with a coefficient of determination, R^2 , of 0.71. This value was substantially lower than that obtained for monotonic shearing of $R^2=0.97$. Also shown on the figure is the best fit for monotonically sheared specimens presented by Zapata-Medina (2012) for the BCF specimens collected at the port of Anchorage.

Most of the specimens fell on or above the trend line, however, several specimens obtained normalized post-cyclic strength significantly lower than the trend line. The OCR of these data points ranged from 1.0 to 2.0. For specimens with OCR higher than 2.0, the post-cyclic strength fell in the range of the best fit obtained for monotonic and post-cyclic specimens. The reduction in normalized post-cyclic strength for specimens with $OCR \leq 2.0$ implies that there may be factors other than stress history that affect the post-cyclic strength of BCF clay.

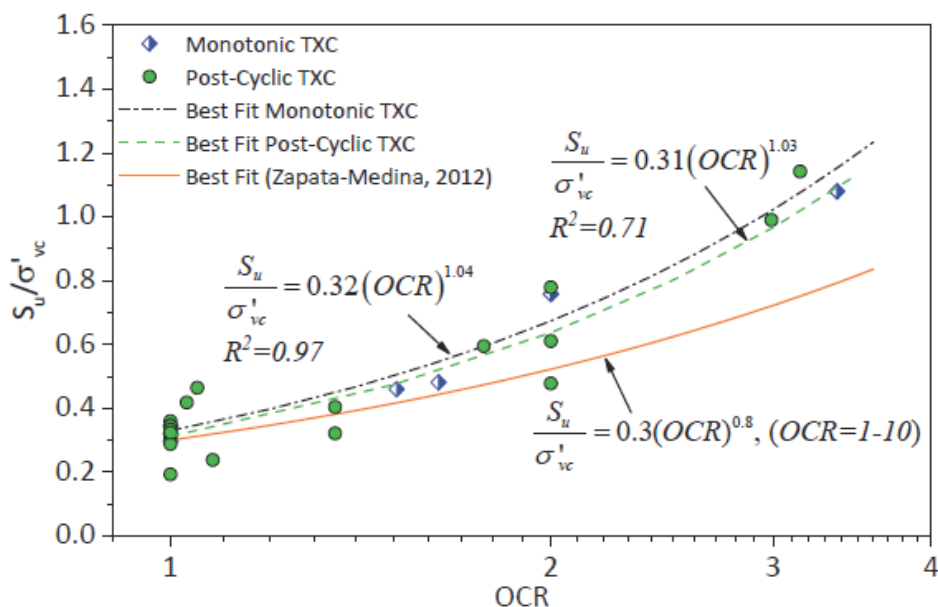


Figure 5.14. Normalized Undrained Shear Strength for Post-Cyclic Compression

Figure 5.15 presents the post-cyclic data points and failure line of the specimens sheared under undrained compression after cyclic loading. It also shows the failure line developed for NC specimens under monotonic conditions as shown in Figure 4.13. Results of post-cyclic undrained strength indicated that the post-cyclic specimens had a failure surface with an intercept in p' - q space. Using Equation 4.5 and Equation 4.6, the friction angle, ϕ' , and the cohesion, c , can be calculated as 29° and 14.0 kPa, respectively. Andersen et al. (1980) showed that the apparent cohesion in the post-cyclic envelope (and missing in the NC envelope) might be explained as a result of the apparent overconsolidation developed during cyclic loading. This apparent condition depends on whether the clay structure is destroyed or not during cyclic loading. The hypothesis of this work is that the degradation of clay specimens during post-cyclic shearing is related to the degradation of the apparent cohesion of the BCF clays. The parameters that caused the apparent cohesion will be explained in more detail in the following sections.

Figure 5.16 presents the effective stress path during cyclic and post-cyclic shearing of same

three specimens shown in Figure 5.13. All specimens developed net positive pore water pressures during cyclic loading. The vertical and horizontal effective stresses after cyclic loading are less than those at the end-of-consolidation condition as a result of the excess pore water pressure developed during cyclic loading.

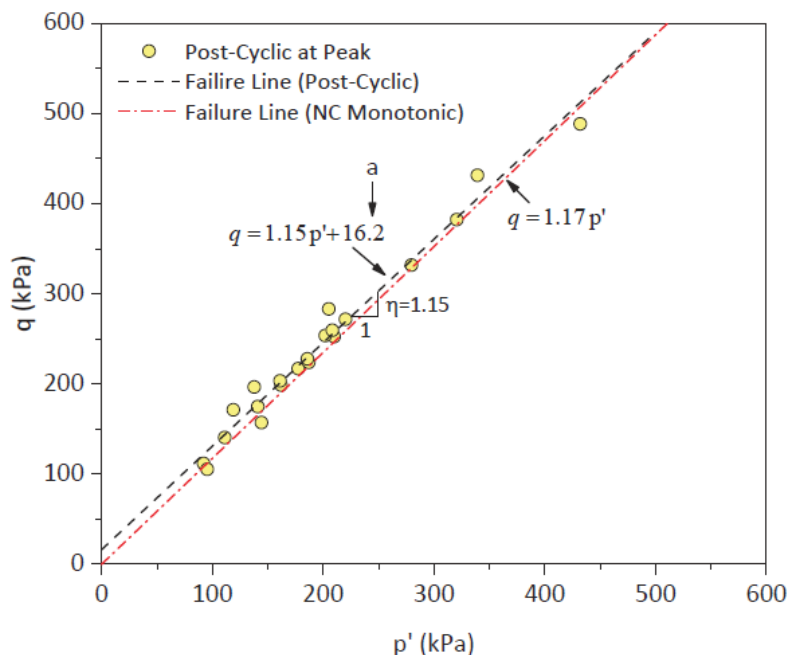


Figure 5.15. Best Fit of Post-Cyclic Sheared specimens in p' - q Space

During post-cyclic shearing, the specimens had a tendency to reduce the initial excessive pore water pressure accumulated during cyclic loading as shown in Figure 5.13, even for initially NC specimens. This result agrees with Andersen et al. (1980) who showed that the effective stress response of initially NC specimens under post-cyclic undrained shearing was similar to those with a higher OCR value. The post-cyclic undrained strength, shown in Figure 5.16, was compared to the monotonic undrained strength obtained from Equation 4.2. These specimens did not exhibit reduction in undrained strength when compared to the best fit from specimens subjected to monotonic loading only. In fact, normalized undrained strength values for specimens with $OCR=1.05$ (b) and 2.0 (c) are significantly higher than the reference monotonic ones.

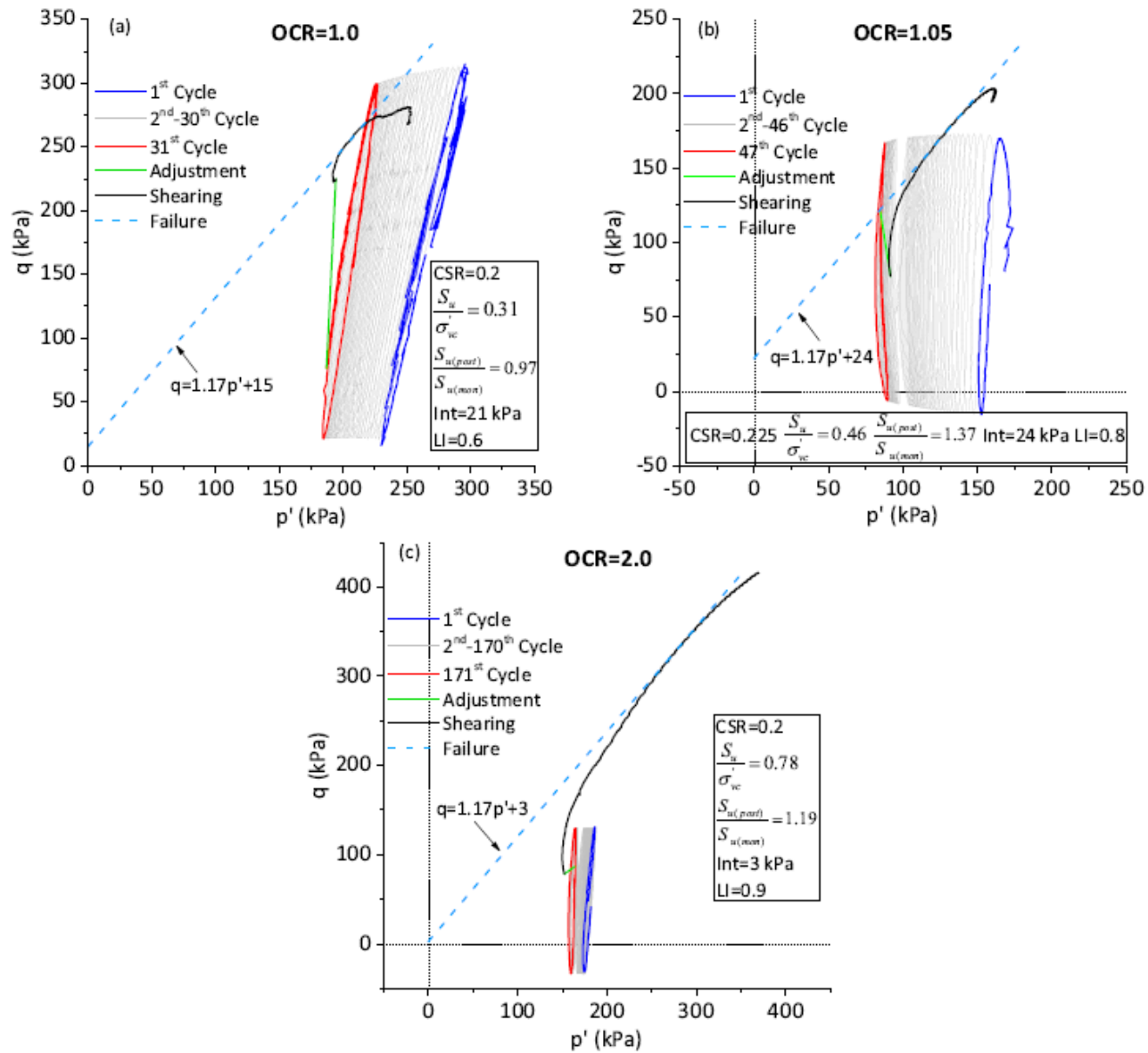


Figure 5.16. Effective Stress Path $OCR=1.0, 1.05, 2.0$ specimens in p' - q Space

5.3.2 Degradation of Undrained Strength of Specimens due Cyclic Loading

This section presents the analysis the post-cyclic and degradation of strength of BCF clay specimens. The post-cyclic degradation is evaluated in terms of the CSR, the cyclic and total strain prior the post-cyclic shearing, and strain energy.

5.3.2.1 Degradation of Strength with Cyclic Stress Ratio. Zapata-Medina (2012) noted that for the contingency level earthquake (CLE) for the Port of Anchorage (POA) project, the established number of cycles and the CSR were 40 and 0.2, respectively, for an earthquake of magnitude (M) of 9 and subsurface conditions at POA. Specimens with OCR of 2.0 required at least a CSR of 0.3 and more than 40 cycles to accumulate 5% axial strain during cyclic loading, as shown in Table 5.1 and 5.2. Given this observation, this section focuses on the post-cyclic strength mainly of NC and lightly OC BCF specimens.

Figure 5.17 shows the variation of the normalized post-cyclic strength with the CSR for specimens which reached 5% axial strain during cyclic loading at a different number of cycles. The ranges of normalized strength are included as a reference for recompression specimens and those with OCR=1.0 and OCR=2.0. No specimen showed degradation of post-cyclic strength for CSR less than 0.2. For all SHANSEP specimens, both OCR=1.0 and 2.0, the degradation was first noted when CSR was equal to 0.25. For lightly OC specimens, the post-cyclic strength was larger than that of NC specimens with the exception of 1 test with OCR=1.08 which showed a lower normalized strength at CSR equal to 0.2. This result will be discussed in more detail later.

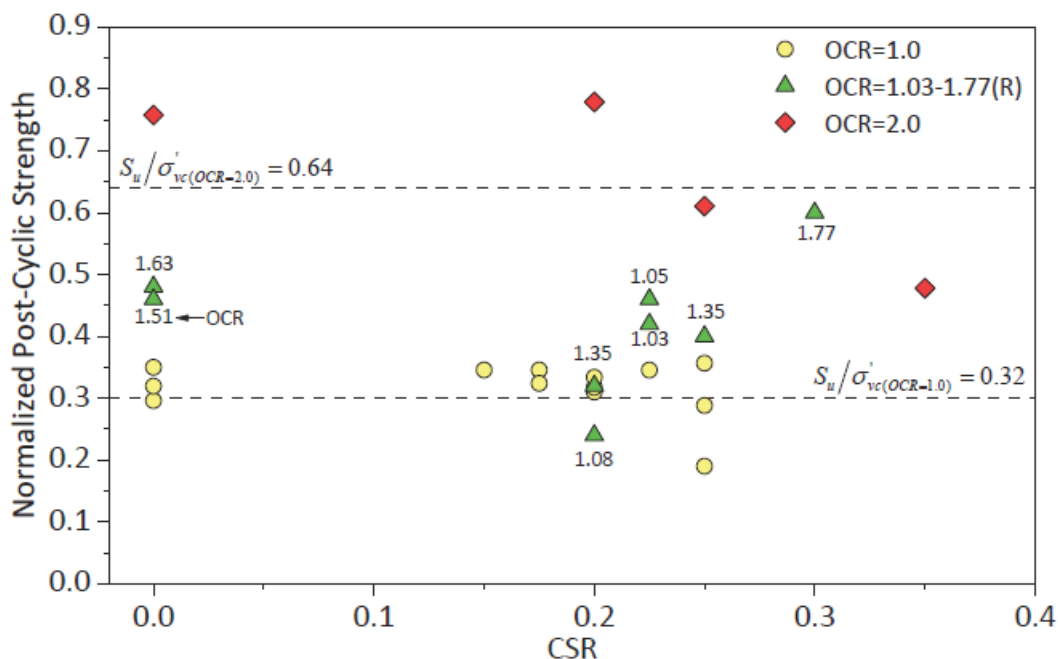
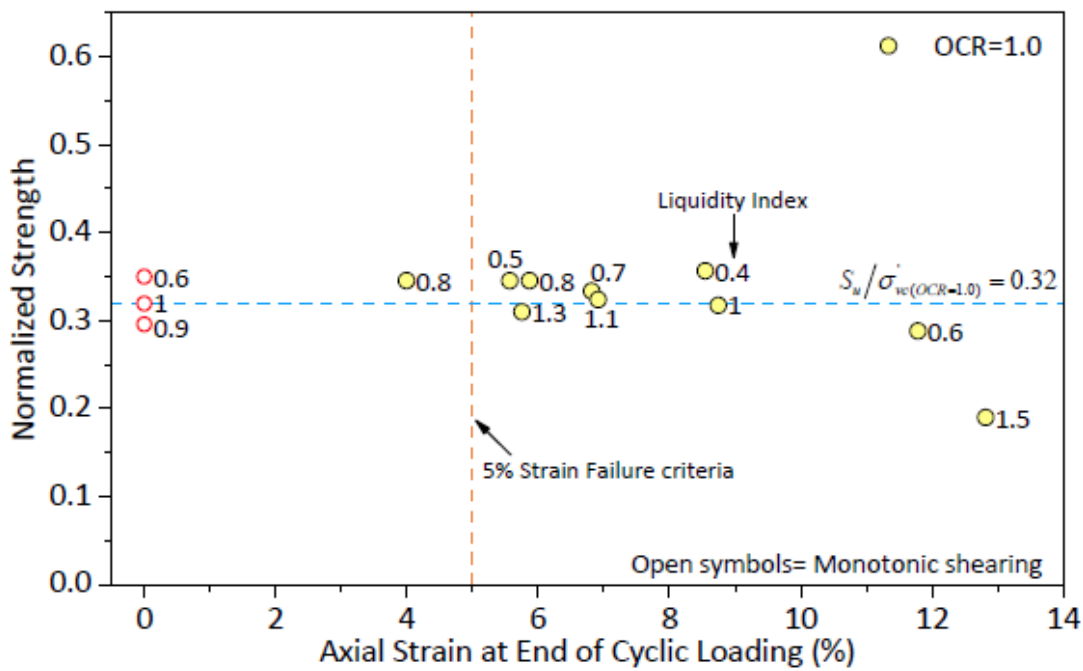


Figure 5.17. Post cyclic Undrained Strength Versus the Cyclic Stress Ratio

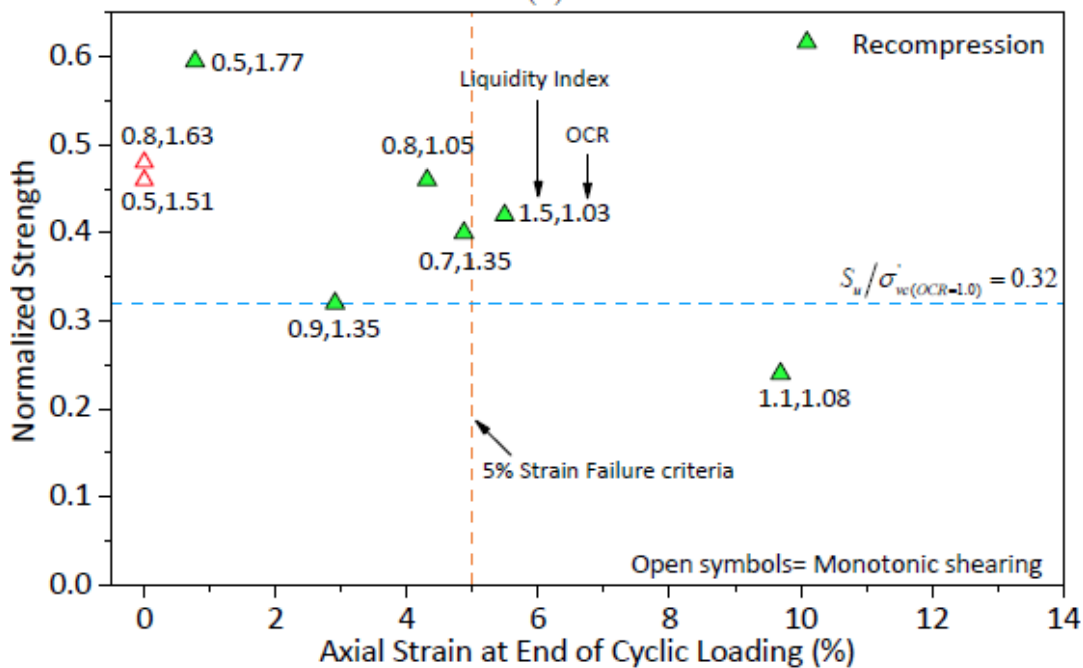
5.3.2.2 Degradation of Strength with Cyclic Axial Strain. Two main approaches have been developed to evaluate the degradation of the post-cyclic strength: the accumulation of the axial strain during cyclic loading (Thiers and Seed, 1969; Castro and Christian, 1976; Koutsoftas, 1978; Andersen et al., 1980; Perlea, 2000) and the accumulation of excess pore water pressure during cyclic loading to estimate the post-cyclic strength (Yasuhara et al., 1992; Yasuhara, 1994). Because a SHANSEP technique was used to prepare many of the specimens, the large axial strains resulting from stressing the specimen beyond the preconsolidation pressure can potentially destructure the clay specimen to some degree. The analysis presented herein considers both the axial strain that developed during cyclic loading and axial strain accumulated during both consolidation and cyclic loading.

Figure 5.18 presents the variation of the post-cyclic undrained strength with axial strain developed during cyclic loading for specimens consolidated by SHANSEP and *recompression* techniques. The numbers next to the data points in the figure correspond to the liquidity index, I_L ,

of each specimen. The corresponding OCRs also are included in Figure 5.18b for *recompression* specimens. Results of monotonic shearing were included as a reference strength and plotted at an axial strain equal to zero. The 5% failure criterion during cyclic loading was included as a reference to show that no significant degradation of strength was noted for any NC specimens prior 11% axial strain (see Figure 5.18a). *Recompression* specimens showed significant scatter when compared to the axial strain developed at the end of the cyclic loading. Two lightly OC specimens had a post-cyclic strength equal or below that of the normalized strength for NC specimens.



(a)



(b)

Figure 5.18. Undrained Strength Versus Axial Strain Developed During Cyclic Loading(a)

SHANSEP (b) Recompression

The influence of the liquidity index, I_L , in undrained strength degradation can be seen in Figure 5.18. According to Mitchell and Soga (2005), the I_L is highly correlated to the sensitivity of clay. NC specimens with higher I_L had slightly smaller normalized strengths at similar values of accumulated axial strain. At strains greater than 11%, the specimen with $I_L = 1.5$ showed more degradation as compared to that with $I_L = 0.6$. The trends in the *recompression* specimens are not as clear, although for the most part, the lowest post-cyclic normalized strengths have the highest I_L values. Results showed in Figure 5.18 indicate that, all other things being equal, sensitive specimens are more susceptible to undrained strength degradation due to cyclic loading than relative insensitive clay.

Given that cyclic strains of either 3% or 5% usually constitute “failure” in cyclic tests, the NC specimens prepared by the SHANSEP technique exhibited no significant reduction in normalized undrained strength when this strain-based “failure” was induced during cyclic loading. Since the goal of the cyclic testing in this research was to reach 5% axial strain or more, only one specimen fell in the range of 3 to 5%, and it exhibited no degradation of normalized undrained strength. Specimens which accumulated 5 to 7% axial showed similar normalized undrained strength when compared to monotonic specimens. The results in this figure indicate significant degradation did not occur until more than 11% strains had accumulated. In the case of specimens consolidated by *recompression*, some specimens degraded before reaching the 5% axial strain failure criteria. However, no reductions below the monotonic NC normalized undrained strength occurred until more than 9% strains had accumulated. The design guidelines presented in Chapter 2 did not include the accumulation of axial strain as a parameter to quantify the post-cyclic strength degradation.

5.3.2.3 Degradation of Strength with Total Axial Strain Prior Post-Cyclic Shearing. The relationship between the normalized undrained strength and the total axial strain prior to monotonic shearing is shown in Figure 5.19 for different OCR. For monotonically-loaded specimens, the total axial strains as a result of consolidation prior to shearing are shown in the figure. Results on this figure show that normalized undrained shear strength decreases with increasing total axial strains prior to monotonic shearing. A best fit equation for the data also is shown with an R^2 value of 0.62. This trend holds for both cyclic and monotonic tests, irrespective of OCR. Thus, one should consider the total strain prior to post-cyclic shearing when evaluating the degradation of normalized undrained strength due to cyclic loading, because destructuring can occur during consolidation as well as cyclic loading.

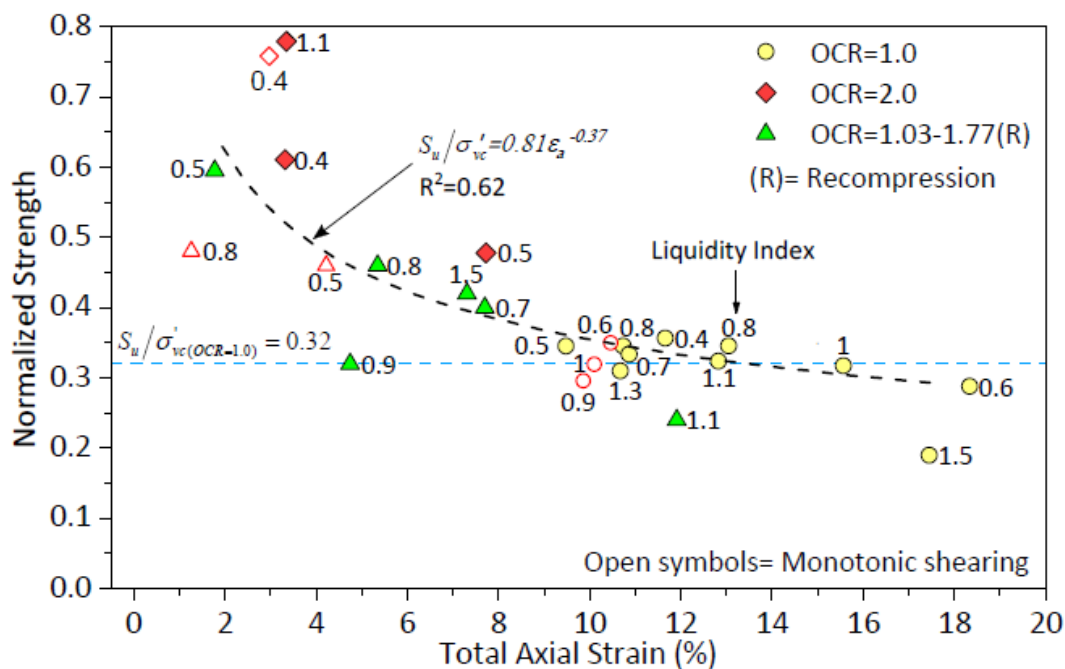


Figure 5.19. Undrained Strength Versus the Total Axial Strain Prior to Monotonic Shearing

NC specimens generally accumulated larger total axial strains prior to post-cyclic undrained shearing (at least 9%) than the *recompression* specimens. This difference largely

occurred because of the smaller consolidation-induced strains caused by the smaller vertical effective stresses applied to a *recompression* specimen during consolidation. In addition, as shown in section 5.2.3, NC specimens had a weaker response to cyclic loading leading to more accumulated axial strain than *recompression* or $OCR=2.0$ specimens.

In general, at a given strain level, specimens with a higher I_L had lower post-cyclic undrained strengths.

The results shown in Figure 5.19 indicate that the axial strain accumulated during the entire test affected the normalized post-cyclic and monotonic undrained strength of BCF clay. As one would expect, this implies that destructuration occurs during both consolidation and cyclic loading stages, a factor that has not yet been recognized in literature regarding post-cyclic strength evaluation of clay. Results based on specimens consolidated using the SHANSEP technique thus can be considered as a conservative approach because more destructuration would occur due to the high consolidation stresses needed for the SHANSEP specimens.

5.3.2.4 Degradation of Strength with the Strain Energy. The accumulation of axial strain at the end of the cyclic loading implicitly incorporates the effect of the number of cycles and the amount of stress applied, represented as the CSR. Strain energy involves the combined effect of the three variables mentioned above as well as the strains that accumulate during consolidation.

The strain energy can be expressed as:

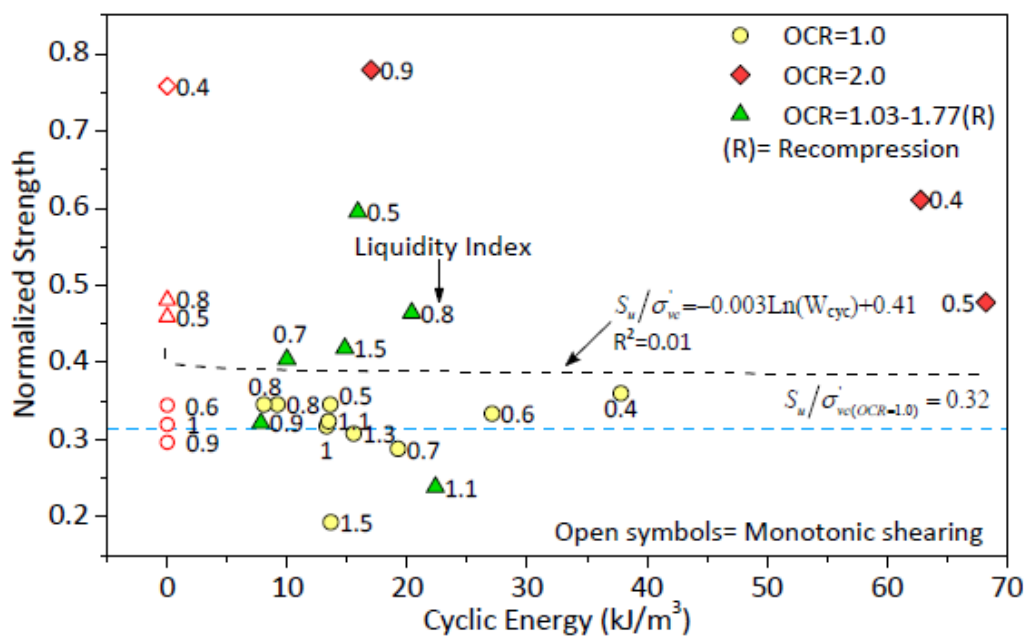
$$(5.2) \quad W = \sum_{i=1}^{i=n} \frac{(\Delta\sigma_{a(i+1)} + \Delta\sigma_{a(i)})}{2} (\varepsilon_{a(i+1)} - \varepsilon_{a(i)})$$

where, $\Delta\sigma_a$ represents the increment of total axial stress and ε_a is the axial strain. Both strain energy developed during cyclic loading and that developed during the entire test prior post-cyclic shearing

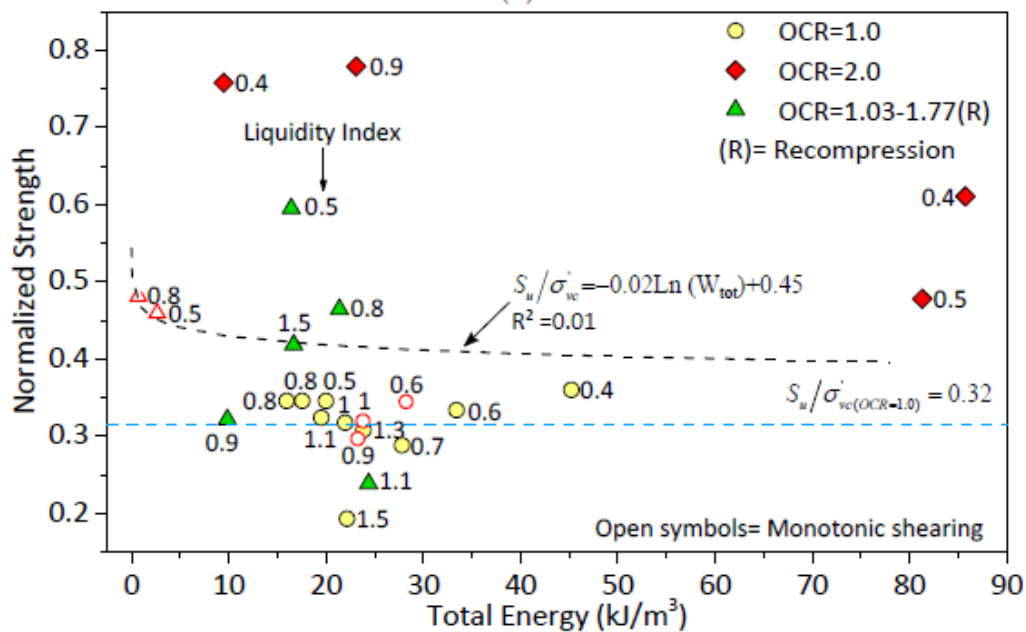
are considered in this section. For the purpose of this research, the total strain energy encompasses the summation of the strain energy from the consolidation, creep, cyclic loading, and equalization (if applies) phases of the experiments.

Figure 5.20 presents the normalized strength as a function of the cyclic and total strain energy. Both post-cyclic and monotonically sheared specimens are included in both plots. Figure 5.20a and 5.20b show no real trend in the normalized strength as the energy accumulated increase. Zergoun (1991) performed a similar analysis for Cloverdale clay and concluded no relationship could be found between the cyclic energy and the degradation of post-cyclic normalized strength. In his case, the results showed an initial degradation of strength as strains first accumulated, then as the total strain energy increased no further reduction of strength was observed.

As shown in Figure 5.19, specimens with high I_L showed a tendency have a lower normalized undrained strength than specimens with lower I_L and same amount of total strain energy. However, given the R^2 value of 0.01 for the relationship shown in Figures 5.19 and 5.20 neither total nor cyclic strain energy cannot be used as an indicator of post-cyclic normalized undrained strength for the results presented herein.



(a)



(b)

Figure 5.20. Normalized Undrained Strength Related to (a) Cyclic Strain Energy and (b) Total Strain Energy

5.3.2.5 Degradation of Strength with the Pore Water Pressure. Figure 5.21 presents the results of the normalized post-cyclic undrained strength as a function of the normalized pore water pressure accumulated at the end of the cyclic loading. The pore water pressure in most of the specimens was not equalized at the end of the cyclic loading and values shown in Figure 5.21 might differ from the uniform value within the specimen as shown in section 5.2.2. An equalization period was allowed in seven specimens (see Table 5.3) and the pore water pressure is expected to be uniform and more accurate within these specimens. Two of those specimens failed during cyclic loading, then only five are included in Figure 5.21. As a reference, results of monotonic tests are shown assuming normalized pore water pressure is zero. Results showed that cyclically-induced pore water pressure has a poor correlation with the post-cyclic undrained strength for normally and slightly overconsolidated specimens. The lack of accuracy in the pore water pressure in specimens with no equalization affects the accuracy with one could predict the degradation of post-cyclic undrained response of normally consolidated and slightly overconsolidated BCF specimens.

For specimens with OCR of 2.0, the pore water pressure shows a reasonable agreement with the post-cyclic strength. When pore water pressure accumulated increased lower post-cyclic undrained strength was observed. Two of the specimens with OCR of 2.0 were subjected to equalization period and that would improve the accuracy of the pore water pressure to predict the degradation of post-cyclic strength. However, the data are limited for OCR of 2.0 and more tests should be required allowing equalization period after cyclic loading and before post-cyclic shearing.

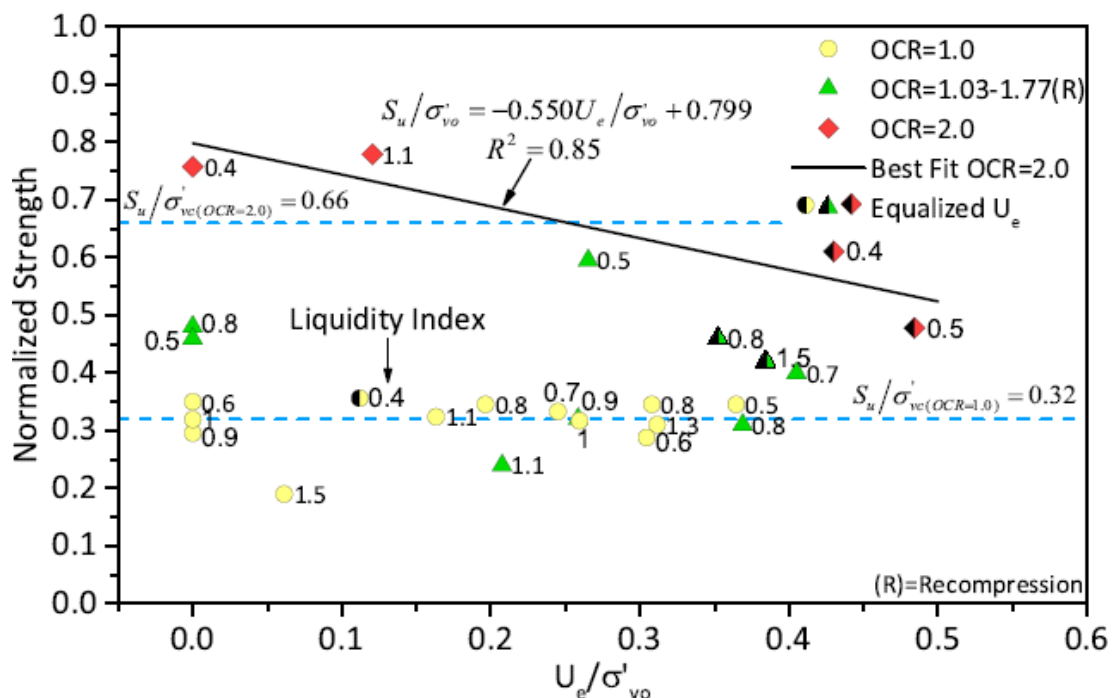


Figure 5.21. Normalized Undrained Strength Related to Pore Water Pressure at the End of Cyclic Loading

5.3.3 Effective Stress Parameters Mobilized during Post-Cyclic Shearing

As shown in section 5.3.2, the post-cyclic normalized undrained strength can be predicted better as a function of the accumulation of axial strain throughout the tests process. The effective stress strength parameters also may be affected by these factors. As shown in section 5.3.1, results of cyclic loading generally indicate an apparent cohesion contributes to the strength. However, this apparent cohesion is not present in all results. The hypothesis of this work is that the degradation of clay specimens during post-cyclic shearing is related to the degradation of the structure, as noted by the apparent cohesion, of the BCF clays.

Typical effective stress paths for different OCR states during cyclic and post-cyclic shearing are presented in Figure 5.22. The parameters in p' - q space, M and a , that correspond to the effective stress failure envelope defined by ϕ' and c , were obtained by keeping M constant and

equal to that defined in monotonic compression tests ($M=1.17$) and placing the failure line such that it includes the maximum effective stress ratio during post-cyclic undrained shearing. From this approach, one can obtain M and a , and by using Equation 4.5 and Equation 4.6 calculate ϕ' and c . Figure 5.22a, 5.22b and 5.22c did not show degradation of post-cyclic undrained strength for the different OCR and “ a ” was always greater than zero. Specimens (d), (e), and (f) showed degradation of post-cyclic undrained strength when compared to the monotonic undrained strength. In this case, “ a ” was zero for specimens (d) and (e) corresponding to $OCR=1.0$ and $OCR=1.08$.

Table 5.6 summarizes the intercept, slope, and internal friction angle mobilized during post-cyclic shearing of the NC and slightly OC specimens. The effective stress paths and failure envelopes of specimens summarized in Table 5.6 are shown in Appendix B. The mobilized friction angle, ϕ' was assumed to remain constant at 29° , corresponding to a M value of 1.17, based on monotonic results. Zapata-Medina (2012) reported an average ϕ' of 28° for triaxial compression of BCF specimens (Facies IV) at the Port of Anchorage. The mobilized intercept varied between 0 to 46 kPa. Two specimens exhibited an intercept of zero. These two specimens showed the highest reductions in undrained strength and had I_L greater than 1.0.

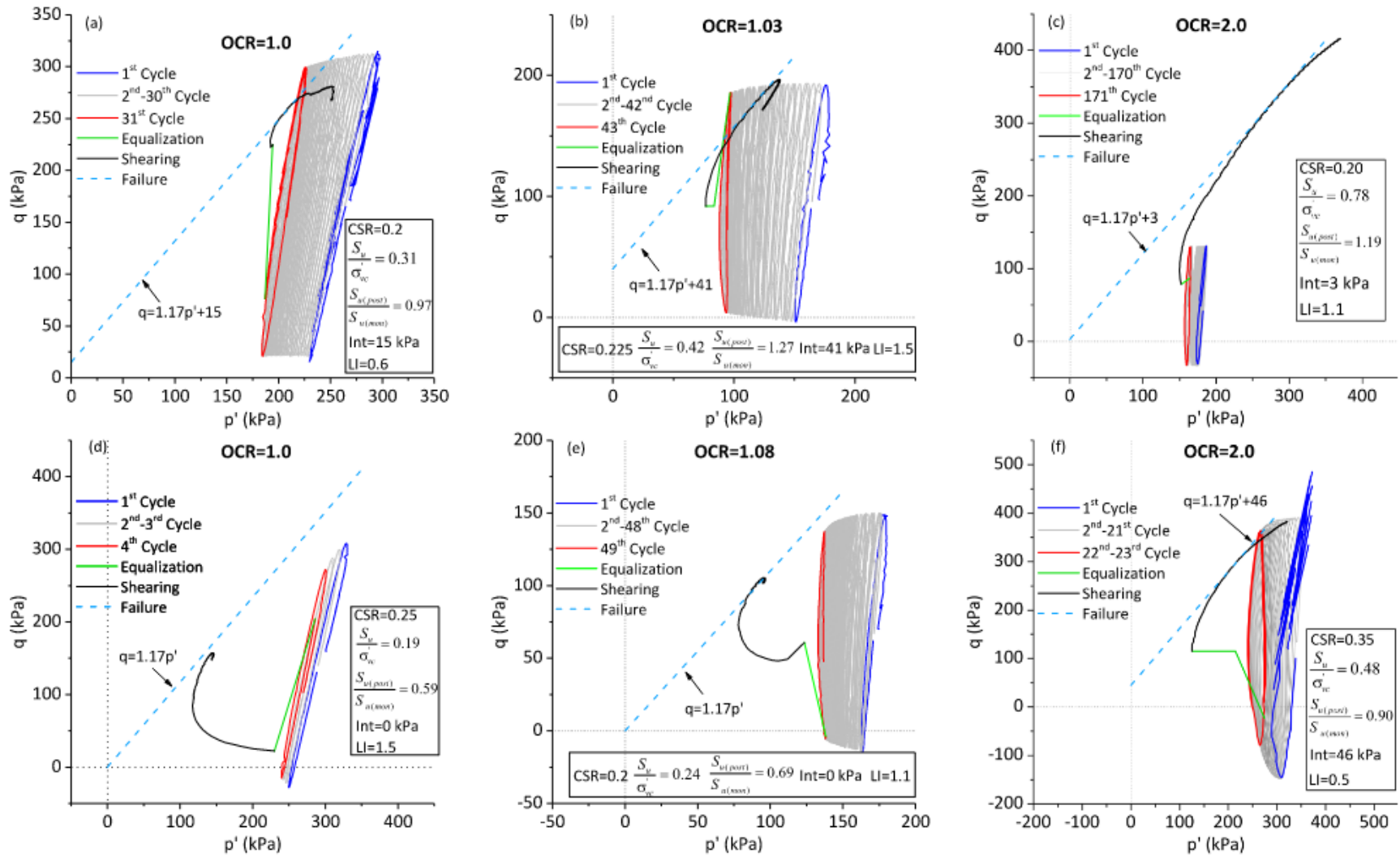
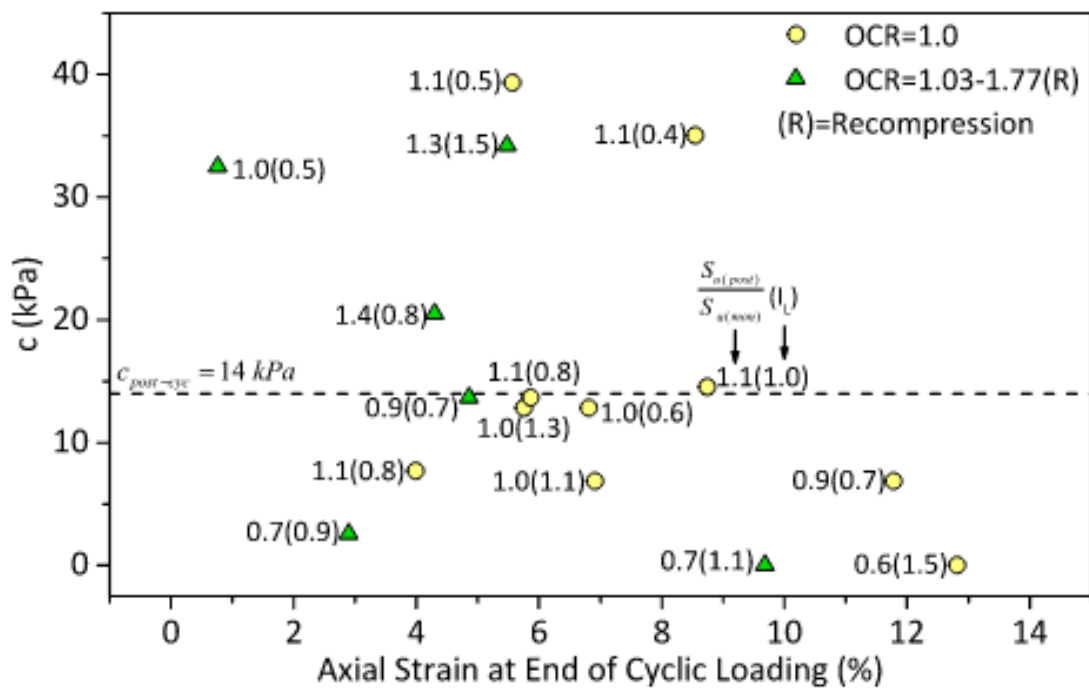


Figure 5.22. Effective Stress Path of NC and Lightly Overconsolidated Specimens in p' - q Space

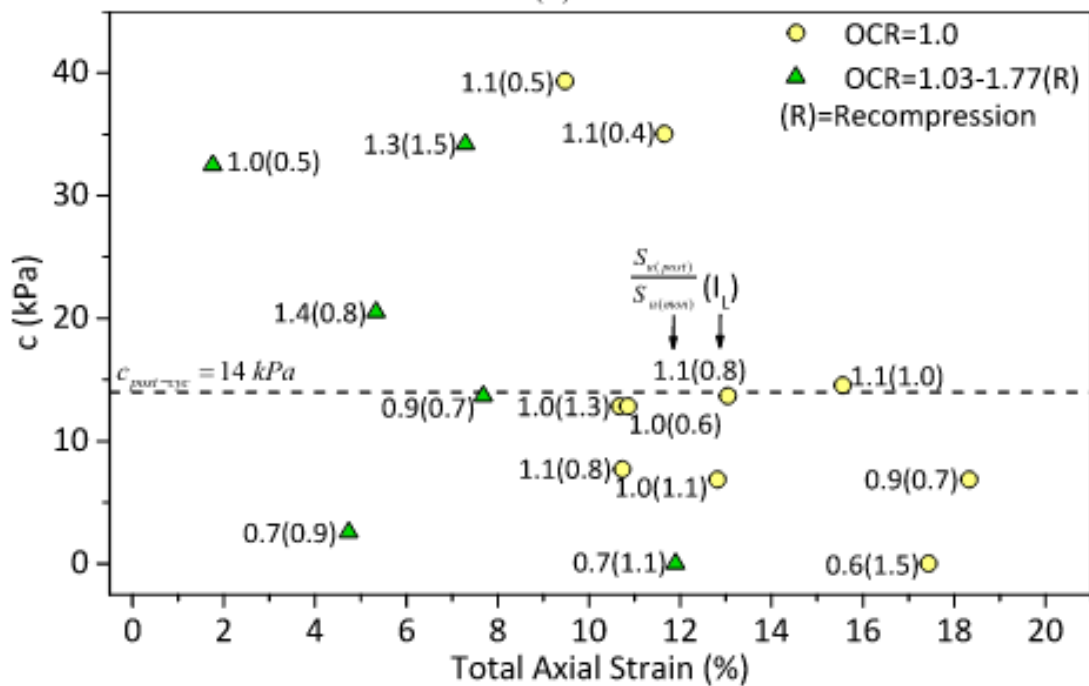
Table 5.6. Results of Effective Strength Parameters for Post-Cyclic Shearing of NC and Slightly Overconsolidated BCF specimens

Specimen	OCR	I_L	S_u/σ'_{vc}	Intercept (kPa)	M	ϕ'
NU-1 17-19	1	0.4	0.36	41		
NU-1 60-62 (2)	1	1.5	0.19	0		
NU-1 60-62 (3)	1	1.3	0.31	15		
NU-1 65-67 (2)	1	0.5	0.35	46		
NU-3 47-49	1	1.0	0.32	17		
NU-3 47-49 (2)	1	0.8	0.35	9		
NU-3 47-49 (3)	1	0.8	0.35	16		
NU-3 55-57	1	0.6	0.33	15	1.17	29
NU-3 55-57 (2)	1	0.7	0.39	8		
NU-3 60-62	1	1.1	0.32	8		
NU-1 37-39 (2)	1.77	0.5	0.6	38		
NU-1 47-49	1.35	0.9	0.32	3		
NU-1 47-49 (2)	1.35	0.7	0.4	16		
NU-1 60-62	1.08	1.1	0.24	0		
NU-1 62-64 (3)	1.05	0.8	0.46	24		
NU-1 65-67	1.03	1.5	0.42	36		

Figure 5.23 shows the apparent cohesion versus the (a) axial strain accumulated during cyclic loading only and (b) axial strain accumulated during the entire test. The apparent cohesion was computed using Eq. (4.6) and the intercept values shown in Table 5.6. Values of undrained strength ratio (i.e. $S_{u(post)}/S_{u(mon)}$) and I_L and are included for each specimen. Also, the apparent cohesion ($c_{post-cyc}$) computed from the intercept in Figure 5.14 is included as a reference. Results showed no direct correlation between the apparent cohesion and the axial strain. This was expected because as shown previously, the cyclic and post-cyclic response is also affected by the I_L of the specimen. Specimens with an apparent cohesion lower than $c_{post-cyc}$ showed, in general, a reduction in undrained strength. This is an indication that the degradation of post-cyclic strength is related to the degradation of the clay structure represented as the apparent cohesion. No reduction of undrained post-cyclic strength was observed when apparent cohesion was higher than $c_{post-cyc}$. Undrained strength ratios higher than 1.0 are attributed to material variability.



(a)



(b)

Figure 5.23. Apparent Cohesion Versus Axial Strain (a) End of Cyclic Loading (b) Total

5.3.3.1 Introduction to Boundary Surface and Degradation Framework. Figure 5.24 shows the effective stress path of specimens (a) NU-3 55-57 and (b) NU-1 60-62(2). The figure includes the boundary surface proposed by Shi (2016) at end-of-consolidation condition. Shi (2016) developed a model that includes two boundary surfaces to consider the intrinsic behavior and soil structure. The structured boundary surface shown in the figure accounts for the material structure that is related to a stronger response of undisturbed samples when compared to reconstituted ones. Figure 5.24(a) presents results of specimen NU-3 55-57 that was cyclically loaded at $CSR=0.20$. This results in a total accumulation of axial strain of 10.9%. Specimen NU-3 55-57 exhibited no degradation undrained strength. In terms of effective stress analysis, the effective stress path during post-cyclic shearing extends beyond the initial boundary surface and the apparent cohesion is higher than zero. These results suggest that no significant destructuration occurred in the specimen during cyclic loading additional to the changes in the structure imposed during consolidation to reach normally consolidated state.

Specimen NU-1 60-62(2) was cyclically loaded at $CSR=0.25$ with a total axial strain accumulation of 17.9% (shown in Figure 5.24(b)). This specimen has the highest undrained strength degradation in this testing program and its effective stress path lies completely within the end-of-consolidation boundary surface. The magnitude of the load and the number of cycles for this specimen was apparently large enough to accumulate enough strain to significantly destructure the clay producing a reduction of post-cyclic strength and reducing the apparent cohesion to zero. In this case, the boundary surface that controls the material is reduced below that of the consolidation condition as a result of destructuration during cyclic loading to accurately capture the post-cyclic strength of the specimen.

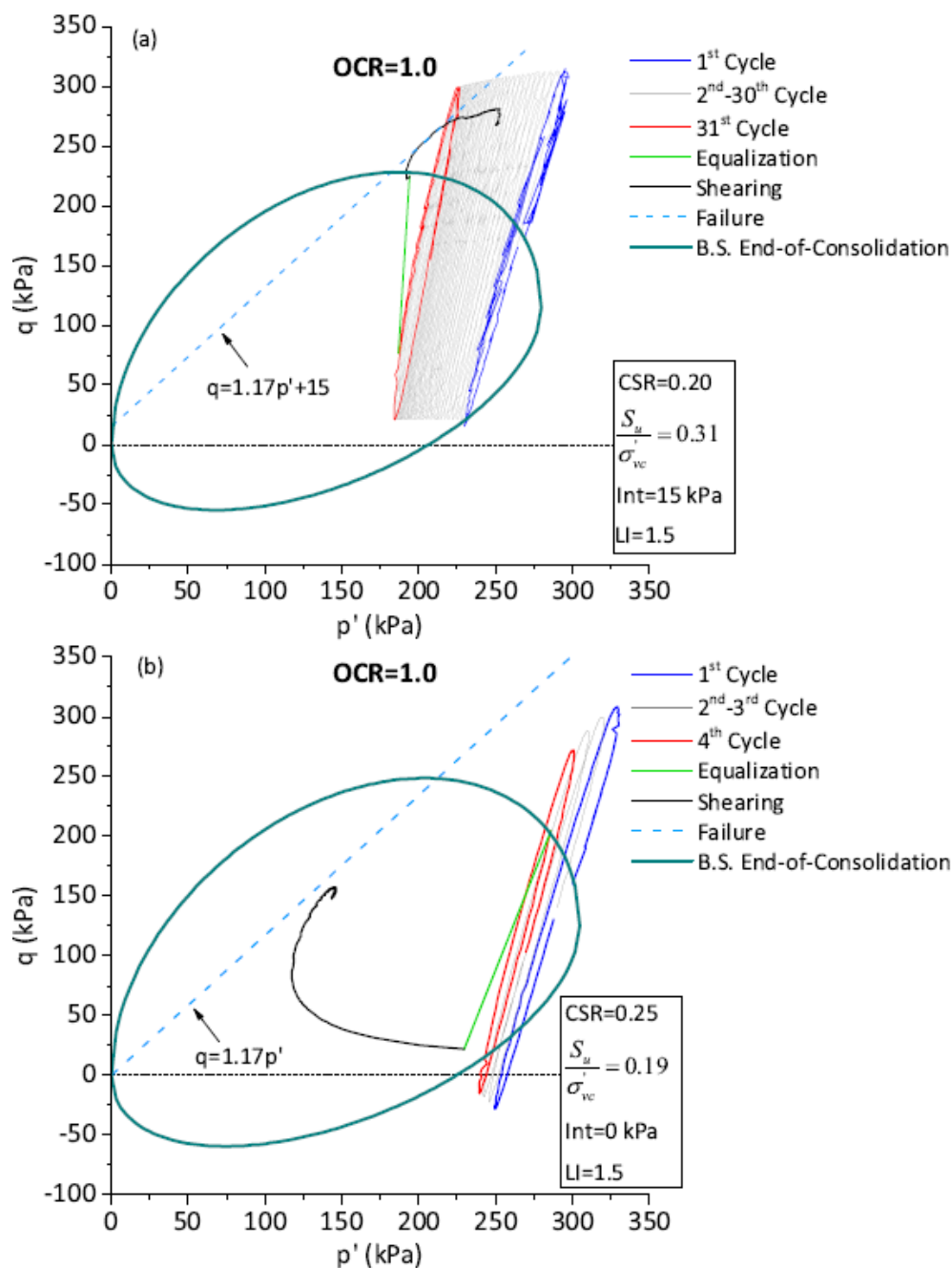


Figure 5.24. Effective Stress Path of NC Specimens Including Boundary Surface

5.4 Summary and Conclusions

This chapter presents and analyzes the cyclic and post-cyclic responses of BCF clay specimens. Some post-cyclic tests included a period of constant total stress between cyclic loading and post-cyclic shearing, in essence an undrained creep period to allow excess pore water pressures

to equilibrate after cyclic loading. For specimens that did not collapse during cyclic loading, the cyclic strength is defined as the relation of the cyclic stress ratio (CSR) and number of cycles to reach 5% axial strain, the failure criterion used in this research. This failure criterion is analyzed in terms of the effective stress at failure. A limited study of the cyclic loading rate was made to illustrate its effects on the cyclic responses of clay. The post-cyclic normalized undrained strength of BCF clay is evaluated in terms of CSR, axial strain during both cyclic loading and the total value prior to post-cyclic shearing, and strain energy.

Based on the results of the cyclic and post-cyclic undrained shearing triaxial tests, the following conclusions can be drawn:

- (1) The cyclic loading generated axial strain in the BCF clay that was dependent on the OCR of the specimen. Normally consolidated to slightly overconsolidated specimens tended to develop higher axial strain than those with higher OCR at the same cyclic stress ratio (CSR). Specimens with OCR higher than 2.0 accumulated negligible axial strain at the end of cyclic loading.
- (2) The cyclic loading generated excess pore water pressure in the BCF clay. For normally consolidated specimens, the excess pore water pressure at the end of each cycle was always positive. Overconsolidated specimens showed negative excess pore water pressure for the first cycles, then as the number the cycles increased the excess pore water pressure became positive. However, the excess pore water pressures at the end of cyclic loading are unreliable indicators of the excess pore pressures throughout the specimen due to the rapid loading rates associated with a testing frequency of 1 Hz.

- (3) NC specimens developed an apparent overconsolidation as a result of positive excess pore water pressure developed during cyclic loading.
- (4) The cyclic strength for BCF clay obtained based on a 5% axial strain failure criterion is a function of the OCR. The cyclic strength relation obtained for NC specimens consolidated by SHANSEP is described by $CSR=0.32-0.097\log(N)$ with a correlation coefficient of 0.83.
- (5) Normally consolidated specimens prepared using the SHANSEP approach exhibited a smaller normalized cyclic strength compared to those slightly overconsolidated by *recompression* when OCR was close to 1.0. These results showed that cyclic strength from specimens prepared by SHANSEP are conservative and may be more representative of the intrinsic behavior of BCF clay.
- (6) At similar CSR and axial strain at the end of consolidation, BFC specimens exhibited lower cyclic strength when their liquidity index was close or higher than 1.0.
- (7) Within the limitations of the pore water pressure measurements, comparison between effective stresses at the end of cyclic loading and the effective stress failure envelope determined by monotonic tests results show that the 5% axial strain failure criterion is not failure in terms of fully mobilizing the BCF shearing resistance. Thus, this approach is conservative.
- (8) The rate of loading produced a significant difference in the stress-strain and excess pore water pressure-strain responses of specimens subjected to cyclic loading. The strain controlled specimens resulted in more degradation when compared to the stress controlled specimens cyclically loaded at 1 Hz.

- (9) Results indicated that the post-cyclic normalized undrained strength of BCF specimens depends on the total strain prior the post-cyclic shearing (i.e., axial strain from consolidation and cyclic shearing. This result implies that a SHANSEP approach will lead to conservative results. The accumulation of axial strain is not recognized in the design guidelines mentioned in this work that only provide a range of degradation based on the magnitude of the earthquake.
- (10) For NC SHANSEP specimens, no reduction of post-cyclic undrained normalized strength was observed until approximately 17% axial strain had accumulated during consolidation (6% axial strain) and cyclic loading (11% axial strain).
- (11) Results showed the influence of the liquidity index in the degradation of the post-cyclic undrained strength. Some of the specimens with a liquidity index above 1.0 exhibited significant loss of post-cyclic undrained strength for the imposed CSR.
- (12) Cyclically-induced pore water pressures are not a satisfactory indicator of the post-cyclic strength degradation because in cyclic tests with a frequency of 1 Hz, measured values of pore water pressure are not representative and do not reflect “uniform” value for the specimen since the time is too short for pore water pressure equalization to occur. Furthermore, degradation of structure can also occur during consolidation.
- (13) The apparent cohesion during post-cyclic shearing poorly correlated to the axial strain accumulated at the end of cyclic loading and from the whole test. Results indicated that this apparent cohesion also depends on the liquidity index. Specimens with a liquidity index higher than 1.0 generally showed lower values of apparent cohesion at similar axial strain accumulated.

- (14) Some specimens that accumulated large axial strains during consolidation and cyclic loading mobilized zero or near zero effective cohesion. This is an indication that the degradation of post-cyclic strength is related to the degradation of the clay structure represented as the apparent cohesion.
- (15) Based on this research results, a reduction of 10 to 15% of the post-cyclic undrained strength to account for cyclic loading can be unrealistic for all conditions. More degradation can occur in specimens that accumulate large axial strains. In this work, reduction of post-cyclic undrained strength reached a maximum of 40% at axial strain accumulated during cyclic loading of 11% for a sensitive specimen with a liquidity index of 1.5.

CHAPTER 6

6 SUMMARY AND CONCLUSIONS

6.1 Summary

The goal of this research is to understand the cyclic behavior and post-cyclic degradation of Bootlegger Cover Formation (BCF) clay. The analysis of cyclic loading during earthquakes is a key procedure in the design of slopes and foundations in seismically active zones. The landslides that occurred in Anchorage, Alaska during the 1964 Alaska earthquake are clear evidence that clay slopes can fail under cyclic loading. While undrained strengths approaching residual values were determined based on the movements of the slides after failure was initiated, the triggering conditions have not been quantified. This research utilized samples collected at Lynn Ary Park, adjacent to the Turnagain Heights landslide escarpment. This location is the same as that used by USGS (Updike et al., 1988) in their evaluations of the sensitivity of the BCF clay. This research establishes index properties, consolidation characteristics and monotonic strength of the BCF clay at this location based on field and laboratory testing. It also examines the cyclic and post-cyclic response of BCF specimens tested in a triaxial device.

Chapter 2 presents a literature review describing the BCF properties and cyclic and post-cyclic behavior of soft and sensitive clays. The index properties and stratigraphy at Lynn Ary Park and the Fourth Avenue slide are summarized. Cyclic and post-cyclic shear strength of clays from eastern Canada, Norway, and Sweden are presented. The cyclic behavior is discussed in terms of axial strain failure criteria, rate of shearing, sensitivity, initial shear stresses and consolidation history. This chapter also summarizes the response of sensitive clay to post-cyclic undrained shearing based on axial strain and pore water pressure accumulated during cyclic loading.

Chapter 3 presents the testing procedures employed in this research to study the cyclic and post-cyclic behavior of BCF specimens collected at Lynn Ary Park. The cyclic triaxial equipment

and procedures for the monotonic and cyclic testing are described, as are specimen preparation techniques. The stages of each test include residual stress and saturation, consolidation by SHANSEP or recompression techniques and drained creep. Then either undrained monotonic shearing or cyclic loading was conducted. When collapse did not occur during cyclic loading, then post-cyclic undrained shearing was applied, either with or without an undrained creep stage for pore pressure equalization prior to the shearing. For every specimen, the shear wave velocity was measured during consolidation and monotonic shearing.

Chapter 4 summarizes the stratigraphy and soil parameters of the BCF clay at Lynn Ary Park at the location of the Northwestern field investigation. It also presents the soil profile and facies description based on the in situ exploration conducted by Updike et al. (1988). The logs for NU-1 and NU-3 borings are presented and include a description of the samples, soil classification, index properties, field vane and sensitivity, stress history and undrained strength. The index properties and shear wave velocity collected in this research are compared to those presented by USGS (Updike et al., 1988). The stress history of the deposit is based on the results of the reconsolidation of the laboratory specimens prepared by SHANSEP techniques. The preconsolidation pressure, OCR, and the coefficient of earth pressure at rest are presented. Results of specimen quality are evaluated based on the shear wave velocity and the axial strain that develops as each specimen is first reconsolidated to its in situ vertical effective stress. The undrained strength is based on the results of monotonic triaxial compression tests, CPT results (Updike et al., 1988) and field vane results. The sensitivity of the BCF clays based on field vane and CPT results are compared to those given by Shannon and Wilson Inc. (1964) and Updike et al. (1988).

Chapter 5 presents and analyzes the cyclic and post-cyclic responses of BCF clay specimens. Results of cyclic triaxial testing are expressed in terms of the accumulation of axial strain and pore water pressure. Some post-cyclic tests included a period of constant total stress between cyclic loading and post-cyclic shearing, in essence an undrained creep period to allow excess pore water pressures to equilibrate after cyclic loading. The cyclic strength is presented as the relation of the cyclic stress ratio (CSR) and number of cycles to reach 5% axial strain, the failure criterion used in this research. This failure criterion is analyzed in terms of the effective stress at failure. A limited study of the loading rate was made to illustrate its effects on the cyclic responses of clay. The post-cyclic undrained strength of BCF clay is evaluated in terms of CSR, axial strain during both cyclic loading and the total value prior to post-cyclic shearing, and strain energy.

6.2 Conclusions

From the results of the boring, and field strength testing and index and consolidation testing, the following conclusions can be drawn:

- (1) The soil profile at Lynn Ary Park consists of an approximately 6 m thick surficial granular soil, geologically called the Naptowne outwash. The BCF is found below the outwash and extended to the bottom of the field investigation conducted as part of this work. A stiff clay (facies IV as defined by Updike) lies directly beneath the outwash and is interbedded with silty sand lenses up to depth of 12 m (El. 8.4 m). Underlying the stiff clay, there is a wet, medium stiff to soft clay (facies III). The medium to soft clay extends to the bottom of the boring at 20.4 m (El. 0 m); however, the continuity of this clay layer is interrupted at an approximately 15 m

(El. 5.4 m) depth by a 0.6 m thick layer of medium dense fine sand. The water table at the time of the Northwestern field work was located 3.6 m (El. 16.8 m) below the ground surface.

- (2) Atterberg limits indicated the facies III and IV of BCF clay are a low plasticity clay (CL) with similar liquid and plastic limits. Because of the higher natural water contents found in the facies III clays, the average liquidity index was 0.8 for facies III compared to 0.50 from facies IV. Liquidity indexes as high as 1.5 occasionally were found in facies III.
- (3) Consolidation test results indicated that OCR decreased with depth, presumably as a result of desiccation. The OCR in facies III decreased from 1.8 at the top of the stratum to 1.03 at elevation 0 m.
- (4) The SHANSEP parameters α and m in the normalized monotonic undrained triaxial compression strength were 0.32 and 1.04, respectively. Specimens used to determine this relation were from both facies III and IV. Zapata- Medina (2012) reported values of 0.3 and 0.8 for the same shearing mode of BCF clay specimens from facies IV at the Port of Anchorage. The drained stress friction angle, ϕ' , based on results on triaxial compression tests on normally consolidated specimens, was 29°.
- (5) Undrained strength from CPT and field vane tests generally decreased with depth consistent with the observation that OCR decreased with depth.
- (6) When the CPT results were plotted in the normalized soil behavior type (SBTn) chart (Robertson, 1990), most of data indicated soil type 3 (clay to silty clay). The facies IV data indicated that the layer was overconsolidated whereas that from

facies III was typically normally consolidated. No data from facies III, which was deemed sensitive by USGS, plotted as soil type 1 a sensitive, fine grained soil. CPT results plotted in an updated SBTn chart that included sensitivity contours (Robertson, 2009) indicated that the sensitivity of the clays was less than or equal to 5.

- (7) Results from the field vane conducted by Northwestern University indicated that the sensitivity of the facies III stratum varied between 2 and 5 with the highest sensitivity near the sand layer in facies III. These findings agreed with the results presented by Shannon and Wilson Inc. (1964). In contrast, the maximum sensitivity obtained by Updike et al. (1988) was obtained in the middle of the facies III layer.

Based on the results of the cyclic and post-cyclic undrained shearing triaxial tests, the following conclusions can be drawn:

- (1) The cyclic loading generated axial strain in the BCF clay that was dependent on the OCR of the specimen. Normally consolidated to slightly overconsolidated specimens tended to develop higher axial strain than those with higher OCR at the same cyclic stress ratio (CSR). Specimens with OCR higher than 2.0 accumulated negligible axial strain at the end of cyclic loading.
- (2) The cyclic loading generated excess pore water pressure in the BCF clay. For normally consolidated specimens, the excess pore water pressure at the end of each cycle was always positive. Overconsolidated specimens showed negative excess pore water pressure for the first cycles, then as the number the cycles increased the excess pore water pressure became positive. However, the excess pore water

pressures at the end of cyclic loading are unreliable indicators of the excess pore pressures throughout the specimen due to the rapid loading rates associated with a testing frequency of 1 Hz.

- (3) NC specimens developed an apparent overconsolidation as a result of positive excess pore water pressure developed during cyclic loading.
- (4) The cyclic strength for BCF clay obtained based on a 5% axial strain failure criterion is a function of the OCR. The cyclic strength relation obtained for NC specimens consolidated by SHANSEP is described by $CSR=0.32-0.097\log(N)$ with a correlation coefficient of 0.83.
- (5) Normally consolidated specimens prepared using the SHANSEP approach exhibited a smaller normalized cyclic strength compared to those slightly overconsolidated by *recompression* when OCR was close to 1.0. These results showed that cyclic strength from specimens prepared by SHANSEP are conservative and may be more representative of the intrinsic behavior of BCF clay.
- (6) At similar CSR and axial strain at the end of consolidation, BFC specimens exhibited lower cyclic strength when their liquidity index was close or higher than 1.0.
- (7) Within the limitations of the pore water pressure measurements, comparison between effective stresses at the end of cyclic loading and the effective stress failure envelope determined by monotonic tests results show that the 5% axial strain failure criterion is not failure in terms of fully mobilizing the BCF shearing resistance. Thus, this approach is conservative.

- (8) The rate of loading produced a significant difference in the stress-strain and excess pore water pressure-strain responses of specimens subjected to cyclic loading. The strain controlled specimens resulted in more degradation when compared to the stress controlled specimens cyclically loaded at 1 Hz.
- (9) Results indicated that the post-cyclic normalized undrained strength of BCF specimens depends on the total strain prior the post-cyclic shearing (i.e., axial strain from consolidation and cyclic shearing). This result implies that a SHANSEP approach will lead to conservative results. The accumulation of axial strain is not recognized in the design guidelines mentioned in this work that only provide a range of degradation based on the magnitude of the earthquake.
- (10) For NC SHANSEP specimens, no reduction of post-cyclic undrained normalized strength was observed until approximately 17% axial strain had accumulated during consolidation (6% axial strain) and cyclic loading (11% axial strain).
- (11) Results showed the influence of the liquidity index in the degradation of the post-cyclic undrained strength. Some of the specimens with a liquidity index above 1.0 exhibited significant loss of post-cyclic undrained strength for the imposed CSR.
- (12) Cyclically-induced pore water pressures are not a satisfactory indicator of the post-cyclic strength degradation because in cyclic tests with a frequency of 1 Hz, measured values of pore water pressure are not representative and do not reflect “uniform” value for the specimen since the time is too short for pore water pressure equalization to occur. Furthermore, degradation of structure can also occur during consolidation.

- (13) The apparent cohesion during post-cyclic shearing poorly correlated to the axial strain accumulated at the end of cyclic loading and from the whole test. Results indicated that this apparent cohesion also depends on the liquidity index. Specimens with a liquidity index higher than 1.0 generally showed lower values of apparent cohesion at similar axial strain accumulated.
- (14) Some specimens that accumulated large axial strains during consolidation and cyclic loading mobilized zero or near zero effective cohesion. This is an indication that the degradation of post-cyclic strength is related to the degradation of the clay structure represented as the apparent cohesion.
- (15) Based on this research results, a reduction of 10 to 15% of the post-cyclic undrained strength to account for cyclic loading can be unrealistic for all conditions. More degradation can occur in specimens that accumulate large axial strains. In this work, reduction of post-cyclic undrained strength reached a maximum of 40% at axial strain accumulated during cyclic loading of 11% for a sensitive specimen with a liquidity index of 1.5.

References

- Åhnberg, H., Larsson, R., & Holmén, M. (2013). *Degradation of clay due to cyclic loadings and deformations*. Paper presented at the Proceedings of the 18th international conference on soil mechanics and geotechnical engineering ICSMGE, Paris.
- Andersen, K. H., Rosenbrand, W. F., Brown, S. F., & Pool, J. H. (1980). Cyclic and static laboratory tests on Drammen clay. *Journal of the Geotechnical Engineering Division*, 106(5), 499-529.
- Andresen, A. (1979). The NGI 54-mm Samplers for Undisturbed Sampling of Clays and Representative Sampling of Coarser Materials, State of the Art on Current Practice of Soil Sampling. Paper presented at the Progressing of The International Symposium of Soil Sampling, Singapore, 1979.
- Ansal, A. M., & Erken, A. (1989). Undrained behavior of clay under cyclic shear stresses. *Journal of Geotechnical Engineering*, 115(7), 968-983.
- ASTM D854-14. (2014). Standard test methods for specific gravity of soil solids by water pycnometer: ASTM international.
- ASTM D1587 / D1587M-15. (2015). Standard Practice for Thin-Walled Tube Sampling of Fine-Grained Soils for Geotechnical Purposes: ASTM International.
- ASTM D2216-10. (2010). Standard test methods for laboratory determination of water (moisture)

content of soil and rock by mass: ASTM International.

ASTM D2573 / D2573M-15. (2015). Standard Test Method for Field Vane Shear Test in Saturated Fine-Grained Soils: ASTM International.

ASTM D4186 / D4186M-12e1. (2012). Standard Test Method for One-Dimensional Consolidation Properties of Saturated Cohesive Soils Using Controlled-Strain Loading: ASTM International.

ASTM D4318-17e1. (2017). Standard Test Methods for Liquid Limit, Plastic Limit, and Plasticity Index of Soils: ASTM International.

ASTM D4452-14. (2014). Standard Practice for X-Ray Radiography of Soil Samples: ASTM International.

ASTM D4767-11. (2011). Standard test method for consolidated undrained triaxial compression test for cohesive soils: ASTM International.

Azzouz, A. S., Malek, A. M., & Baligh, M. M. (1989). Cyclic behavior of clays in undrained simple shear. *Journal of Geotechnical Engineering*, 115(5), 637-657.

Baligh, M. M. (1985). Strain path method. *Journal of Geotechnical Engineering*, 111(9), 1108-1136.

Baligh, M. M., Azzouz, A. S., & Chin, C.-T. (1987). Disturbances due to “ideal” tube sampling. *Journal of Geotechnical Engineering*, 113(7), 739-757.

Becker, D., Crooks, J., Been, K., & Jefferies, M. (1987). Work as a criterion for determining in situ and yield stresses in clays. *Canadian Geotechnical Journal*, 24(4), 549-564.

Bjerrum, L. (1973). Problems of soil mechanics and construction on soft clays, State of the art report, Session 4. *Proc. of 8th ICSMFE, Moscow*, 3, 109-159.

Boulanger, R. W., & Idriss, I. (2006). Liquefaction susceptibility criteria for silts and clays. *Journal*

- of geotechnical and geoenvironmental engineering, 132(11), 1413-1426.
- Boulanger, R. W., & Idriss, I. (2007). Evaluation of cyclic softening in silts and clays. *Journal of geotechnical and geoenvironmental engineering*, 133(6), 641-652.
- Cho, W., Holman, T. P., Jung, Y.-H., & Finno, R. J. (2007). Effects of swelling during saturation in triaxial tests in clays. *Geotechnical Testing Journal*, 30(5), 378-386.
- Clayton, C., & Heymann, G. (1999). Stiffness of geomaterials from small strain triaxial and field geophysical tests. Paper presented at the Proceedings of the Second International Symposium on Pre-failure Deformation Characteristics of Geomaterials.
- Farrar, J. A., Torres, R., and Crutchfield, L. G. (2008). Cone penetrometer testing, scoggins dam, tualatin project, oregon. Technical report, Engineering Geology Group Bureau of Reclamation, Technical Services Center, Denver, Co (Report No. 86-68320). Retrieved from
- Finno, R. J., & Chung, C.-K. (1992). Stress-strain-strength responses of compressible Chicago glacial clays. *Journal of Geotechnical Engineering*, 118(10), 1607-1625.
- Finno, R. J., & Kim, T. (2012). Effects of stress path rotation angle on small strain responses. *Journal of geotechnical and geoenvironmental engineering*, 138(4), 526-534.
- GDS Instruments Ltd. (2013). *The GDS 2Hz/5Hz/10Hz Dynamic Testing System Hardware Handbook*: GDS Instruments Ltd.
- GDS Instruments Ltd. (2015). *The GDS Bender Elements System Hardware Handbook for Vertical and Horizontal Elements*: GDS Instruments Ltd.
- Hanna, A. M., & Javed, K. (2008). Design of foundations on sensitive Champlain Clay subjected to cyclic loading. *Journal of geotechnical and geoenvironmental engineering*, 134(7), 929-937.

- Hanna, A. M., & Javed, K. (2014). Experimental investigation of foundations on sensitive clay subjected to cyclic loading. *Journal of geotechnical and geoenvironmental engineering*, 140(11), 04014065.
- Holman, T. P., & Finno, R. J. (2005). Maximum shear modulus and incrementally nonlinear soils. Paper presented at the Proceedings of the International Conference on Soil Mechanics and Geotechnical Engineering.
- Holtz, R. D., Kovacs, W. D., & Sheahan, T. C. (2011). *An introduction to geotechnical engineering* (2nd Edition ed. Vol. 733): Prentice-Hall Englewood Cliffs, NJ.
- Houston, W. N., & Mitchell, J. K. (1971). Property interrelationships in sensitive clays. *Journal of Soil Mechanics & Foundations Div.*
- Idriss, I. M., Dobry, R. u., & Sing, R. (1978). Nonlinear behavior of soft clays during cyclic loading. *Journal of geotechnical and geoenvironmental engineering*, 104(ASCE 14265).
- Jaky, I. (1944). The coefficient of earth pressure at rest. *Journal Soc. of Hungarian Architects and Engineers*, 355-358.
- Jamiolkowki, M. (1988). New developments in field and laboratory testing of soils. Paper presented at the International conference on soil mechanics and foundation engineering. 11.
- Kavazanjian, E. (2011). *LRFD Seismic Analysis and Design of Transportation Geotechnical Features and Structural Foundations: Reference Manual*: US Department of Transportation, Federal Highway Administration, National
- Koutsoftas, D. (1978). Effect of cyclic loads on undrained strength of two marine clays. *Journal of geotechnical and geoenvironmental engineering*, 104(ASCE 13751).
- Kramer, S. (1996). *Geotechnical earthquake engineering*, Prentice Hall Upper Saddle River. New

Jersey.

- Ladd, C. C. (1991). Stability evaluation during staged construction. *Journal of Geotechnical Engineering*, 117(4), 540-615.
- Ladd, C. C., & DeGroot, D. J. (2004). Recommended practice for soft ground site characterization: Arthur Casagrande Lecture: Massachusetts Institute of Technology.
- Ladd, C. C., & Foott, R. (1974). New design procedure for stability of soft clays. *Journal of geotechnical and geoenvironmental engineering*, 100(Proc Paper 10064).
- Ladd, C. C., & Lambe, T. W. (1964). The strength of "undisturbed" clay determined from undrained tests. In *Laboratory shear testing of soils*: ASTM International.
- Lade, P., Updike, R. G., & Cole, D. A. (1988). Cyclic triaxial tests of the Bootlegger Cove formation, Anchorage, Alaska: US Government Printing Office.
- Lee, K. L. (1979). Cyclic strength of a sensitive clay of eastern Canada. *Canadian Geotechnical Journal*, 16(1), 163-176.
- Lee, K. L., & Focht Jr, J. A. (1976). Strength of clay subjected to cyclic loading. *Marine Georesources & Geotechnology*, 1(3), 165-185.
- Lefebvre, G., LeBoeuf, D., & Demers, B. (1989). Stability threshold for cyclic loading of saturated clay. *Canadian Geotechnical Journal*, 26(1), 122-131.
- Lefebvre, G., & Pfendler, P. (1996). Strain rate and preshear effects in cyclic resistance of soft clay. *Journal of Geotechnical Engineering*, 122(1), 21-26.
- Lunne, T., Berre, T., Andersen, K. H., Strandvik, S., & Sjørnsen, M. (2006). Effects of sample disturbance and consolidation procedures on measured shear strength of soft marine Norwegian clays. *Canadian Geotechnical Journal*, 43(7), 726-750.
- Lunne, T., & Kleven, A. (1981). Role of CPT in North Sea foundation engineering. *Cone*

Penetration Testing and Experience, 76-107.

Lunne, T., Powell, J. J., & Robertson, P. K. (1997). Cone penetration testing in geotechnical practice. Retrieved from

Matsui, T., Ito, T., & Ohara, H. (1980). Cyclic stress-strain history and shear characteristics of clay. *Journal of the Geotechnical Engineering Division*, 106(10), 1101-1120.

Meigh, A. C. (2013). *Cone penetration testing: methods and interpretation*: Elsevier.

Mitchell, J. K. (1973). Sensitivity and geotechnical properties of Bootlegger Cove clay. The great Alaska earthquake of 1964, 157-178.

Mitchell, J. K., & Soga, K. (2005). *Fundamentals of soil behavior (Vol. 3)*: John Wiley & Sons New York.

Mortezaie, A. R., & Vucetic, M. (2013). Effect of frequency and vertical stress on cyclic degradation and pore water pressure in clay in the NGI simple shear device. *Journal of geotechnical and geoenvironmental engineering*, 139(10), 1727-1737.

Olsen, H. W. (1989). Sensitive strata in Bootlegger Cove formation. *Journal of Geotechnical Engineering*, 115(9), 1239-1251.

Perlea, V. G. (2000). Liquefaction of cohesive soils. In *Soil Dynamics and Liquefaction 2000* (pp. 58-76).

Robertson, P. K. (1990). Soil classification using the cone penetration test. *Canadian Geotechnical Journal*, 27(1), 151-158.

Robertson, P. K. (2009). Interpretation of cone penetration tests—a unified approach. *Canadian Geotechnical Journal*, 46(11), 1337-1355.

Rosenqvist, I. T. (1953). Considerations on the sensitivity of Norwegian quick-clays. *Geotechnique*, 3(5), 195-200.

- Santagata, M. C., & Germaine, J. T. (2002). Sampling disturbance effects in normally consolidated clays. *Journal of geotechnical and geoenvironmental engineering*, 128(12), 997-1006.
- Schmidt, B. (1966). Earth pressures at rest related to stress history. *Canadian Geotechnical Journal*, 3(4), 239-242.
- Seed, B., & Lee, K. L. (1966). Liquefaction of saturated sands during cyclic loading. *Journal of Soil Mechanics & Foundations Div*, 92(ASCE# 4972 Proceeding).
- Seed, H. B., & Wilson, S. D. (1967). The turnagain heights landslide, Anchorage, Alaska. *Journal of Soil Mechanics & Foundations Div*, 93(4), 325-353.
- Shannon and Wilson Inc. (1964). Report of Anchorage Area Soil Studies. Retrieved from Anchorage, Alaska:
- Shi, Z. (2016). Numerical modelling of cyclic degradation of natural clay. (PhD), Northwestern University,
- Skempton, A., & Northey, R. (1952). The sensitivity of clays. *Geotechnique*, 3(1), 30-53.
- Skempton, A. W., & Northey, R. D. (1952). The sensitivity of clays. *Geotechnique*, 3(1), 30-53.
- Stark, T. D., & Contreras, I. A. (1998). Fourth Avenue landslide during 1964 Alaskan earthquake. *Journal of geotechnical and geoenvironmental engineering*, 124(2), 99-109.
- Thiers, G. R., & Seed, H. B. (1969). Strength and stress-strain characteristics of clays subjected to seismic loading conditions. In *Vibration effects of earthquakes on soils and foundations*: ASTM International.
- Urdike, R. G., Olsen, H. W., & Schmoll, H. R. (1988). Geologic and geotechnical conditions adjacent to the Turnagain Heights landslide, Anchorage, Alaska: Department of the Interior, US Geological Survey.
- Vucetic, M., & Dobry, R. (1988). Degradation of marine clays under cyclic loading. *Journal of*

Geotechnical Engineering, 114(2), 133-149.

Vyalov, S. S. (2013). Rheological fundamentals of soil mechanics: Elsevier.

Washington Department of Transportation. (2015). Geotechnical design manual. Retrieved from Olympia, Washington:

Wichtmann, T., Andersen, K. H., Sjursen, M. A., & Berre, T. (2013). Cyclic tests on high-quality undisturbed block samples of soft marine Norwegian clay. *Canadian Geotechnical Journal*, 50(4), 400-412.

Yasuhara, K. (1994). Postcyclic undrained strength for cohesive soils. *Journal of Geotechnical Engineering*, 120(11), 1961-1979.







Yasuhara, K., Hirao, K., & Hyde, A. F. L. (1992). Effects of cyclic loading on undrained strength and compressibility of clay. *Soils and Foundations*, 32(1), 100-116.




Zapata-Medina, D. (2012). Evaluation of Dynamic Soil Parameter Changes Due to Construction Induced Stresses. (PhD), Northwestern University,






Zergoun, M. (1991). Effective stress response of clay to undrained cyclic loading. (PhD), University of British Columbia,



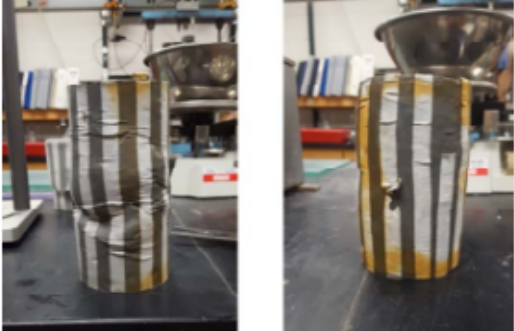

Appendix A




Appendix A. Boring Logs with Photos


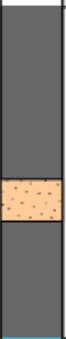



 Northwestern University		Log of Boring NU-1		Project: BCF exploration Location: Anchorage, AK Start Date: 07/13/2015 End Date: 7/14/2015 Elevation: 20.42 m	Page 1 of 7
Depth (m)	Eleva. (m)	Graphic log	Material Description	Photos of Samples	
5					
	15		<p>(SP-SM) Fine sand (post-BCF) from top to 12" with a presence of gravel on top. (CL) Gray, dry, stiff clay with presence of several thin silty sand lenses to the bottom of the tube</p>		
6					
	14		<p>(SP-SM) Fine sand (post-BCF) from top to 9" with a presence of gravel on top. (CL) Gray, dry, stiff clay with presence of several thin silty sand lenses to the bottom of the tube. Higher water content at the contact with sand</p>		
7			<p>(CL) Gray, dry, stiff clay with presence of several thin silty sand lenses along the cross section of the samples. 1" thick lense at 7" from the top of the tube</p>		

 Northwestern University		Log of Boring NU-1		Project: BCF exploration Location: Anchorage, AK Start Date: 07/13/2015 End Date: 7/14/2015 Elevation: 20.42 m	Page 2 of 7
Depth (m)	Eleva. (m)	Graphic log	Material Description	Photos of Samples	
13					
8					
12			(CL) Material from cutting from top to 6". From 6", stiff clay with presence of some silty sand lenses		
9					
11					

 Northwestern University		Log of Boring NU-1		Project: BCF exploration Location: Anchorage, AK Start Date: 07/13/2015 End Date: 7/14/2015 Elevation: 20.42 m	Page 3 of 7
Depth (m)	Eleva. (m)	Graphic log	Material Description	Photos of Samples	
10			From top to 6" material from the cutting. (CL) From 6" to 10", stiff clay with presence of silty sand lenses. 7" to bottom, homogeneous stiff clay. No silty sand lenses were observed		
10					
11					
9			From 0 to 8" material from cutting, very disturbed. (CL) Homogeneous Gray, dry, stiff clay. Cracks have silty sand material.		
12					

 Northwestern University		Log of Boring NU-1		Project: BCF exploration Location: Anchorage, AK Start Date: 07/13/2015 End Date: 7/14/2015 Elevation: 20.42 m	Page 4 of 7
Depth (m)	Eleva. (m)	Graphic log	Material Description	Photos of Samples	
8			(CL) Homogeneous Gray, medium stiff clay. Material is softer and wetter compared to shallower samples.		
13			From top to 3" material from the cutting. (CL) From 3" to bottom homogeneous, Gray, wet and soft clay. So silty sand lenses observed.		
7					
14			Material from cutting from top up to 12". (CL) From 12" to bottom homogeneous, Gray, wet and soft clay.		

 Northwestern University		Log of Boring NU-1		Project: BCF exploration Location: Anchorage, AK Start Date: 07/13/2015 End Date: 7/14/2015 Elevation: 20.42 m	Page 5 of 7
Depth (m)	Eleva. (m)	Graphic log	Material Description	Photos of Samples	
6			From top to 3" material from the cutting. (CL) From 3" to bottom homogeneous, Gray, wet, soft clay. So silty sand lenses observed.		
15					
5			(CL) From top to 6" of homogeneous, Gray, wet, medium stiff clay. (SP-SM) Fine sand with 7% of fines from 16" to bottom		
16					
4					

 Northwestern University		Log of Boring NU-1		Project: BCF exploration Location: Anchorage, AK Start Date: 07/13/2015 End Date: 7/14/2015 Elevation: 20.42 m	Page 6 of 7
Depth (m)	Eleva. (m)	Graphic log	Material Description	Photos of Samples	
17			From top to 13" material from the cutting, probably a mixed of clay and sand. (CL) From 13" to 16" a fine sand layer (SP-SM). From 16" to the bottom Gray, wet, medium stiff clay, no silty sand lenses observed		
3					
18					
2			From top to 3" material from the cutting. (CL) From 4" to bottom homogeneous, Gray, wet, soft clay. So silty sand lenses observed		
19					



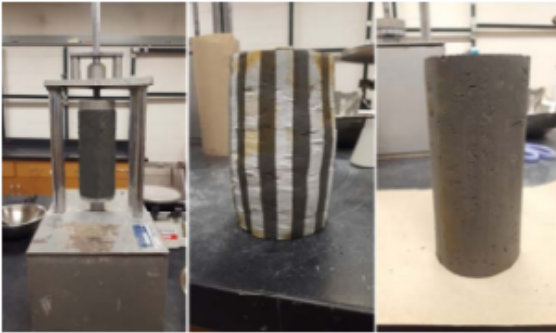

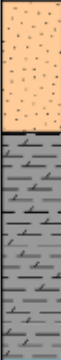


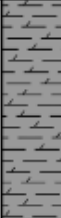


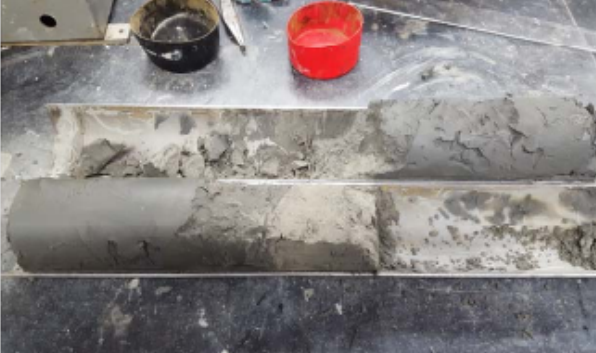











 Northwestern University		Log of Boring NU-1		Project: BCF exploration Location: Anchorage, AK Start Date: 07/13/2015 End Date: 7/14/2015 Elevation: 20.42 m	Page 7 of 7
Depth (m)	Eleva. (m)	Graphic log	Material Description	Photos of Samples	
1			From top to 4" material from the cutting. (CL) From 4" to bottom homogeneous , Gray, wet, soft clay. So silty sand lenses observed		
20			From top to 4" material from the cutting. (CL) From 3" to bottom homogeneous , Gray, wet, soft clay. Inside the samples, silty sand lenses observed		
0					



Figure A.1. Boring Log NU-1

 Northwestern University		Log of Boring NU-3		Project: BCF exploration Location: Anchorage, AK Start Date: 07/16/2015 End Date: 7/16/2015 Elevation: 20.42 m	Page 1 of 6
Depth (m)	Eleva. (m)	Graphic log	Material Description	Material Description	
13					
8			<p>(SP-SM) From top to 8" fine sand very wet that leaked during the cutting.</p> <p>(CL) From 8" to the bottom was composed of dry, stiff clay with presence of silty sand lenses</p>		
12					
9					

 Northwestern University		Log of Boring NU-3		Project: BCF exploration Location: Anchorage, AK Start Date: 07/16/2015 End Date: 7/16/2015 Elevation: 20.42 m	Page 2 of 6
Depth (m)	Eleva. (m)	Graphic log	Material Description	Material Description	
11			(CL) Homogeneous clay along the tube, Gray, stiff. Silty sand lenses are present at 20" to 23" from the top of the tube.		
10					
10					
11			(CL) From 6" to 13" uniform Gray, stiff clay. (SP) Presence of silty sand lense of 4" thick with some presence of clay. (CL) From 17" to bottom, same stiff clay present as 6" to 13"		
9					

 Northwestern University		Log of Boring NU-3		Project: BCF exploration Location: Anchorage, AK Start Date: 07/16/2015 End Date: 7/16/2015 Elevation: 20.42 m		Page 3 of 6
Depth (m)	Eleva. (m)	Graphic log	Material Description	Material Description		
12						
8			<p>(CL) From 5" to 12" Gray, medium stiff clay, similar to that one present in NWU1 40-42. From 12" to 19" the material is drier with high presence of silty sand lenses. From 19" to bottom the material is similar to upper one</p>			
13			<p>From top to 6" material from the cutting. (CL) From 6" to bottom homogeneous, Gray, wet and soft clay. So silty sand lenses observed</p>			
7						

 Northwestern University		Log of Boring NU-3		Project: BCF exploration Location: Anchorage, AK Start Date: 07/16/2015 End Date: 7/16/2015 Elevation: 20.42 m		Page 4 of 6
Depth (m)	Eleva. (m)	Graphic log	Material Description	Material Description		
14						
6			<p>(CL) From top to 19" Gray, wet, soft clay with presence of silty some silty sand lenses. From 19" to the bottom sand layer</p>			
15						
5			<p>(ML) Top to 5" consists a silt very wet with very sensitive lenses. (CL) From 5" to the bottom fine sand with a 7% fine content</p>			

 Northwestern University		Log of Boring NU-3		Project: BCF exploration Location: Anchorage, AK Start Date: 07/16/2015 End Date: 7/16/2015 Elevation: 20.42 m		Page 5 of 6
Depth (m)	Eleva. (m)	Graphic log	Material Description	Material Description		
16						
4						
17			From top to 6" material from the cutting. (CL) From 6" to bottom homogeneous, Gray, wet and soft clay. No silty sand lenses observed			
3						
18						




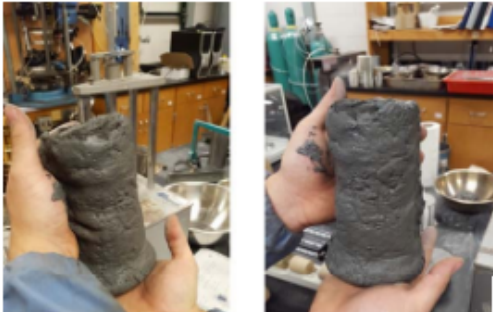
 Northwestern University		Log of Boring NU-3		Project: BCF exploration Location: Anchorage, AK Start Date: 07/16/2015 End Date: 7/16/2015 Elevation: 20.42 m		Page 6 of 6
Depth (m)	Eleva. (m)	Graphic log	Material Description	Material Description		
2			From top to 10" material from the cutting. (CL) From 10" to the bottom Gray, wet, soft clay. No silty sand lenses observed			
19			(CL) Very disturbed Gray, wet, soft clay. 6" of material recovered			
1						
20			(CL) Very disturbed Gray, wet, soft clay. The material was collpasing by its own weight. 12" of material recovered			

Figure A.2. Boring Log NU-3

Appendix B

Appendix B. Triaxial Results of BCF Specimens

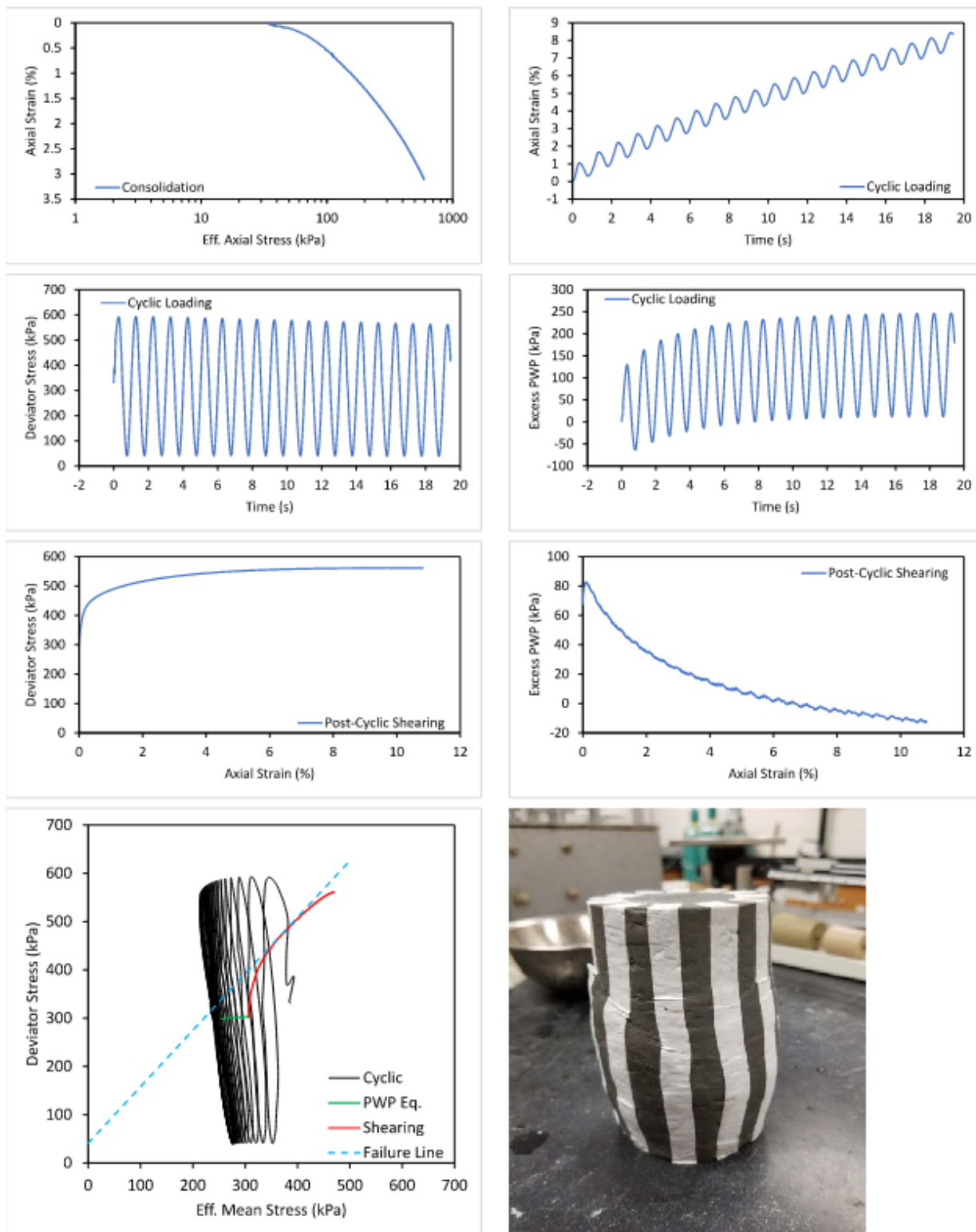


Figure B.1. Specimen NU-1 17-19

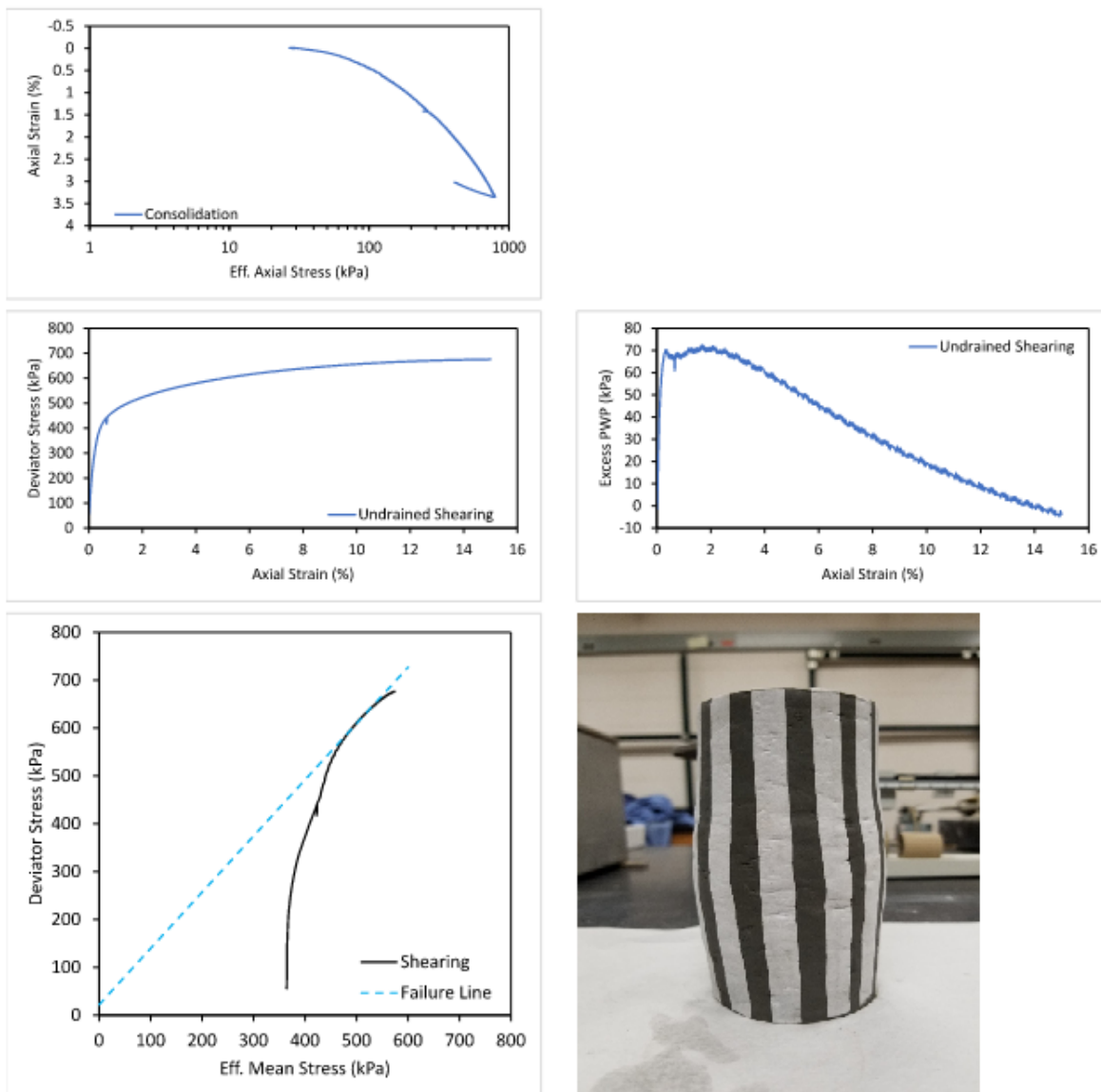


Figure B.2. Specimen NU-1 20-22

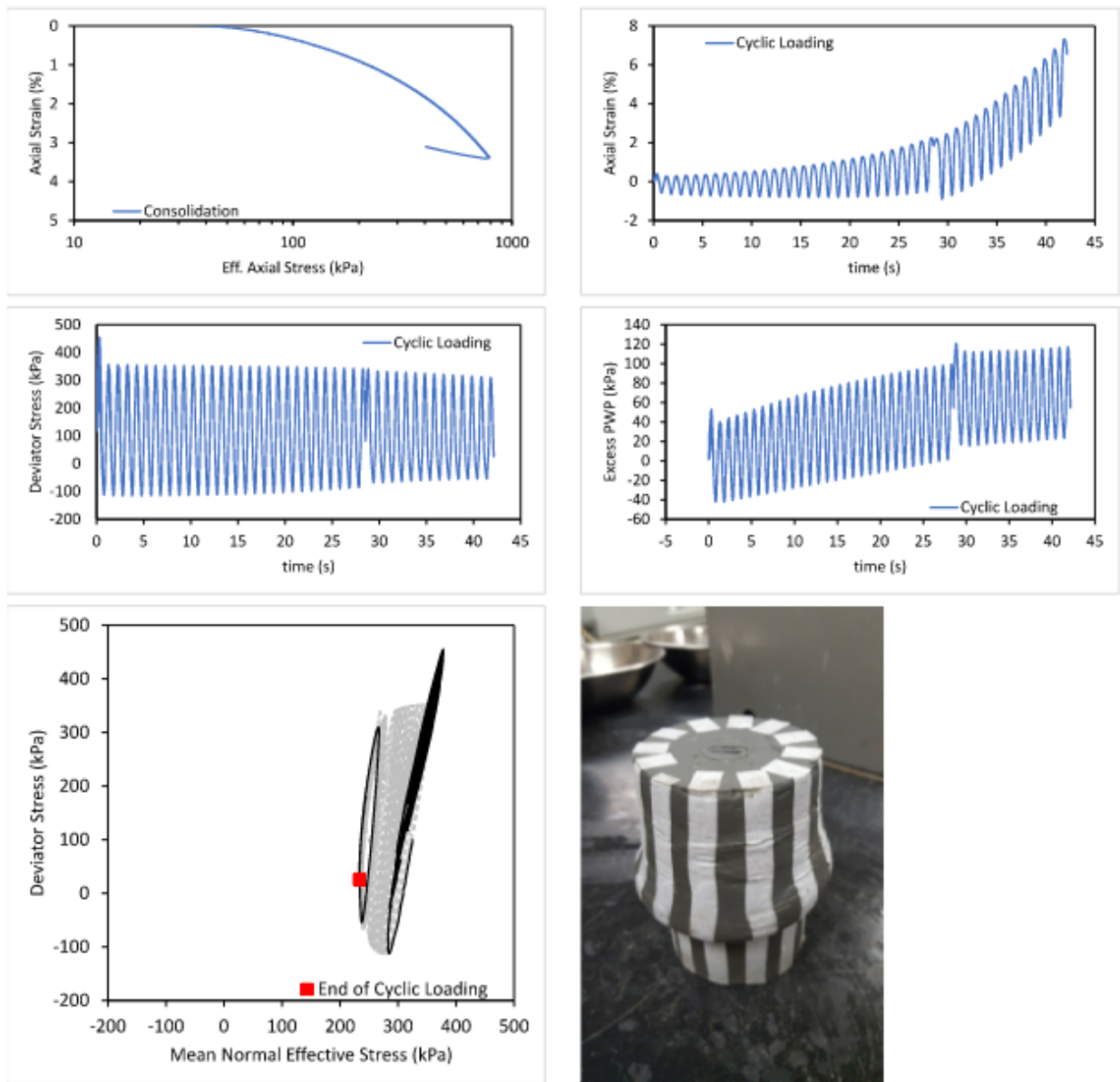


Figure B.3. Specimen NU-1 22-24

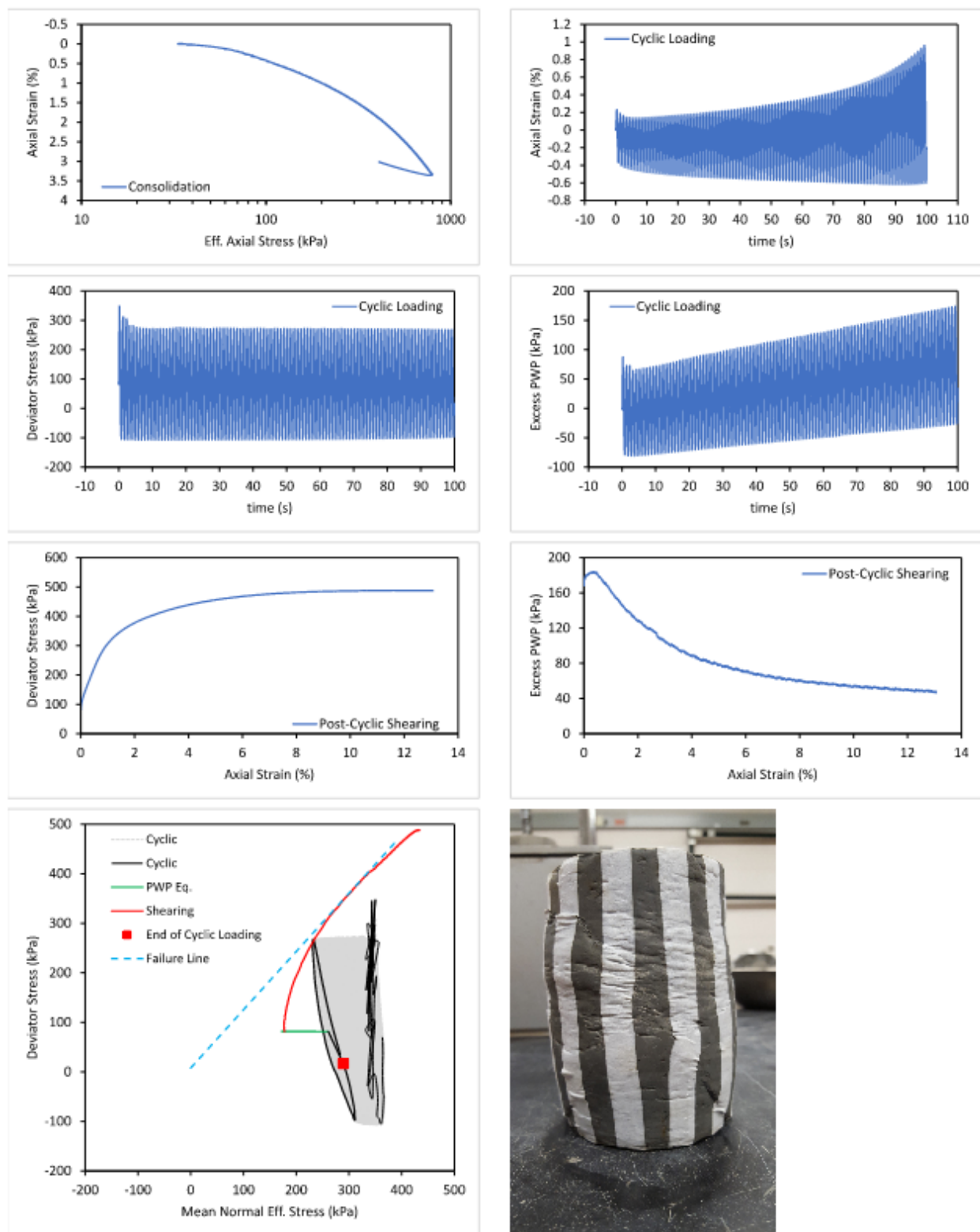


Figure B.4. Specimen NU-1 22-24(2)

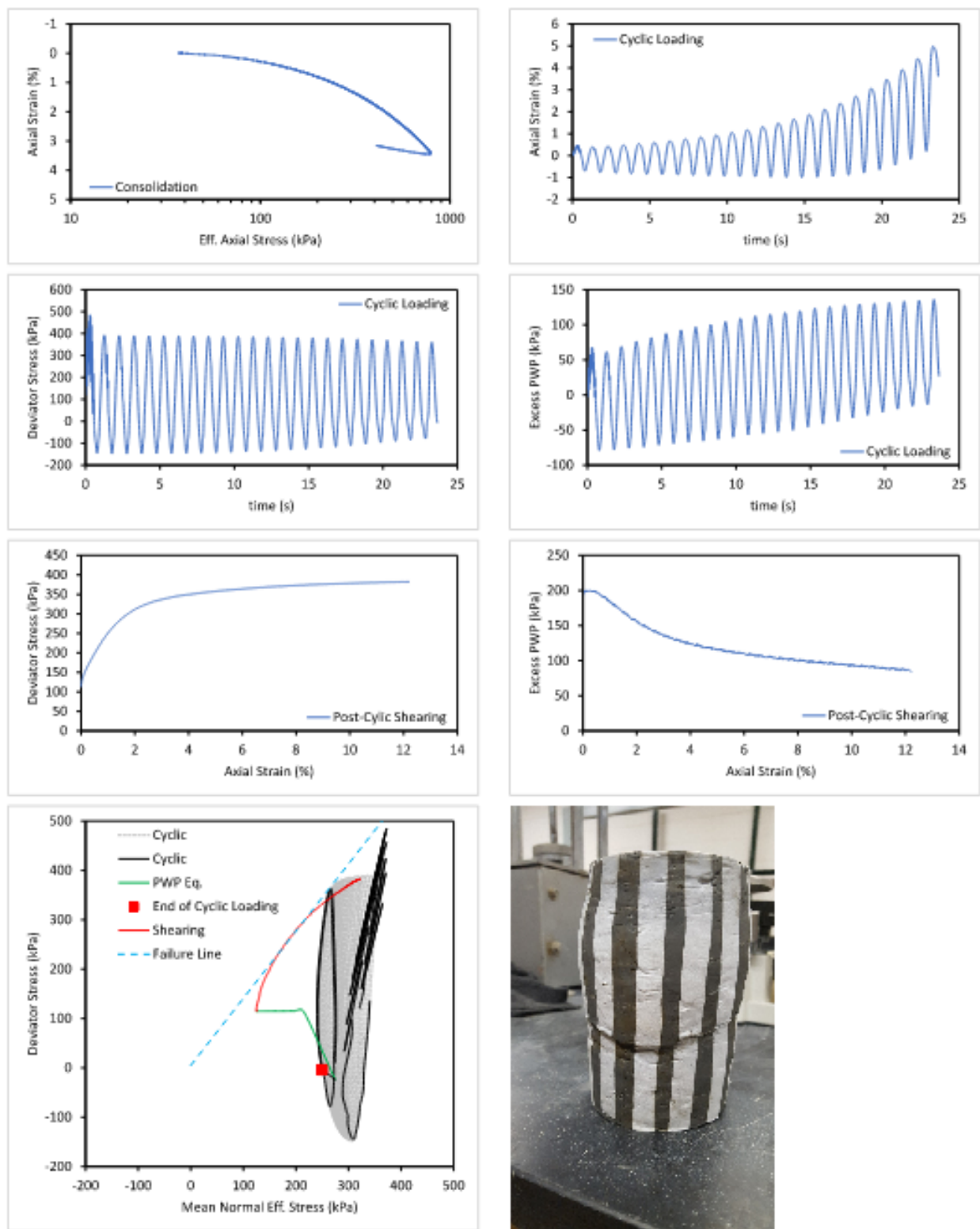


Figure B.5. Specimen NU-1 22-24(3)

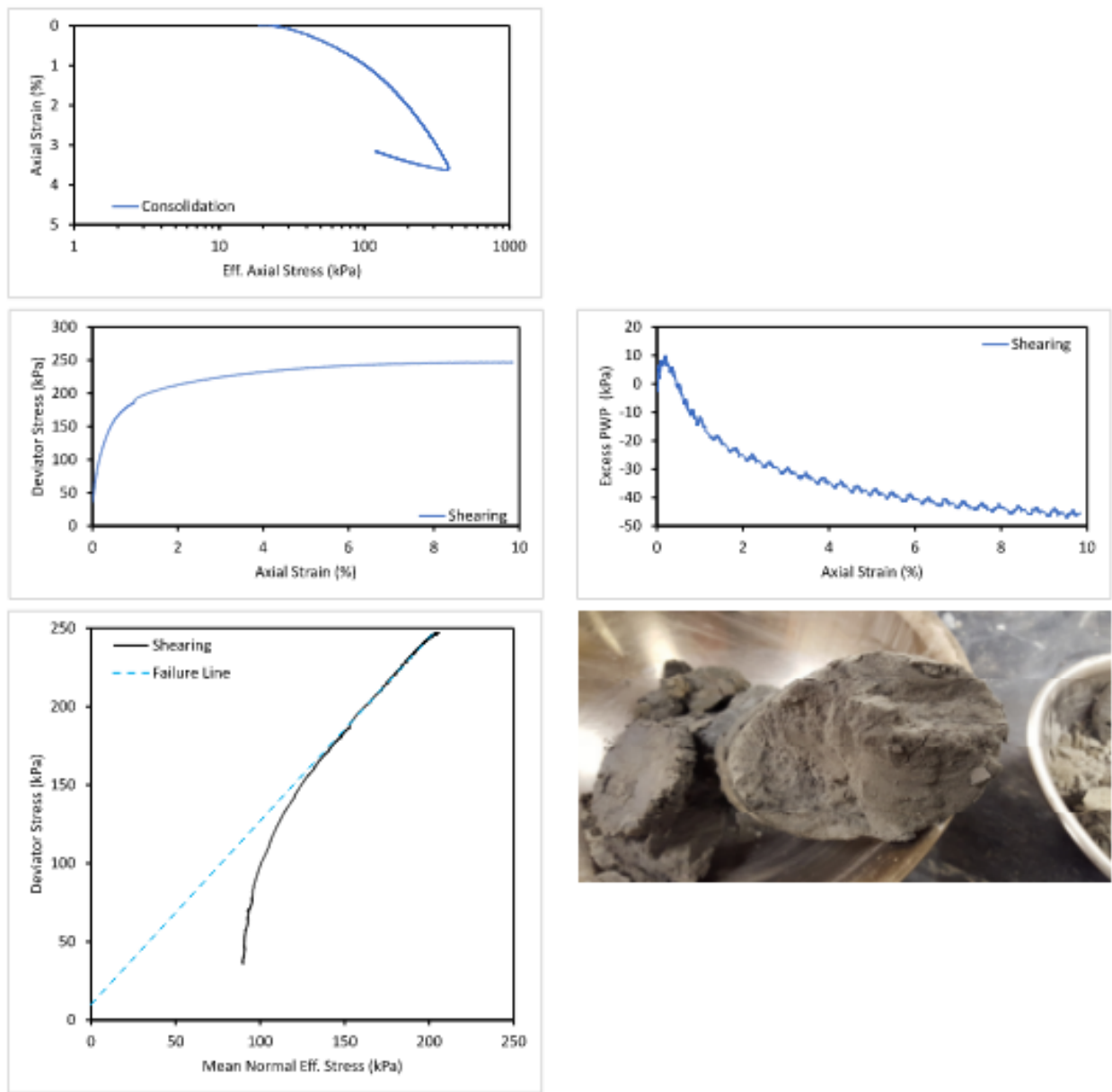


Figure B.6. Specimen NU-1 27-29

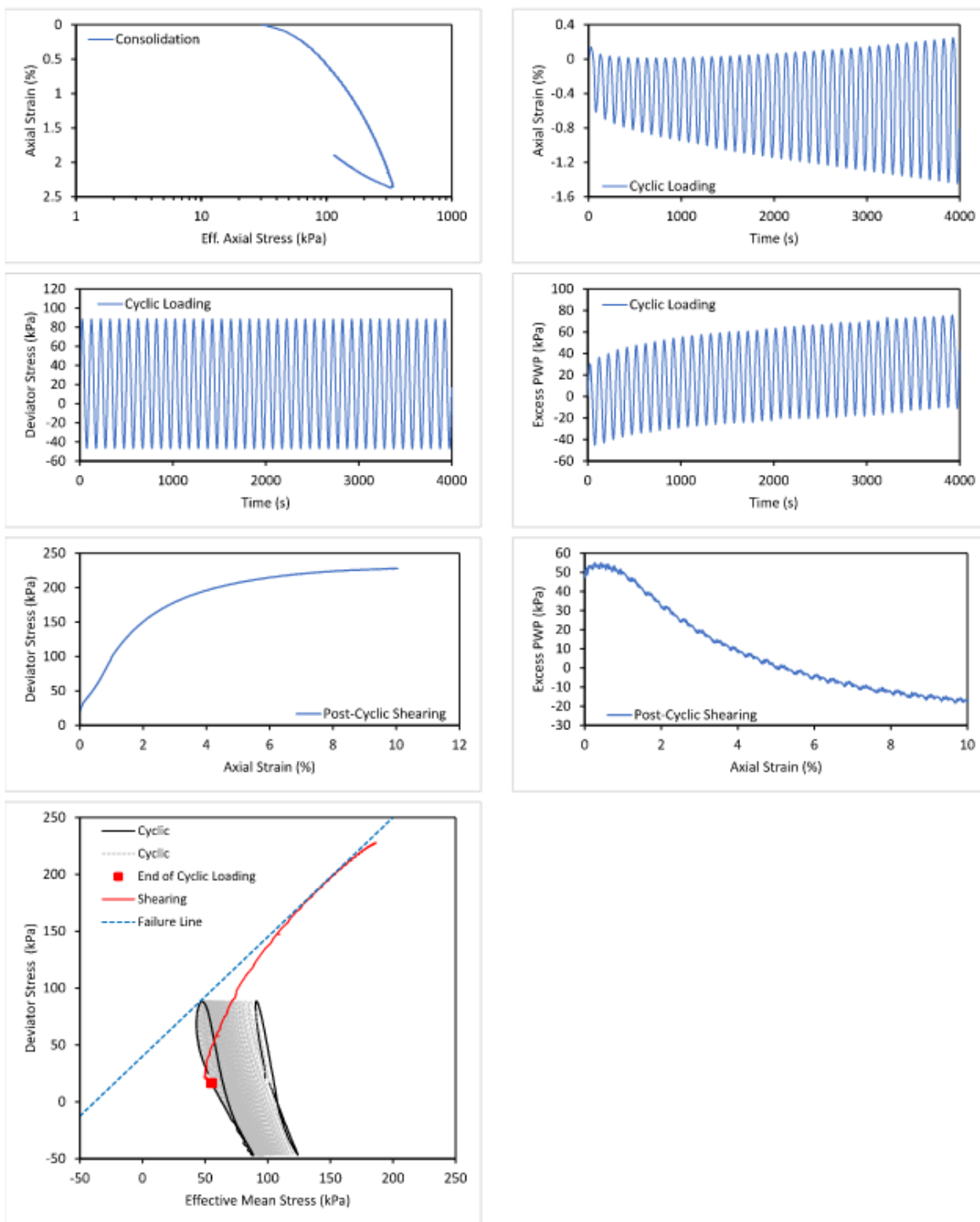


Figure B.7. Specimen NU-1 27-29(2)

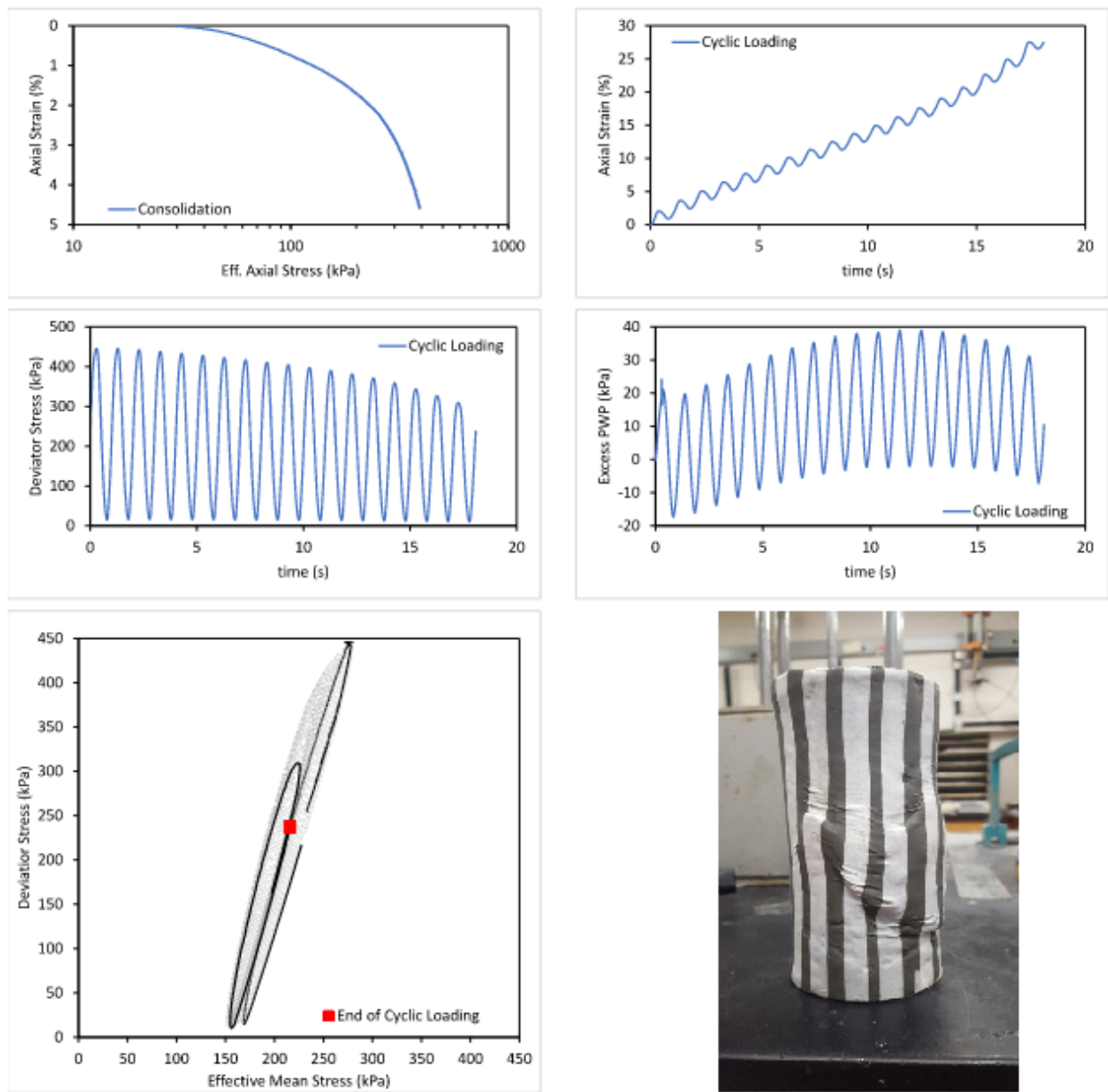


Figure B.8. Specimen NU-1 32-34(3)

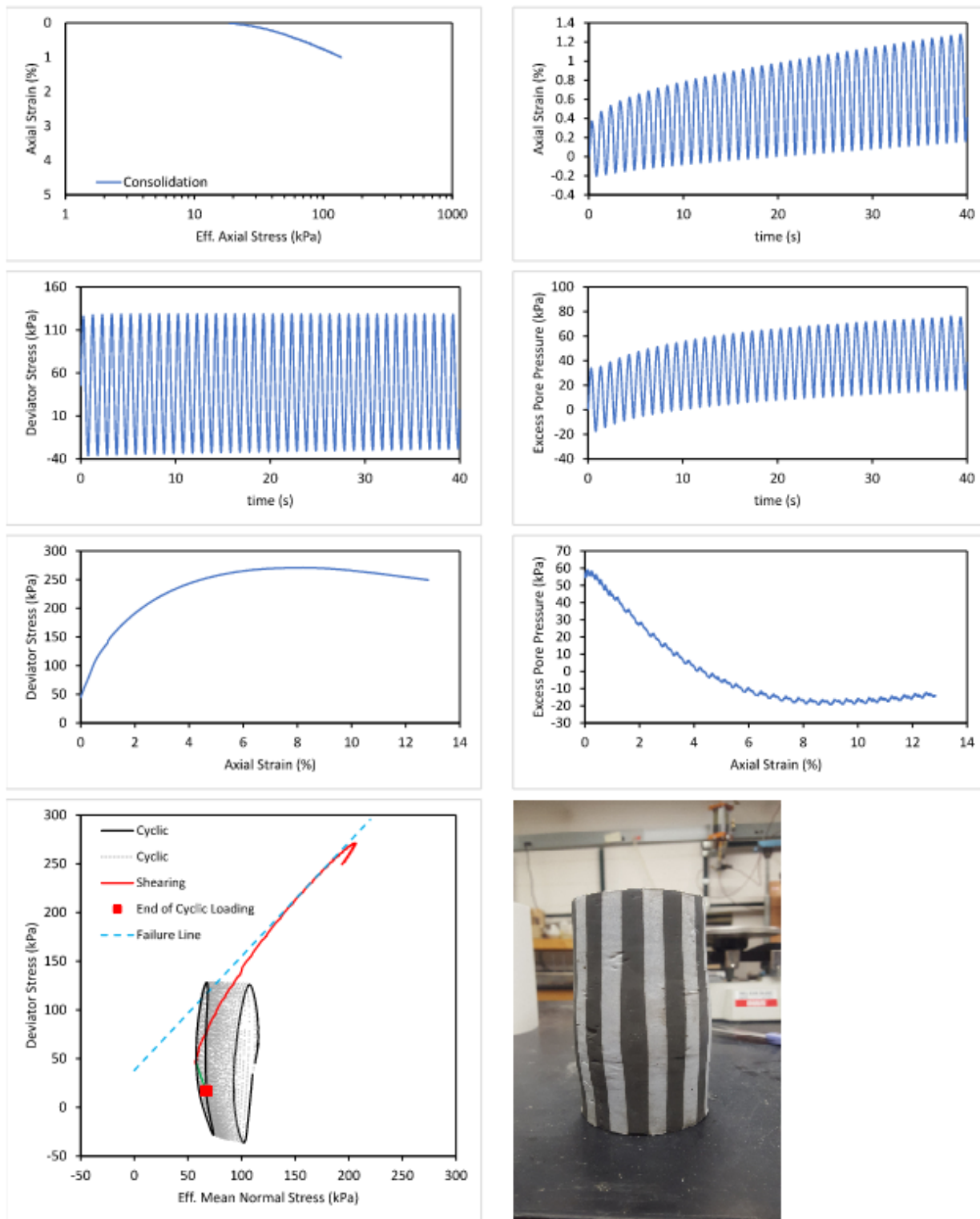


Figure B.9. Specimen NU-1 37-39(2)

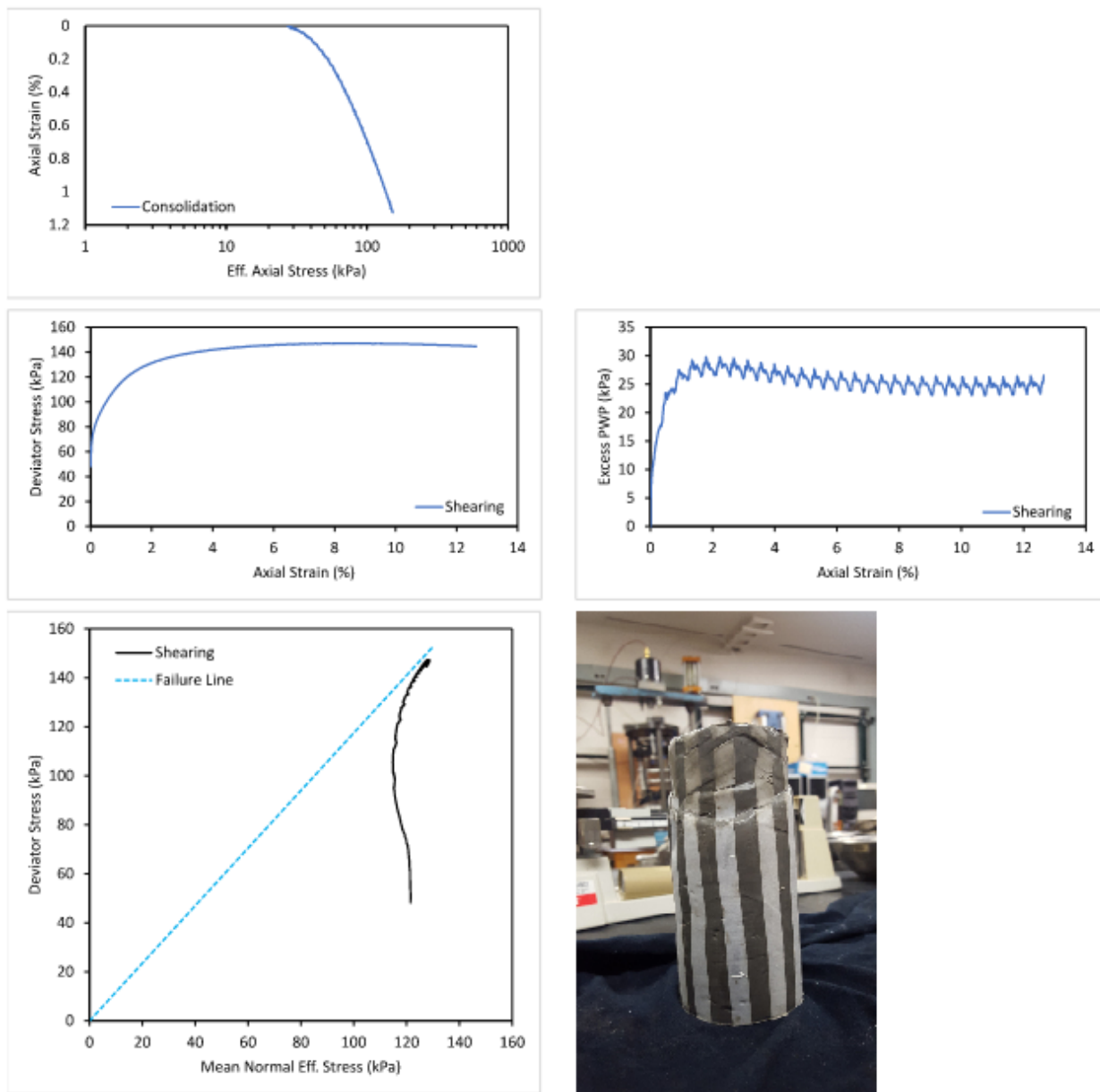


Figure B.10. Specimen NU-1 40-42

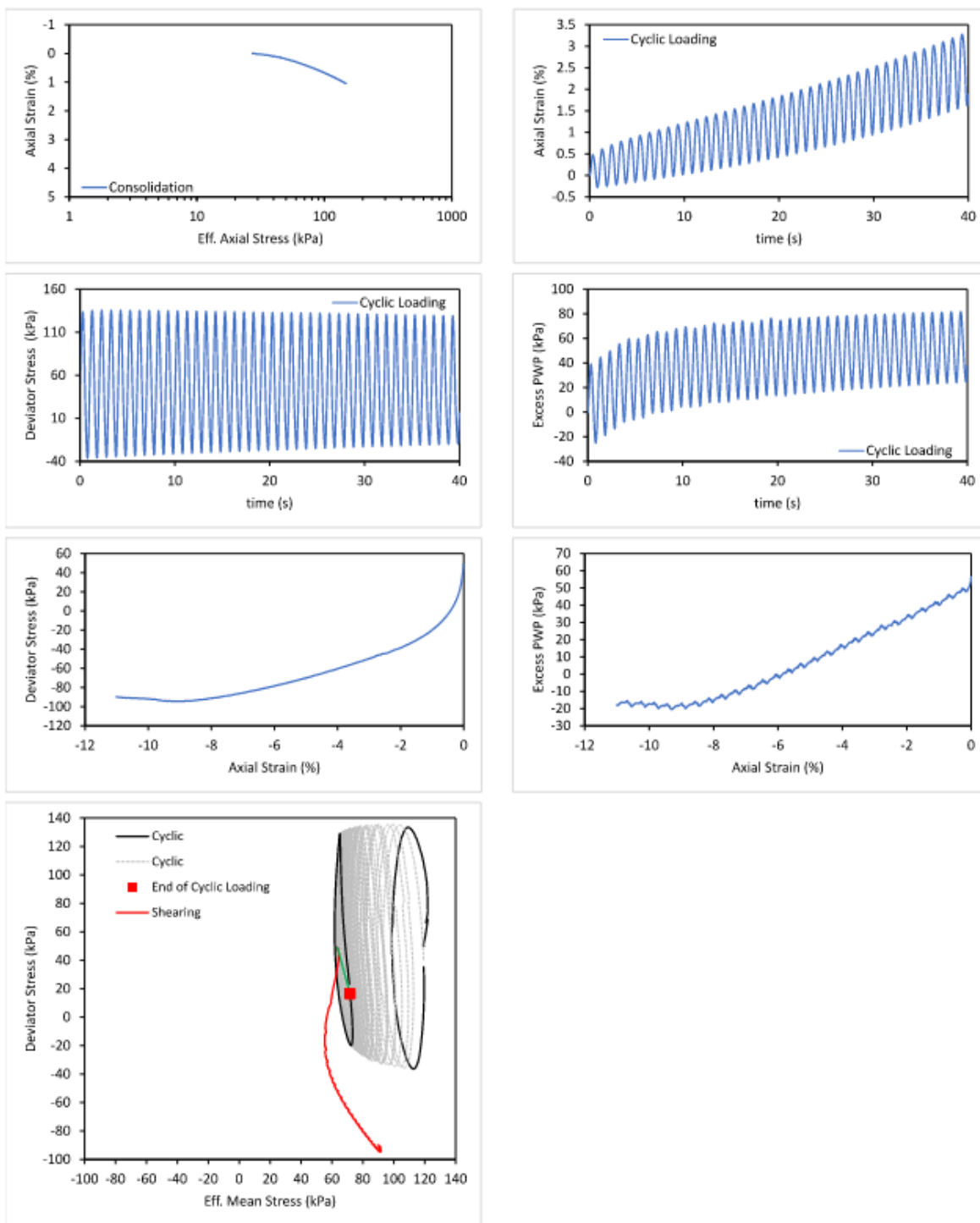


Figure B.11. Specimen 40-42(2)

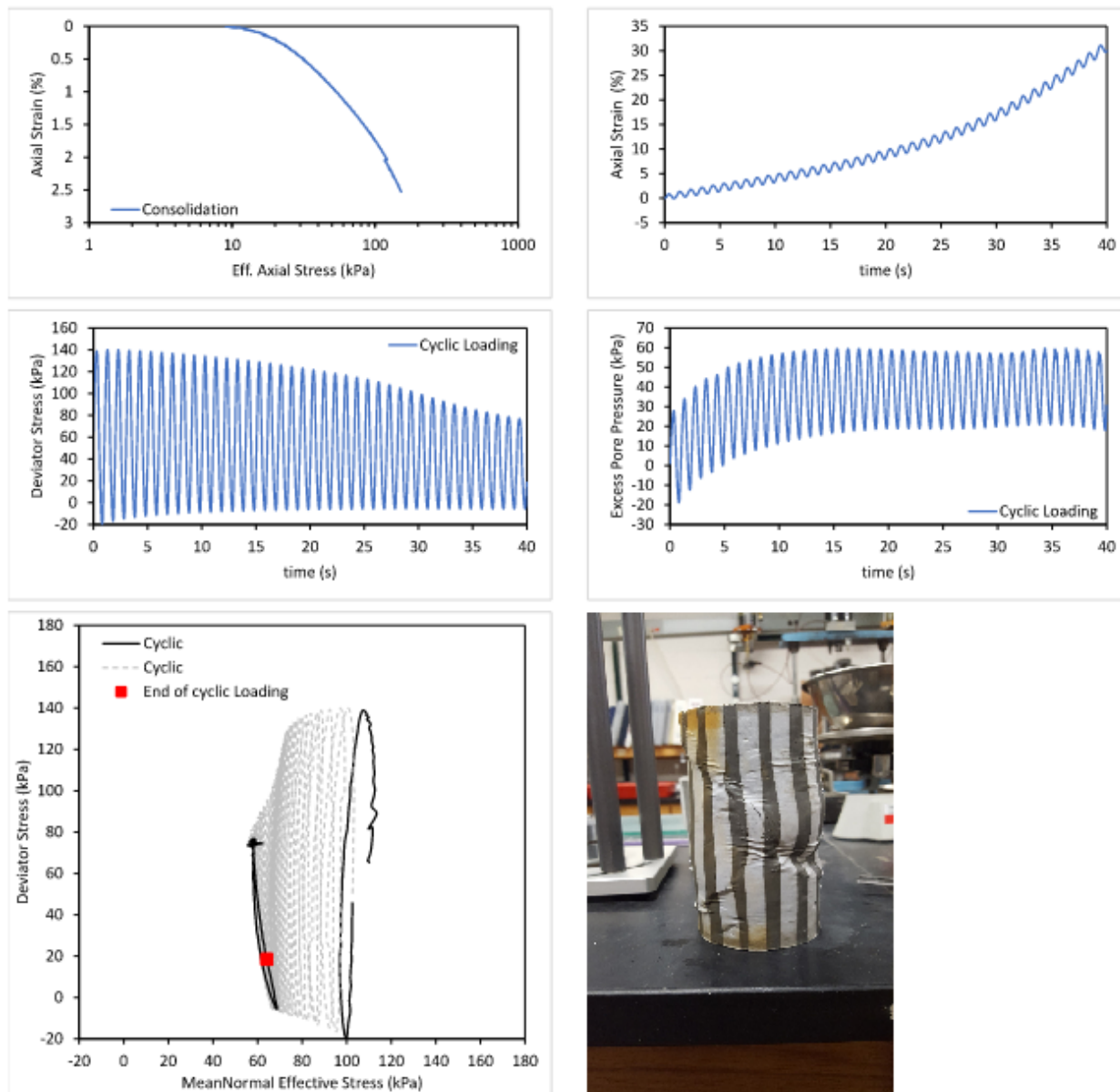


Figure B.12. Specimen 42-44(2)

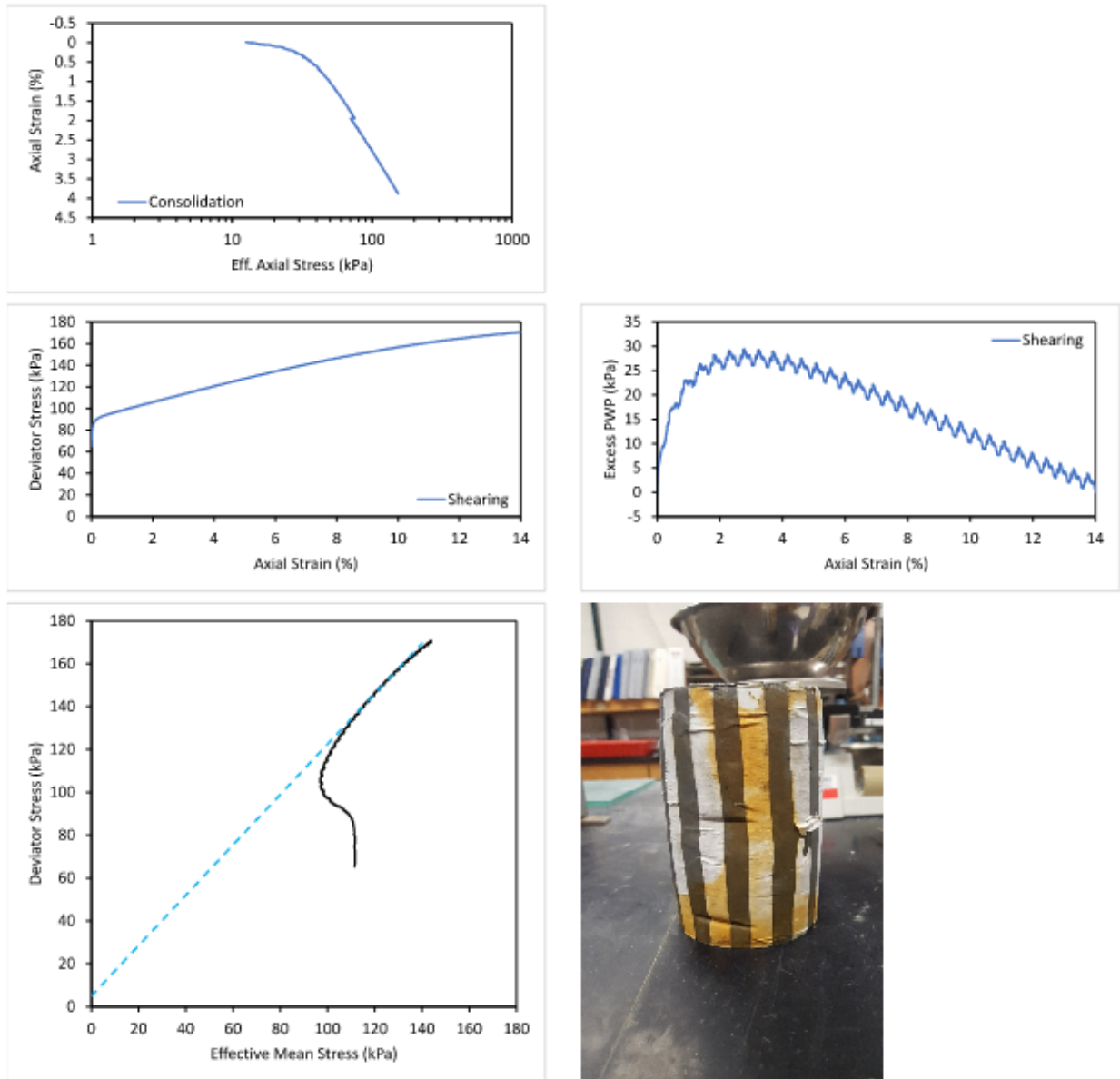


Figure B.13. Specimen NU-1 42-44(3)

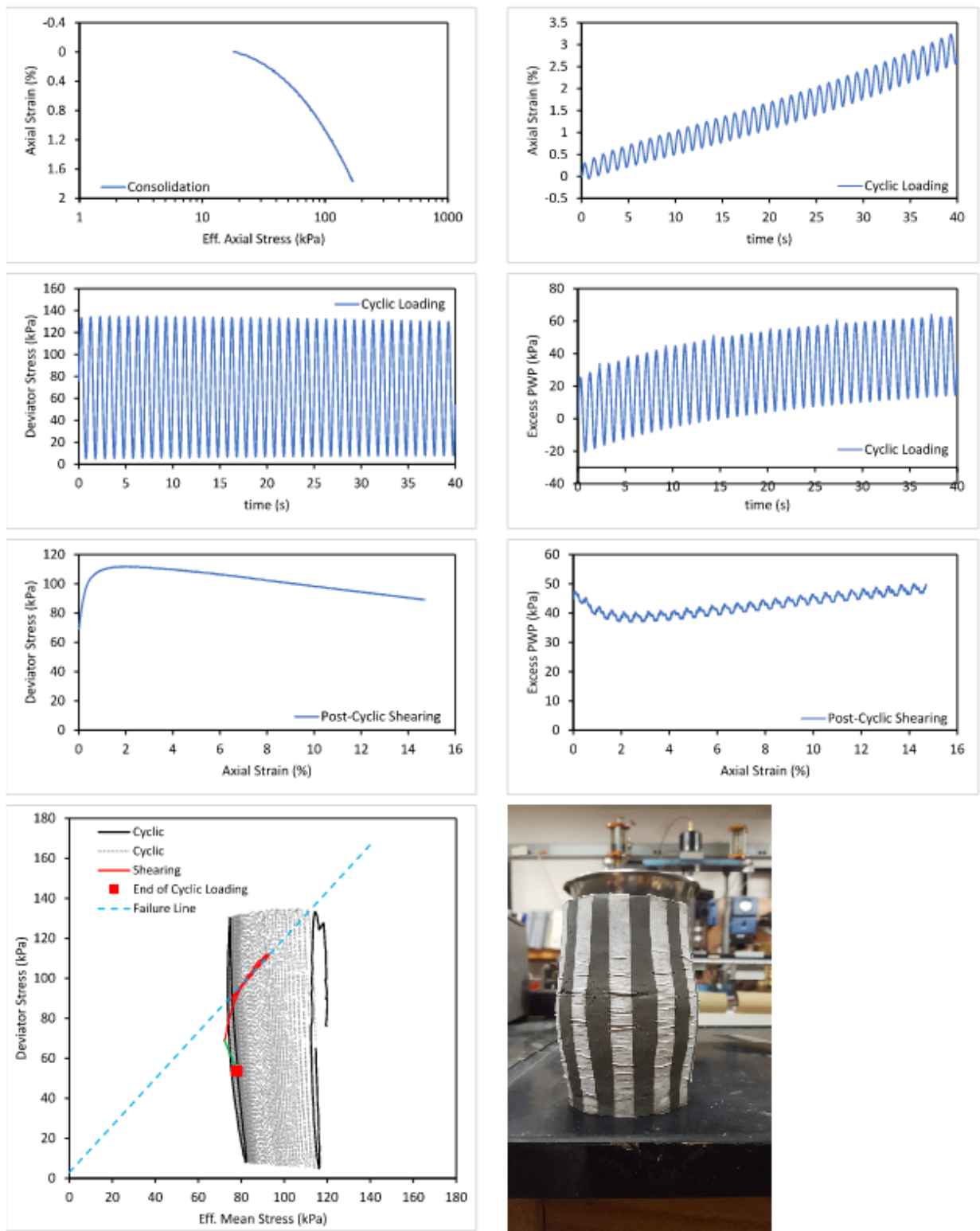


Figure B.14. Specimen NU-1 47-49

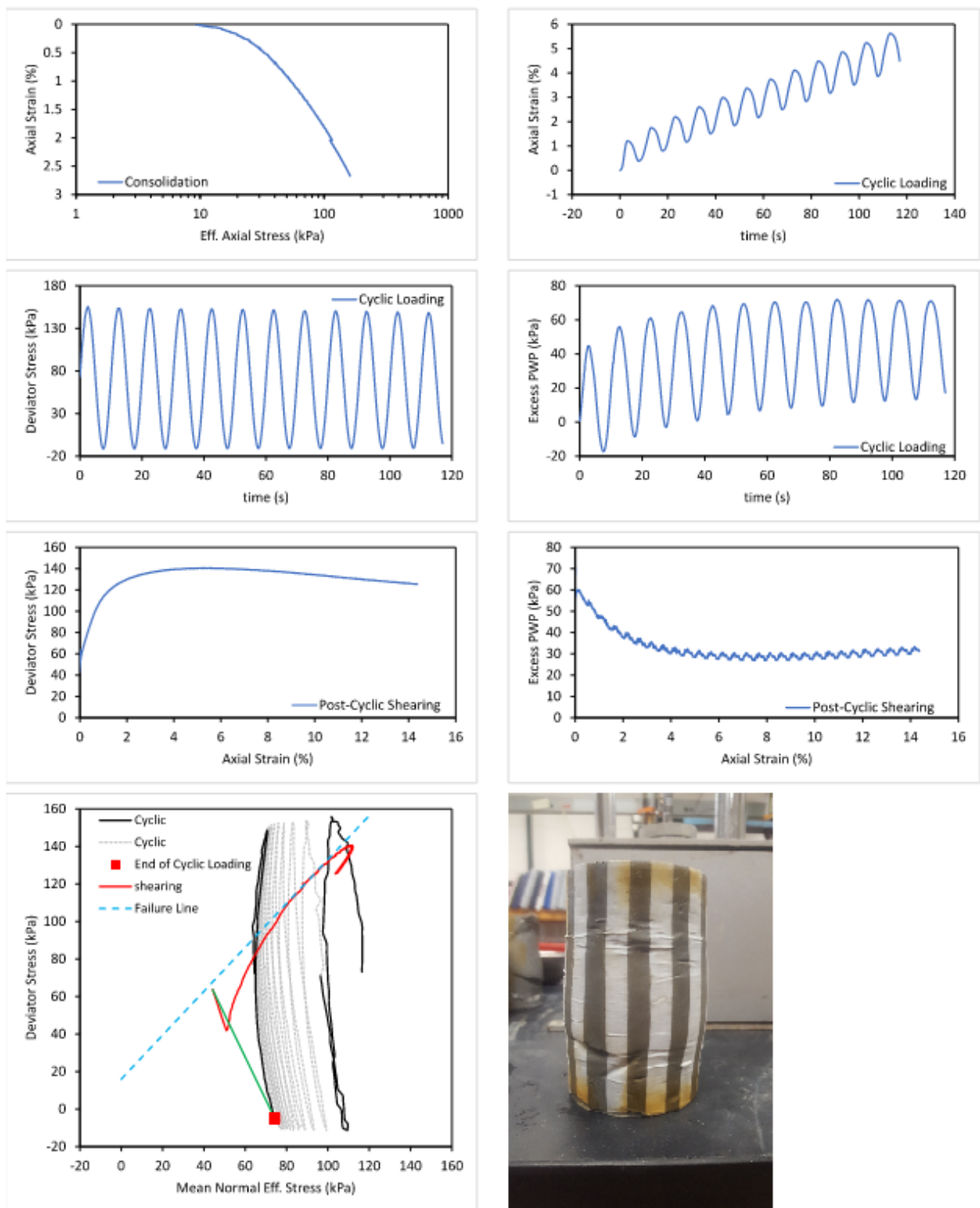


Figure B.15. Specimen NU-1 47-49(2)

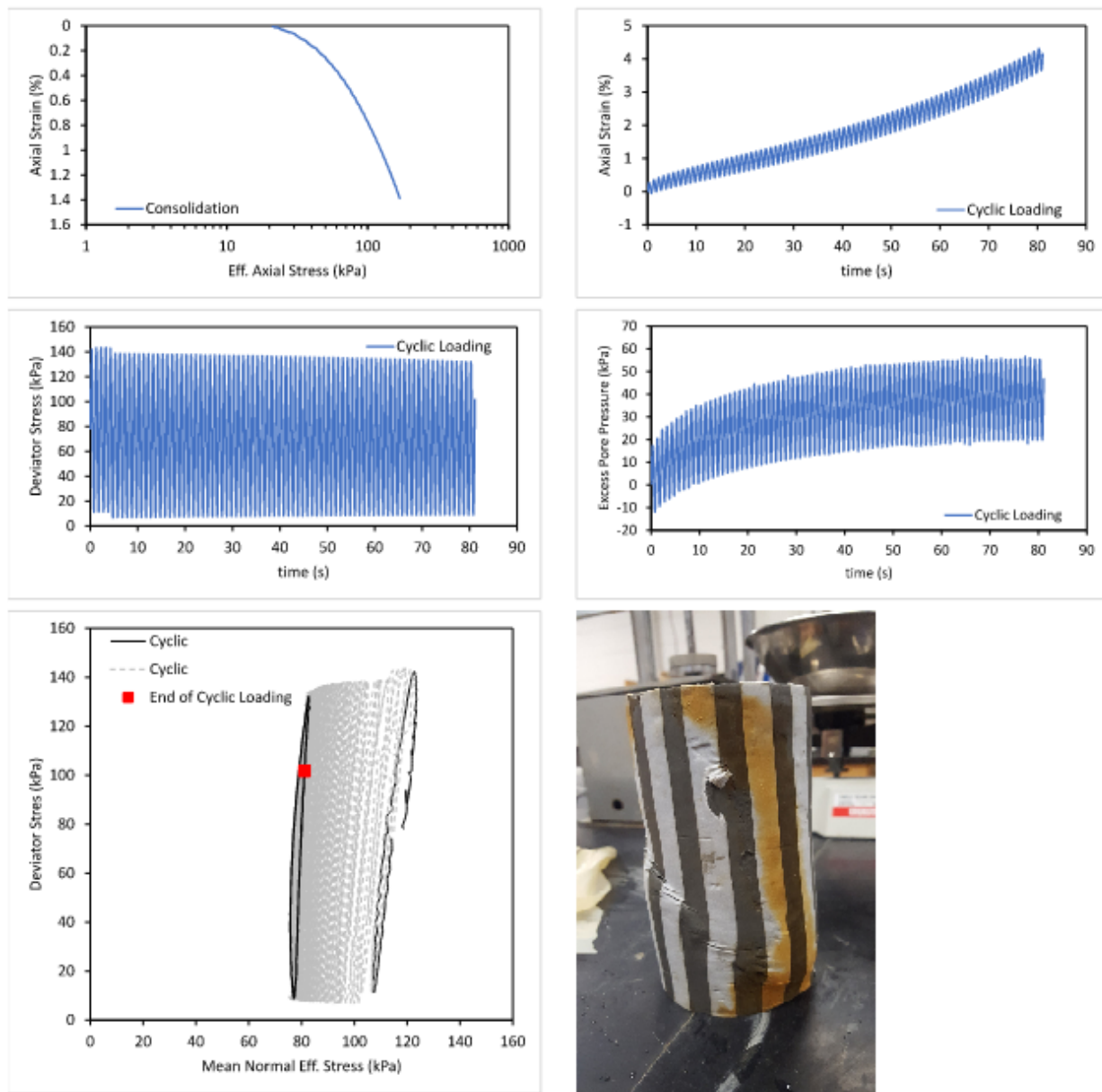


Figure B.16. Specimen NU-1 47-49(3)

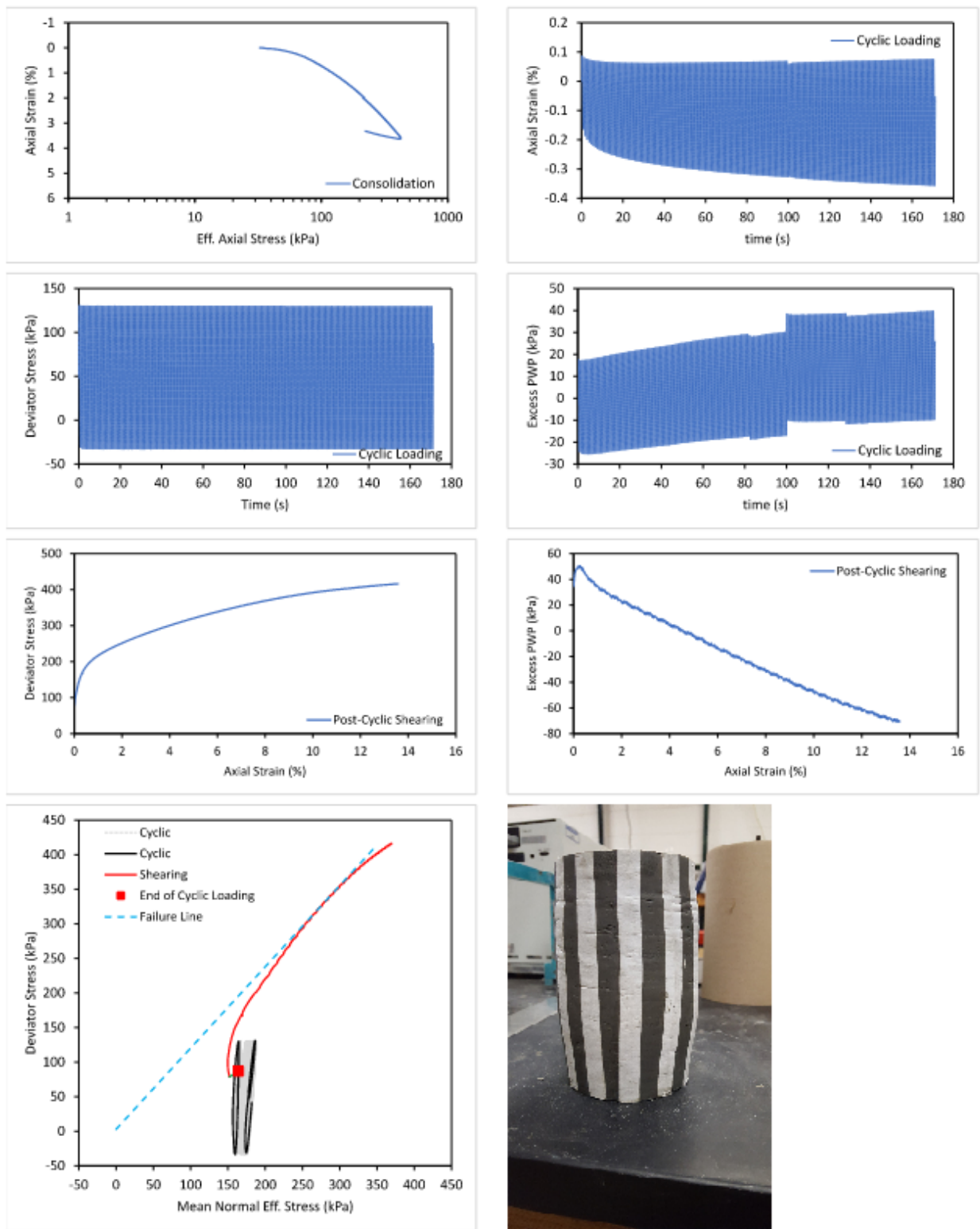


Figure B.17. Specimen NU-1 55-57

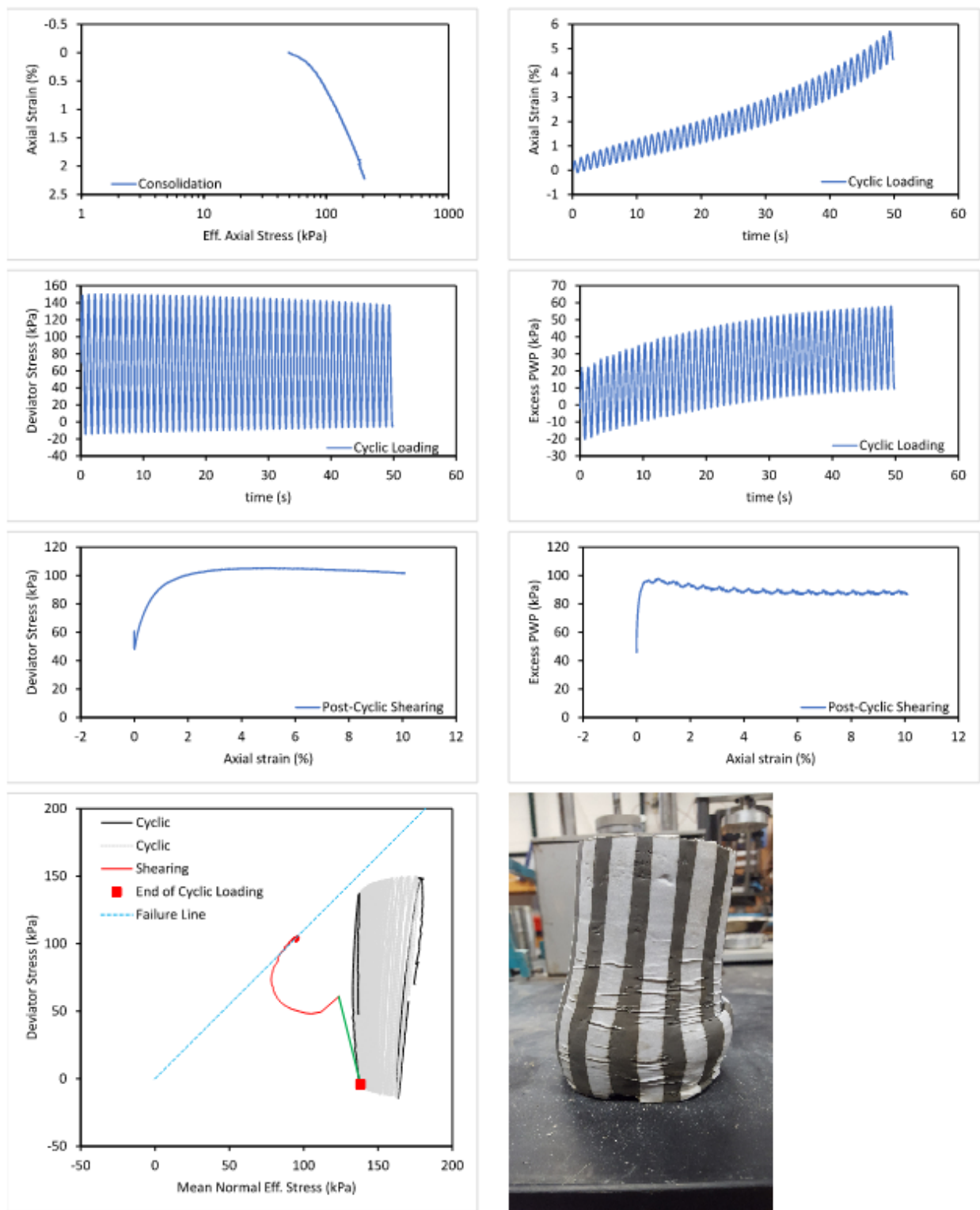


Figure B.18. Specimen NU-1 60-62

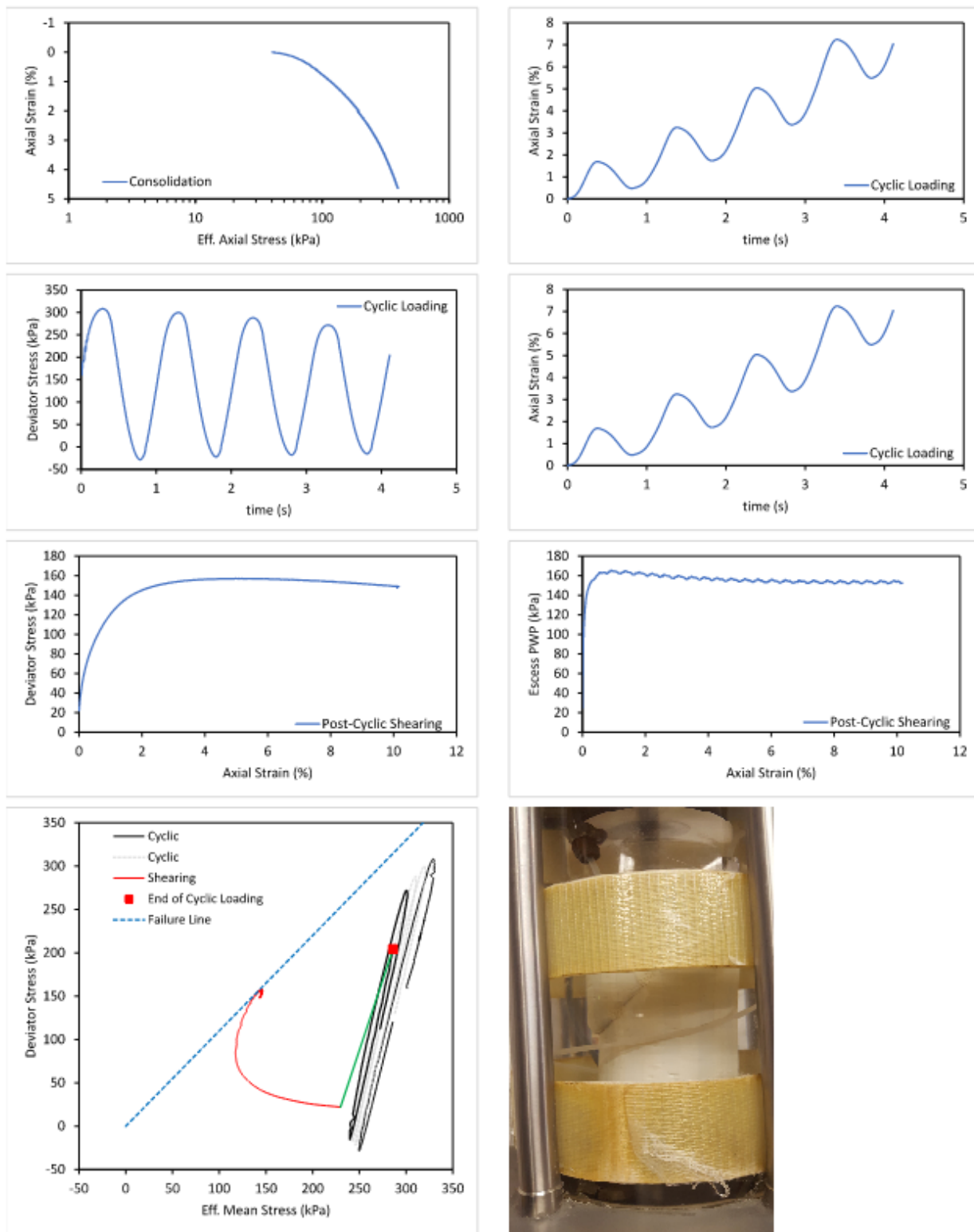


Figure B.19. Specimen NU-1 60-62(2)

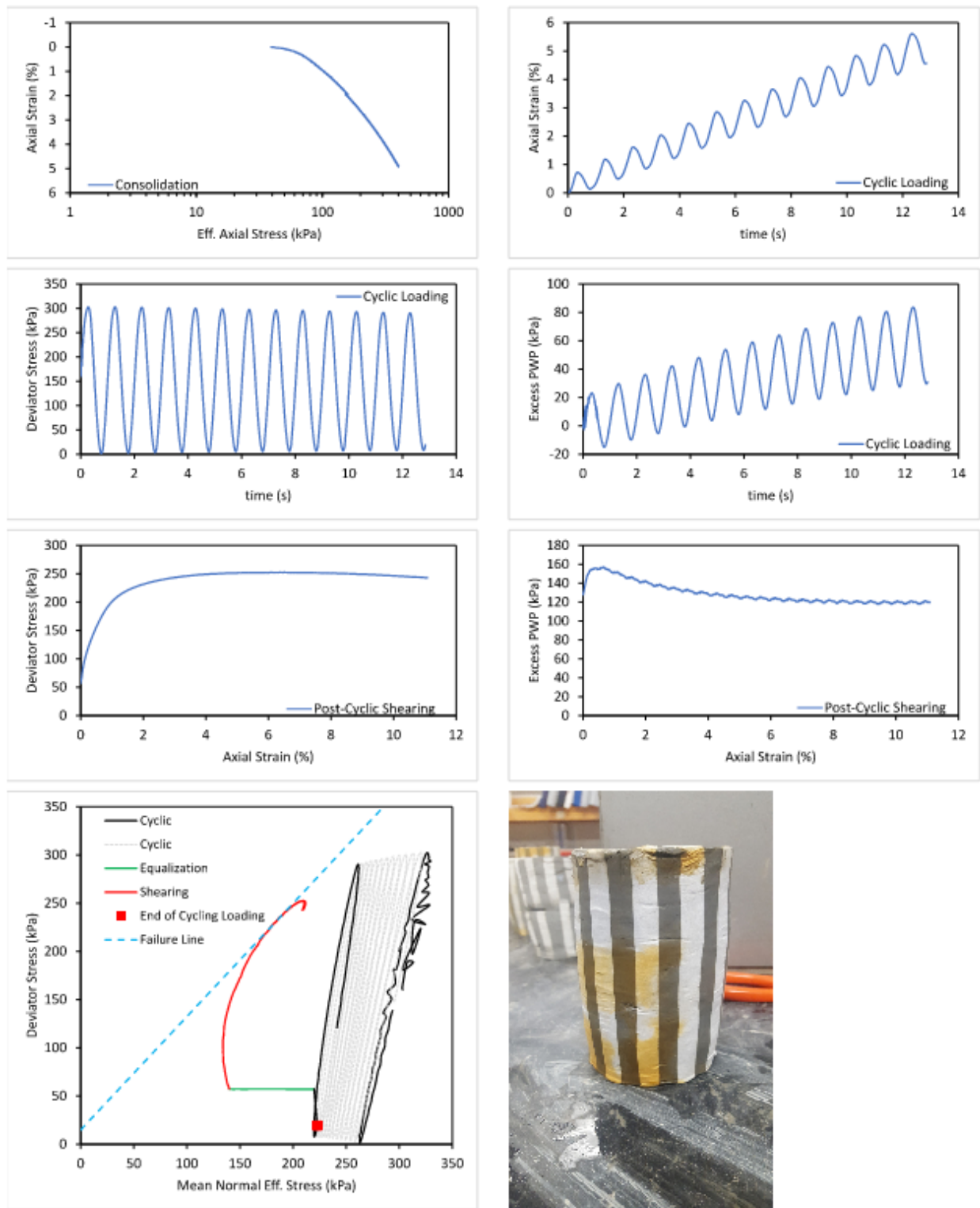


Figure B.20. NU-1 60-62(3)

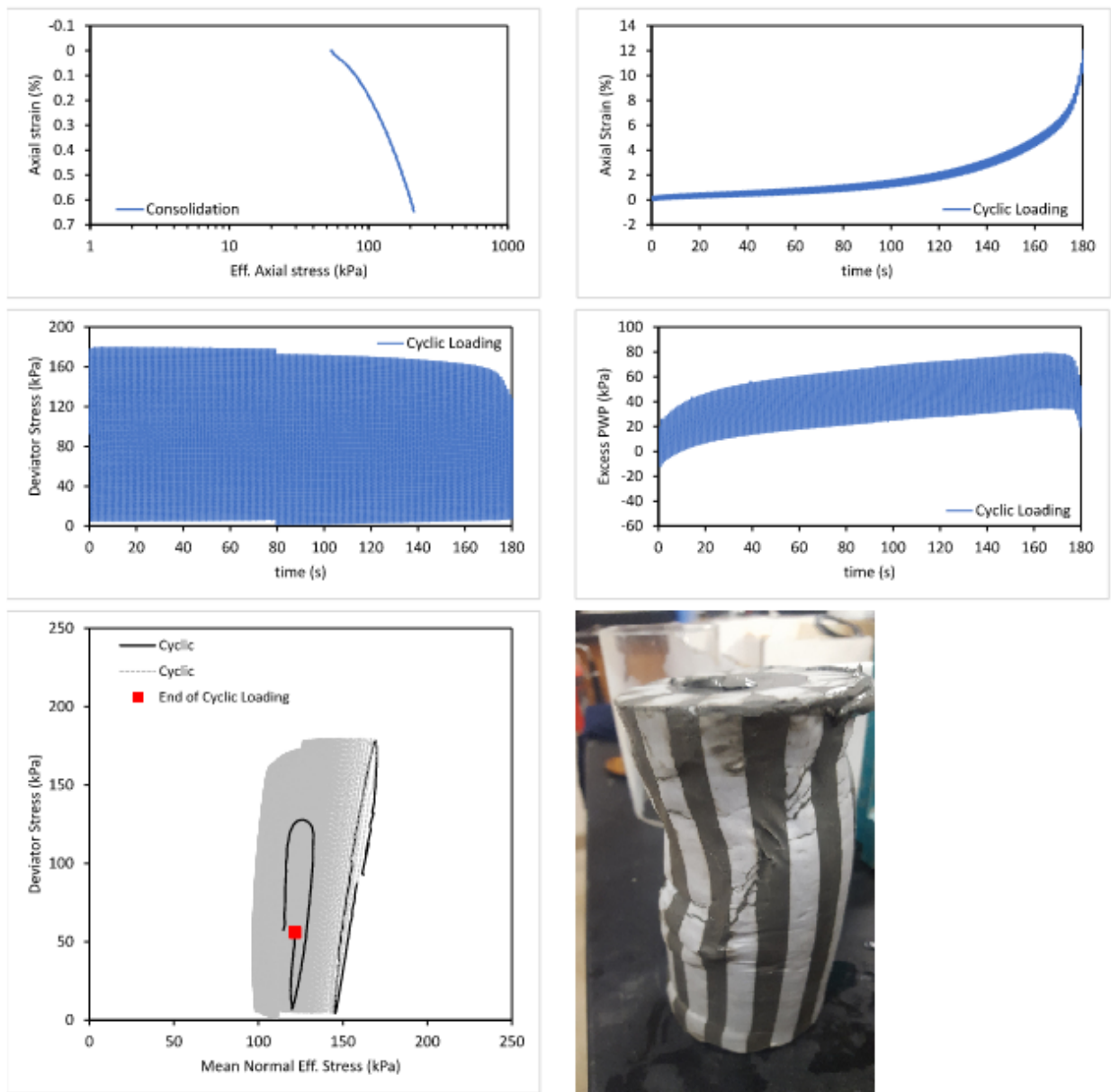


Figure B.21. Specimen NU-1 62-64

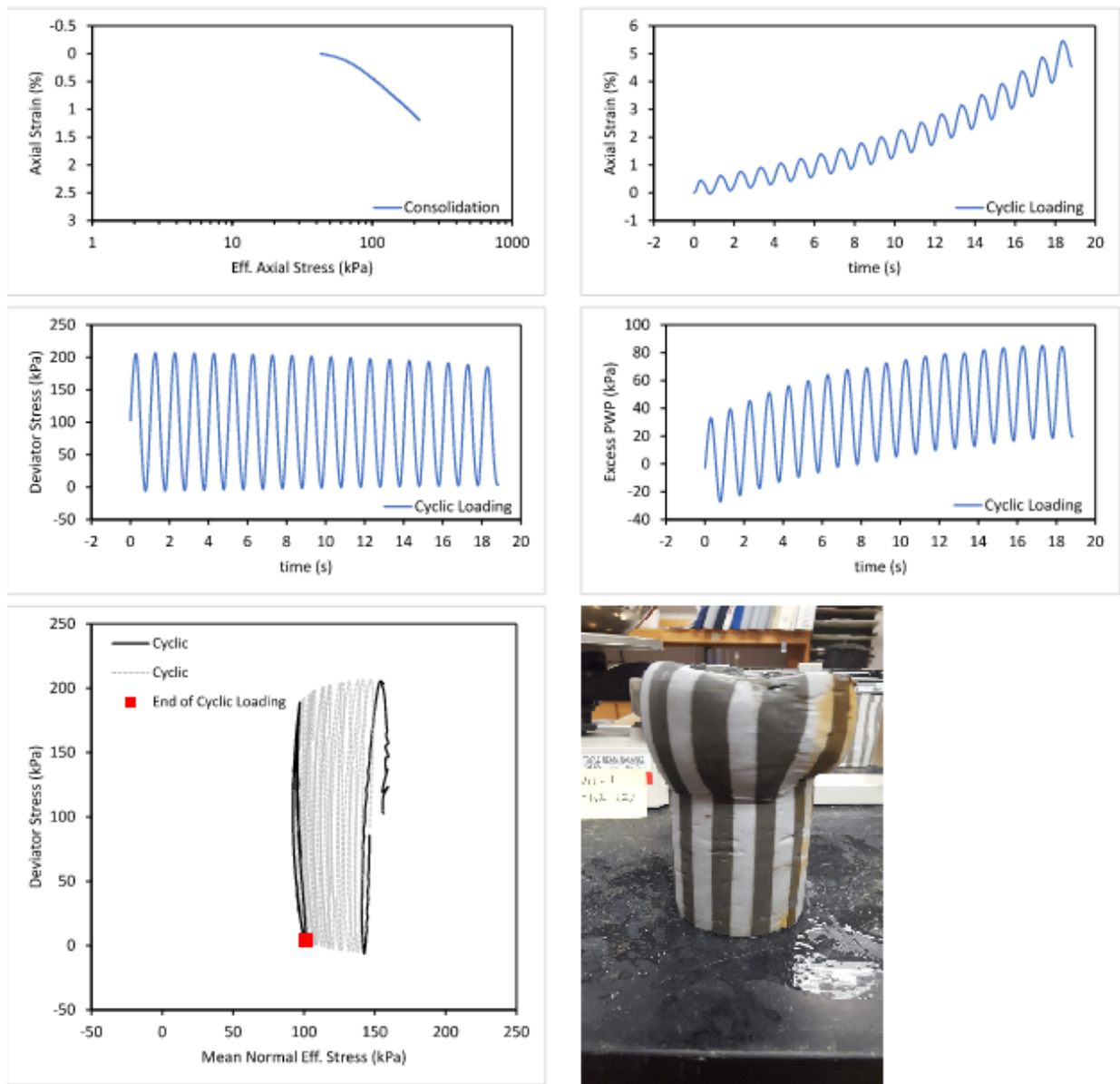


Figure B.22. NU-1 62-64(2)

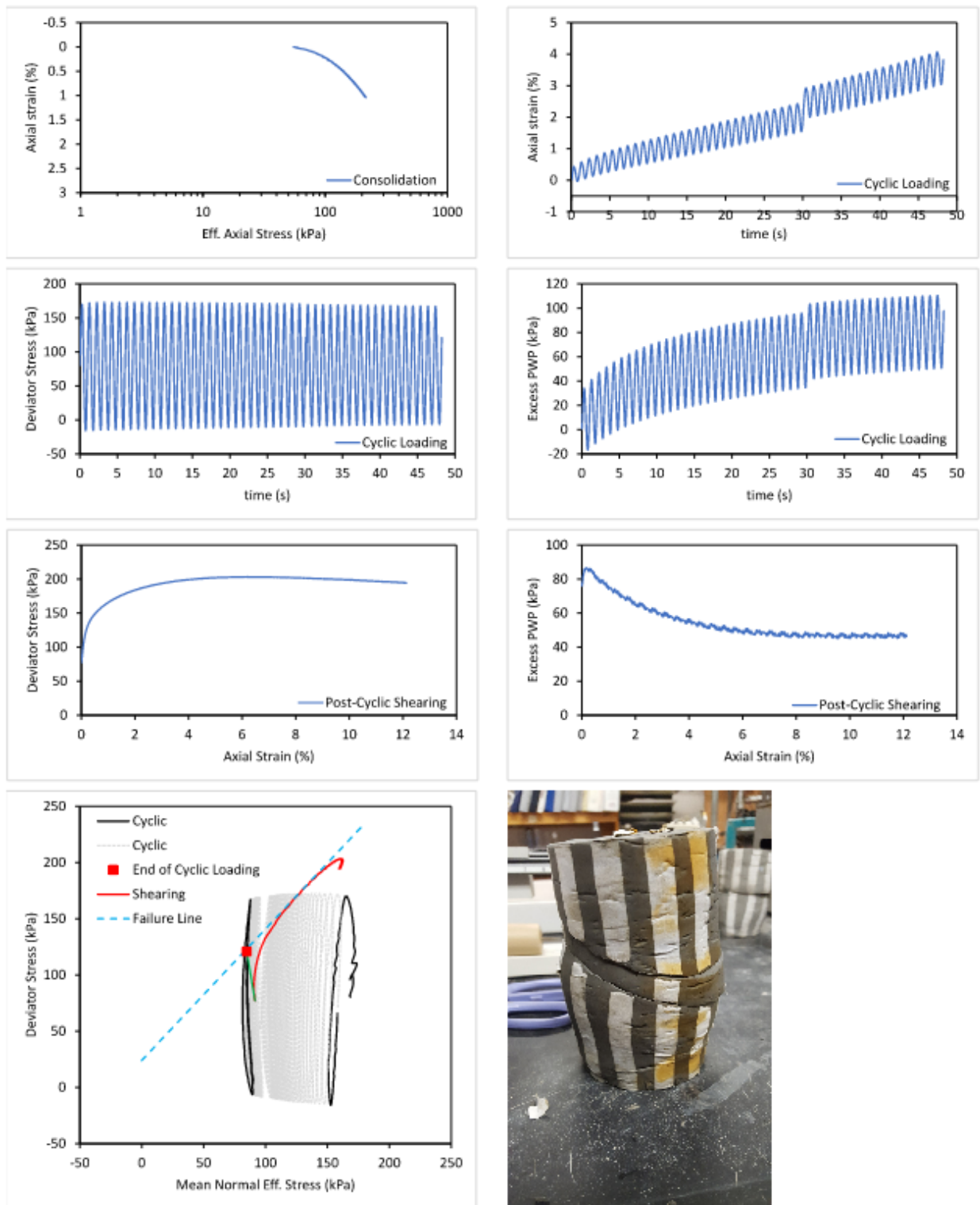


Figure B.23. Specimen NU-1 62-64(3)

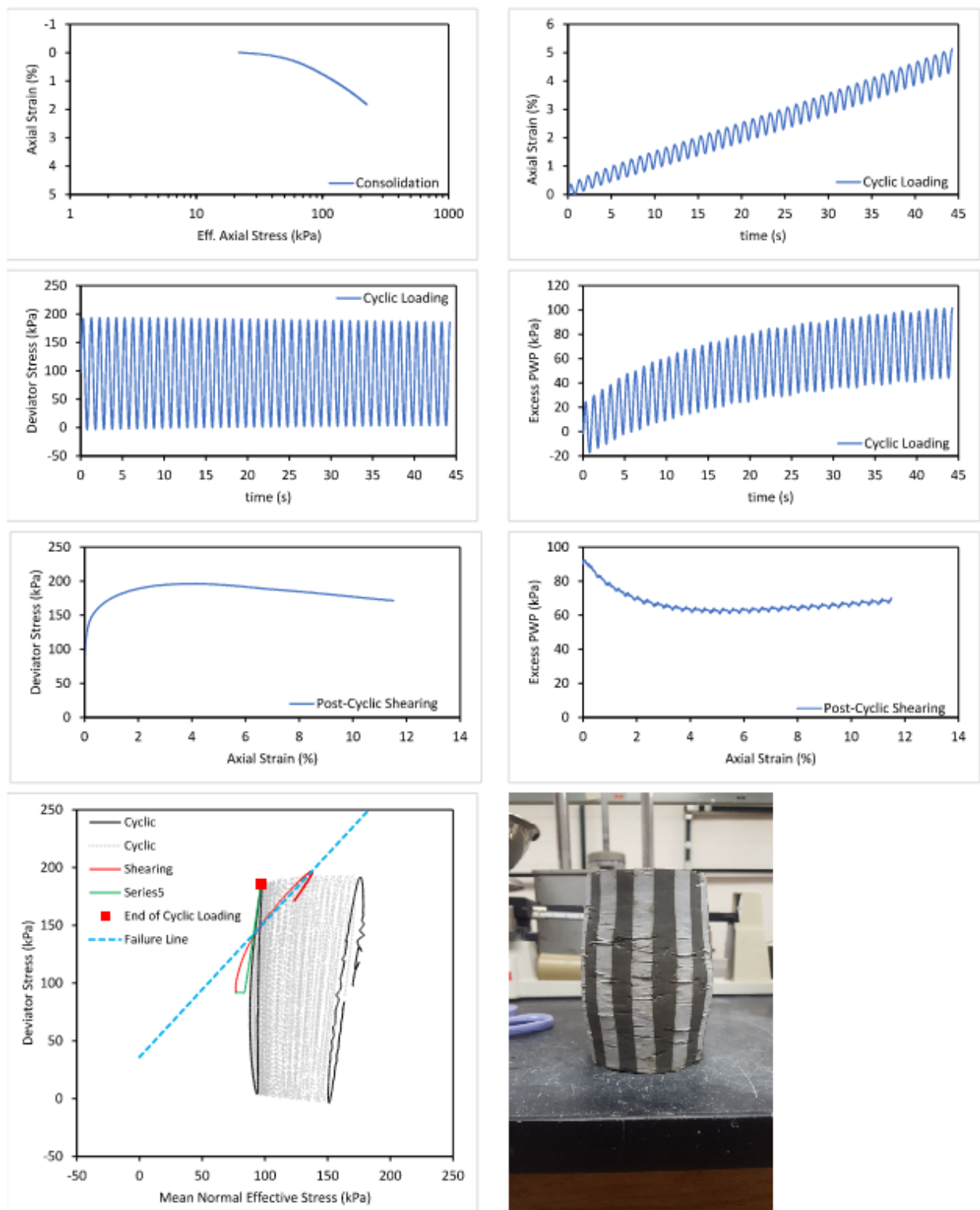


Figure B.24. Specimen NU-1 65-67

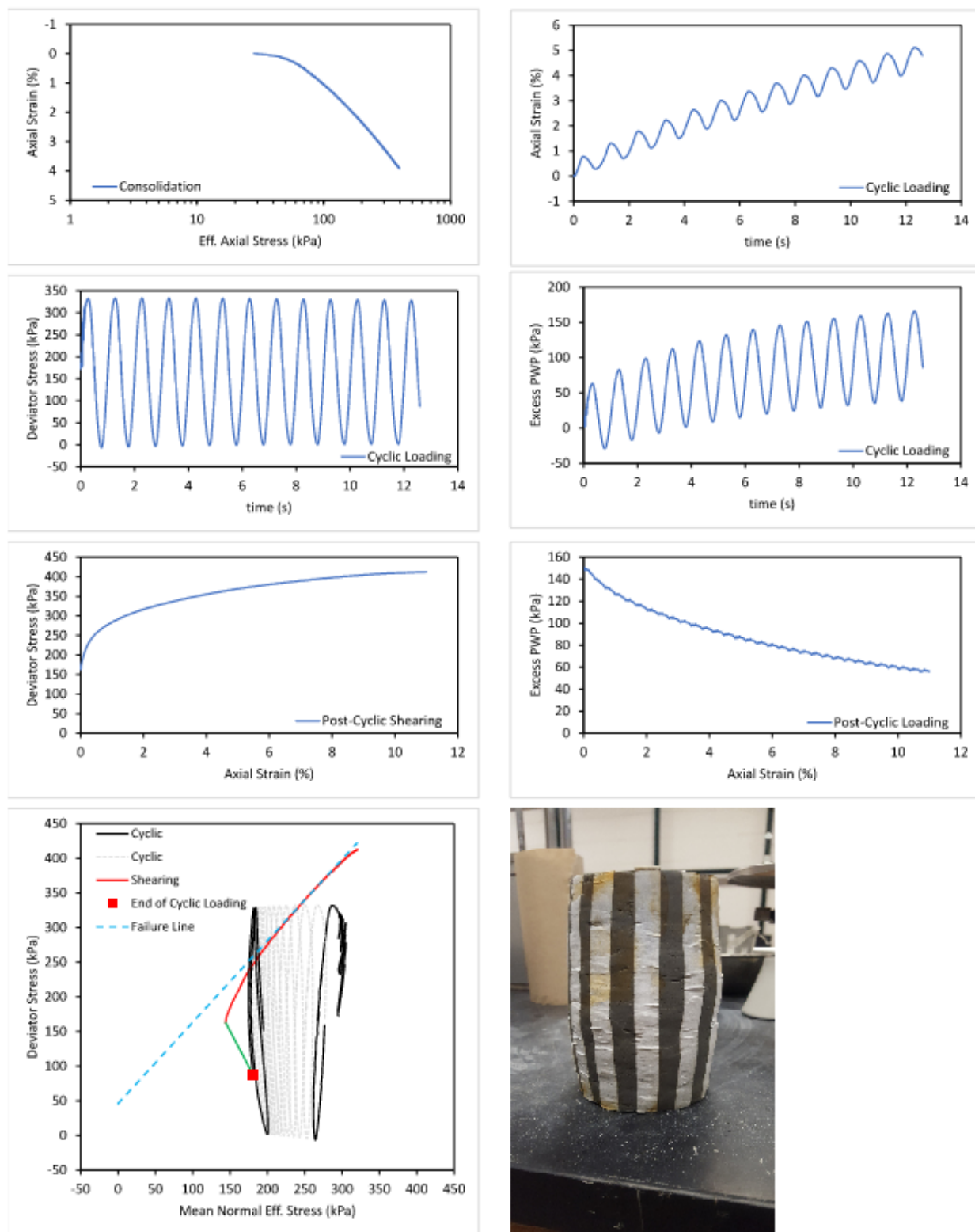


Figure B.25. Specimen NU-1 65-67(2)

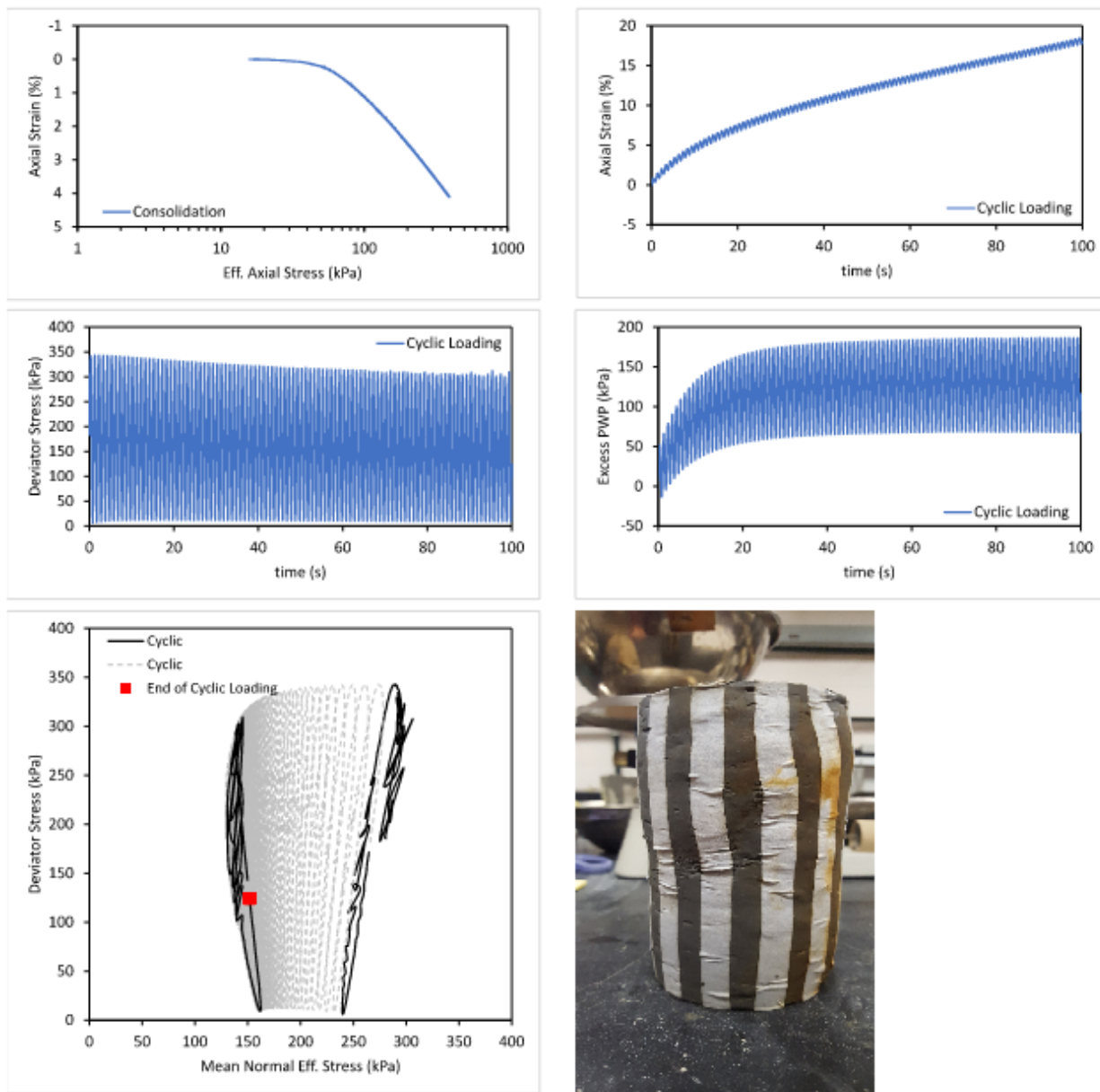


Figure B.26. Specimen NU-1 65-67(3)

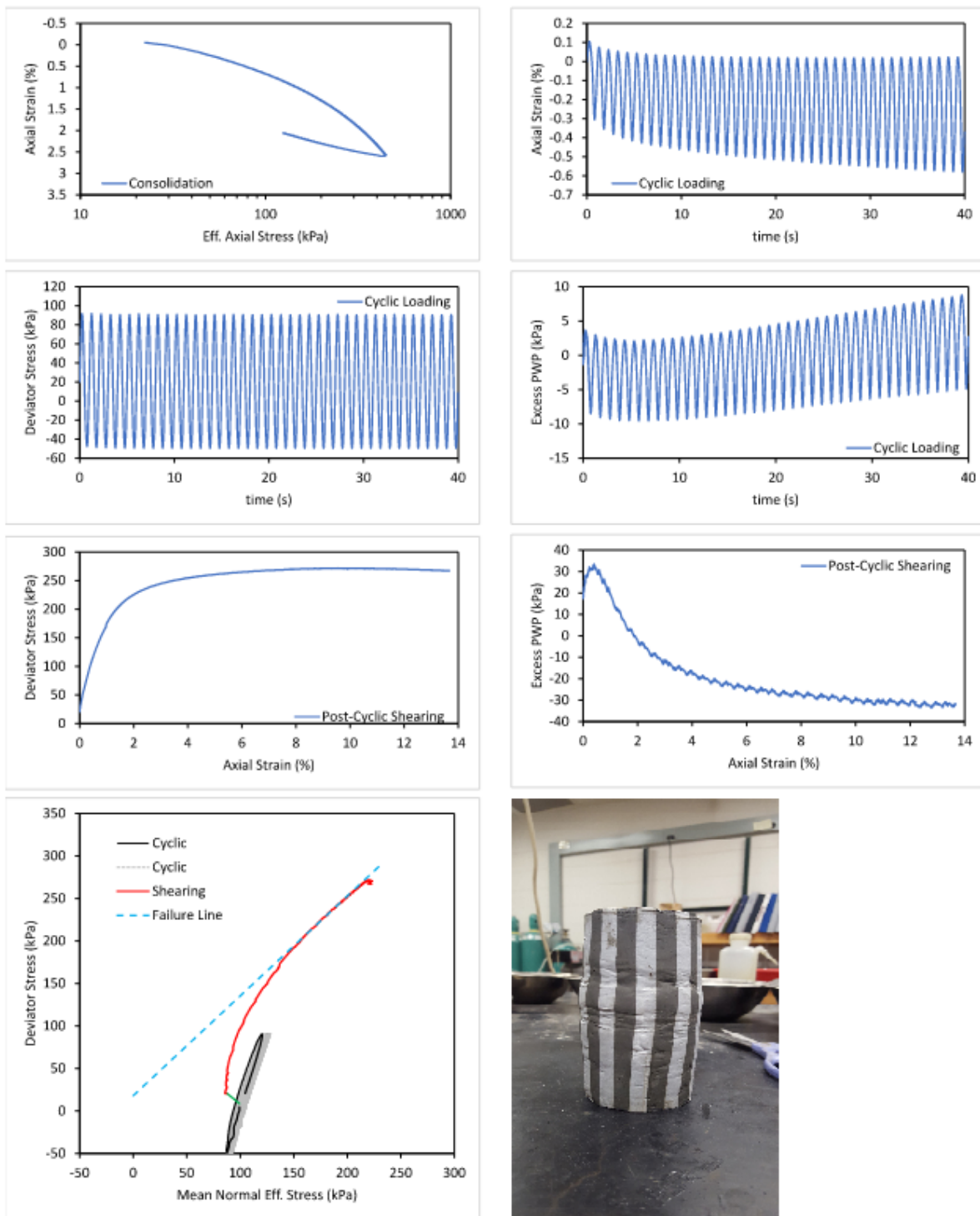


Figure B.27. Specimen NU-3 25-27

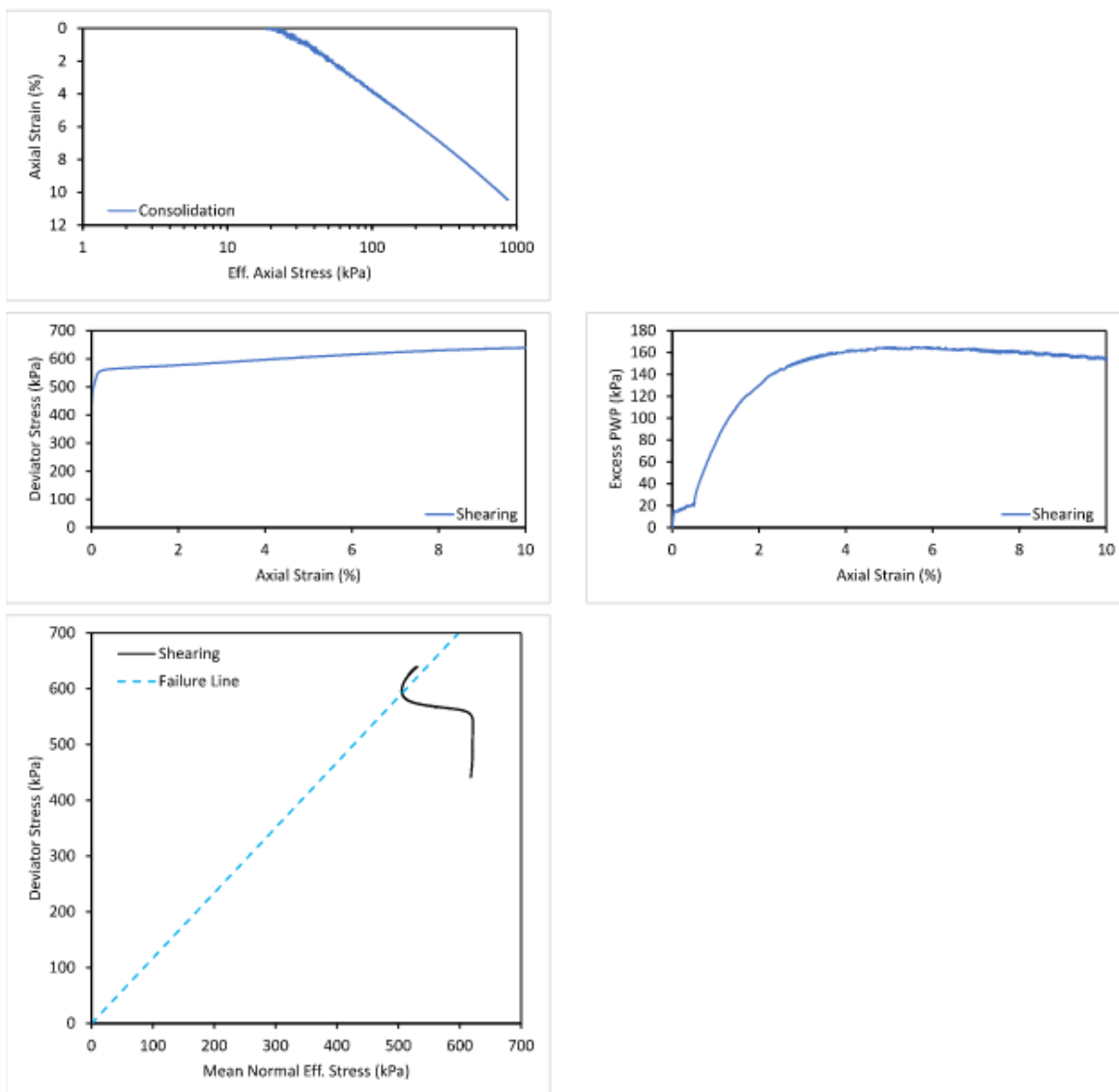


Figure B.28. Specimen NU-3 30-32

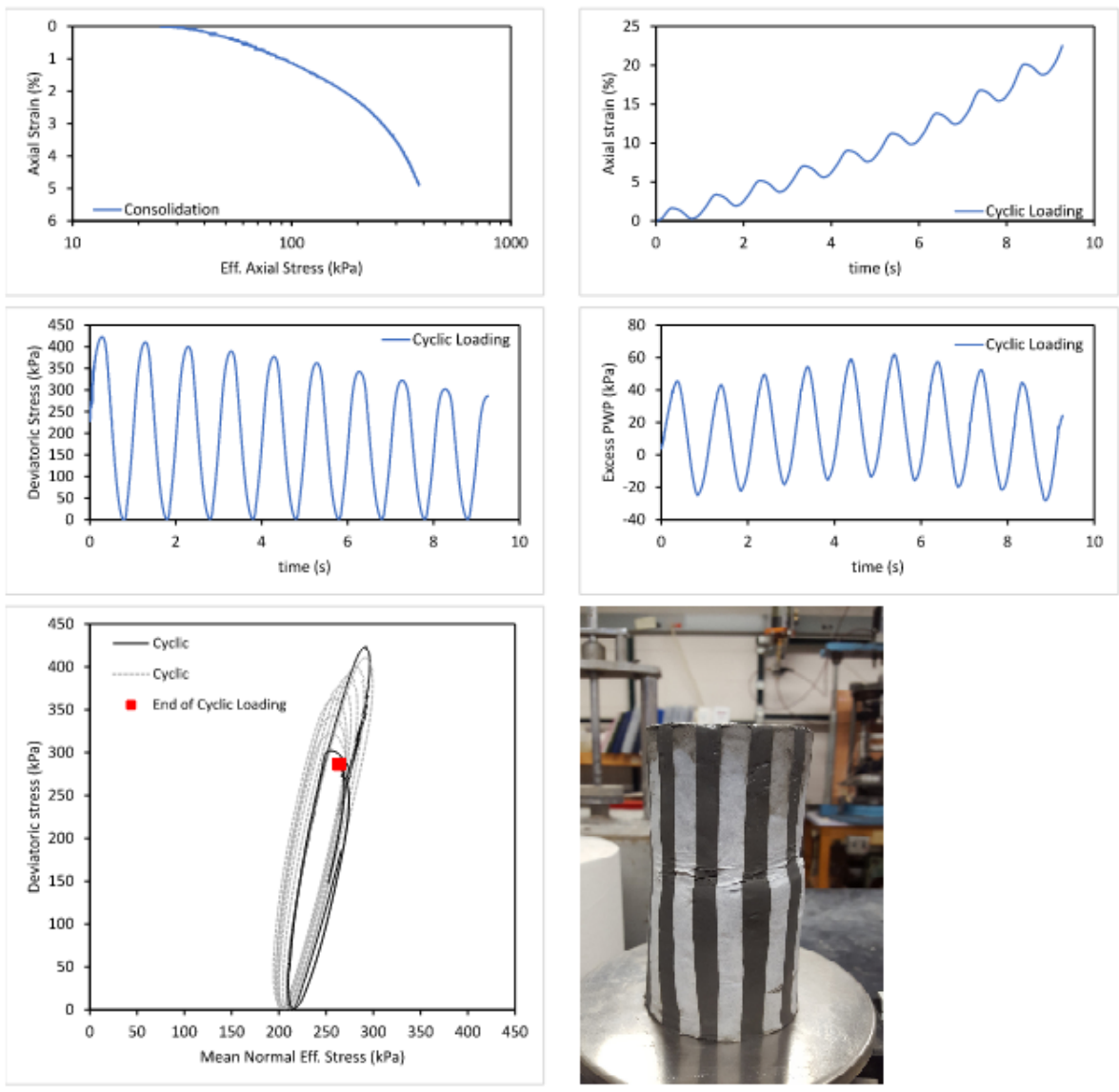


Figure B.29. Specimen NU-3 40-42

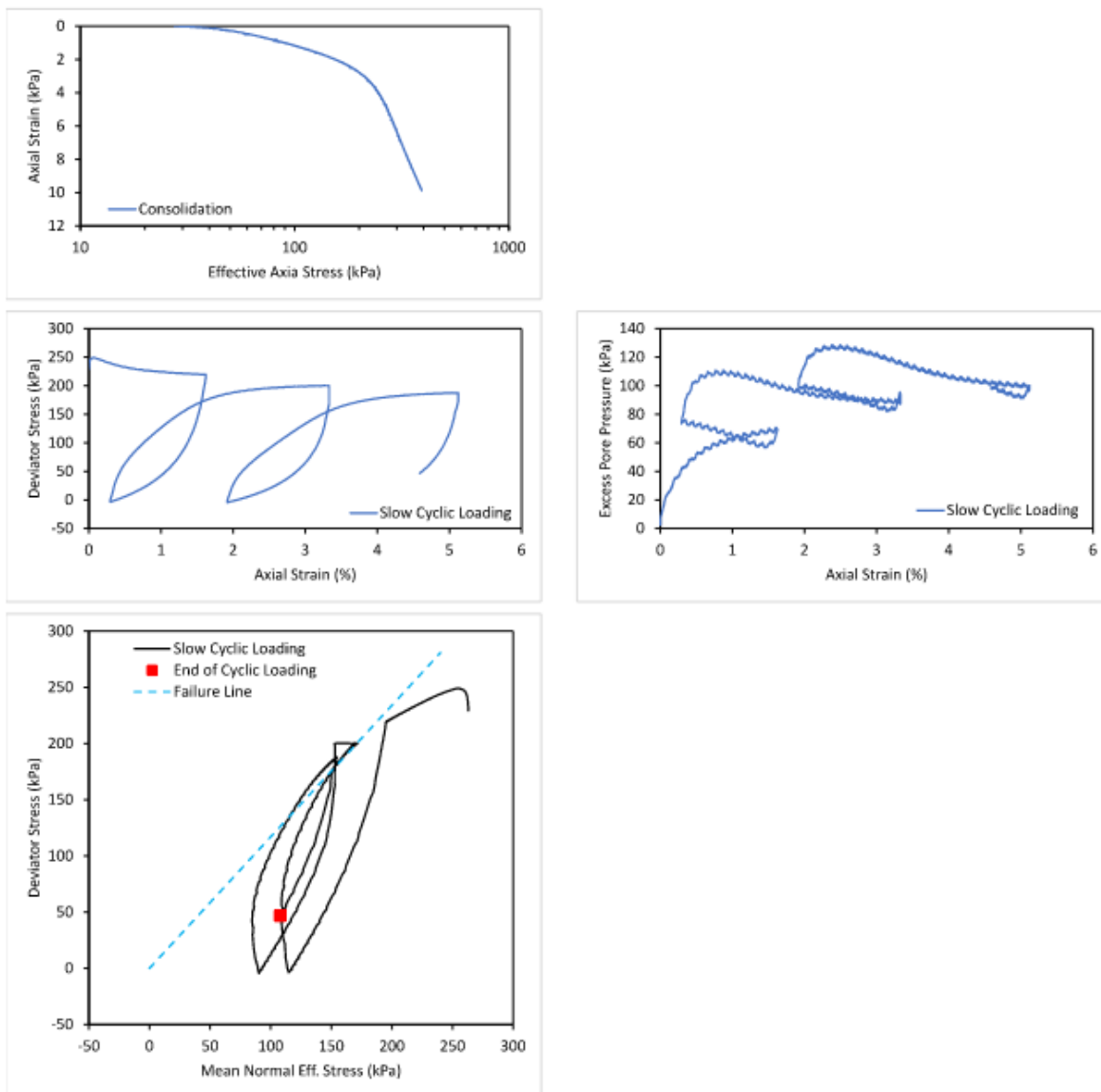


Figure B.30. Specimen NU-3 42-44

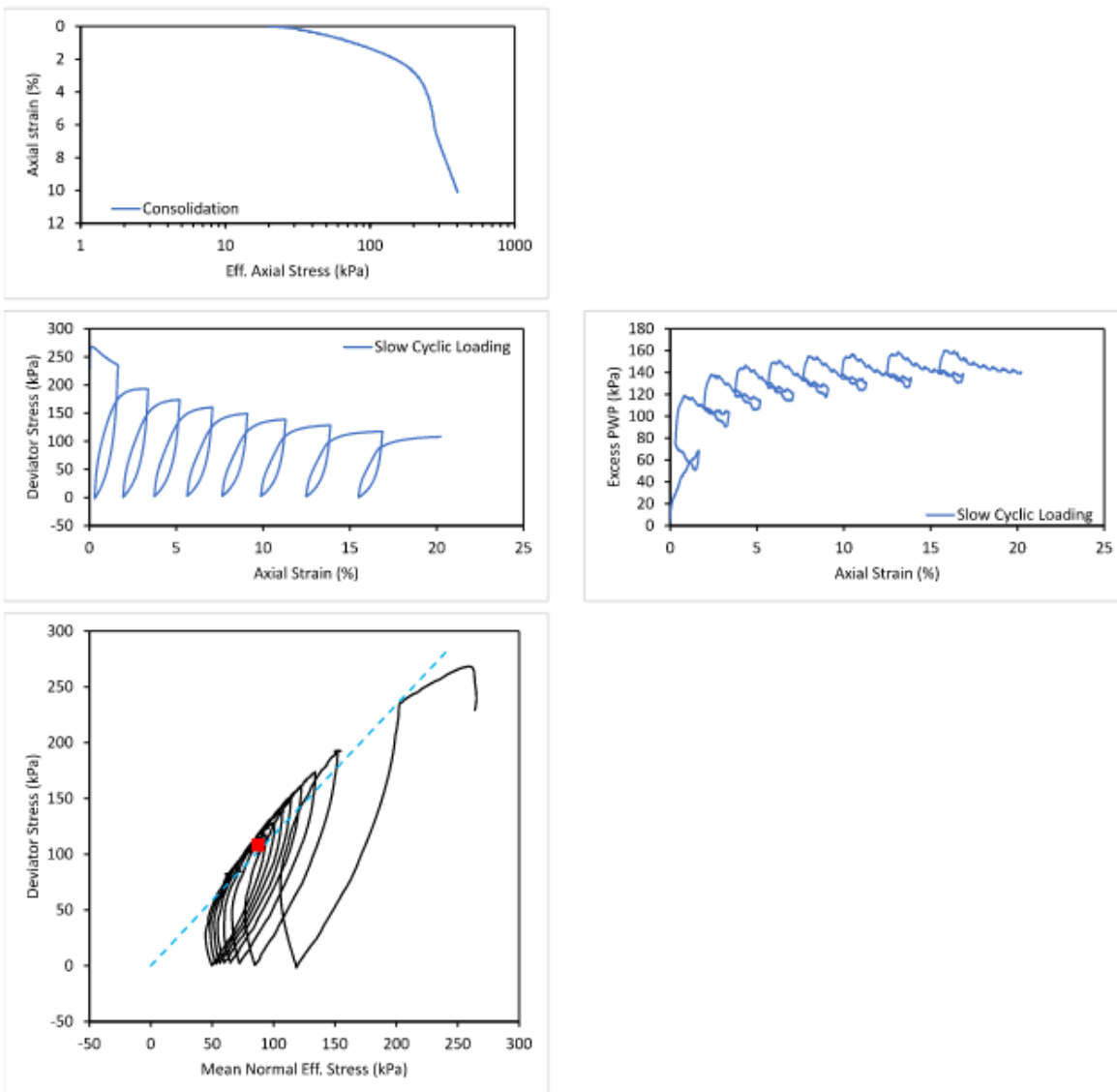


Figure B.31. Specimen NU-3 42-44(2)

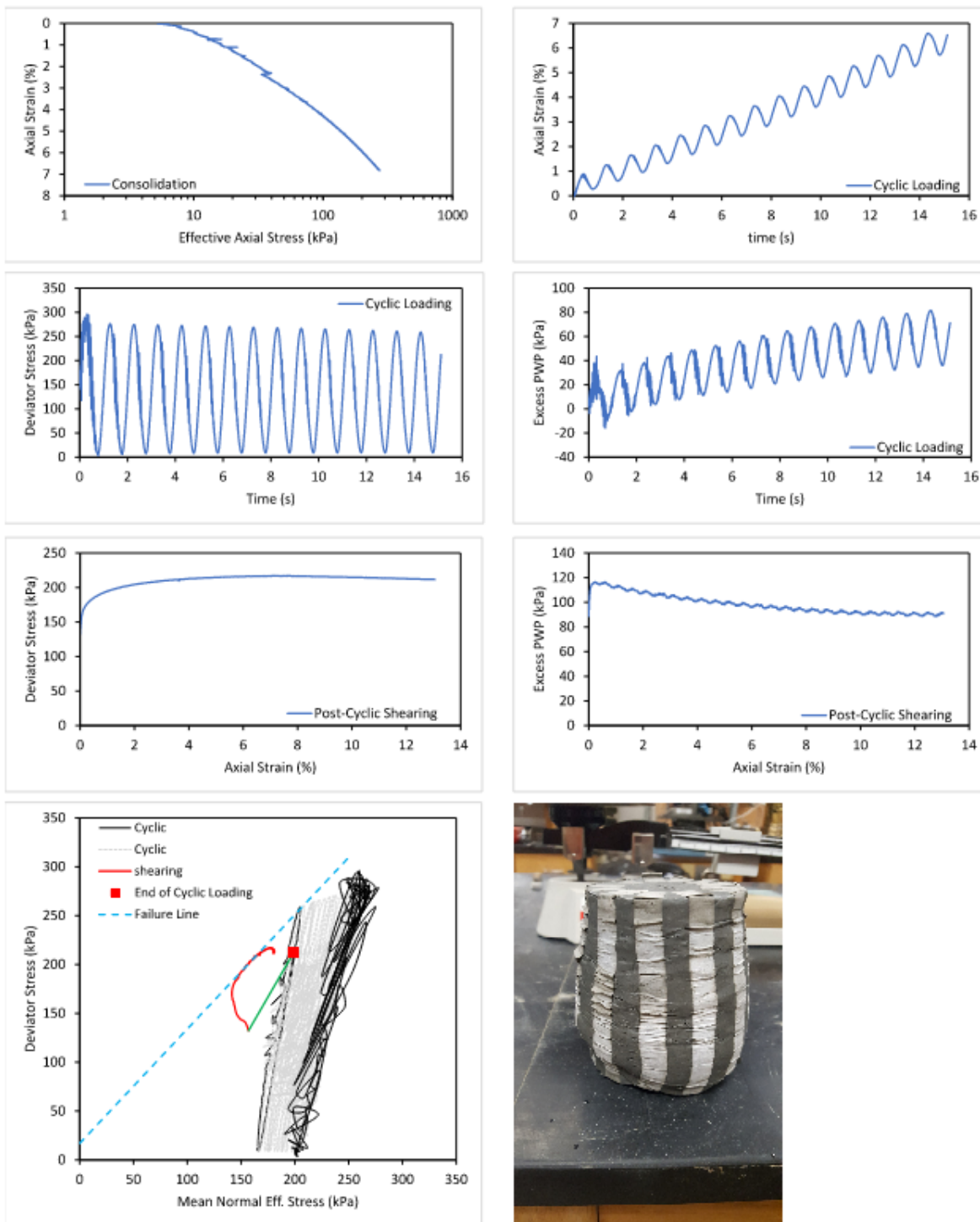


Figure B.32. Specimen NU-3 47-49

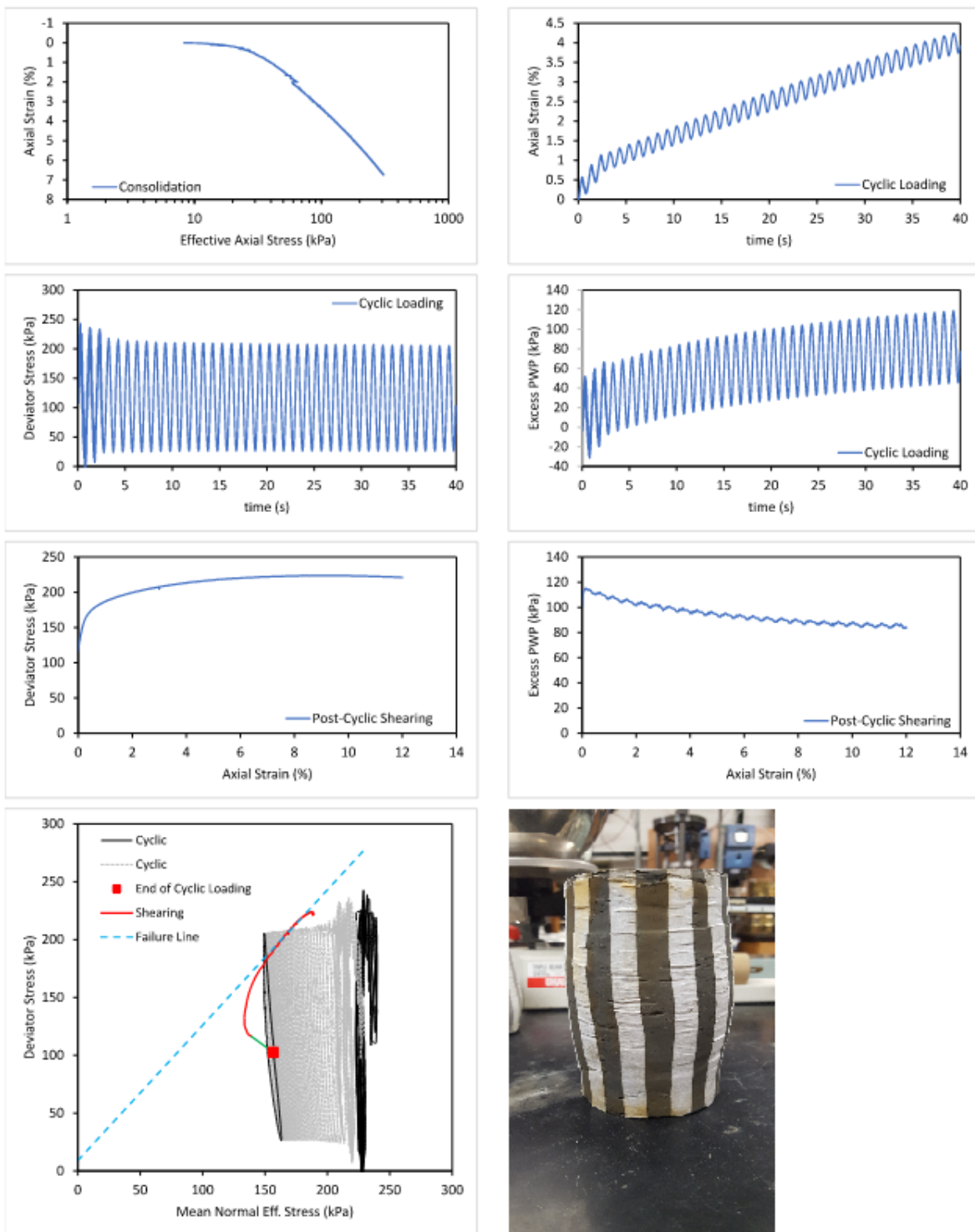


Figure B.33. Specimen NU-3 47-49(2)

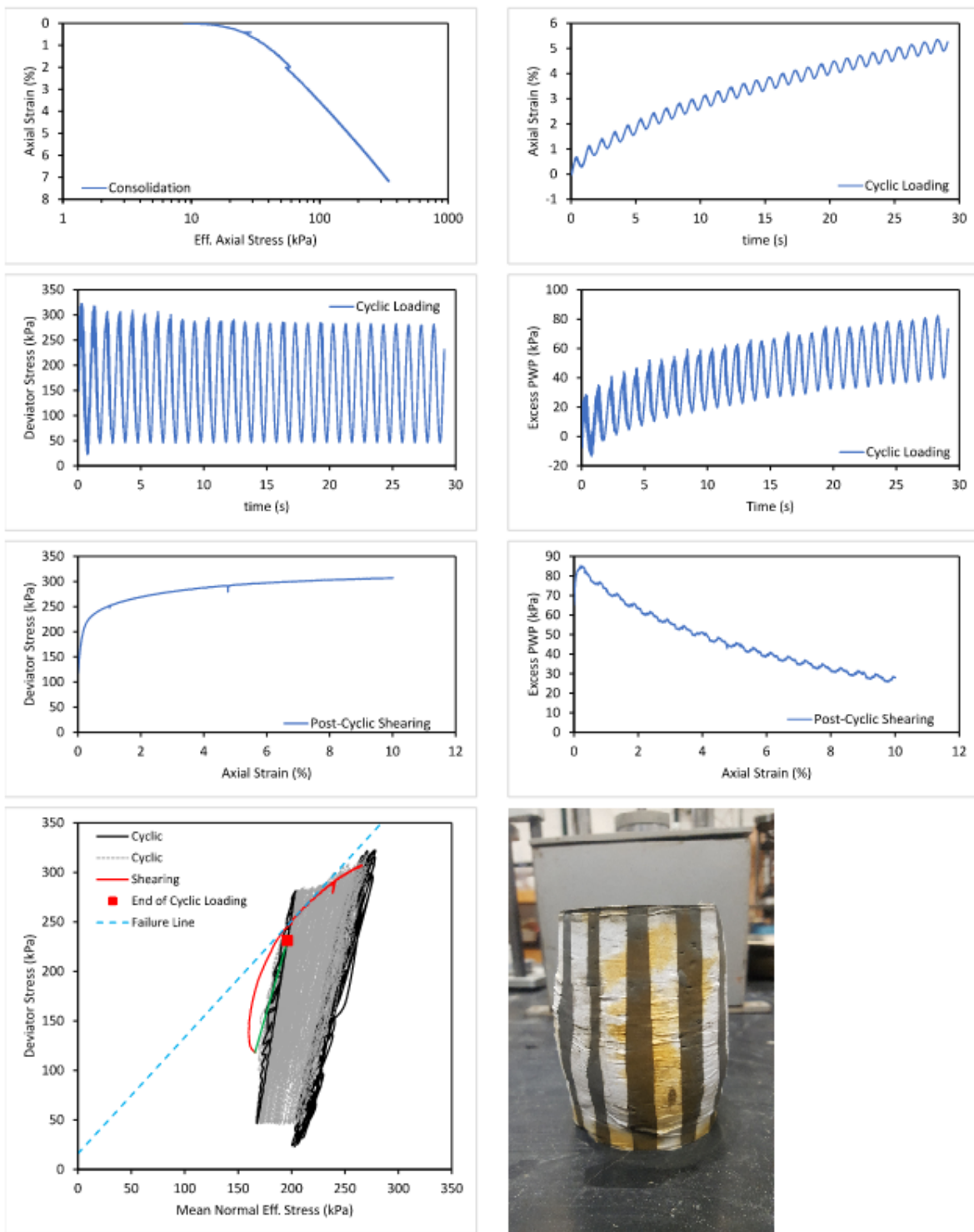


Figure B.34. Specimen NU-3 47-49(3)

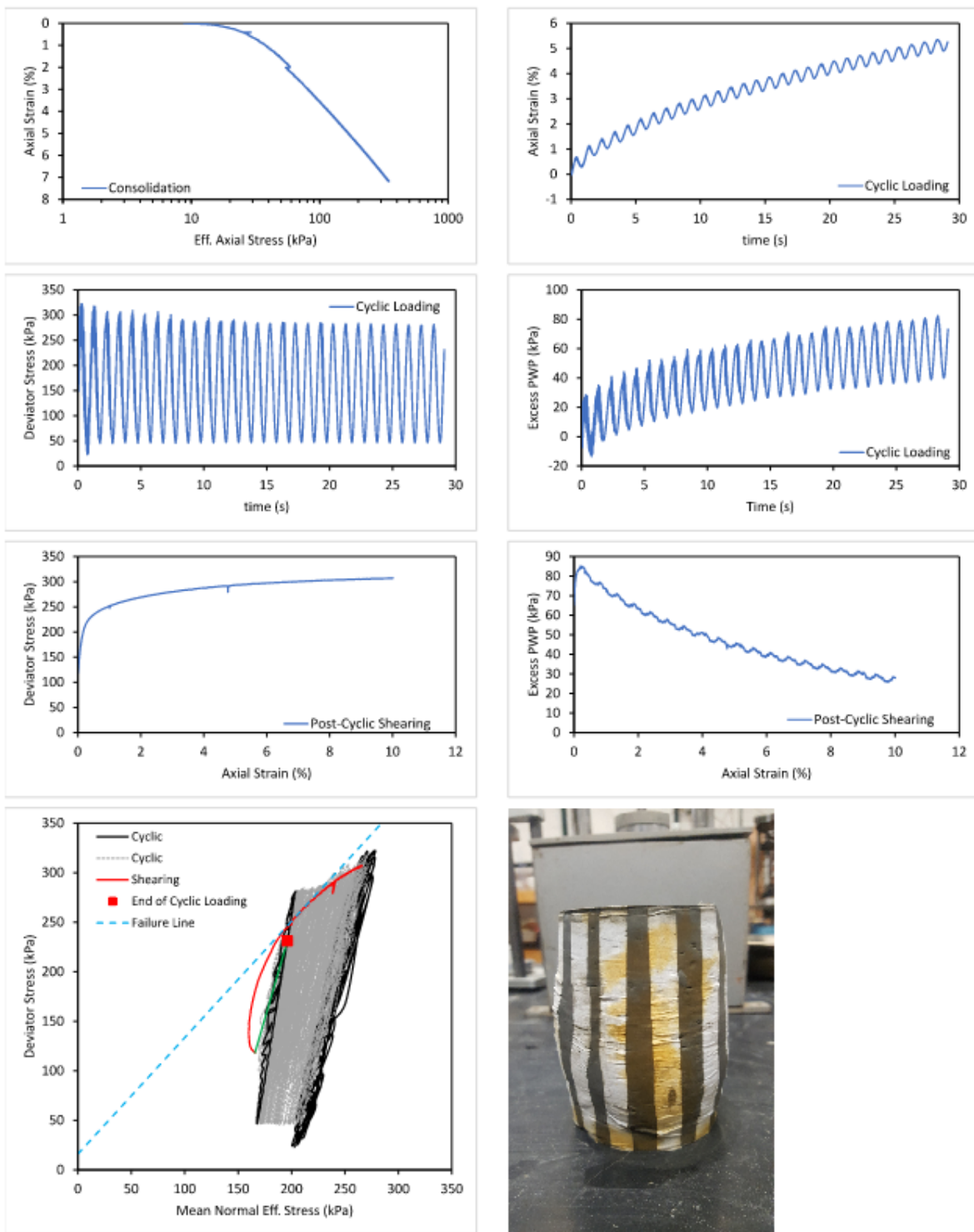


Figure B.35. Specimen NU-3 55-57

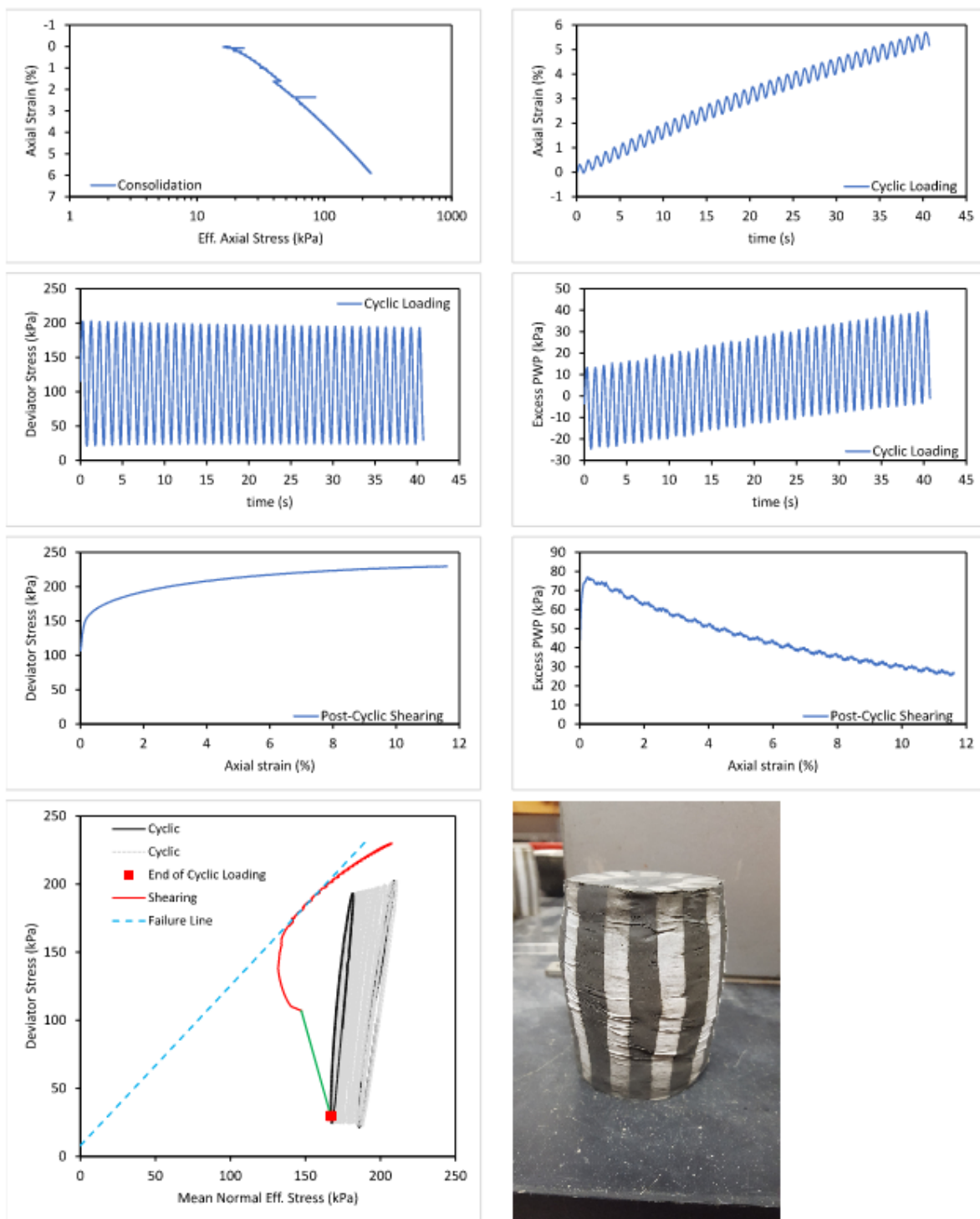


Figure B.36. Specimen NU-3 60-62